TOOLS FOR DESIGN OF HIGH TEMPERATURE BOREHOLE STORAGE IN DISTRICT HEATING PRODUCTION

TERMISKA ENERGILAGER

Energiforsk

Tools For Design of High Temperature Borehole Storage In District Heating Production

JOSÉ ACUÑA, ALBERTO LAZZAROTTO, JOSÉ GARCIA, WILLEM MAZZOTTI PALLARD,
MONIKA TOPEL, MAX HESSELBRANDT, MALIN MALMBERG AND MOHAMMAD ABUASBEH

Foreword

Det här projektet genomfördes för att utveckla en modell för design av ett borrhålslager i ett fjärrvärmesystem med hänsyn till grundvattenflöden. Här har ett beräkningsverktyg tagits fram som till exempel kan användas av energibolag i samband med förstudier där potentialen för högtemperaturlagring i borrhål undersöks. En öppen källkod har också genererats inom projektet som kan användas för att undersöka inverkan av grundvattenrörelse på ett lagers prestanda.

Projektet Tools for Design of High Temperature Borehole Storage in District Heating Production har letts och genomförts av KTH genom José Acuña, Alberto Lazzarotto, José Garcia, Willem Mazzotti Pallard, Monika Topel, Max Hesselbrandt, Malin Malmberg och Mohammad Abuasbeh.

Projektet ingår i programmet Termiska Energilager vars långsiktiga mål är att visa hur, var och när termiska energilager kan utformas och användas och vilken ekonomisk och miljömässig nytta de kan ge med finansiering från Energimyndighetens TERMO-program.

En fokusgrupp, tillika programmets styrgrupp, har följt och granskat projektet. Styrgruppen består av Henrik Lindståhl (ordförande) (Tekniska verken i Linköping AB), Lennart Hjalmarsson (Göteborg Energi AB), Per Haker (Hässleholm Miljö AB), Einar Port (Mälarenergi AB), Per Kallner (Vattenfall R&D AB), Lina Hoffert (Öresundskraft Kraft & Värme AB), Morgan Romvall (Halmstad Energi och Miljö AB), Ted Edén (Norrenergi AB) och Erik Holmén (ENA Energi) och Julia Kuylenstierna (adjungerade Energiforsk).

Suppleanter har bestått av Ulf Hagman (Göteborg Energi), Marianne Allmyr, (Mälarenergi AB), Mile Elez (Tekniska verken i Linköping AB), Jesper Baaring (Öresundskraft Kraft & Värme AB), Mats Svensson (Halmstad Energi och Miljö AB), Staffan Stymne (Norrenergi AB) och Patric Jönnervik (Jönköping Energi AB).

April 2021

Julia Kuylenstierna
Programansvarig, Energiforsk

Kort sammanfattning på svenska

Geoenergilager för att ta hand om spillenergi vid temperaturer under 100 ° C har varit föremål för diskussion i Sverige under de senaste åren, inom ramen för fjärrvärmeproduktion genom centrala kraftvärmeverk. (Forman et al. 2016) visar att ungefär hälften av den globala produktionen av primär energi går till spillo och att ca 60% av denna genereras inom detta temperaturområde.

Även om några tidigare och värdefulla svenska och internationella erfarenheter inom geoenergilagring vid högre temperaturer har dokumenterats i (Nordell, 1994), (Nordell et al, 2016) och (Malmberg, 2017) är många design- och praktiska frågor fortfarande öppna. Beräkningsverktyg för att utvärdera genomförbarhet och prestanda för högtemperaturborrhålslager behövs.

Detta projekt har fokuserat på utvecklingen av fristående beräkningsverktyg för design, simulering och optimering av dessa system, via värmeenergilagring i borrhål som kan interageras med kraftvärmeverk. De resulterande verktyg hjälper att bestämma, för givna begränsningar och användarkrav, en preliminär storlek på ett borrhålslager och värmepumpsystem, samt att studera påverkan av olika faktorer på prestanda.

Designen baseras på en förenklad quasi-steady state-metod (Yevankar, 2019), följt av dynamiska simuleringar i programmet TRNSYS (Malmberg et al, 2018). Beräkningsperioden väljs av användaren. Energieffektivitet och nuvärdet kan sedan användas som optimeringsmål och optimala lösningar (Pareto front) för motstridiga mål tillhandahålls för vissa typiska fall för att ge användarna extra hjälp vid dimensionering och simuleringsarbete.

Med ett krav för urladdningstemperatur och urladdningseffekt samt ett utbildat och projektspecifikt val av övriga inputs kan verktyg användas i samband med förstudier där potentialen för hög temperaturlagring i borrhål undersöks, inom effektområdet 10–50 MW.

Eftersom värmeöverföringsprestanda i borrhålslagren är beroende av markens termiska egenskaper men också av porositeten eller närvaron av sprickor i bergmassan, har detta projekt också inkluderat utvecklingen av modeller för att kvantifiera det inflytande som grundvattenrörelsen kan ha på denna typ borrhålslager, vilket vanligtvis inte beaktas vid utformningen av dessa system. Två modelleringsmetoder presenteras, en analytisk och en numerisk. Påverkan av grundvattenflöde har kvantifierats för realistiska scenarier. De möjliga effekterna på prestandan presenteras och diskuteras i energi och exergitermer. Som förväntat är effekten av grundvattenflödet svår att generalisera, eftersom varje borrhålslager kan kräva sin egen modell. Även när det kan finnas situationer där effekten av grundvattenflödet är försumbar (eller positiv), visar modellerna som utvecklats i detta arbete att grundvattenflöden av rimlig storlek har en negativ inverkan på prestanda. Även ett valideringsarbete har initierats med både en labbmodell och med uppmätt data från ett befintligt högtemperaturlager i Braedstrup Danmark.

Varje projekt är unikt men beräkningsverktygen som är framtagen i detta projekt bör kunna komma till nytta i de flesta fall. Användaren med viss förståelse för

geoenergisystem kan variera inputs och tolka hur outputs ska användas för ett specifikt ändamål/projekt. Användare med tillgång till TRNSYS kan även, med kännedom om publikationerna som ligger bakom detta projekt, boosta modellerna med fler eller färre systemkomponenter så som styrning, ta bort värmepumpen, distribution vid olika temperaturnivåer mm.

Förutom denna rapport och beräkningsverktyg resulterade detta projekt i fem publikationer där all information om det utförda arbetet presenteras. Publikationerna bifogas denna rapport.

Summary

(Forman et al. 2016) shows that around half of the global production of primary energy is wasted as exhaust or effluent losses, approximately 60% of the wasted heat being generated at temperature levels below 100°C. Borehole Thermal Energy Storages (BTES) for taking care of such losses have been a subject of discussion in Sweden during the last years, in the context of district heating production through central combined heat and power plants. Although a few earlier and valuable Swedish and international experiences in the subject have been documented in (Nordell, 1994) (Nordell et al, 2016) and (Malmberg, 2017), many design and practical questions remain still open and tools for evaluating feasibility and performance of high temperature borehole storages are needed.

This project has focused on the development of a Stand-alone calculation tool for design, simulation and optimization of High Temperature (HT, operating around 50 to 100⁰C) borehole thermal energy storage interacting with a combined heat and power plant. The resulting tool proposes, for given constrains and user requirements, the size of a borehole storage and heat pump system based on a simplified quasi steady state approach (Yevankar, 2019), followed by TRNSYS based dynamic simulations (Malmberg et al, 2018) for a period (years) chosen by the user. Exergy efficiency and the net present value can then be used as optimization objectives and a range of optimal solutions (Pareto front) for these conflicting objectives is provided for some simulated cases, allowing the tool users to have some extra help when carrying out own design and simulation work.

As heat transfer performance in borehole storages is closely dependent on ground thermal properties but also on the porosity or presence of fractures in the rock mass, this project has also included the development of models for quantifying the influence that groundwater movement may have on this type of HT-BTES storages, which is usually not considered when designing these systems. Advection-diffusion based heat transport processes have received far less attention and, in high temperature applications, any groundwater flow around the boreholes might be intuitively detrimental for the performance of the storage). Two modeling approaches are therefore presented, one analytical and one numerical. The influence of groundwater flow has been quantified for realistic scenarios of HT-BTES and the possible effects due to porosities, connectivity between voids or interconnected permeable joints and fractures is discussed in terms of energy and exergy performance. As expected, the effect of groundwater flow is difficult to generalize, as each storage local condition may require its own model. Even when there might be situations when the effect groundwater flow is negligible (or positive), the models developed in this work show that groundwater flows of reasonable size have a negative impact on the performance of HT-BTES. Attempts for validating the work have been made using both a laboratory scale model and real measured data from an existing high temperature storage in Braedstrup Danmark.

Besides this report and the calculation tool (distributed by Energiforsk and KTH), this project includes five publications where all details about the performed work are presented. The publications are appended to the report.

List of content

Energiforsk

OMFATTNANDE SAMMANFATTNING

Cirka 50 % av den globala produktionen av primärenergi går till spillo och cirka 60 % av spillenergin genereras vid temperaturnivåer under 100 °C. Användning av geoenergiborrhål vid hög temperatur (HT-BTES) verkar vara ett lovande tillvägagångssätt för storskalig säsongslagring av överskottsvärme i fjärrvärmesystem, som kan bidra till utfasning av fossila bränslen som idag utnyttjas för spetsvärmeproduktion. Behovet av fristående beräkningsverktyg för design av dessa gav upphov till detta projekt.

Projektet heter WP3.1 och är en del av Energiforsks forskningsprogram "Termiska Energilager", som godkändes av Energimyndigheten den 28 mars 2018 med Diarienummer 2018-001356, projektnummer 45976-1. Projektets mål är att:

1. Utveckla ett flexibelt verktyg för design av central energilagring med hög temperatur i borrhål.

2. Utveckla en analytisk och en numerisk modell som kvantifierar påverkan av grundvattenflöde på prestanda för lagring av värmeenergi med hög temperatur.

3. Föreslå metoder för teoretisk prestandaoptimering av lagring av värmeenergi för borrhål med hög temperatur.

Projektet omfattar följande tre arbetspaket (se figur 1):

WP1: Fristående beräkningsverktyg (kopplat till mål 1)

WP2: Simulering av grundvattenflöde (kopplad till mål 2)

WP3: Exergi och teknisk-ekonomisk optimering (kopplad till mål 1&2)
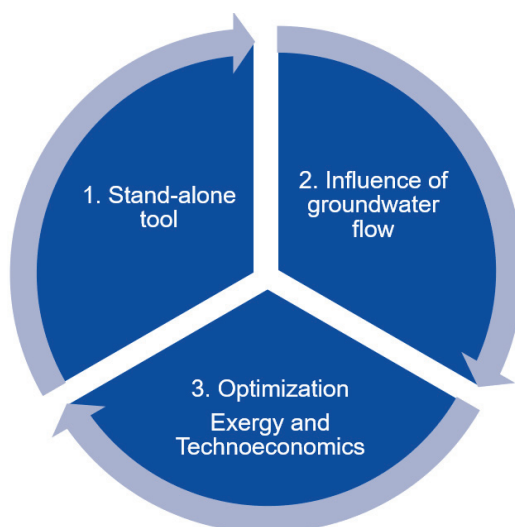
Figur 1. Projektets arbetspaket.

Värmeöverföringen i borrhålslager är beroende av markens termiska egenskaper, men också av eventuella grundvattenströmningar genom sprickor i bergmassan

som omger borrhålen. Det senare beaktas vanligtvis inte vid modellering av BTES-system då värmetransport genom värmeledning ofta antas vara den enda dominerande värmeöverföringsmekanismen. Så var fallet i det fristående beräkningsverktyget som togs fram i projektet.

I applikationer med hög temperatur kan ett eventuellt grundvattenflöde runt borrhålen vara skadligt för lagrets prestanda. De flesta modeller som tidigare har tagits fram för att hantera detta förutsätter förenklade förhållanden som homogena markegenskaper och grundvattenflöden medan ett fåtal tar hänsyn till varierande grundvattenflöden i t.ex. vertikalt skiktade porösa medier. Denna studie presenterar två modelleringsmetoder, en analytisk och en numerisk, där påverkan av grundvattenflöde har kvantifierats för realistiska scenarier av HT-BTES. Dessa är inte direkt kopplade till det fristående verktyget som tas fram i WP1.

Beräkningsresultaten i samtliga arbetspaket presenteras i termer av exergiprestanda, eftersom exergi tar hänsyn till mängden värme som utbyts men även till temperaturen vid vilken denna värme utbyts. Livscykelkostnaderna har också beaktats i arbetspaket 1 och 3, och en optimeringsalgoritm har använts för att uppskatta optimala kurvor efter att upprepade gånger ha kört BTES-simuleringar genom det fristående verktyget. Ett antal designparametrar varierades vid varje körning.

Detaljerade resultat för projektet hittas i den engelska versionen av denna rapport samt i fem publikationer som projektet resulterade i:

1. Lazzarotto A, Mazzotti Pallard W, Abuasbeh M, Acuna J. 2021. Performance evaluation of borehole thermal energy storage through energy and exergy analysis. World Geothermal Congress.

2. Hesselbrandt M. 2020. Performance analysis of a high temperature borehole thermal energy storage under influence of groundwater flow". MSc thesis. KTH.

3. Mazzotti Pallard W, Lazzarotto A, Acuna J, Palm B. 2020. Design methodology for laboratory scale borehole storage: an approach based on analytically-derived scaling laws and numerical simulations. Geothermics 2020.

4. Yevalkar, Amol. 2019. "Integrated Combined Heat and Power Plant with Borehole Thermal Energy Storage." Master thesis, Stockholm, Sweden: KTH Royal Institute of Technology. http://urn.kb.se/resolve?urn=urn:nbn:se:kth:diva-266787.

5. Malmberg, Malin, Mazzotti Willem, Acuña José, Lindståhl Henrik, and Lazzarotto Alberto. 2018. "High Temperature Borehole Thermal Energy Storage - A Case Study." In *Research Conference Proceedings*. Stockholm, Sweden.

BERÄKNINGSVERKTYGET

Utveckling av ett fristående verktyg för design och simulering av ett högtemperaturborrhålslager kopplat till fjärrvärmeproduktion har varit ett huvudmål för detta projekt. Systemet som simuleras visas i ett förenklat diagram i figur 2, i vilken borrhålslagret som visas längst ner i figuren är kärnan i modellen. Observera att det också finns en värmepump i systemet, då det inte är möjligt att från lagret hämta samma temperaturer som skickats ner under tidigare laddningsperioder. Det är dock fortfarande möjligt att erhålla komplett information för lagret och varje komponent i systemet, ifall användaren önskar koppla lagret på ett annat sätt.
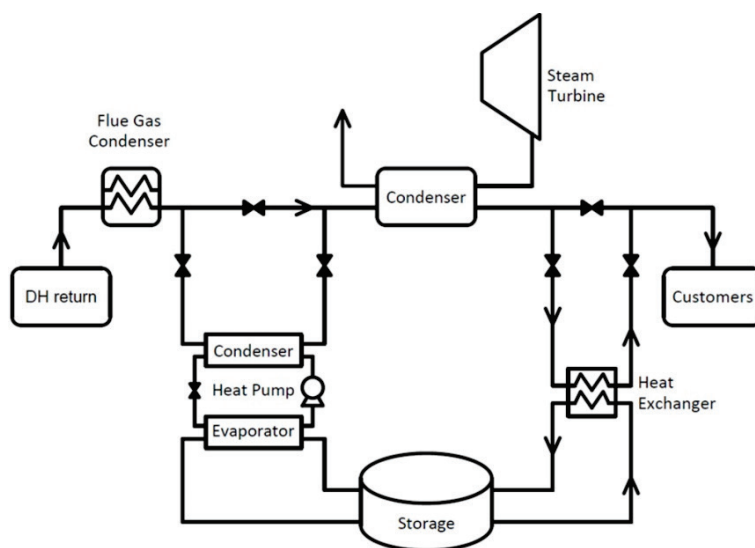
Figur 2. Schema som illustrerar systemet som modelleras i projektet.

Det finns två driftfall i beräkningsverktyget, sommar och vinter. Under sommaren laddas HT-BTES-systemet med varmvatten från kraftvärmeanläggningens kondensor. Urladdningen sker med hjälp av en värmepump under vintern och värmen används för att förvärma inloppet till kondensorn. Under vinterdriften används en värmepump för att öka vattentemperaturen.

Ett antal versioner för beräkningsverktyget har delats med styrgruppen för Termiska Energilager. Versionen som denna rapport bygger på kallas version 5, och den går att ta del av via Energiforsk eller genom att kontakta författarna. Gränssnitten illustreras i figur 3.
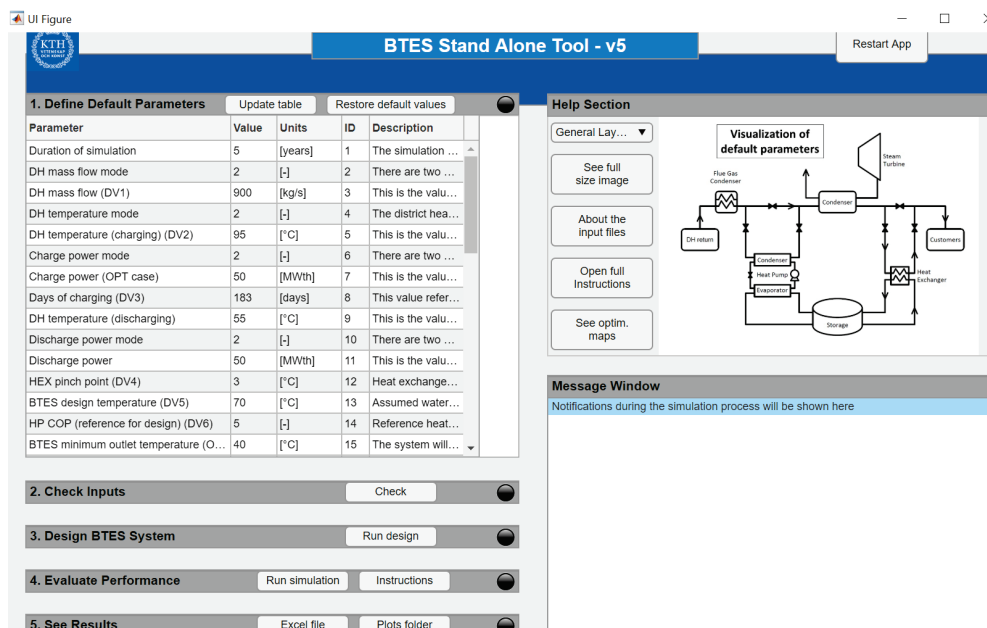
Figur 3. Användargränssnitt.

Verktyget fungerar i två steg:

Först via en generell quasi-steady-state dimensioneringsmodell utvecklad för systemets tre huvudkomponenter: värmeväxlare, värmepump och borrhålslagret. Borrhålslagrets erforderliga effektkapacitet, temperaturer och flöden är inputs. Komponenterna är dimensionerade för effekt mellan 10 och 50 MW. Temperaturen i slutet av valfri urladdningsperiod används som ett kriterium för att tillgodose användarnas krav och borrhålslagret måste tillfredsställa värmepumpens kylbelastning under hela simuleringsperioden samt den nödvändiga utloppstemperaturen för HT-BTES. Antalet borrhål justeras iterativt. Detta första steg utförs för att snabbt erhålla en systemstorlek. Se publikation 4 för mer detaljer.

När det preliminära designkriteriet är uppfyllt skapar modellen en inmatningsfil och skriver alla beräknade värden för de olika komponenterna som ingångsparametrar till det andra steget, dynamiska simuleringar. Här simuleras det resulterande systemet i steg 1 under ett antal år som användaren väljer. Därefter kan användaren erhålla simuleringsresultaten för samtliga simulerade år i både grafisk och tabellform.

För mer information om hur verktyget fungerar och hur den användas hänvisas till den engelska slutrapporten.

PRESTANDAOPTIMERING

För att hjälpa användaren att bedöma hur optimalt det simulerade systemet är har ett flertal måloptimeringar genomförts med en optimeringsalgoritm i kombination med det fristående verktyget. När användaren har utfört sina beräkningar med det fristående beräkningsverktyget kan uppskattade Pareto-optimala fronter användas för att trimma in designen och uppnå önskade mål. Fyra st case finns att utgå ifrån, med 2 olika temperaturnivåer för 10 MW respektive 50 MW kapacitet. Dessa visas i figur 4.
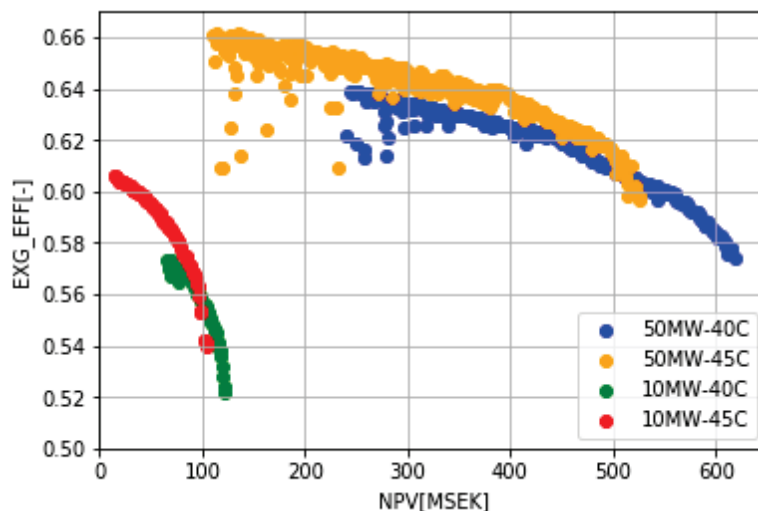
Figur 4. Pareto front for fyra olika optimeringscase.

Varje punkt i figur 4 representerar ett specifikt system med en unik uppsättning av inputs. I grund och botten är varje punkt en specifik körning av det beräkningsverktyget.

Med hjälp av en optimeringsrutin är det möjligt att erhålla prestandan samtidigt som designparametrarna varieras vid varje körning, men eftersom optimeraren inte är en del av det fristående verktyget har ett stort antal simuleringar genomförts för att illustrera vad som kan göras med verktyget när man vill jämföra effekten av olika inputs och systemkrav. Vid varje steg kan nya och gammal inputdata kombineras och de sämre lösningarna/kombinationerna kan tas bort från processen.

Prestandan för borrhålslagret utvärderas med hänsyn till både energi och exergi, både på systemnivå och säsongsbasis, samt inom lagringsvolymen. Lagrets säsongsvisa prestanda beräknas med följande två ekvationer för energi (η) och exergi (ψ), där d och c står för urladdning respektive laddning och den nedre gränsen (0) för laddningsintegralen står för laddningstidens start (inte nödvändigtvis noll). För detaljer i varje parameter som används i ekvationerna hänvisas till publikation 1.

$$\eta \;=\; \frac{Q_d}{Q_c} = \frac{\int_{\tau_c}^{\tau_c+\tau_d} \dot{m}c_p \left(T_{\text{out}}(t) - T_{\text{in}}\right) dt}{\int_0^{\tau_c} \dot{m}c_p \left(T_{\text{in}}(t) - T_{\text{out}}\right) dt}$$

$$\psi \;=\; \frac{\text{Ex}_d}{\text{Ex}_c} = \frac{\int_{\tau_c}^{\tau_c+\tau_d} \dot{m}c_p \left[(T_{\text{out}}(t) - T_{\text{in}}(t)) - T_0 \ln\left(\frac{T_{\text{out}}(t)}{T_{\text{in}}(t)}\right)\right] dt}{\int_0^{\tau_c} \dot{m}c_p \left[(T_{\text{in}}(t) - T_{\text{out}}(t)) - T_0 \ln\left(\frac{T_{\text{in}}(t)}{T_{\text{out}}(t)}\right)\right] dt}$$

Innanför lagringsvolymen beräknas energi och exergiprestanda enligt följande:

$$\eta_{\text{storage}}(V,t) = \frac{Q_{\text{stored}}(V,t)}{Q_{\text{exchanged}}(t)} = \frac{\int_V \rho_g c_{p_g} \left(T(\mathbf{x}, T) - T_0\right) dV}{\int_0^t m_f c_{p_f} \left(T_{\text{in}}(t) - T_{\text{out}}(t)\right) dt}$$

Energiforsk

$$\psi_{\text{storage}}(V, t) \;=\; \frac{\text{Ex}_{\text{stored}}(V, t)}{\text{Ex}_{\text{exchanged}}(t)} = \frac{\int_V \rho c_p \left[(T(\mathbf{x}, t) - T_0) - T_0 \ln\left(\frac{T(\mathbf{x},t)}{T_0} \right) \right] \, dV}{\int_0^t \dot{m} c_p \left[(T_{\text{in}}(t) - T_{\text{out}}(t)) - T_0 \ln\left(\frac{T_{\text{in}(t)}}{T_{\text{out}(t)}} \right) \right] \, dt}$$

Inte all energi eller exergi som lagras i kontrollvolym är återhämtningsbar, men dessa prestandaindikatorer gör det möjligt att kvantifiera lagrets förmåga att bibehålla den energi som injiceras och som kan delvis kan urladdas. För beräkning av exergi med hjälp av ekvationerna ovan använder man absoluta temperaturer uttryckta i Kelvin. Referenstemperaturen T_0 betraktas i denna rapport som markens ostörda temperatur men den kan väljas godtyckligt.

Energiforsk

PÅVERKAN AV GRUNDVATTENFLÖDE

En del av värmen som lagras i marken under laddningssäsongen kan på grund av grundvattenflöde transporteras bort från lagringsvolymen och kan därmed inte hämtas under urladdningssäsongen. Även om detta är intuitivt ur en kvalitativ synvinkel är den kvantitativa bedömningen av denna effekt svår att utföra. En fråga som uppstår är var man drar gränsen mellan acceptabelt och oacceptabelt grundvattenflöde. Svaret går inte att generalisera då varje projekt har specifika krav och förutsättningar. Effekten av grundvattenflöde i borrhålslager med högtemperatur har dock undersökts genom energi- och exergianalys med analytiska och numeriska modeller. Undersökningen görs för borrhålskonfigurationen vid ett verkligt borrhålslager i Braedstrup, Danmark. Systemet laddas via de inre borrhålen under sommaren och från de yttre borrhålen under vintern. Se figur 5.

Om berget i ett borrhålslager skulle ha sprickzoner så skulle grundvattenflödet förekomma i flödesvägar som beror på spricksystemets lokala geometri, och inte på det sättet som illustreras i figur 5. Varje fall är projektspecifikt och påverkan som grundvattenflöde har går ej att kvantifiera på ett generellt sätt utan är starkt beroende på lokala förutsättningar i varje projekt.
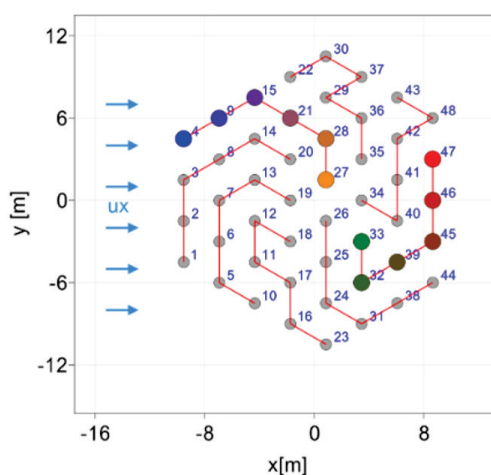
Figur 5. Borrplan Braedstrup. Hypotetiskt grundvattenflöde från vänster till höger. Mätning av fram och returledningstemperatur i två färgmarkerade borrhålskretsar, nedströms och uppströms.

Marken i detta projekt har antagits vara homogen och uppträder som ett poröst medium, antingen hela volymen eller delar av den. Medelegenskaperna har antagits vara stabila och relativt konstanta över ett givet område av utrymmet.

Beräkningarna har gett tillfälle att testa två metoder för modellering av högtemperaturlagring som integrerar värmeöverföring i porösa medier med hjälp av en semi-analytisk och en numerisk metod. De erhållna resultaten är inte alls allmänna, eftersom de beror på modellernas projektspecifika parametrar och de lokala förhållandena för varje lagringsplats, men de ger en indikation på storleken på effekten som grundvattenflödet kan ha på prestanda.

Den numeriska modellen som har utvecklats i detta projekt representerar det termiska beteendet av lagret i Danmark, och mätdata har använts för validering

med bra överenskommelse mellan uppmätta och beräknade värden (se figur 6). Som för de flesta numeriska modeller krävs en lång simuleringstid. Ett antal hypotetiska scenarier med olika hydrauliska gradienter har dock testats. Figur 7 visar simuleringsresultatet för dessa.
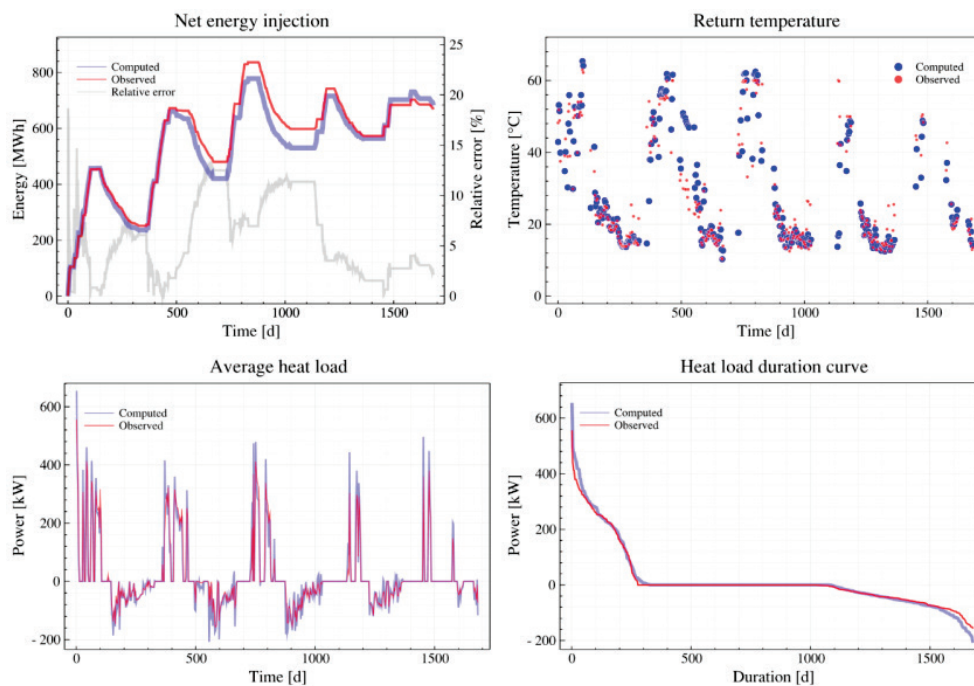
Figur 6. Jämförelse mellan uppmätt och beräknat data. Numeriska modell.

Enligt resultatet i figur 7 har ett litet grundvattenflöde (liten hydraulisk gradient) faktiskt en förbättringseffekt i lagringsprestandan under den fjärde lagringscykeln, troligtvis på grund av förbättrad värmetransport och därmed minskad värmemotstånd. Både när det gäller lagrets säsongsvisa systemenergi och exergiprestanda sker en gradvis ökning som sedan stabiliseras med tiden. Ett mer stationärt tillstånd tenderar att inträffa mycket tidigare i fall av högt grundvattenflöde (stor hydraulisk gradient). Den relativa förändringen av energieffektiviteten blir från år till år mindre.

Dessa tendenser kan även observeras i resultaten från den analytiska metoden (se nedan). Det är dock viktigt att notera att tider för laddning / urladdning, liksom flöden och temperaturer är mycket oregelbundna i det numeriska fallet eftersom det är driftsdata från Braedstrup som används som input.
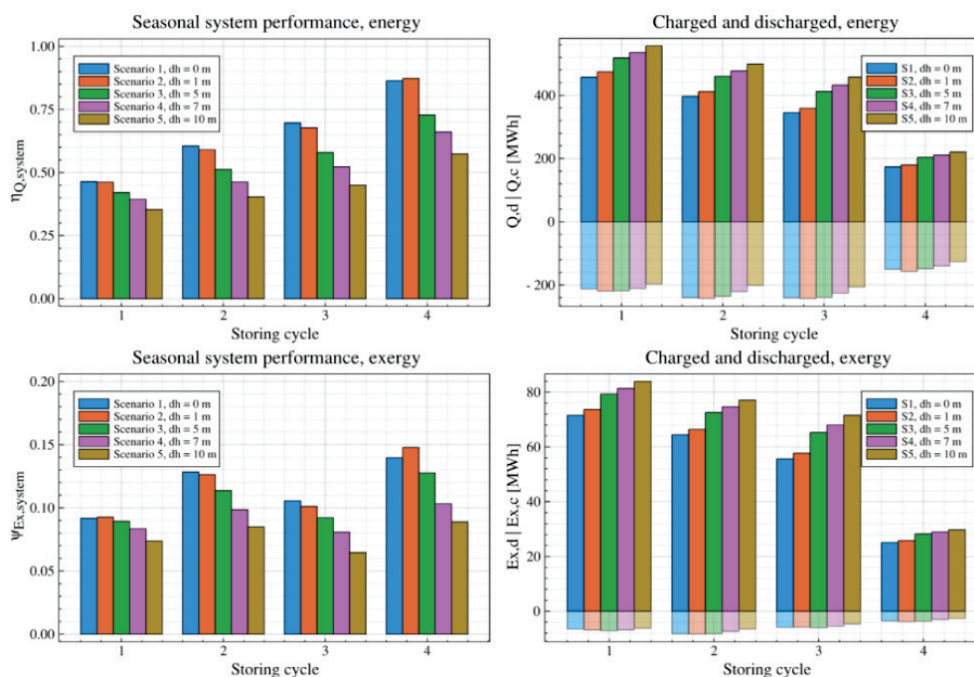
Figur 7. Energi and exergi for olika hydrauliska gradienter i borrhålslagret i Braedstrup, Danmark.

I den analytiska lösningen antas homogena hydrauliska och termiska egenskaper. Modellen är endast giltig under en begränsad uppsättning av villkor men är snabbare och gör det möjligt att utforska fler fall. Den är baserad på så kallat rörliga finita linjekällteorin (moving finite line source), som erhålls genom att integrera effekten av en rörlig punktkälla inbäddad i en oändlig volym med homogena termiska och hydrauliska egenskaper längs borrhålets längd. Temperaturen beräknas för vilken punkt i bergvolymen och i tiden som helst (x, y, z och t) och temperaturfältet runt flera borrhål i borrhålslagret erhålls med hjälp av superposition och summeringen av effekten av varje linjekällas bidrag, vilket är möjligt eftersom differentialekvationen som styr värmetransporten i porösa medier är linjär under det betraktade tillståndet.

Borrhålsfältet påverkas av regionalt grundvattenflöde med hastighet u_x, vilket uttrycks i ekvationerna ovan. Braedstrups borrhålskrets med seriekopplingar (en på uppströmsdelen av borrhålsfältet och en på nedströmsdelen) visas i figur 5. Temperaturerna, energi och exergi har beräknats för att belysa lagringsbeteendet i närvaro av grundvatten, vid två olika hastigheter för grundvattenflödet, 0,5 cm/dag and 1 cm/dag. Dessa jämförs med fallet utan grundvattenflöde. Beräkningsverktyget finns att hämta här:
https://gitlab.com/alblaz/BTESGroundWaterSimulator

ground water speed 0.01 m/day
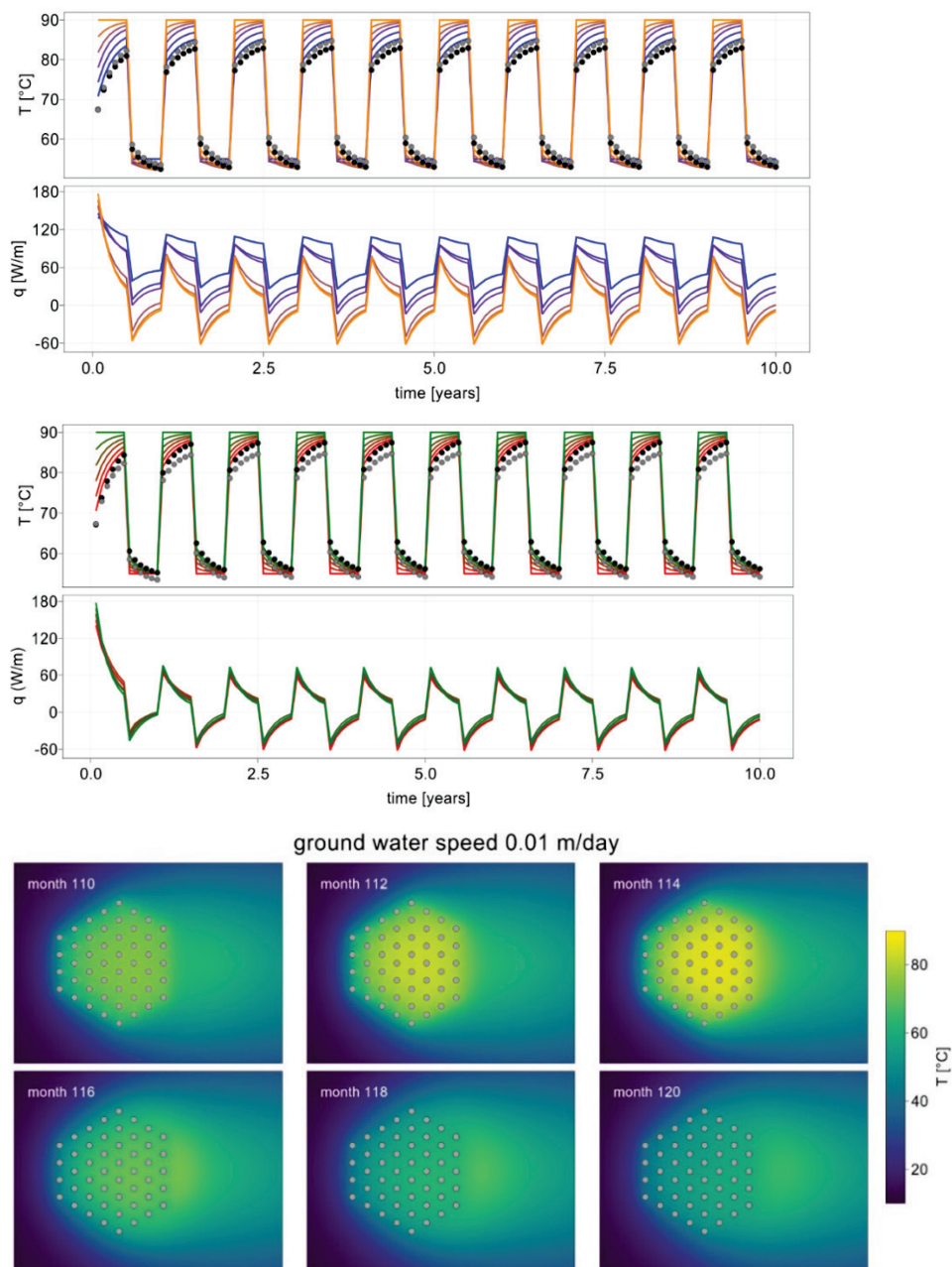
Figur 8 Beräknade temperaturer, grundvattenhastighet u_x = 1 cm/dag.

För fall där det inte finns något regionalt grundvattenflöde är inlopps- och utloppstemperaturerna från de två borrhålskretsarna mycket lika trots att deras position inte är exakt symmetrisk. Effektuttaget är också mycket lika.

När grundvattenflödet ökar börjar effekten på inlopps- och utloppstemperaturen i de två kretsarna att avvika (se utloppstemperaturen i figur 8 som inte sammanfaller). Uppströms belägna borrhål är kallare än borrhålen nedströms, och de tre sista borrhålen i uppströmsserien är vid temperaturer under den tillförda inloppstemperaturen. Dessa borrhål dumpar värme (istället för att extrahera värme) under urladdningsperioden. Konturdiagrammet visar hur en del av värmen förskjuts helt i slutet av extraktionsperioden, dvs den kan inte längre återvinnas med hjälp av borrhålen.

Mängden energi som plockas ut och laddas i systemet beror på grundvattenflödets hastighet, temperaturen som tillförs borrhålslagret och på de termiska (och hydrauliska) förhållandena i lagret självt. Figur 9 och 10 visar prestandan för de tre flödeshastigheter som studerats, för två olika fall vid inloppet för laddning vid 90 eller 80°C och urladdning vid 55 respektive 20°C.

När grundvattenhastigheten ökar kan systemet lagra mer energi i marken, men det extraherar mindre under vintern. De låga energinivåerna speglar det faktum att "lågkvalitetsvärme" utvinns efter att ha laddat in "högre kvalitet" under föregående säsong (man kan fortfarande ladda ur stora mängder energi även om värmekvaliteten är låg). Vid högre urladdningstemperaturer blir dessa värden bättre.

Beräkningarna i figur 9 och 10, och även de i figur 7, visar att både energi- och exergiprestanda försämras med ökande grundvattenflöde.

Exergiindikatorn verkar vara mindre känslig än energiindikatorn trots att det inte är helt uppenbart från figurerna ovan. Den exergi som extraheras från borrhålslagret är ganska låg. Den stora skillnaden mellan laddnings- och urladdningsperioder visar på betydande energiförluster. Även om lägre grundvattenflöden bidrar till något högre exergilagringseffektivitet efter ett par lagringscykler, detta verkar det inte vara av betydelse för den totala prestandan. Det är dock av mer betydelse i fallet 90/55°C.

Användning av höga laddningstemperaturer, samtidigt som värme laddas ur vid temperaturer relativt nära referenstemperaturen, främjar energiutvinning och lagringstemperaturerna hålls på måttliga nivåer, men exergiprestanda straffas om den ostörda marktemperaturen används som referens, dvs man främjar hög energiprestanda genom att använda låga inloppstemperaturer vid urladdning (vilket automatiskt innebär närmare ostörda temperaturen), men det innebär också att man måste kompromissa med exergiprestandan.
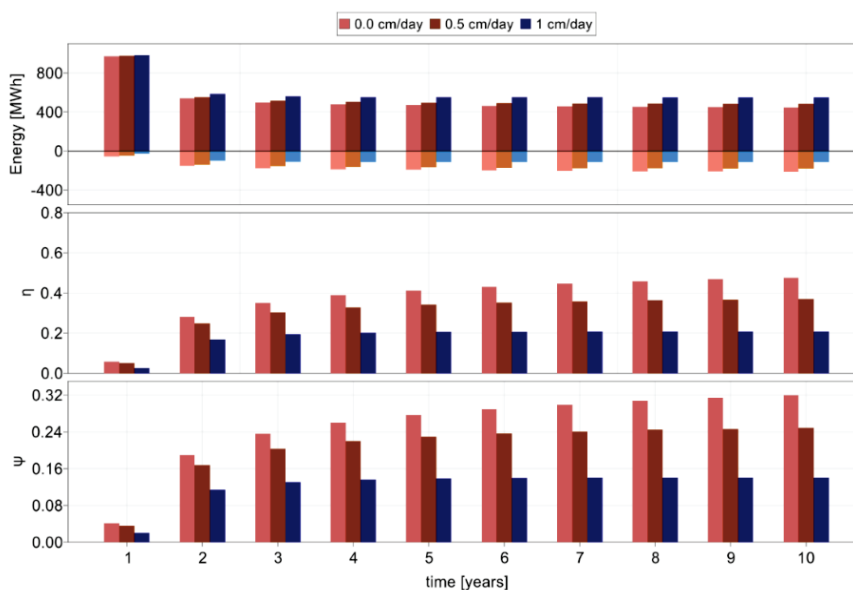
Figur 9. Sammanställning av energi och exergiverkningsgrad (inloppstemperaturen är 90°C vid laddning och 55°C vid urladdning)
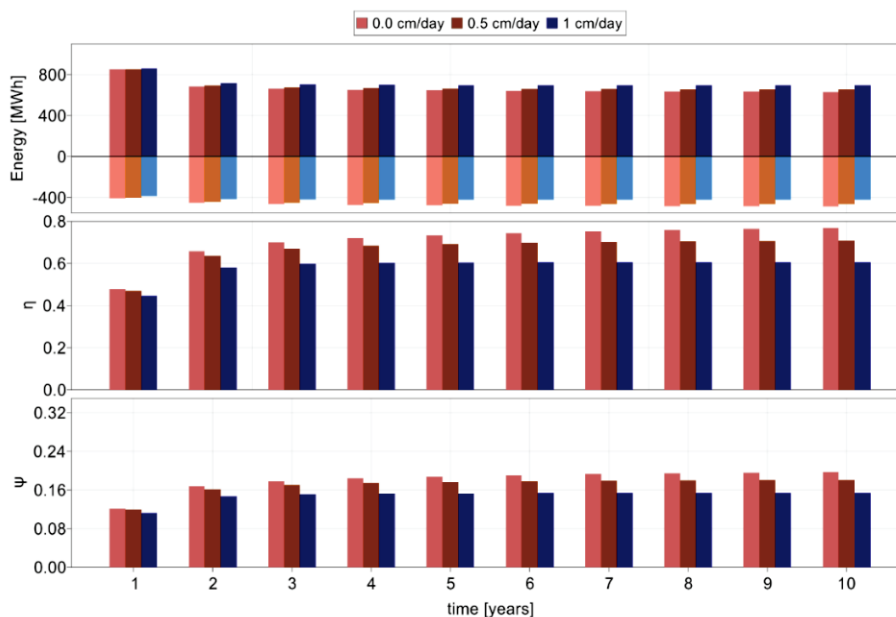
Figur 10. Sammanställning av energi och exergiverkningsgrad (inloppstemperaturen är 80˚C vid laddning och 20˚C vid urladdning)

SLUTSATS

Detta projekt har fokuserat på utvecklingen av ett fristående beräkningsverktyg för design, simulering och optimering av borrhålslager integrerade med kraftvärmeverk. Verktyget hjälper att bestämma, för givna begränsningar och användarkrav, en preliminär storlek på ett borrhålslager och värmepumpsystem.

Designen baseras på en förenklad quasi-steady state-metod följt av dynamiska simuleringar i programmet TRNSYS. Beräkningsperioden väljs av användaren. Energieffektivitet och nuvärdet kan sedan användas som optimeringsmål och optimala lösningar (Pareto front) kan tillhandahållas för vissa typiska fall för att ge användarna extra hjälp vid dimensionering och simuleringsarbete.

Projektet har inkluderat utvecklingen av modeller för att kvantifiera det inflytande som grundvattenrörelsen kan ha på högtemperaturborrhålslager, vilket vanligtvis inte beaktas vid utformningen av dessa system. Två modelleringsmetoder presenteras, en analytisk och en numerisk. Påverkan av grundvattenflöde har kvantifierats för realistiska scenarier. De möjliga effekterna på prestandan presenteras och diskuteras i energi- och exergitermer. Som förväntat är effekten av grundvattenflödet svår att generalisera, varje borrhålslager kräver sin egen specifika modell.

Även när det kan finnas situationer där effekten av grundvattenflödet är försumbar (eller positiv), visar modellerna som utvecklats i detta arbete att grundvattenflöden av rimlig storlek har en negativ inverkan på prestanda i högtemperatur borrhålslager.

1   INTRODUCTION

1.1   BACKGROUND AND MOTIVATION

Flexible tools for calculating how to harness waste heat through thermal energy storage are needed. Waste heat is an inevitable by-product of every energy conversion process. Estimations show that around 50% of the global production of primary energy is wasted as exhaust or effluent losses, out of which approximately 60% are generated at temperature levels below 100 °C (Forman et al. 2016). Waste heat recovery has been recognized as a means to improve overall energy efficiency and reduce greenhouse gas emissions (U.S. Department of Energy 2008; Cabeza 2015). Borehole thermal energy storage (BTES) or more specifically high temperature BTES (HT-BTES), appears to be a promising approach for large-scale, long-term, sensible thermal storage of excess heat from combined heat and power (CHP) plants (Reuss 2015), possibly allowing to eliminate fossil fuels during peak winter hours and to lower life cycle costs. This project is born in the need of having a standalone tool that designs and quantifies performance for central large-scale HT-BTES together with generic CHP plants.

Borehole storages consists mainly of two parts, vertical boreholes and the surrounding ground. The ground is used as storage medium and the vertical U-pipe or coaxial Borehole Heat Exchangers (BHE) as the interaction components between production plants and the storage medium. A heat transfer fluid is circulated through the BHE network and exchanges heat with the surrounding ground. Heat transfer performance in each borehole is mainly dependent on the type of BHE used. Although BHEs with coaxial pipe configuration show better thermal performance than the more common U-tube BHEs (Acuña 2013), single and double closed-loop U-tube BHEs have been used in most existing HT-BTES implementations (Sibbitt et al. 2012; Tordrup, Poulsen, and Bjørn 2017; Nußbicker et al. 2003; Mangold and Deschaintre 2015; Grycz, Hemza, and Rozehnal 2014). Coaxial type BHE installations have been tested to a minor scale (Acuña 2013; Alkiswani and Regander 2019; Nordell 1994; Nordell et al. 2016).,

Heat transfer performance in the bedrock is closely dependent on the ground thermal properties but also on the tightness (porosity or presence of fractures) of the rock mass surrounding the boreholes. The latter is usually not considered when designing low temperature BTES systems. Heat transport by conduction is often the only heat transfer mechanism considered. In high temperature applications, however, any groundwater flow around the boreholes might be intuitively detrimental for the performance of the storage.

While heat conduction models have been thoroughly investigated and established in design tools used for both academic and commercial purposes (Zhang, Wang, Liu, Kong, Wang 2018), approaches to model advection-diffusion based heat transport processes have received far less attention (Banks 2015). A noteworthy study dealing with analytical modeling of coupled groundwater flow and heat transfer in porous media is (Diao, Li, Fang 2004), who developed a ground resistance model based on the Moving Infinite Line Source (MILS) solution to the advection-diffusion equation. (Molina-Giraldo, Blum, Zhu, Bayer, Fang 2011a,b)

Energiforsk

further developed the MILS theory by introducing a solution to the moving finite line source (MFLS) problem to account for axial effects and constant surface temperature, and (Katsura, Shoji, Sakata, Nagano 2020) derived an approximate solution of the moving infinite cylinder source model. (Molina-Giraldo, Bayer, Blum 2011) and (Chiasson, O'Connell 2011) also considered the effect of thermal dispersion upon advective and conductive heat transport. All these models presume simplified conditions such as homogeneous and isotropic ground material properties, uniform and steady groundwater flow, and constant ground surface temperature. However, recently developed analytical models have made it possible to account also for spatial and temporal variations in ground surface temperature (Rivera, Blum, Bayer 2015), and non-uniform groundwater flow in vertically-layered porous media (Hu 2017). Considering this background, this study presents two modeling approaches (not directly connected to the stand-alone tool), one analytical and one numerical, where the influence of groundwater flow has been quantified for realistic scenarios of HT-BTES. The possible effects due to porosities, connectivity between voids or interconnected permeable joints and fractures is discussed and presented in terms of energy and exergy performance.

Exergy considers both the quantity of the heat exchanged as well as the temperature at which this heat is exchanged, which most of the earlier work dealing with BTES have failed to describe (since they have only focused on energy performance, forgetting the temperature at which the thermal energy is exchanged with the BTES.

Exergy analysis (and optimization) should be of interest especially when dealing with High Temperature-BTES systems, as recently presented in Hemmatabady et al. (2020). This work focuses on quantifying exergy performance along with energy performance for HT-BTES systems, considering both pure conduction in solid as well as the presence of regional groundwater flow. In parallel to optimizing exergy, the life cycle costs has also been considered.

In order to account for multiple performance indicators such as exergy and life cycle cost in the selection of optimal configurations, multi-objective optimizations have therefore been suggested in this study. An optimizer algorithm (Leyland, 2002) is used in combination with the standalone tool developed in this project, estimating pareto optimal fronts after running BTES simulations (through the standalone tool) repeated times while varying the design parameters on each run. This is done in the search of fulfilling desired objectives, usually conflicting in nature. Exergy efficiency and the net present value were selected as the objectives of the optimization. As these conflicting objectives provide a range of optimal solutions (Pareto front) instead of one single optimal configuration, this allows to user to make a choice based on the obtained performances and the related input parameters that lead to that optimal configuration.

1.2 OBJECTIVES

1. Develop a general and flexible model for design of central high temperature borehole thermal energy storage.

Energiforsk

2. Develop an analytical and a numerical model that quantifies the influence of groundwater flow on the performance of high temperature borehole thermal energy storage.

3. Suggest methods for theoretical performance optimization of high temperature borehole thermal energy storage.

1.3   WORKING PACKAGES

This project is called WP3.1 and it is part of Energiforsk research program "Termiska Energilager", as approved by Energimyndigheten on 2018-03-27 with Diarienummer 2018-001356, project number 45976-1. The project comprises the following three working packages:

WP1: Development of Stand-alone calculation tool (connected to objective 1)

WP2: Simulation of groundwater flow (connected to objective 2)

WP3: Exergy and techno-economical optimization (connected to objective 1 and 2)

These three working packages are intimately connected with the project objectives as well as with each other, as illustrated in Figure 1. WP1 is connected to objective 1, WP2 to objective 2 and WP3 to objective 1, 2 and 3.
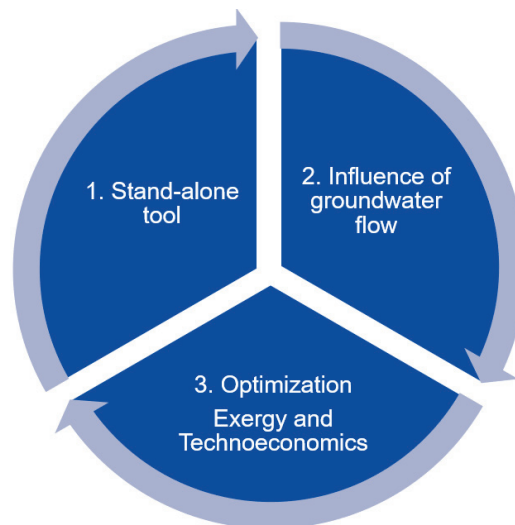
Figure 1. Working packages of the project

A summary on the methodology, results and conclusions of each working package are presented in the following three separate chapters as well as in the different publications from this project:

1. Lazzarotto A, Mazzotti Pallard W, Abuasbeh M, Acuna J. 2021. Performance evaluation of borehole thermal energy storage through energy and exergy analysis. World Geothermal Congress.

2. Hesselbrandt M. 2020. Performance analysis of a high temperature borehole thermal energy storage under influence of groundwater flow". MSc thesis. KTH.

3. Mazzotti Pallard W, Lazzarotto A, Acuna J, Palm B. 2020. Design methodology for laboratory scale borehole storage: an approach based on analytically-derived scaling laws and numerical simulations. Geothermics 2020.

4. Yevalkar, Amol. 2019. "Integrated Combined Heat and Power Plant with Borehole Thermal Energy Storage." Master thesis, Stockholm, Sweden: KTH Royal Institute of Technology. http://urn.kb.se/resolve?urn=urn:nbn:se:kth:diva-266787.

5. Malmberg, Malin, Mazzotti Willem, Acuña José, Lindståhl Henrik, and Lazzarotto Alberto. 2018. "High Temperature Borehole Thermal Energy Storage - A Case Study." In *Research Conference Proceedings*. Stockholm, Sweden. https://doi.org/10.22488/okstate.18.000036.

1.4 REPORT STRUCTURE AND ACKNOWLEDGMENTS

This report is a summary of the work carried out during the project "Kraftvärmeverk i samspel med borrhålslager", part of the research program Termiska Energilager.

The report consists of mainly three chapter, each one summarizing the work of the three working packages. The three chapter do successive reference to several publications that have been delivered as part of the project. These publications should always be included in this report package so that the reader has access to details.

Energiforsk

2 STAND-ALONE CALCULATION TOOL

Developing a stand-alone tool that designs and simulates the behavior of a BTES system coupled to a combined heat and power plant has been one of the major focuses of this project. The system to be simulated is shown in a simplified diagram, Figure 2, the borehole thermal energy storage shown at the bottom of the figure being the core of the model. Observe that there is also a heat pump in the system.

There are two operational modes in the calculation tool, summer and winter. During summer, the BTES system is charged using hot water from the CHP plant's steam condenser outlet. During winter, the BTES system is discharged, and the heat is used to preheat the inlet to the CHP plant's condenser. During the winter operation, a heat pump is used to help rise the water temperature.
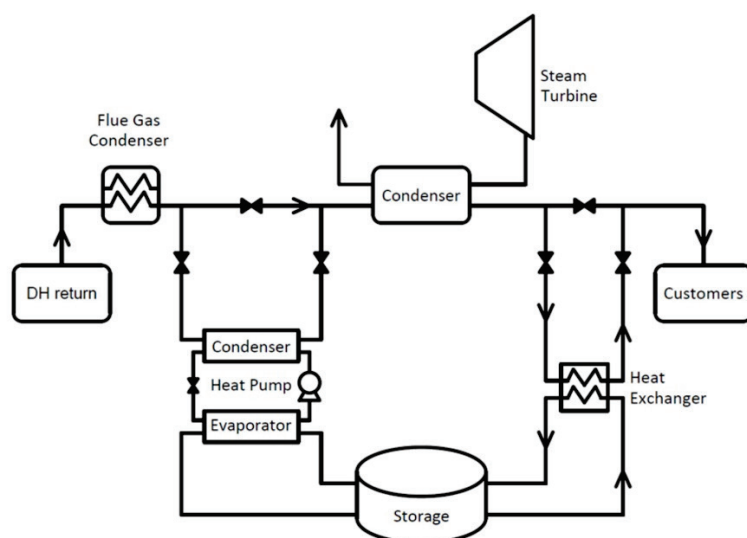
Figure 2. Scheme illustrating the system modelled

A number of tool versions have been shared with the steering group of Termiska Energilager via Energiforsk. The version on which this report is bases is called version 5, V5.

The tool works initially with a generic quasi-steady-state sizing model developed for the three main components of the system: heat exchanger, heat pump and the borehole thermal energy storage. For the BTES, the steady state model is a simplified version of the DST model suggested by (Hellström, 1989). This quasi steady-state model is used to produce a preliminary size, which can then be simulated in a dynamic way, evaluated and optimized. Part of the development work is presented in (Yevalkar, 2019), publication 4. It is described that the preliminary size used the temperature at the end of the 5th discharging period (5th year) as a criterion to size the system / BTES. The number of boreholes is adjusted

iteratively through the N-R method while the power coverage and mass flows are considered as inputs.

Each iteration, based on the original and adjusted input parameters, the model calculates the required heating output and the cooling load of the heat pump, as well as the number of heat pumps needed. The components are sized for powers ranging between 10 and 50 MW. The BTES is designed in such a way that it must satisfy the cooling load of the heat pump for the entire period of the simulation as well as the required outlet temperature of the BTES on the last day of the discharge, set as an input.

Once the preliminary design criterion is satisfied, the model creates an input file and writes all the calculated values for the different components as inputs dynamic simulations which are done using the model developed by Malmberg et al. (2018), also part of this report in publication 5.

The heat pump model used in the simulations was developed for the particular power range 10 to 50 MW, and consists of mathematical correlations derived from data provided by a commercial heat pump manufacturer. This power range is reasonable for centralized HT-BTES that fits well with the chosen heat pump model approach. The charging and discharging power (heat exchange) in thermal systems can be scaled up/down by changing either the temperature levels or changing the mass flows to be handled.

Temperatures have been assumed to be relatively similar for different installations (supply temperature from the flue gas condenser to the heat pump during discharging normally around 55°C, boreholes outlet temperature is around 40-60°C during discharging and charging temperatures summertime at about 95°C). Although the tool has been developed to handle a flexible range of values, it is recommended to use similar temperatures to those described previously. The authors take no responsibilities about any results generated by the stand-alone unless they themselves generate the results.

2.1   HOW TO USE THE TOOL

All the files have been gathered and organized in a main folder called "BTES_StandAloneTool_GUIv5". This main folder can be directly copied and pasted in any location of any PC, as long as the path does not contain any points "." in it. For example, the path in Figure 3 is not valid because of the point character "." in "WP3.1". Any points in the path would cause the application to stop reading the path and the required files would not be found.
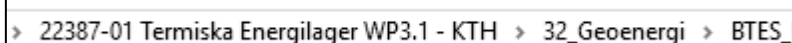

Figure 3. Invalid path for the folder

The main folder contains six items (see Figure 4). The folder "DataFromUser" contains text files with daily averaged information of relevant mass flows and temperatures values, used as inputs for the model if this feature is selected by the user when defining the default parameters in section "1. Define Default

Parameters". A description of this feature and files is provided in the file "About the input files.pdf". The user can access this file by clicking on the button "About the input files" in the help section on the user interface (see Figure 5). The folders "MATLABfiles" and "TRNSYSfiles" contain the files required for the model to work properly. There is no need to open or edit any files within these two folders. The folder "Results" contains the results of the simulations; these are summarized in one excel file, "BTES_simulation_results.xlsx", and supported with additional plots and graphs of some of the key performance indicators. These results are available in this folder; however, they can also be accessed directly via the user interface, section "5. See Results" (see Figure 5).

The other two files in the main folder are "MyAppInstalle_web.exe" for installing MATLAB runtime, and "BTES_StandAloneTool_GUIv5.exe" for starting the stand-alone tool user interface.
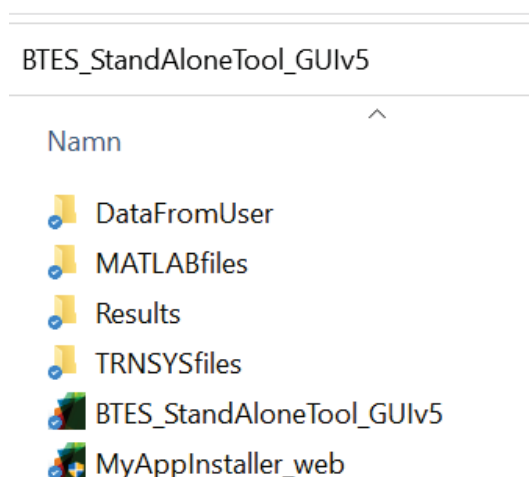
Figure 4. Main Folder

The MATLAB Runtime is a standalone set of shared libraries that enables the execution of compiled MATLAB applications or components without the need of MATLAB licenses. To install MATLAB Runtime, simply double click the file "MyAppInstalle_web.exe" (located in the main folder "BTES_StandAloneTool_GUIv5") and follow the instructions. This step (installing MATLAB runtime) is only required for the first time the application is used. Additional information is available in the file "MATLAB Runtime.txt", in the "MATLABfiles" folder.

To start the application, double click on the file "BTES_StandAloneTool_GUIv5.exe". The application might take a couple of seconds to start, especially when started for the first time.

The user interface is presented in Figure 5. It has seven sections. The sections 1 to 5 follow the simulation process (define inputs, check inputs, design the system, evaluate the performance, see the results). The two additional sections are "Help Section" and "Message Window". In the help section the user can find additional

information about the parameters used in section "1. Define Default Parameters". The user can also access the files "BTES_StandAloneTool_GUIv4.pdf" and "About the input files". In the message window, the user can follow any warnings or results during the simulation process. Note that the full results are available in section "5. See Results".
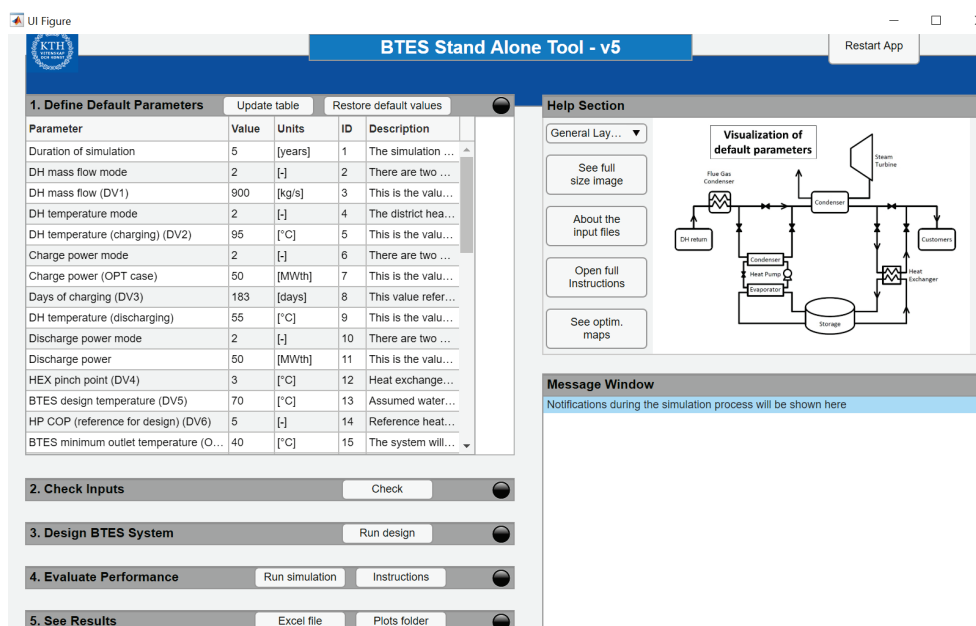
Figure 5. User Interface

2.1.1   Set the default parameters

Before running a simulation, the user can edit the values in the column "Value" of the section "1. Define Default Parameters". Notice that each parameter has an identification number for easier referencing (column "ID"), as well as a description (displayed fully when hoovering the cursor over the description). The user can only edit the fields in the column "value" (i.e. not the units). Once the desired values are entered, click on the button "Update table". The indicator (black circle on the right-hand side of the section heading) will turn green if the inputs have been input correctly. The buttom Restart App can be used to go back to default input values (the default input values can be edited in the excel file DefaultParameters_Names, located in folder…\BTES_StandAloneTool_GUIv5\MATLABfiles).

2.1.2   Check inputs

This section is to make sure the inputs defined are valid without having to run the full simulation. Click on the button "Check". If the inputs are valid, the indicator will turn green, and a message will appear in the message window. If there is a problem with the inputs, you will receive a message with more information about the error. The user has a larger degree of freedom when using own input data files. For users not having this possibility, recommended values are given in the program.

2.1.3   Design BTES system

This section will find a feasible design that satisfies the parameters defined in the first section. To start it, click on the button "Run Design". During the design process, the indicator should turn amber, indicating that the tool is busy sizing the components. Once finished, the indicator turns green, indicating that a design has been found. The preliminary results of the design process are shown in the message window when finished. If there is an error in this stage, the simulation will stop and the error message will appear on the message window.

2.1.4   Evaluate performance

To evaluate the performance of the system designed, click on the button "Run simulation". This will launch the TRNEdit application, which starts the simulation in the dynamic model developed in TRNSYS. Detailed information about how to navigate on the TRNEdit environment can be found in the file "TRNEdit instructions". You can access this file by clicking on the button "Instructions" in the heading of section "4. Evaluate Performance".

2.1.5   See results

Once the dynamic simulation is finished, the information is post-processed (this might take a few seconds, the indicator should turn amber (busy calculating) and relevant information about the status of the process will be displayed in the message window. After post-processing, the results will be available. You can access to these files directly through the buttons in section 5, or going to the folder "Results" in the Windows environment.

The excel file "BTES_simulation_results" has two sheets. In the first sheet, "Summary", there are three sections (see Figure 6).

Section 1 provides a summary of the results including design results (e.g. number of boreholes, ground area required, etc.) and performance results (e.g. energy used for charging, energy delivered, OPEX, NPV, etc.). Since the performance of the system changes from year to year, the OPEX value reported in this section is the average yearly OPEX (averaged considering the lifetime of the system, parameter 43). The energies and profits reported in this section also account for the total lifetime of the system (these are not averaged but totalized). For the NPV calculations, it is assumed that the years after the last simulated year (in this case, years 6 to 20) have the same performance as the last year simulated (year 5). Finally, the las three results reported in this section, efficiency, SPF and exergy, are the results of the last year of the dynamic simulation (year 5).

Section 2 provides with annual values of energies. Only the simulated years are shown (years 1 to 5). As mentioned before, for the techno economic KPIs (e.g. NPV) this values are assumed constant throughout the lifetime of the system (in this case, years 6 to 20).

Section 3 shows warnings (if any). In the example below it is shown how the model could not find a design able to provide the required discharge power. Instead, it

found the maximum discharge power such system could provide. It also shows what would be a tentative COP value to reach the required original discharge power (this condition is further explained in the next section of this document).

The second sheet of the file, "Hourly results", has daily averaged values of relevant variables such as temperatures in and out of the components, mass flows, powers, etc.
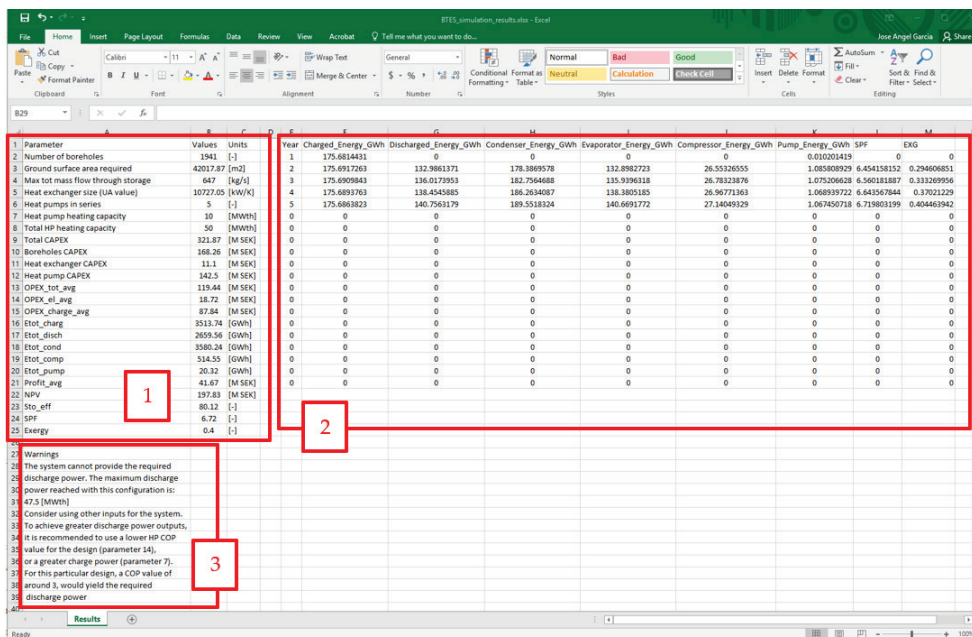
Figure 6. BTES_simulation_results

2.2 ADDITIONAL INFO ABOUT THE TOOL

2.2.1 Chronology of calculation steps

Once the default parameters are defined, the following calculation steps are done.

1. There is a first guess of the number of boreholes. With that and the defined mass flow rate per BH loop, a total BH mass flow is calculated.

2. The HEX is sized. Both mass flows (hot, or MF4, and cold, or MF6) are known. See the flow chart in Figure 2 to understand the numbers referring to where in the system the variables are referring to.

3. The two inlet temperatures (hot, or T4, and cold, or T6) are known at this point. The UA value of the HEX will be such that the difference between the hot inlet and the cold outlet is equal to the defined HEX pinch point (HEX PP). This means that changing the decision variable "design temperature" (arbitrarily defined at the beginning) effectively changes the size of the HEX. This is the only use of this variable and was introduced as a decision variable to allow the optimizer to explore solutions with different HEX sizes.

4. The heat pump system is sized based on its heating capacity. The heating capacity is the same as the discharge power defined. The heat pump system is composed of single heat pump units connected is series, 10MW$_{th}$ each. There is also a scaling factor, that accounts for the DH mass flow (DH_MF). It is assumed that the HP system was designed to handle 900 kg/s. Should the DH_MF be lower or greater than that, the scaling factor will "correct" this.

    For example,
    - 50MW$_{th}$ with a "normal MF" → 5 HPs in series;
    - 50MW$_{th}$ with larger MF → 4 HPs in series (but these are 4 larger HPs, scaled up);
    - 50MW$_{th}$ with lower MF → 6HPs in series (but these are 6 smaller HPs, scaled down).

    The heat pump system size is determined only based on its heating capacity. The COP is used to determine what the required cooling capacity is. Therefore, the COP will determine how much heat the boreholes must provide to the heat pumps. Lower COP values will "demand" less power from the boreholes and vice-versa. In the dynamic model (TRNSYS) the heat pump model has the two mass flows (district heating and borehole sides) as well as the temperature from the borehole side as inputs. This means that choosing different COP values (in the default parameters) will put the same heat pump under different conditions. Meaning, for a fixed discharge power (→ a fixed heating capacity → a fixed heat pump system size), choosing a lower or higher COP means having the same heat pump system, just that in one case the borehole will be sized so that there is more or less cooling capacity. This effect is seen in the results, designs with lower COP show more electric consumption since it must compensate for the lack of heat provided by the borehole storage.

5. The BTES is sized. In this context, sizing the BTES means finding the number of boreholes required (for a pre-defined depth and other borehole characteristics) such that a certain condition is met. This condition has been defined as being able to deliver water at a minimum of 40°C on the last day of the discharging period of the 5th year. In the process, the BTES is subjected to a charging/discharging scheme defined by the powers time series defined. When it is being charged, the maximum heat input to the BTES is the predefined "charging power", as long as the charging temperature for such power is feasible (the temperature of the water being heated up in the HEX cannot be higher than the charging temperature minus the pinch point). When discharging, it is assumed that a constant heat (Q2) is extracted from the storage; this will cause it to cool down. If at the end of the 5th year the outlet temperature of the BTES is "close enough" to 40°C, the sizing of the BTES is complete. If not, step 6.

6. The code starts the sizing process again with a new value of number of boreholes and continues to evaluate the condition. The new number of boreholes is not a random guess but rather an estimation using the Newton Raphson method. All the required information is then passed onto the dynamic model for evaluating the system's performance.

2.2.2 Notifications and messages

It is possible that the tool does not find a solution for the input parameters set by the user. For example, if the charging power (provided for charging the BTES by the combined heat and power plant during summer) is too low as compared to the discharging power required (provided by the BTES during winter), the model might not find a solution because there will not be enough heat stored in the BTES for covering the demand.

There are plenty of variables and parameters the user can change for the model to find a solution. The main three parameters are the "Charge power" (parameter ID 7 in the tool), the "Discharge power" (parameter ID 11 in the tool) and the COP of the heat pump (parameter ID 14 in the tool). By increasing the charging power or decreasing the discharging power, the model will be able to find a solution, i.e. would find a design that satisfies the requirements. This option has been programmed to occur automatically:

The approach adopted to work around this is to use the discharging power (power required by the user) as an "aiming target". The design process will start as usual but if the code does not find a number of boreholes such that the required condition is met, the discharging power will be "relaxed". Then, the discharge power will be re-written to a fraction of its original value (e.g. 97% of its original value), and the process will start again. Eventually the code will find a solution and report this situation in the final results. This explains that under the conditions defined (charging and discharging powers, temperatures, mass flows, etc.) the required discharge power was not met, and the maximum power achieved by the system was 97% of its original value (or whatever that final value is). It is also shown in the results what would be a tentative COP value for the system to reach the required discharging power.

In a similar way, a plan B can be to lower the COP (defined as the heat pump heating capacity to electric power ratio), the model may then converge to a solution since this parameter effectively changes the ratio of heat output from the HP to heat input to the HP, Q1 and Q2. In such case (lowering the COP) the boreholes would need to store less energy and the heat pump compressor would consume more electricity to cover the required demand. The user should keep in mind that this "plan B" might just be a way of playing with the program in order to converge. COP is not adjustable and lowering the COP of a system is, of course, nothing that the authors recommend.

If the model cannot find a solution for the parameters set by the user, it will automatically try to find a recommended COP value. This condition will be notified in the message window. Then, with the original COP defined by the user, the tool will determine what is the maximum discharge power possible for the system and continue the simulation for this new discharging power.

Three additional messages may occur:

Message 1: Occurs if the difference between the temperature of the district heating water used for charging the storage (temperature of water entering the hot side of the heat exchanger, parameter ID 5) and the BTES design temperature (temperature of water leaving the BTES and entering the cold side of the heat exchanger at the design point, parameter ID 13) is less than the pinch point temperature (parameter ID 3).

Message 2: Occurs when the model did not find a solution for the requirements defined by the user, then tried to find a recommended COP value or a maximum discharge power possible but did not succeed.

Message 3: Occurs when the charging power (parameter ID 7) is less than 50% of the discharging power (parameter ID 11). In this case, the model will not even look for a recommended COP value nor will it find the maximum discharge power achievable. The recommended action is either to lower the discharge power requirement or to increase the charging power available.

2.2.3   About the input files

Input files can be used for more customized simulations, instead of using the input value list in the tool. There are five text files in the folder "BTES_StandAloneTool_vx\DataFromUser":

File 1 - TemperatureFile_Amb: It is a one-column table that contains daily averaged values of the ambient temperature in [°C]

File 2 – FlowRateFile: It is a one-column table with daily averaged values of the district heating mass flow in [kg/h]. This mass flow is shown in the images "DH mass flow 1 – ID3" and "DH mass flow 2 – ID3" in the "Help Section" of the Stand Alone Tool.

File 3 - PowerLimitFile_HEF: It is a one-column table with daily averaged values of the surplus heat generated by the CHP plant in [kJ/h]. This value is used as "power limit" for the BTES system since it is the maximum available heat to be injected in the storage. This power is shown in the image "Charging power – ID7" in the "Help Section" of the Stand Alone Tool.

File 4 - TemperatureFile_DH: It is a one-column table that contains daily averaged values of the water temperature, in [°C], entering and leaving the CHP plant´s steam condenser. For the charging period, summer, the value refers to the temperature of DH water leaving the steam condenser and going into the heat exchanger (image "DH temp charging – ID5" in the "Help Section" of the Stand Alone Tool). For the discharging period, winter, the value refers to the temperature of the DH water leaving the CHP plant´s flue gas condenser and entering the heat pump´s condenser (image "DH temp discharging – ID9" in the "Help Section" of the Stand Alone Tool).

File 5 - PowerLimitFile_HP: It is a one-column table with daily averaged values of the allowed heat injection into the DH system (heat pump maximum output) [kJ/h]. This power is shown in the image "Discharging power – ID11" in the "Help Section" of the Stand Alone Tool.

File 1 is always used by the model. Files 2, 3, 4 and 5 are used as inputs for the model if it is defined by the user with the "mode parameters" (parameter ID2, ID4, ID6 and ID10) in the section "1. Define Default Parameters").

These files can be replaced with others containing new data, however, the name of the files and its format must be the same. Notice that each file has 366 data points. The first point is used as a starting point (day 0). The other 365 points represent the value of each day of the year. These last 365 points are repeated for simulations longer than one year. The simulation (and the data files) considers "day 1" as the first day of the charging period. Therefore, the first half* of the file contains data for the charging period, and the second half*, for the discharging period. Be aware of the decimal separator "." not "," and the units [kg/h], not [kg/s] and [kj/h] not [MW].

* It is half by default, but the user can choose the length of the charging period with the parameter 7 "Charging period length".

Energiforsk

3 PERFORMANCE OPTIMIZATION

Multi-objective optimizations were carried out using an optimizer algorithm in combination with the standalone tool. The optimizer that was implemented is called OSMOSE, developed at the industrial energy systems laboratory in Lausanne (Leyland, 2002).

The optimizer was set to estimate Pareto optimal fronts from a population based evolutionary algorithm. With the optimizer routine, it was possible to run the performance on the BTES through the standalone tool repeated times while varying the design parameters on each run. Each iteration provides a new "individual" to the population, which contributes to the solution. The initial population changes at each step by means of cross-over and mutation, both of which serve to generate improved solutions. The new population is then combined with the old one and the worse solutions are removed from the process. This is done in the search of fulfilling desired objectives. The optimizer is not part of the stand-alone tool, but a large number of simulations were carried out to illustrate what can be done and hereby give an extra help to the stand-alone tool users when doing different simulation runs. The key performance indicators of exergy efficiency and the net present value were selected as the objectives of the optimization. The former is defined as presented in section 3.1. The latter is well known.

3.1 ENERGY AND EXERGY PERFORMANCE

BTES system performance is commonly assessed using the ratio of injected to extracted thermal energy. This can be done over several durations, e.g. over one storing cycle. Assessing the storage performance only by energy analysis leads to loss of information on availability and quality of the heat being stored and discharged, which leads to the need of performing exergy analyses. Analyzing exergy allows evaluating the quality of the heat being injected, stored and extracted. This has been applied in studies of BTES and GSHP systems but has not been established as a standard method in shallow geothermal system design. Publication 1, appended to this report, presents an approach for exergy and temperature analysis, formulated and evaluated at storage boundaries and within the storage itself, i.e., at inlet and outlet but also with respect to a subsurface interface between the storage volume and surrounding ground.

The performance of the borehole storage is evaluated both at a system level (inlet-outlet) on a seasonal basis, but also within the storage volume at any time t. The seasonal performance is calculated using the following two equations for energy (η) and exergy (ψ), where d and c stand for discharge and charge, respectively, and the lower limit (zero) of the charging integral is that start of the charging time, not necessarily 0.

$$\eta = \frac{Q_d}{Q_c} = \frac{\int_{\tau_c}^{\tau_c+\tau_d} \dot{m} c_p \left(T_{\text{out}}(t) - T_{\text{in}}\right) dt}{\int_0^{\tau_c} \dot{m} c_p \left(T_{\text{in}}(t) - T_{\text{out}}\right) dt}$$

Energiforsk

$$\psi \ = \ \frac{\text{Ex}_d}{\text{Ex}_c} = \frac{\int_{\tau_c}^{\tau_c + \tau_d} \dot{m} c_p \left[(T_{\text{out}}(t) - T_{\text{in}}(t)) - T_0 \ln \left(\frac{T_{\text{out}}(t)}{T_{\text{in}}(t)} \right) \right] \, dt}{\int_0^{\tau_c} \dot{m} c_p \left[(T_{\text{in}}(t) - T_{\text{out}}(t)) - T_0 \ln \left(\frac{T_{\text{in}}(t)}{T_{\text{out}}(t)} \right) \right] \, dt}$$

Within the storage volume, the two indicators are calculated as

$$\eta_{\text{storage}}(V, t) = \frac{Q_{\text{stored}}(V, t)}{Q_{\text{exchanged}}(t)} = \frac{\int_V \rho_g c_{p_g} \left(T(\mathbf{x}, T) - T_0 \right) dV}{\int_0^t m_f c_{p_f} \left(T_{\text{in}}(t) - T_{\text{out}}(t) \right) dt}$$

$$\psi_{\text{storage}}(V, t) \ = \ \frac{\text{Ex}_{\text{stored}}(V, t)}{\text{Ex}_{\text{exchanged}}(t)} = \frac{\int_V \rho c_p \left[(T(\mathbf{x}, t) - T_0) - T_0 \ln \left(\frac{T(\mathbf{x},t)}{T_0} \right) \right] dV}{\int_0^t \dot{m} c_p \left[(T_{\text{in}}(t) - T_{\text{out}}(t)) - T_0 \ln \left(\frac{T_{\text{in}}(t)}{T_{\text{out}(t)}} \right) \right] \, dt}$$

For exergy calculation the temperatures are absolute temperatures expressed in Kelvin and the reference temperature T_0 considered is the undisturbed temperature of the ground. This reference temperature can though be chosen to be different. The subindex "stored" indicates stored in the storage volume and "exchanged" the cumulative injected and extracted in to the BTES system, for both energy and exergy.

The control volume for the storage around the boreholes has been chosen to contain a percentage 1-ϵ of the overall heat injected after a time τ_d corresponding to the time for the discharge cycle, motivated because the discharging time is a relevant time for extracting useful heat from the storage volume. So, for the calculations, the family of points with maximum distance from the boreholes equal to r_ϵ (radius of the control volume) are identified as being contained in the storage volume.

Not all the energy or exergy stored in this control volume is recoverable, but this approach allows measuring the capability of the BTES of maintaining the energy injected in the surrounding of the borehole system at distance from which it can be partly discharged.

The full report about this suggested approach is presented in publication 1 and it includes some study cases used for calculations. Exergy has also been calculated and used to evaluate optimum Pareto fronts based on multiple simulations using the stand-alone tool, as explained below. Moreover, these indicators have been used to evaluate the effect that groundwater flow may have on the performance of high temperature BTES. Details about this are discussed in chapter 4.

3.2   OPTIMIZATION MAPS

As mentioned above, the optimization has been set to find solutions that maximize both objectives exergy and net present value. The reason behind selecting these two was to comprise a combination of both technical and economic performances of the BTES system, which in turn, also happen to be conflicting. In principle, any two KPIs could be selected as objectives for the optimization. However, conflicting objectives provide a range of optimal solutions (Pareto front) instead of one single optimal configuration. This allows user to then make a choice based on obtained

performances and the related input parameters leading to that optimal configuration.

The results of the optimization are shown in the form of plots that one objective in each axis: the exergy of the system on the Y axis and the NPV on the X axis. Four BTES cases were optimized, each corresponding to a different BTES storage size and discharge temperature:

- Case A: 50 MW – 40°C discharge power and temperature
- Case B: 50 MW – 45°C discharge power and temperature
- Case C: 10 MW – 40°C discharge power and temperature
- Case D: 10 MW – 45°C discharge power and temperature

Figure 7 shows the corresponding Pareto front for each optimization case.
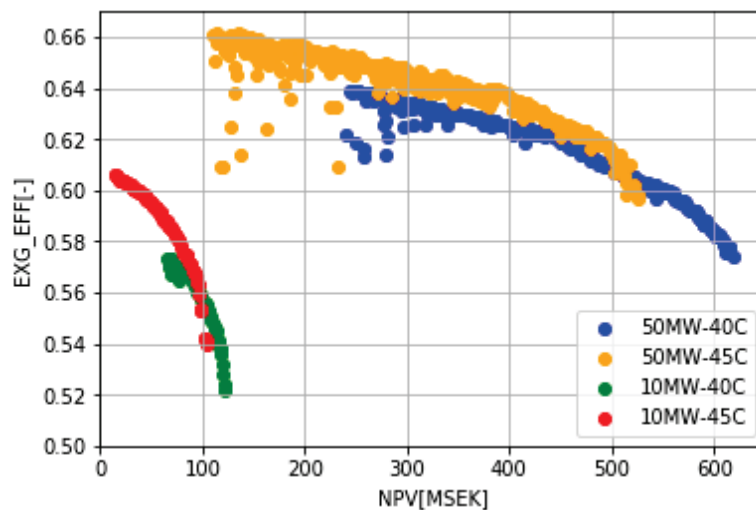
Figure 7. Pareto front for each optimization case

It is important to highlight that each point in the optimization plot represents a different system with a unique set of decision variables values. Essentially, each point is a different run of the standalone tool. Since the optimizer is not directly coupled to the standalone tool, figures such as Figure 8 and Figure 9 have been added in order to to let the user appreciate the relationship between these input parameters and the optimal configurations. In that way, the user can check these before deciding for an input value in the standalone too. All figures for all cases are found in the working folder of the tool.
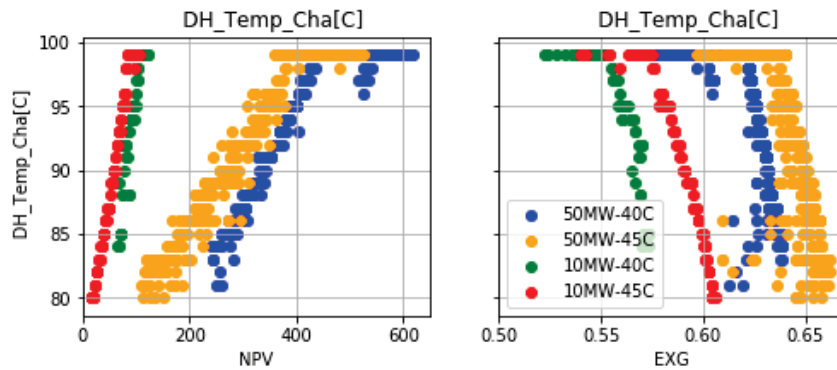
Figure 8. Example of exergy and NPV vs district heating charging temperatures
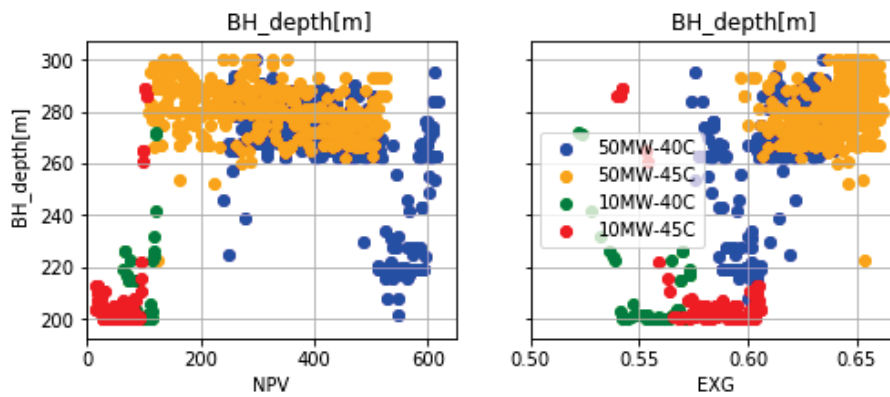
Figure 9. Example of Example of exergy and NPV vs borehole depth

Other produced maps, also available through the standalone tool, by clicking on the button "See optim. Maps" indicated in Figure 10. Observe that these maps are not directly connected to the user's own calculations. They come from a large number of runs for typical power and temperature ranges. The maps are suggested to be used as a help tool for choosing design inputs through qualitative interpolation between the presented cases.

Figure 10. Screen shot of the stand-alone tool indicating how to find the optimization maps

4 GROUNDWATER FLOW

Groundwater flow can have a negative effect in borehole storage systems performance. Part of the heat stored in the subsurface during the charging season can be transported away from the storage volume and thereby cannot be retrieved via the borehole heat exchangers during the extraction season. While this is fairly intuitive from a qualitative standpoint, quantitative assessment of the ef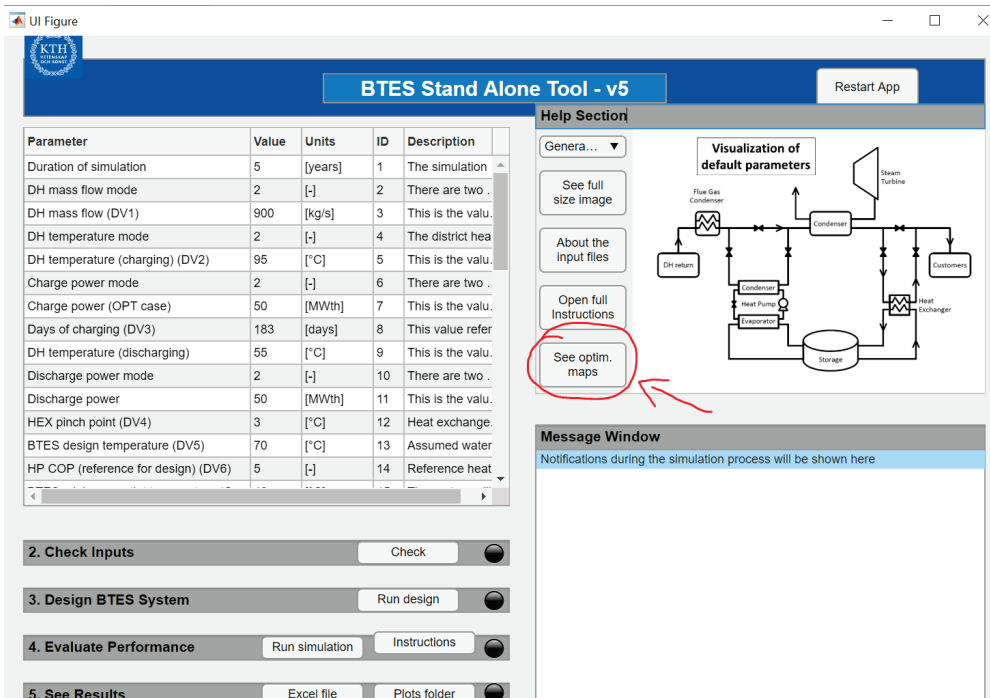fect of groundwater is necessary to understand the impact of different level of groundwater flows. A question that arises is where to draw the line between acceptable and unacceptable groundwater flow.

A wide variety of modeling approaches and conceptual models have been developed and adopted to face the challenges related to scale effects, heterogeneity, and flow in porous and fractured media. Considering that many problems involve investigation of large domains at e.g. aquifer or regional scale levels, continuum approaches have been widely used for modeling groundwater flow and subsurface transport processes in porous and fractured media.

Earlier studies on real borehole storages have used numerical models to get a better representation of the ground conditions. They have been developed as continuum models where the ground is assumed to be homogeneous, behaving as a porous medium, which is valid for most soils and some porous rocks, i.e. this implies that the groundwater flow occurs uniformly across sections of the rock volume.

If the rock in the borehole storage is fractured, the groundwater flow can though occur in preferential flow paths that depend on the local geology and geometry of the fractures. Assuming a porous medium requires then that average properties of the modelled media should be stable and relatively constant over a given range of the space. Heterogeneities can then appear further away.

Some fractured rocks do not allow being treated as porous medium. For example, a large fracture crossing the volume of a borehole storage, through which a dominant groundwater flow occurs, would imply not being able to treat the storage as porous media in an accurate manner. There are, however, also methods where exact geometries of fractures can be accounted for (so-called discrete fracture network approaches) and/or where the fracture geometries are upscaled and re-represented with the help of statistical methods so that equivalent properties over the whole domain are obtained. This is, though, more complex, time consuming and less suitable for being added to a possible extension of the stand-alone tool. Coupled groundwater and heat transport in fractured rock, and applications of discrete fracture network approaches in BTES modeling, should be subject of further research.

Numerical models based on finite element can accurately portrait the hydraulic and thermal behavior on the subsurface. Ground surface profiles, ground layers stratigraphy as well as hydraulic and thermal properties can be modelled. These numerical models require, however, long simulation time, which limits the number of cases that can be explored to study a given system.

Models based on analytical solutions have the opposite features compared to the numerical models. They are less flexible since the analytical solutions are valid only under a limited set of conditions. They are, however, usually faster and they allow to explore more cases. The stratigraphy of the ground is not modeled in detail and the ground is assumed to have uniform hydraulic and thermal properties. No detailed description of the ground surface profile can be either utilized. Instead, a uniform gradient is assumed in the whole borehole field, yielding to a uniform Darcy velocity in the ground.

The effect of groundwater flow on the thermal performance of high temperature borehole storage has been investigated through energy and exergy analysis for different groundwater flow rate scenarios, using both analytical and numerical models.

Section 4.1 presents the use of a semi-analytical method for investigation of the effect of groundwater flow on a high temperature borehole thermal energy storage system. The original idea was to include this calculation method in the stand alone delivered in this project, but this was not done due to constrains (computational, time and programing language compatibility). This could, however, be done at possible future continuation stage. Section 4.2 presents a hypothetical groundwater system that has been treated numerically, extending a validated pure conduction model to account for advective effects.

The validation has been done for pure conduction case, against measured data from an existing storage located in dry soil. Even the design and construction of a laboratory scale model has been. See publication 2 and 3 as well as (Blomfelt et al 2021). The knowledge obtained during the work by (Abuasbeh et al, 2021) has also contributed to the understanding of groundwater flow theory.

4.1 ANALYTICAL MODEL BASED ON MOVING FINITE LINE SOURCE

The model used to simulate the thermal behavior of borehole within a porous media affected by ground water flow is based on the solution by (Molina Giraldo et al, 2011) for the moving finite line source problem. The tool developed in this project is available for download here: https://gitlab.com/alblaz/BTESGroundWaterSimulator

The solution is obtained by integrating along the length of the borehole the effect of a moving point source embedded in an infinite volume with uniform thermal and hydraulic properties. The boundary condition at the surface is enforced using the method of images. In the paper by Molina Giraldo the condition used is the zero temperature boundary condition at the surface, obtained by placing sinks $-q'$ symmetrical to the sources q' with respect to the surface. Thanks to the symmetry, the heat flux lines are perpendicular to the surface and as a result the surface is isothermal. The temperature solution at a generic point (x, y, t) a time t, for zero surface temperature boundary condition is:

$$\Delta T(x,y,z,t) = \frac{q'}{2\pi\lambda} \exp\left(\frac{v_T r}{2\alpha}\right)\left(\int_D^H f(x,y,z,t)\, dz' - \int_{-H}^{-D} f(x,y,z,t)\, dz'\right)$$

$$f(x,y,z,t) = \frac{1}{4r}\left[\exp\left(-\frac{v_T r}{2\alpha}\right) erfc\left(\frac{r - v_T t}{2\sqrt{\alpha t}}\right) + \exp\left(\frac{v_T r}{2\alpha}\right) erfc\left(\frac{r + v_T t}{2\sqrt{\alpha t}}\right)\right]$$

$$r = \sqrt{x^2 + y^2}$$

$$v_T = u_x \frac{\rho_w c_w}{\rho\, c}$$

Where q' [W/m] is the power per meter injected, λ and α are respectively the thermal conductivity and thermal diffusivity of the ground, D, H are respectively the buried depth of the borehole and its length, v_T the effective heat transport velocity and, $\rho_w c_w$ is the volumetric capacity of the water and $\rho\, c$ is the volumetric capacity of the porous media.

Another boundary condition that can be easily obtained through the method of images is the adiabatic boundary condition. This is a relevant boundary condition for storage application where a layer of insulation is often placed on top of the storage surface. Although this layer cannot completely cancel heat losses from the top surface, a zero-flux boundary condition is more useful than a zero-temperature boundary condition, especially for high temperature applications where the heat losses from the top surface may be high, leading to an underestimated solution. On the other hand, it is important to keep in mind, that the solution obtained imposing adiabatic condition is overestimating the solution.

The adiabatic condition is obtained by placing sources $+q'$ instead of sinks $-q'$ on the negative z axis. The symmetry of the sources forces the heat flux line to be parallel at the surface yield a zero- flux boundary condition at the top surface.

The temperature solution at a generic point (x, y, z) at time t, for adiabatic boundary condition at the surface is:

$$\Delta T(x, y, z, t) = \frac{Q}{2\pi\lambda} \exp\left(\frac{v_T}{2\alpha}\right) \left(\int_D^H f(x, y, z, t)\, dz' - \int_{-H}^{-D} f(x, y, z, t)\, dz' \right)$$

This solution is utilized as a building block to obtain the temperature field when multiple boreholes are placed nearby using superposition and summing the effect of the contribution of each source. Superposition of the effect is allowed since the differential equation governing the heat transport in porous media is linear under the condition considered.
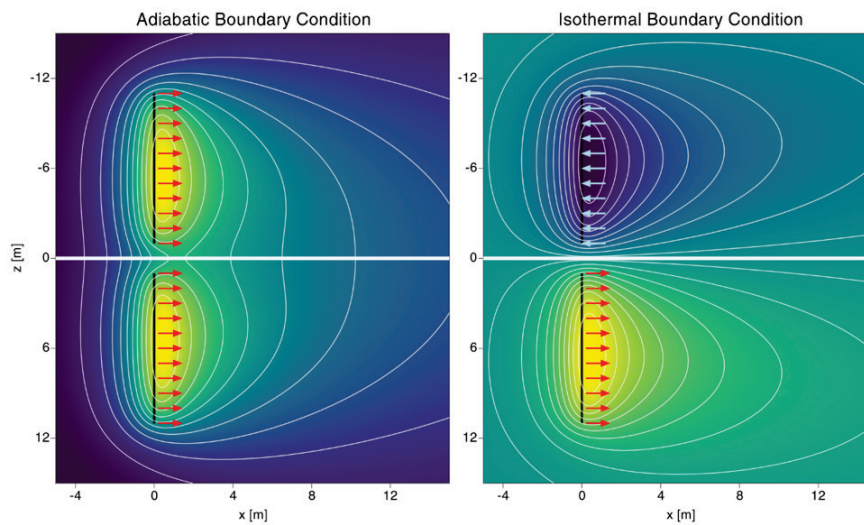
Energiforsk

Figure 11. Example of application of the method of images to compute the temperature field around a linear heat source after time t and enforce adiabatic or isothermal boundary conditions at the surface z = 0 . The linear source is embedded in a semi-infinite porous media with uniform thermo-physical properties and with uniform flow along the x direction.

Figure 11 shows an example of application of the method of images to compute the temperature field around a linear heat source after time t and enforce adiabatic or isothermal boundary conditions at the surface z = 0. The linear source is embedded in a semi-infinite porous media with uniform thermo-physical properties and with uniform flow along the x direction.

4.1.1   The study case, a HT-BTES with and without groundwater flow

An example of model of high temperature storage affected by groundwater flow is provided in this section in order to the get an idea of how the flow velocity affects the performance of the storage, a key objective of this project.

The example provides the occasion to test a methodology for the modeling of high temperature storage that integrates heat transfer in porous media using a semi-analytical approach. The results obtained are by no means general, since they depend on the specific parameters of the model and the local conditions of each storage site, but they provide an indication of the magnitude of the effect that groundwater flow could have on the performance.

The model simulates an array of borehole heat exchangers consisting of several hydraulic loops connected in parallel such that each loop is provided with the same inlet temperature. The model enables evaluating the performance of the BTES given the bore field geometry and hydraulic arrangement (Cimmino, 2018; Lazzarotto, 2014).

Figure 12 shows the study case that is considered: 8 separate (non-identical) loops are fed in parallel with constant inlet mass flow at 90 °C during the summer and 55°C during the winter. Later in this chapter, the study case is even simulated with constant inlet mass flow at 80 °C during the summer and 20°C during the winter.

The borehole configuration and the arrangement studied are the ones of an actual pilot borehole storage (Tordrup et al., 2017). The system is fed from the internal borehole during summer and from the external boreholes during winter. The output temperature and the heat exchanged by the system are not directly imposed and are the result of the specific borehole configuration and operational strategy. The borehole field is affected by regional groundwater flow with velocity u_x, as expressed in the equations above.

In Figure 12, two of the loops with series connections are color coded, one on the upstream section of the borehole field and one on the downstream section are color coded. Temperature and heat flows for these boreholes will be presented in the results section to highlight the storage behavior in presence of groundwater.

4.1.2 The modelling strategy

The ground is modelled using the moving finite line source with adiabatic boundary condition as presented earlier in this chapter. For the sake of simplicity each borehole is modeled assuming uniform power q' along borehole segments of length H placed at buried depth D (and along the relative image). The borehole temperature is evaluated at the mid-point D+H/2.
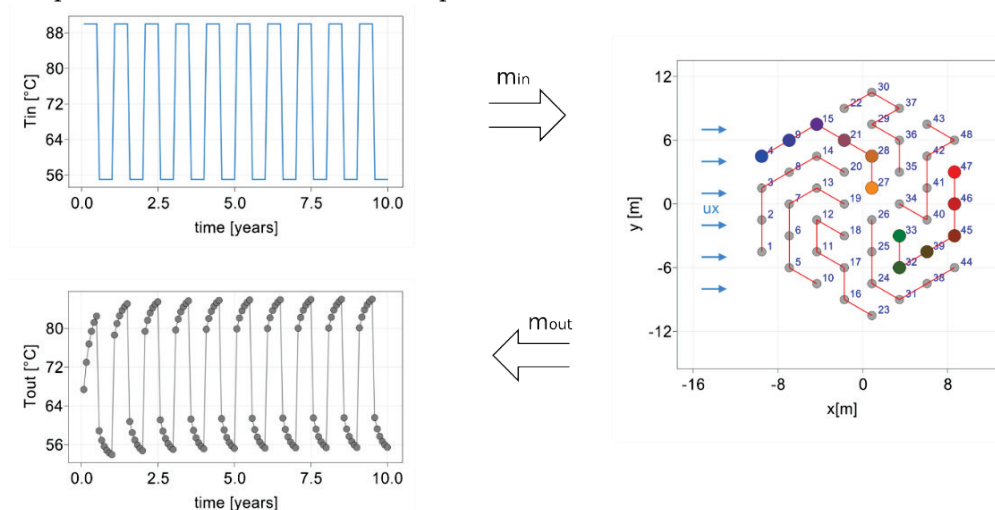

Figure 12 Borehole field configuration modeling scheme. The borehole is supplied with a constant flow at a temperature Tin and output a temperature Tout. Two loops along series connections are color coded

Given a borehole storage with N boreholes, the unknowns of the problems are the inlet temperature in the boreholes $T_{in}^{(i)}(t)$, the outlet temperature from the boreholes $T_{out}^{(i)}(t)$, the borehole wall temperature $T_b^{(i)}(t)$ and the power per meter exchanged by each borehole $q'_b^{(i)}(t)$ for a total of 4N unknown at each time step in the simulation. The system can be modelled using a set of 4N linear equations that models the ground, the borehole, the interaction between the ground and the borehole and the topology of the hydraulic network.

4.1.3 The ground and the boreholes

The interaction between boreholes is modelled using the following expression:

$$T_b^{(i)}(t) - \frac{1}{2\pi k_g} \sum_{j=1}^{N} q'^{(j)}(t)\ g\left(\Delta x_{j,i}, \Delta y_{j,i}, D + \frac{H}{2}, t_{step}\right) = T_0 +$$
$$\frac{1}{2\pi k_g} \sum_{k=1}^{N_t-1} \sum_{j=1}^{N} (q'^{(j)}(t_k) - q'^{(j)}(t_{k-1}))\ g\left(\Delta x_{j,i}, \Delta y_{j,i}, D + \frac{H}{2}, t_{N_{t-1}-t_k}\right)$$

where $\Delta x_{j,i}$, $\Delta y_{j,i}$ are the distances between borehole j and i along the x and y directions respectively, and g is the thermal response factor which in this case is based on the moving finite line source with adiabatic boundary condition.

It is worth noting that the term on the right-hand side of the equation are values that can be computed given the load history of the storage. The equation is written to collect on the left-hand side all the unknowns and the relative coefficients. On the right-hand side, the given terms.

The borehole has been modelled according to the method introduced by (Cimmino, 2016). The model is fairly general and can be applied to stepwise constant borehole temperature. In this initial work we consider only the simple case of uniform borehole temperatures. The equation used is of the following form:

$$a_{in}T_{in} + a_{out}T_{out} + a_b T_b = 0$$

Where only the linear relationship between T_{in}, T_{out} and T_b are reported in the equation. The formulation for the coefficients a_{in}, a_{out} and a_b can be found in (Cimmino, 2016).

The heat balance in the borehole is (H being the borehole length):

$$m\ c_{p_f}T_{in}^{(i)}(t) - m\ c_{p_f}T_{out}^{(i)} - q_b'^{(i)}(t)\ H = 0$$

Imposing the outlet to a value $T_{in}^{(i)}(t) = f(t)$ and connecting the outlet of borehole j to the inlet of borehole by $T_{in}^{(i)}(t) - T_{out}^{(j)}(t) = 0$ enable any possible hydraulic topology for the borehole loop.

The equations presented in this section (4.1.3) can be expressed in matrix form as system of equation Ax=b with 4N equations and 4N unknowns. The system is fairly flexible and several matrices A can be built corresponding to different topology and operation. This enables for instance switching flow direction during operation which may be a desirable feature when studying borehole connected in series.

The seasonal performance of the borehole storage is evaluated at a system level (inlet-outlet) on a seasonal basis. Performance is evaluated both in terms of energy and exergy, as presented in section 3.1.

4.1.4 Temperature and power at different groundwater flows

As introduced in section 4.1.1, in order to show some quantitative values about how relevant groundwater flow can be on the performance of a high temperature storage, the configuration showed in Figure 12 has been used in a couple of test cases. Table 1 gives an overview of the parameters utilized to model the ground and the boreholes.

The boreholes are connected in series and they are supplied with a temperature of 90 or 80°C during summer and 55 or 20°C during winter time, respectively. A flow of 0.5 kg/s per loop is imposed and circulation goes from the center to the outer region of the boreholes during summer and in the opposite direction during wintertime, i.e. six months each.

Simulations are performed with a monthly time step and for a time horizon of ten years. In the reference case the regional groundwater velocity is 0 cm/day. The system is then simulated for a groundwater velocity of 0.5 and 1 cm/day.

**Table 1. Properties utilized to define the test cases**

Property	Symbol	Value	Units
borehole radius	r_b	0.0575	m
borehole length	H	50	m
ground conductivity	k_g	2	W/(m K)
ground heat capacity	C_g	$1.7 \cdot 10^6$	J/(m^3 K)
grout conductivity	k_b	1.5	W/(m K)
grout heat capacity	C_b	$3.1 \cdot 10^6$	J/(m3 K)
boreholes distance	B	3	m
mass flow rate per loop	$\dot{m}$	0.5	kg/s
density fluid	ϱ_f	1000	kg/m^3
specific heat capacity fluid	cp_f	4182	J/(kg K)
arrangement	-	Series	-
inlet temperature summertime	$T_{in,s}$	90 or 80	°C
inlet temperature wintertime	$T_{in,w}$	55 or 20	°C
undisturbed temperature	T_0	8	°C
Groundwater velocity	u_x	0	cm/day
Porosity	φ	0.2	-

The model was used to obtain the solutions for the temperatures T_{in}, T_{out} and T_b, and for the heat rates q_b' for the test cases. The results are presented in Figure 13, Figure 14 and Figure 15 for the three different groundwater velocities, 0, 0.5 and 1.0 cm/day respectively, where each figure contains several plots. The first plot reports temperatures and heat per meter exchanged in a borehole series in the upstream section of the borehole. The second plot reports the results for a branch in the downstream section of the borefield. The color codes of Figure 12 are utilized when plotting inlet fluid temperatures and heat rates to distinguish each individual borehole. Outlet temperature from the branch (black dots) and from the borehole field (grey dots) are also plotted. The third plot, contour plot, shows the temperature field at 6 times during the 10th year of operation is used to show how the temperature field change in the surrounding of the borehole field in presence of groundwater.

For the case when there is no regional ground water flow (Figure 13), the inlet and outlet temperatures from the two branches is very similar even though their

Energiforsk
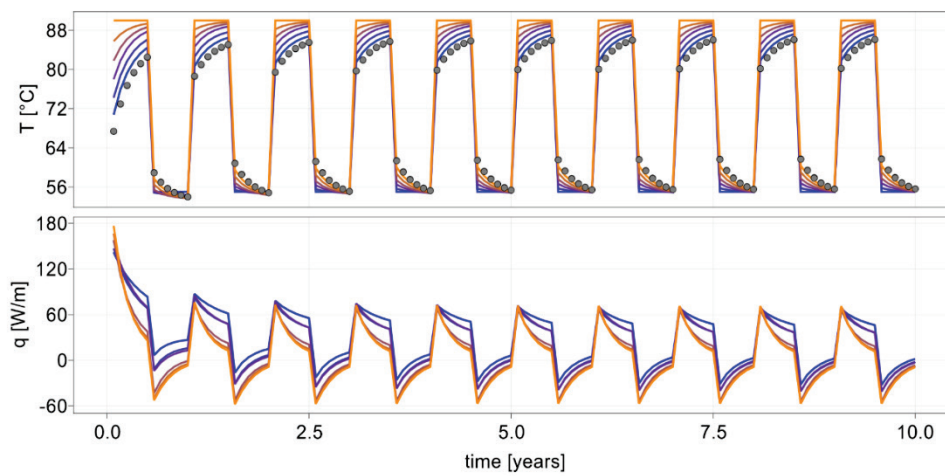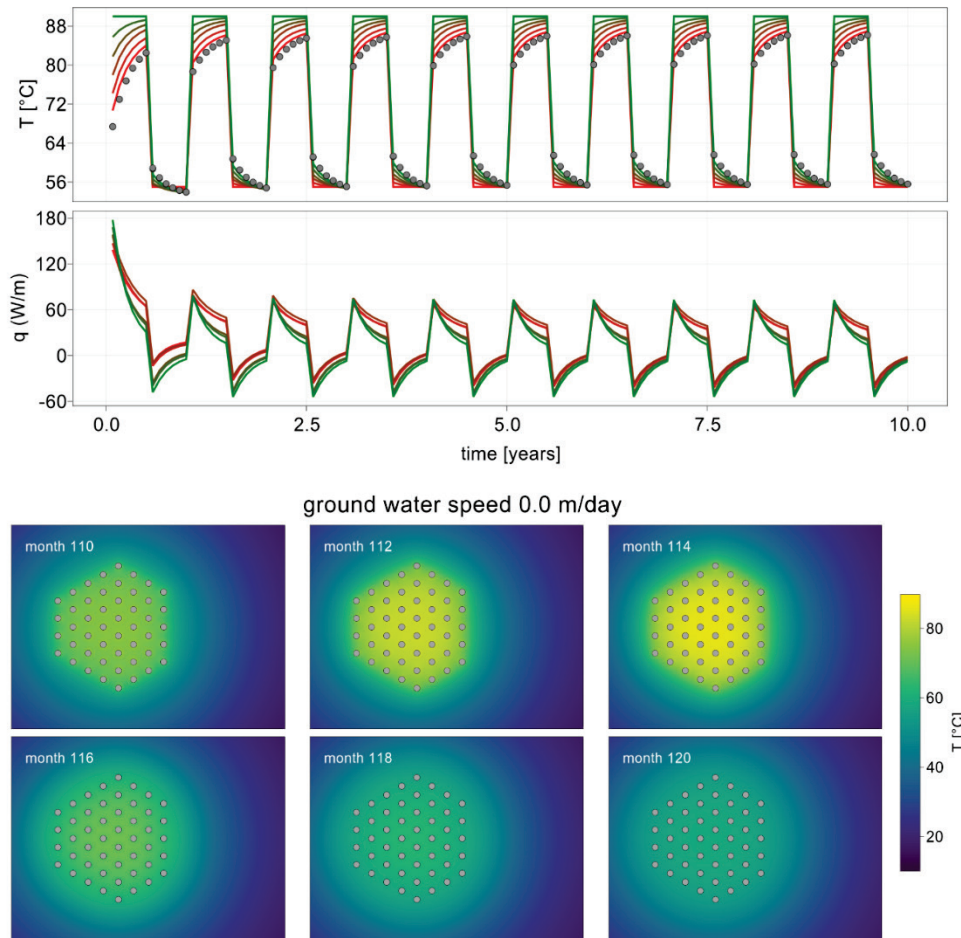
Figure 13 Results for u_x = 0 cm/day.

As groundwater flow increases (Figure 14 and Figure 15), the effect on the inlet and outlet temperatures in the two branches start to diverge. This can be easily appreciated as the outlet temperature from the branches and the outlet temperature from borehole field do not coincide anymore. The upstream boreholes are colder than the downstream boreholes, and the last three boreholes in the upstream series are at temperatures below the inlet temperature supplied. As a result, these boreholes inject heat (instead of extracting) during the extraction period. The contour plots for these two cases during the 10th year of operation show how the heat is fully displaced by the end of the extraction season and cannot be recovered anymore by means of the boreholes in the field.

Figure 14 Results for u_x = 0.5 cm/day.

Figure 15 Results for u_x = 1 cm/day.

4.1.5 Performance indicators at different groundwater flows

The amount of energy extracted and injected into the system is not predefined in the test cases. Instead, this depends on the flow rate and temperature supplied to the storage and on the thermal conditions within the storage itself. It is therefore of

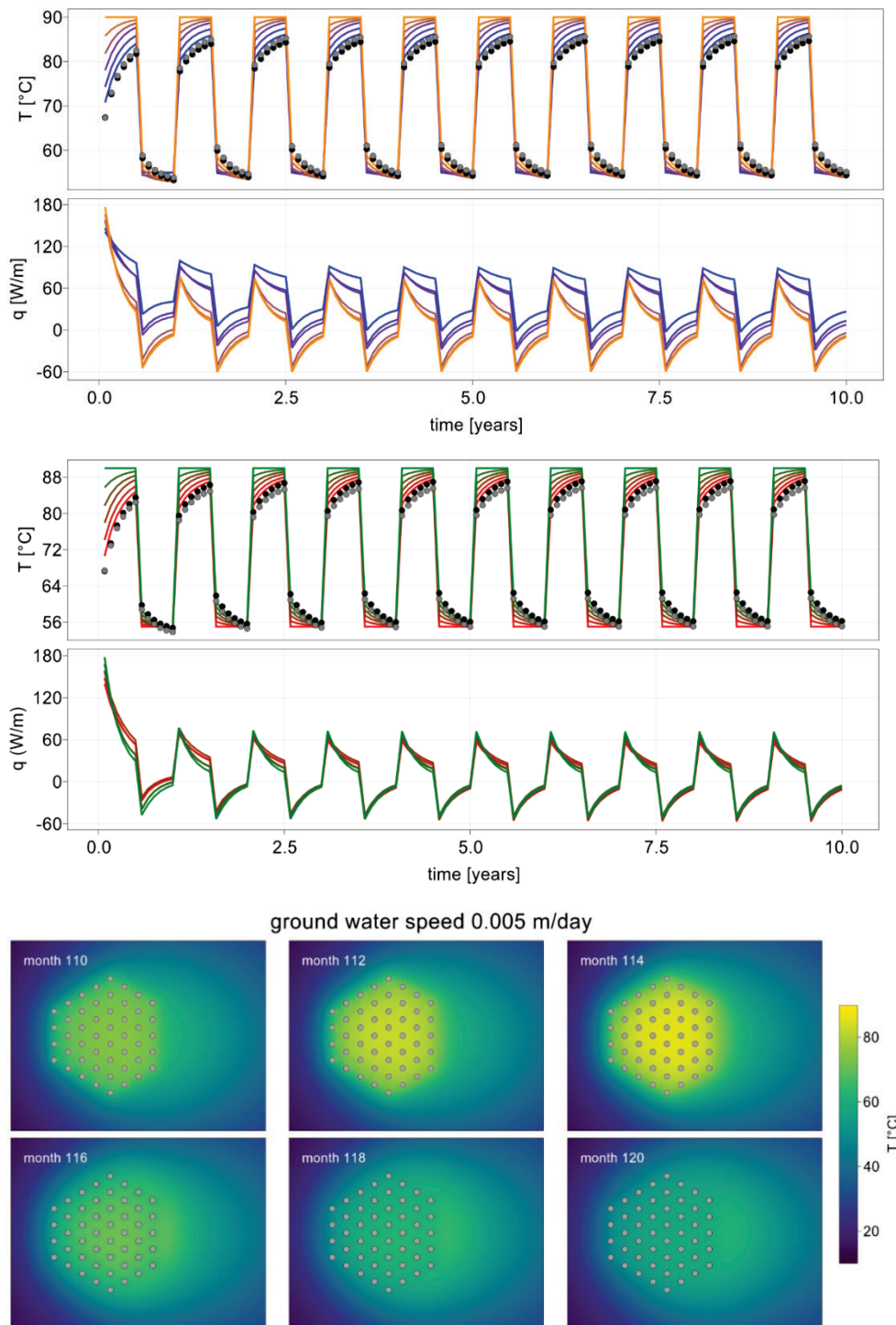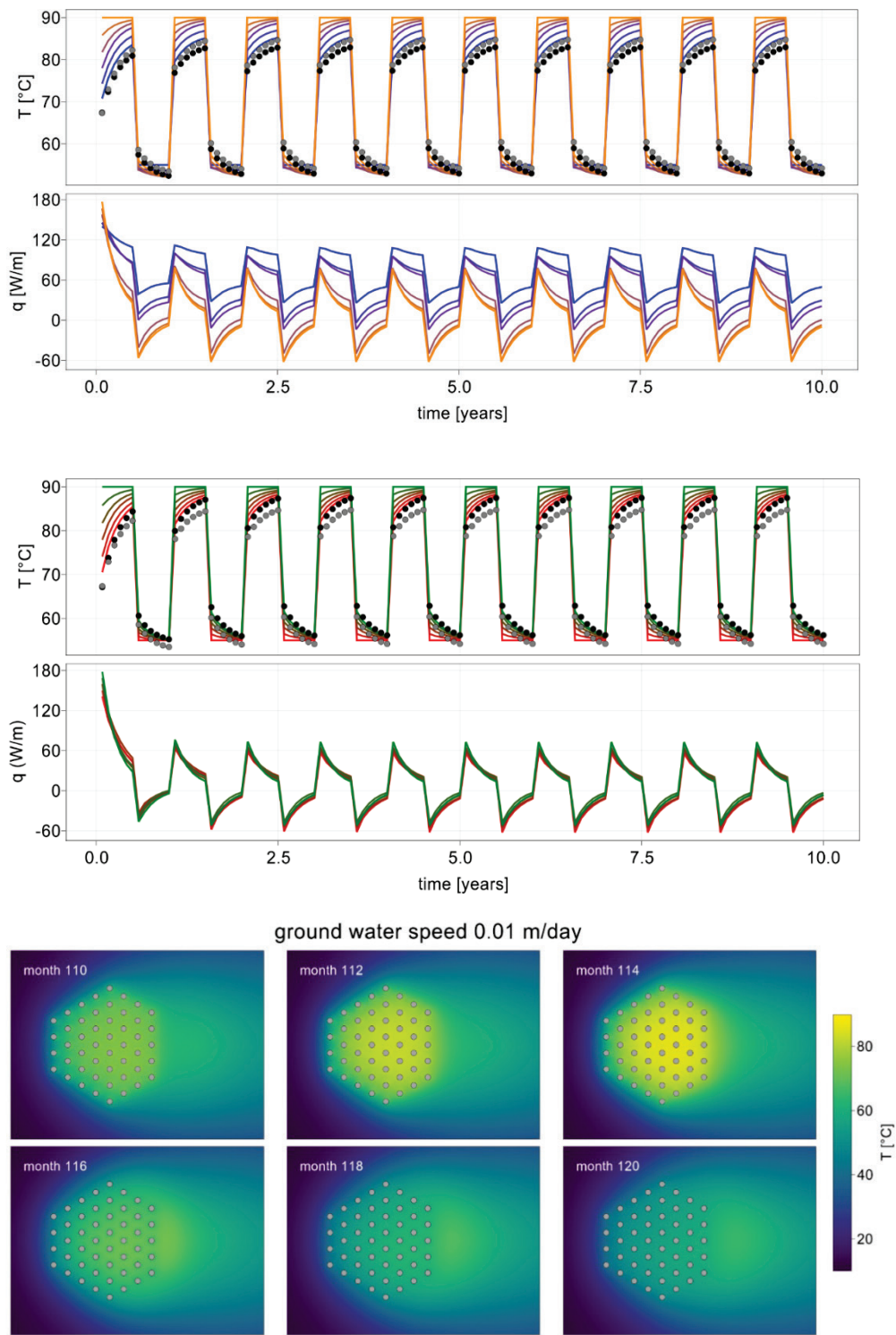interest evaluating the energy injected and extracted each year from the storage, and evaluate the relative seasonal performance in terms of energy and exergy, as suggested in our work presented in publication 1.

Figure 16 shows these for the three flow speeds studied for the case when charging temperature of 90°C and discharging temperature of 45 °C. A great dependency between each of the groundwater speeds can be observed. As the groundwater speed increases the system is capable of injecting more energy into the ground, but it extracts less during winter time. The seasonal energy efficiency at the 10th year η_{10} drops from 45% to 38% and down to 20% for the three groundwater velocities, while the seasonal exergy efficiency ψ_{10} drops from 32% to 24%, and all the way down to 7%.

The same simulations are now repeated, but this time using a supply temperature of 80°C and a return temperature of 20°C (similar to the conditions used in the numerical model presented in publication 2). The results are shown in Figure 17. It can be observed that the energy extracted is significantly larger. The energy efficiency η_{10} is as high as 78% for the no flow case and down to 60% for the 1 cm/day flow. On the other hand, the exergy efficiency ψ_{10} drop to values 18% and 15% which is much lower values when compared to the previous case. These results reflect the fact that we are extracting "low grade" heat after injecting "higher grade" heat in the previous season.

One observation is that the effect of groundwater on energy and exergy efficiency is now less important as compared to the case of 90°C charging and 55°C discharging. For the case of 80°C charging and 20°C discharging, the net energy exchanged with the storage is relatively small and the operation of the system is rather balanced. As a consequence, there is not a great temperature build up in the storage volume and the temperature in the storage is rather close to the undisturbed ground temperature T_0. Moreover, the extraction temperature is 20°C which is also relatively close to the undisturbed temperature. These two facts explain the relatively lower impact of the groundwater flow on the estimated performance indicators.
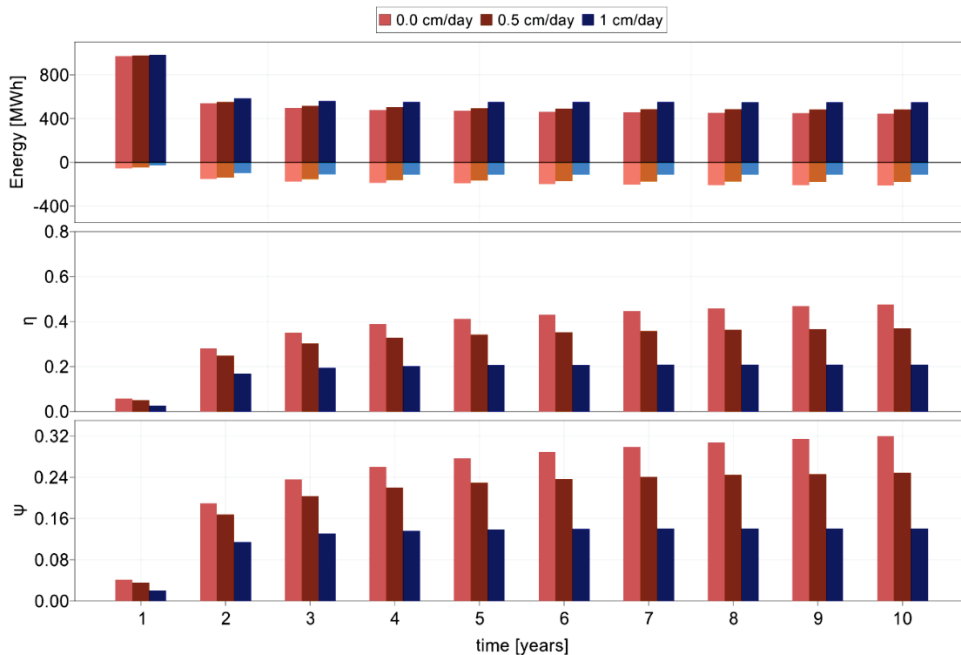
Figure 16: Energy flows, Seasonal Energy Efficiency and Seasonal Exergy Efficiency for the three cases studied.
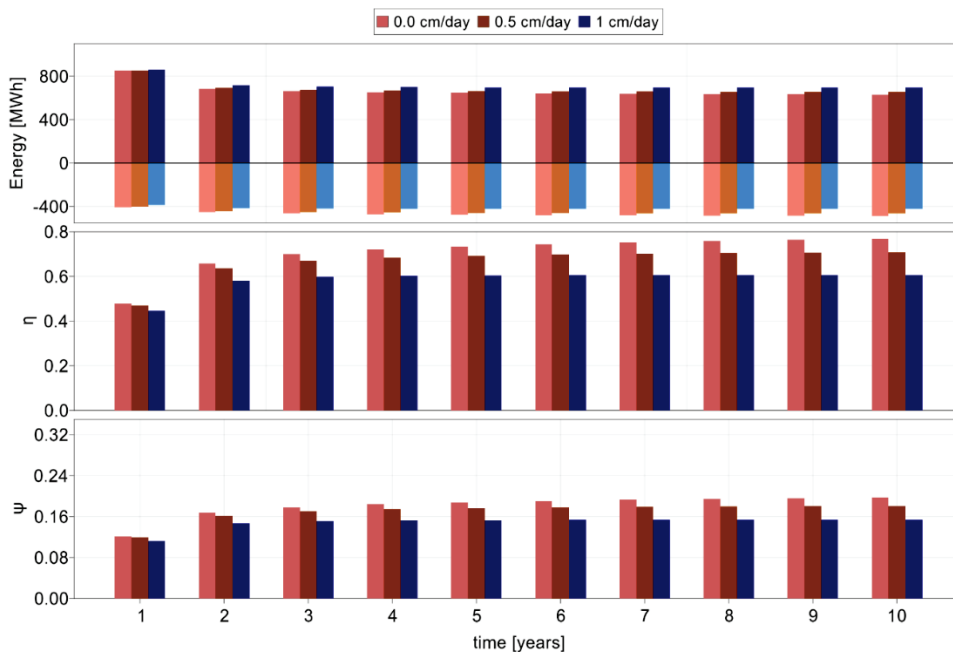
Figure 17: KPIs for the three study cases when simulating injection temperature 80˚C and extraction temperature 20˚C

4.2   NUMERICAL MODEL

Numerical models based on finite element have the advantage that they are flexible allowing to accurately portrait the hydraulic and thermal behavior on the subsurface. With these models we can model the ground surface profile and the

ground layers stratigraphy and its hydraulic and thermal properties. Numerical models require though long simulation time, limiting the number of cases that can be explored to study a given system.

In this project, the tool FEFLOW has been used to develop a model of the same borehole field geometry presented in Figure 12, an existing borehole storage in Braedstrup, Denmark. This storage is dry, all boreholes are above the groundwater level, see details in (Tordrup et al., 2017), and it has been in operation since 2012. With the help of measured operation temperature data, the model has been validated for the case of groundwater flow equal to zero, and it has subsequently been extended to study several cases with hypothetical groundwater flow rate scenarios. Energetic and exergetic performances of the HT-BTES were performed based on all results, following an approach similar to the one suggested in publication 1. Figure 18 shows an illustration of the model geometry and mesh (see more details in publication 2).
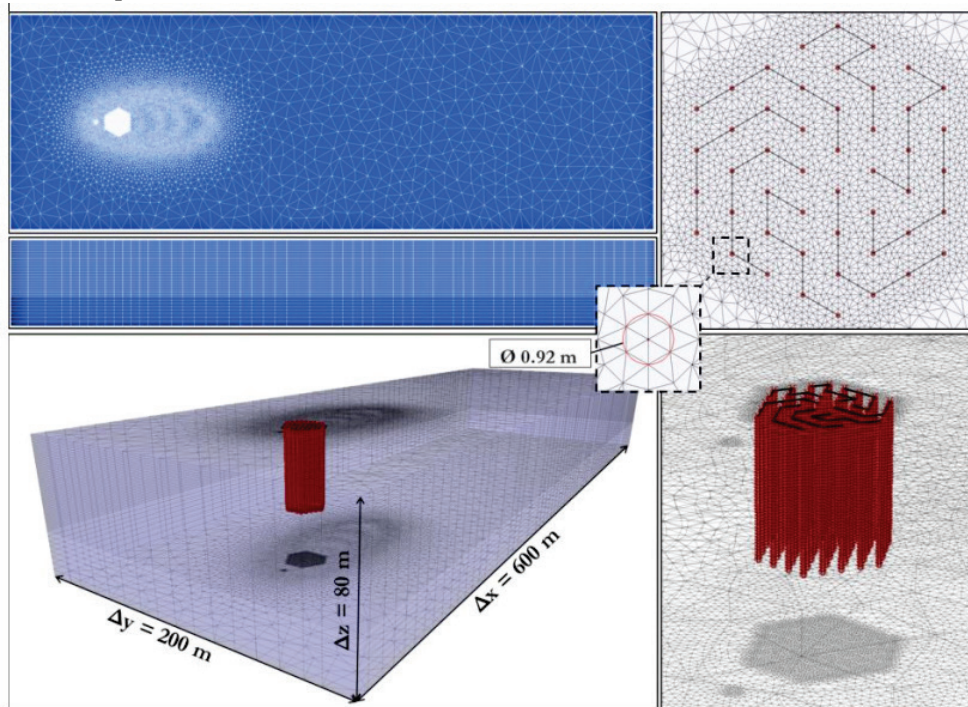

Figure 18. Illustration of the numerical model geometry

A plug-in for enabling simulation of series-connected BHEs with flow direction control was developed using the C++ programming language with the APIs available for FEFLOW. This plug-in tool for switching the flow direction was also indirectly validated.

The general results from the simulation results with Darcy flux equal to zero and those including heat advection (by defining a hypothetical confined groundwater system within the model domai and imposing a uniform hydraulic gradient across the storage site) are presented in Figure 19. It is obvious that it decreases in the presence of groundwater flow. A small rate of groundwater flow, however, seems actually to improve storage performance during the fourth storing cycle, probably

because of enhanced heat transport and thus reduced ground thermal resistance. This effect was also observed by (Bauer et al., 2009).

Both in terms of seasonal system energy and exergy performance, there is a gradual increase which then stabilizes as time goes on. A quasi-stationary condition tends to occur much earlier in cases of high groundwater flow. Also, the relative change in exergy efficiency from year to year is smaller as groundwater velocity/hydraulic head is increased. These observations are even valid when observing the performance results from the analytical approach. It is important to note, however, that times for charging / discharging, as well as flows and temperatures are very irregular in the numerical case (operation data), giving rise to certain tendencies that are difficult to interpret. The analytical results use regular and stable input values.
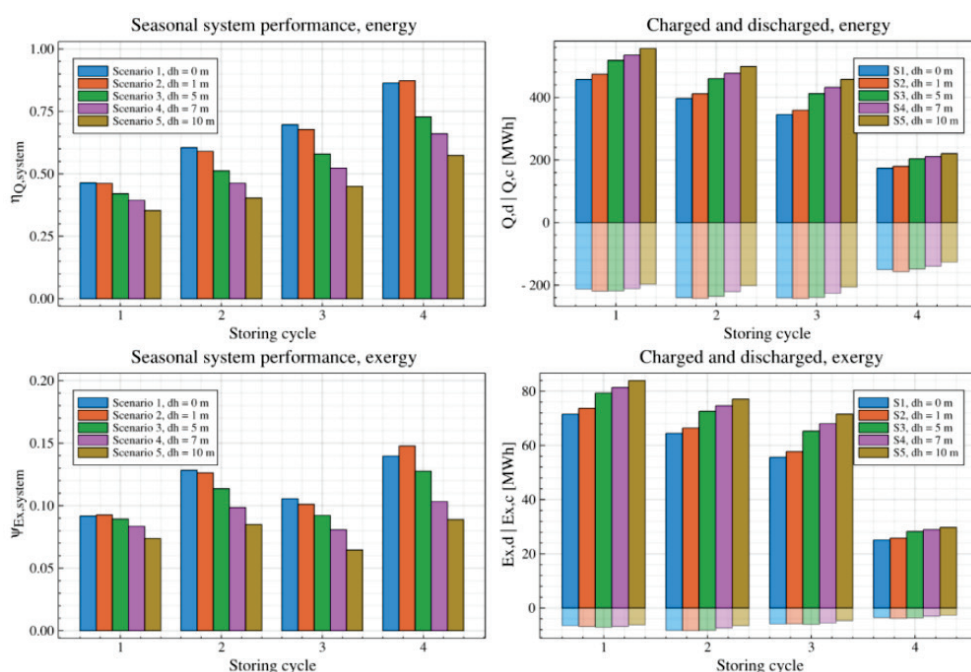
Figure 19. Energy and exergy for all cases (scenarios with different hydraulic heads).

Exergy seems to be less sensitive to groundwater flow rate than energy. The exergy extracted from the storage (negative values in the figure) is rather low and equal for all scenarios. The large difference between charging and discharging periods shows significant exergy losses, in all study cases.

Although it can be seen after a couple of storage cycles that lower groundwater flow velocities contribute to somewhat higher exergy storage efficiency, it seems not to be of importance for the overall performance. The effect of groundwater flow on exergy performance might though be more prominent under other operation and subsurface conditions than the ones set out in this study. Using high charging temperatures (i.e. high quality heat), while discharging heat at temperatures relatively close to the undisturbed ground temperature, energy extraction is promoted and the storage temperatures are kept at moderate levels,

but the exergy performance is penalized if the undisturbed ground temperature is to be used as a reference in the exergy calculation. The reference temperature will affect the quantitative result, but the overall result will not be affected. Complete analyses of the energy and exergy losses are presented in publication 2.

4.3   VALIDATION

4.3.1   Numerical model and measured data från Braedstrup

As mentioned above, the pure conduction numerical model was validated with measured data from the installation in Braedstrup. Figure 20 shows temperatures and computed net energy and power in good agreement between the numerical model and operation data, with some larger deviations in energy magnitudes during the second discharging season. A number of graphs with computed and measured temperatures at different locations in the storage can be seen in a complete validation study presented in publication 2, showing the capabilities of the model.
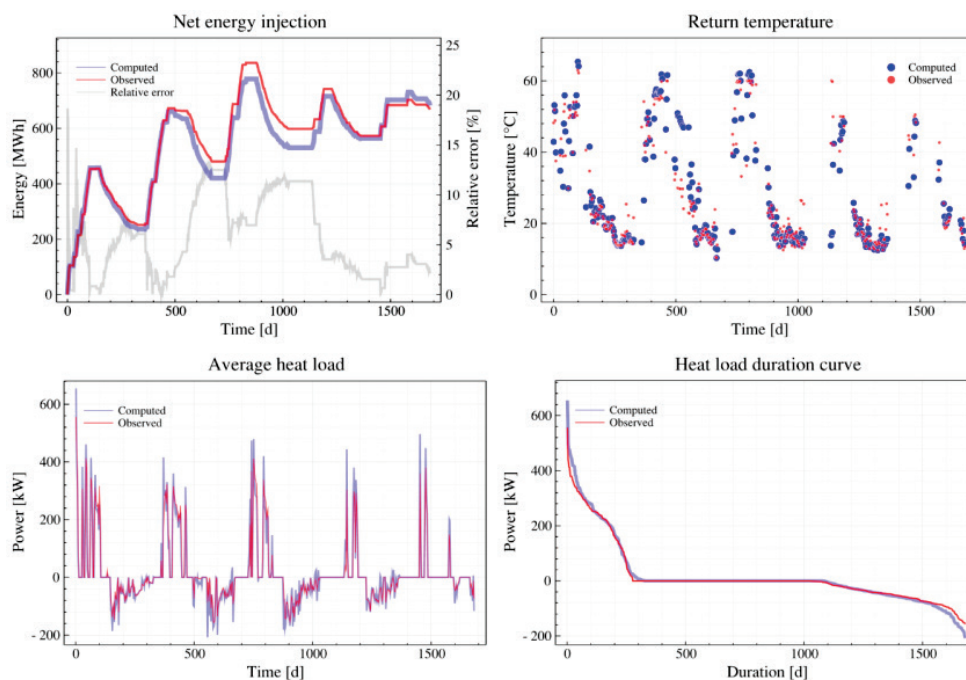
Figure 20. Comparison between the model results and measured energy flow and return temperatures

4.3.2   Laboratory scale model

The validation work presented in the previous section is of primary importance when evaluating the suitability of the tested model, not least because it is based on data from a real installation over several years of operation. Nevertheless, this validation process cannot guarantee that the model will perform equally well in other conditions. For instance, the small differences between data and simulations may be due to the model not capturing all heat transfer mechanisms, wrongful assumptions, biased parameters (e.g. thermal conductivity) or a combination of

those. In that case, it is not possible to conclude on the origin of those small differences because the data is not generated under controlled conditions.

This issue has motivated the design and construction of a laboratory scale model inside our lab at KTH Energy Technology (thus under more controlled conditions). Another advantage of such a Laboratory Scale Borehole Storage (LABS) is that the required testing time is reduced significantly. Indeed, BTES have a very large thermal inertia, making the heat transfer transient during most of their lifetime. Should a model suitably describe heat transfer phenomena in the BTES, it would have to be validated over the BTES lifetime (> 20 years). It is not hard to imagine the challenges of monitoring a real installation over such size and for such long times. Instead, by reducing the scale, the required testing is greatly reduced. This stems from the conservation of the Fourier number.

The lack of reference validation data, borehole storages being designed for long lifetime (years or decades), the thermal processes being so slow, and the difficulty to monitoring such large installations with long time scales, has motivated the design and construction of a laboratory scale model inside our lab at KTH Energy Technology. The time scale and accessibility are then reduced, and controlled conditions may hopefully be achieved.

The lab-scale BTES is being built as quarter of a cylinder with dimensions scaled down with a factor of 600 with respect to reality. The radius and depth (of the storage volume) is 1 meter and.

The design has carefully been done based on invariance requirements analytically derived from the heat equation. Numerical models were then used to verify the found invariance requirements, determine test durations so that time scale ambitions could be achieved, find a suitable size for the LABS, as well as investigate boundary condition (BC) and practical issues. Two scientific articles dealing with the design work have been published and are included to this report as an appendix (see publication 3 for more details).

The invariance of nondimensional numbers, a requirement for generating the lab-scale model was achieved, i.e. a real-scale installation can be represented in the lab, however with a cost of having to scale up boundary conditions (e.g. forced convection applied on the top) proportionally to the geometrical scale factor. Thermal response functions, sometimes also called g-functions, where generated and compared with other studies, allowing to do some new findings as well as validating the design method.

A laboratory scale model was finally set, consisting of a 4 × 4 borehole field and vertical boreholes. A geometrical scale factor of 600 is found suitable, implying simulating a real-scale borehole of 300 m by a 50 cm long "in-lab" borehole. The corresponding test duration is then about 5.5 days. For boreholes of 1 m depth, the borehole temperature increase induced by boundary effects is indeed less than 0.29 K, which is below the determined design uncertainty of the change in average borehole wall temperature. The borehole radius is chosen as 1.25 mm while the spacing is of 3.3 cm. Symmetry is used to reduce the size to a ¼ cylinder, thereby reducing the weight.

The external structure is constituted of a metallic container whose walls are equipped with insulation materials. The outer material of the quarter cylinder is made of 5mm thick stainless steel that has been welded together. A sealant is also used in the joints of the welded steel. Inside the steel, a 100 mm thick insulation layer has been added.

A thin layer of dry sand was put in the bottom as a bed for a heating plate, and a similar layer on top of it. This is to allow heat to dissipate easily on both sides of the heating cable, limiting potential high temperature issues that may arise from direct contact between the heating cables and the insulation layers. The sand layer on top of the plate is followed by two plastic layers for the water tightness. The rest of the tank interior is filled with a mixture of sand and water, which represents the ground.

The saturated sand was chosen in the work presented in publication 3 for its appropriate properties and capability to simulate the real ground. A photo of the lab model as it looks today is shown in Figure 21. It was unfortunately not possible to finish it within the frame of this project. A copper plate with electric heating wires was installed (see Figure 22). The power is controlled with an adjustable voltage transformer and thermocouples are used to measure temperature at different locations.
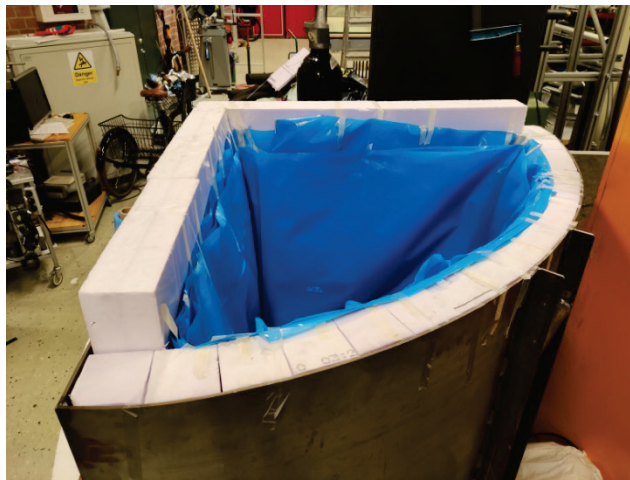
Figure 21. Picture of the laboratory scale model during construction.
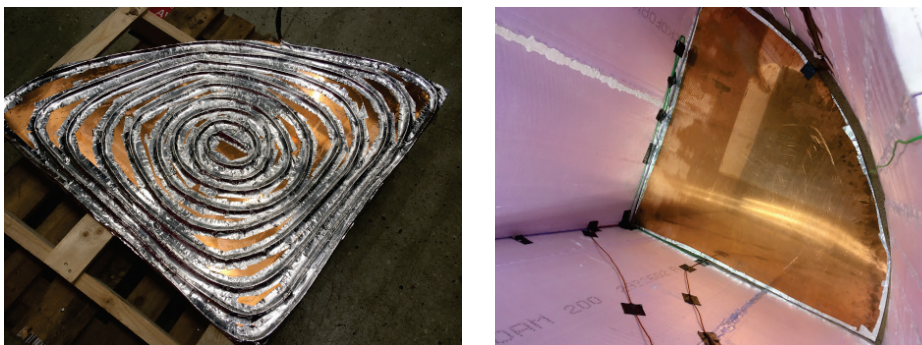
Figure 22. Heating plate

One of the major challenges has been to build borehole heat exchangers (U-pipe 0.7mm in diameter. in this case) that respect the scale of the system, with proper connecting joints and reasonable pressure drops. Pressure drop has been measured for several U-pipe BHEs and system curves have been used to select a proper circulation pump. Complete reports with more details about the design and construction of the laboratory model are included in the report in publication 3 and (Blomfelt et al, 2021).
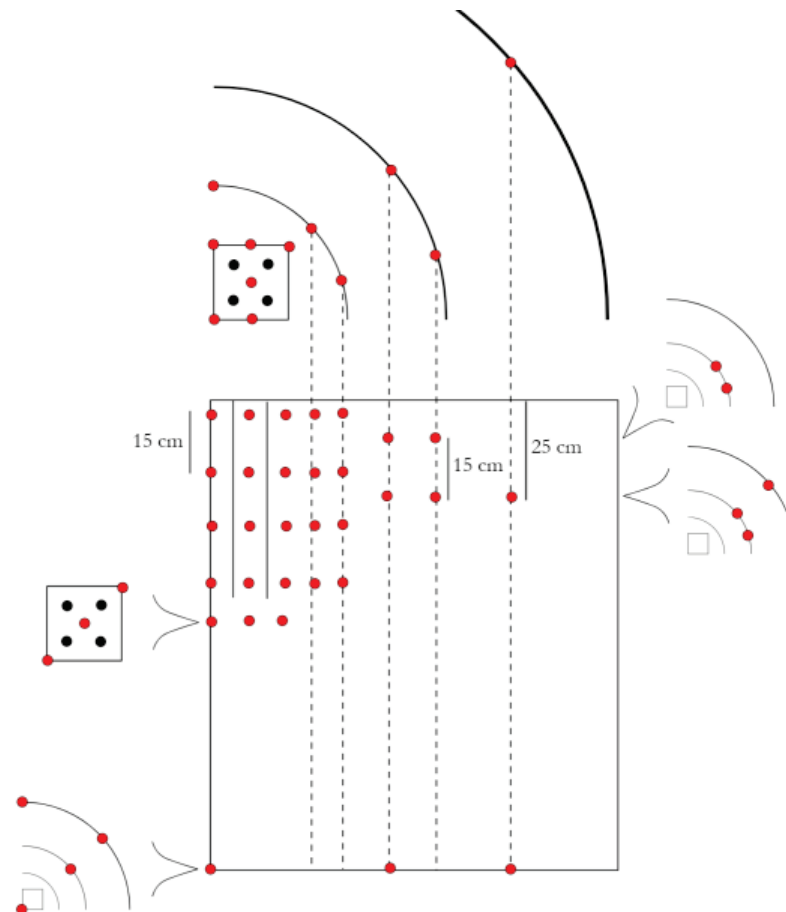
Figure 23. Thermocouple location in the laboratory model

Through this validation work, the authors believe that a solid contribution with identified potential error sources has been made to the scientific community, able to generate reference Thermal Response Functions under controlled conditions and fulfilling a data gap that strengthens the trustworthiness of long-term ground heat transfer models for high temperature borehole thermal energy storages.

5 CONCLUSION

A Stand-alone calculation tool for design, simulation and optimization of High Temperature borehole thermal energy storage interacting has been developed. The tool the size of a borehole storage and heat pump system proposes for given constrains and user requirements. It works based on a simplified quasi steady state approach and dynamic simulations. An analytical and a numerical modeling approach for quantifying the effect of groundwater flow have also been presented, and attempts for validating part of the modelling work have been made using both a laboratory scale model and real measured data from an existing high temperature storage in Braedstrup Danmark.

The influence of groundwater flow has been quantified for realistic scenarios of HT-BTES and the possible effects due to porosities, connectivity between voids or interconnected permeable joints and fractures is discussed in terms of energy and exergy performance. Even when there might be situations when the effect groundwater flow is negligible (or positive), the models developed in this work show that groundwater flows of reasonable size have a negative impact on the performance of HT-BTES. The effect of groundwater flow is though strictly dependent on local conditions and the presented modelling approaches can be adapted to specific sites.

As Exergy takes into account both the quantity of the heat exchanged as well as the temperature at which this heat is exchanged, the results of the work above are presented in terms of exergy efficiency, besides energy efficiency and net present value. Most of the earlier work dealing with BTES have failed to describe the temperature at which the thermal energy is exchanged with the BTES, which should be of interest especially when dealing with High Temperature-BTES systems. Pareto fronts for the conflicting objectives are provided for some simulated cases that give users extra help when carrying out own design, simulation and optimization work.

As summarized here, the project objectives were fulfilled and tools for design and for performance quantification and optimization with and without groundwater flow have been developed. Results shown in the optimization maps or regarding groundwater flow are, however, not generated to any extent in the stand alone tool.

Energiforsk

6 REFERENCES

Abuasbeh M, Acuna J, Lazzarotto A, Palm B. 2021. Key Performance Indicators for Long Term Evaluation of Aquifer Thermal Energy Storage Systems: Esker Case Study in Stockholm. Submitted for publication.

Acuña, José. 2013. "Distributed Thermal Response Tests : New Insights on U-Pipe and Coaxial Heat Exchangers in Groundwater-Filled Boreholes. Doctoral thesis, KTH.

Alkiswani, Mutaz, Claes Regander. 2019. "Säsongslagring Av Överskottsvärme Vid KVV Filborna, Helsingborg." Presented at the Geoenergidagen 2019, Stockholm.

Banks, D. (2015). A review of the importance of regional groundwater advection for ground heat exchange. Environmental Earth Sciences, 73(6), 2555–2565.

Bauer, D., Heidemann, W., Müller-Steinhagen, H., & G Diersch, H.-J. (2009). Modelling and simulation of groundwater influence on borehole thermal energy stores. Proceedings of Effstock, the 11th International Conference on Thermal Energy Storage.

Blomfelt J, Brouillette E, Dong H, Balan C, De Luca S, Kronström C. 2021. Lab-scale borehole thermal energy storage. Final Report, KEX. KTH.

Cabeza, Louisa F. 2015. Advances in Thermal Energy Storage Systems. Methods and Applications. Woodhead Publishing Series in Energy.

Chiasson, A., & O'Connell, A. (2011). New analytical solution for sizing vertical borehole ground heat exchangers in environments with significant groundwater flow: Parameter estimation from thermal response test data. HVAC&R Research, 17(6), 1000–1011.

Cimmino, M.: Fluid and borehole wall temperature profiles in vertical geothermal boreholes with multiple U-tubes. Renewable Energy 96, Part A, (2016), 137–147

Cimmino, M.: G-functions for bore fields with mixed parallel and series connections considering axial fluid temperature variations, in: Proceedings of the IGSHPA Research Track (2018).

Diao, N., Li, Q., & Fang, Z. (2004). Heat transfer in ground heat exchangers with groundwater advection. International Journal of Thermal Sciences, 43(12), 1203–1211.

Forman, Clemens, Ibrahim Kolawole Muritala, Robert Pardemann, and Bernd Meyer. 2016. "Estimating the Global Waste Heat Potential." *Renewable and Sustainable Energy Reviews* 57 (C): 1568–79.

Grycz, David, Petr Hemza, and Zdeněk Rozehnal. 2014. "Charging of the Experimental High Temperature BTES Via CHP Unit - Early Results." *Energy Procedia*, Proceedings of the 2nd International Conference on Solar Heating and Cooling for Buildings and Industry (SHC 2013), 48 (January): 355–60.

Hellström, G., 1989. Duct Ground Heat Storage Model - Manual for Computer Code, Lund: University of Lund, Department of Mathematical Physics

Hemmatabady, Hoofar, Julian Formhals, Bastian Welsch, Daniel Otto Schulte, and Ingo Sass. 2020. "Optimized Layouts of Borehole Thermal Energy Storage Systems in 4th Generation Grids." *Energies* 13 (17): 4405.

Hu, J. (2017). An improved analytical model for vertical borehole ground heat exchanger with multiple-layer substrates and groundwater flow. Applied Energy, 202, 537–549.

Katsura, T., Shoji, Y., Sakata, Y., & Nagano, K. (2020). Method for calculation of ground temperature in scenario involving multiple ground heat exchangers considering groundwater advection. Energy and Buildings, 220, 110000.

Lazzarotto, A.: A network-based methodology for the simulation of borehole heat storage systems. Renewable Energy 62, (2014), 265–275.

Leyland G, 2002, "Multi-Objective Optimization Applied to Industrial energy problems", PhD thesis in Energy Systems, Swiss Federal Technology Institute, Lausanne.

Malmberg, Malin. 2017. Transient modeling of a high temperature borehole thermal energy storage coupled with a combined heat and power plant. Master of Science Thesis EGI 2017: 0106 MSC.

Malmberg, Malin, Willem Mazzotti, José Acuña, Henrik Lindståhl, and Alberto Lazzarotto. 2018. "High Temperature Borehole Thermal Energy Storage - A Case Study." In *Research Conference Proceedings*. Stockholm, Sweden.

Mangold, Dick, and Laure Deschaintre. 2015. "Seasonal Thermal Energy Storage: Report on State of the Art and Necessary Further R+D." IEA SHC Task 45.

Molina-Giraldo, N., Bayer, P., & Blum, P. (2011a). Evaluating the influence of thermal dispersion on temperature plumes from geothermal systems using analytical solutions. International Journal of Thermal Sciences, 50(7), 1223–1231.

Molina-Giraldo, N., Blum, P., Zhu, K., Bayer, P., & Fang, Z. (2011b). A moving finite line source model to simulate borehole heat exchangers with groundwater advection. International Journal of Thermal Sciences, 50(12), 2506–2513.

Energiforsk

Nordell, Bo. 1994. "Borehole Heat Store Design Optimization." Luleå: Luleå University of Technology.

Nordell, Bo, Alberto Liuzzo Scorpo, Olle Andersson, Leif Rydell, and Björn Carlsson. 2016. *Long-Term Long Term Evaluation of Operation and Design of the Emmaboda BTES. : Operation and Experiences 2010-2015*. Luleå tekniska universitet.

Nußbicker, J, D Mangold, W Heidemann, and H Müller-Steinhagen. 2003. "Solar Assisted District Heating System with Duct Heat Store in Neckarsulm-Amorbach (Germany)."

Reuss, M., 2015. The Use of Borehole Thermal Energy Storage (BTES) Systems. In: L. F. Cabeza, ed. Advances in Thermal Energy Storage Systems: Methods and Applications. s.l.:Woodhead Publishing , pp. 117-147. ISBN 978-1-78242-096-5.

Rivera, J. A., Blum, P., & Bayer, P. (2015). Analytical simulation of groundwater flow and land surface effects on thermal plumes of borehole heat exchangers. Applied Energy, 146, 421–433.

Sibbitt, Bruce, Doug McClenahan, Reda Djebbar, Jeff Thornton, Bill Wong, Jarrett Carriere, and John Kokko. 2012. "The Performance of a High Solar Fraction Seasonal Storage District Heating System – Five Years of Operation." *Energy Procedia* 30: 856–65.

Tordrup, K. W., S. E. Poulsen, and H. Bjørn. 2017. "An Improved Method for Upscaling Borehole Thermal Energy Storage Using Inverse Finite Element Modelling." *Renewable Energy* 105 (May): 13–21.

U.S. Department of Energy. 2008. "Waste Heat Recovery: Technology and Opportunities in U.S. Industry." US Department of Energy.

Yevalkar, Amol. 2019. "Integrated Combined Heat and Power Plant with Borehole Thermal Energy Storage." Master thesis, Stockholm, Sweden: KTH Royal Institute of Technology.

Zhang, C., Wang, Y., Liu, Y., Kong, X., & Wang, Q. (2018). Computational methods for ground thermal response of multiple borehole heat exchangers: A review. Renewable Energy, 127, 461–473. https://doi.org/10.1016/j.renene.2018.04.083

Energiforsk

BILAGA - BERÄKNINGSEXEMPEL

STEG 1: INPUTS

Med avsikt att illustrera hur verktyget fungerar utgör denna rapportbilaga ett beräkningsexempel. Läsaren hänvisas också till section 2.1 i rapporten.

Ett specifikt mål med exemplet är att visa den delen av utdatafilen som endast avser borrhålslagret, dvs som visar hur lagret presterar för sig själv, utan värmepump. Till beräkningsexemplet har följande krav/input använts:

Urladdningseffekt 30 MW, en fil med ett årsdata för laddning och urladdning av borrhålslagret samt fjärrvärmeflödet, koaxial borrhålskollektorn, försäljningspris 400 SEK/MWh, kostnad för laddning lika med -140 SEK/MWh, kalkylränta 7%. Övriga inputs enligt defaultvärden.

Filen med inputdata enligt ovan presenteras i Figur 1 där det framgår effektprofiler för lagrets laddning och urladdning, som toppar vid ca **50 MW** respektive **30 MW**, samt fjärrvärmeflödet med ett medelvärde på **704 kg/s** (2 533 m³/h).
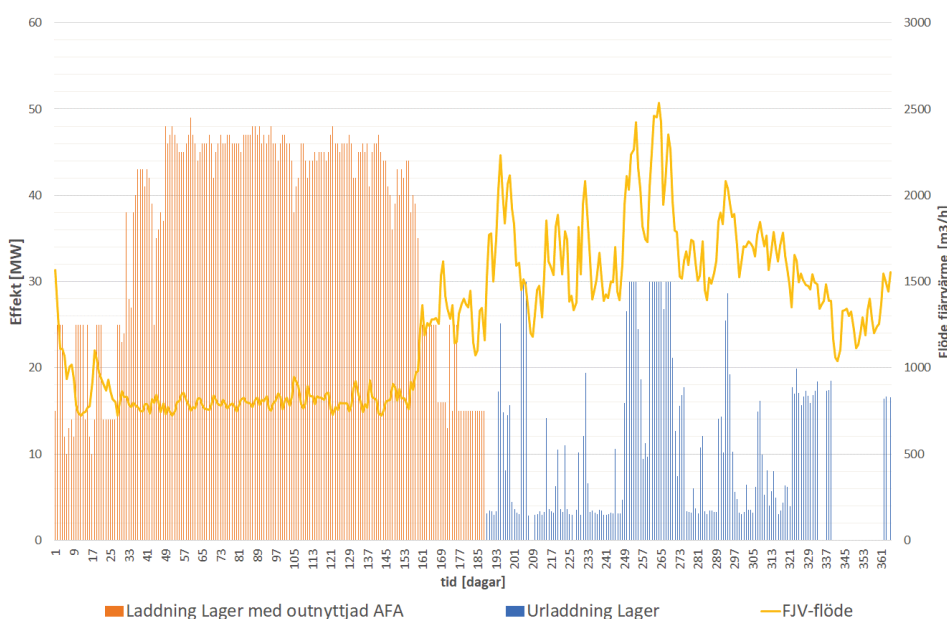
Figur 1. Input. Laddning och urladdningseffekter för lagret

De inputs som enligt ovan har implementerats i exemplet illustreras med rött färg i Figur 2, Figur 3, Figur 4 och Figur 5. För övriga inputs se Figur 7.
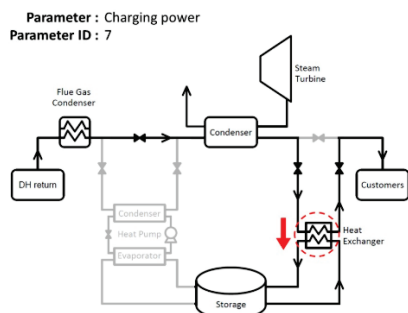
Figur 2. Laddningseffekt
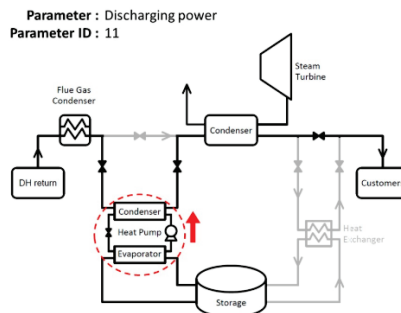
Figur 3. Urladdningseffekt
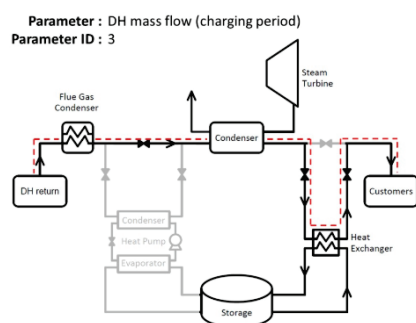
Figur 4. Fjärrvärmeflöde under laddning
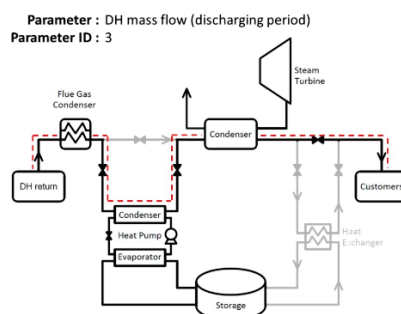
Figur 5. Fjärrvärmeflöde under urladdning

När användaren önskar ändra flera av de mer viktiga default inputs rekommenderas det att göra detta via sheet 1 i filen önskade värden i *DefaultParameters_Names*, se Figur 6, istället för genom användargränssnittet. Detta pga att det senare kräver en manuell uppdatering av inputvärden via en separat knapp via en separat knapp [Update table] och det förekommer ofta att detta glöms bort. I detta specifika fall har den första antaganden för lagrets storlek (antal borrhål) också ändrats till 1000, istället för defaultvärdet 2000 för att undvika iterationsrelaterade buggar.
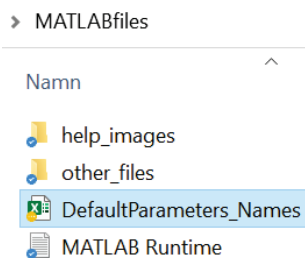
Figur 6. File path till att ändra default parameters

Parameter	Value	Units	ID
Duration of simulation	5	[years]	1
DH mass flow mode	2	[-]	2
DH mass flow (DV1)	704	[kg/s]	3
DH temperature mode	2	[-]	4
DH temperature (charging) (DV2)	95	[°C]	5
Charge power mode	2	[-]	6
Charge power (OPT case)	50	[MWth]	7
Days of charging (DV3)	183	[days]	8
DH temperature (discharging)	55	[°C]	9
Discharge power mode	2	[-]	10
Discharge power	30	[MWth]	11
HEX pinch point (DV4)	3	[°C]	12
BTES design temperature (DV5)	70	[°C]	13
HP COP (reference for design) (DV6)	5	[-]	14
BTES minimum outlet temperature (O…	40	[°C]	15
BH set-point time	5	[years]	16
BH max mass flow per BH loop (DV7)	1	[kg/s]	17
BH depth (DV8)	300	[m]	18
BH radius	0.055	[m]	19
BH number guess	1000	[-]	20
BH spacing (DV9)	5	[m]	21
BH series	3	[-]	22
BH resistance	0.05	[(m.k)/W]	23
BH ground thermal conductivity	2.9	[W/(m.K)]	24
BH ground volumetric heat capacity	2241	[kJ/(m3.K)]	25
BH ground initial temperature	8	[°C]	26
BH years of preheating	1	[years]	27
BH type (1.Utube - 2.Coaxial)	2	[-]	28
BH per collector	50	[-]	29
BH SDR	11	[-]	30
BH U-tube diameter	40	[mm]	31
BH coaxial inside diameter	50	[mm]	32
BH coaxial outside diameter	115	[mm]	33
BH intermediate pipe diameter	40	[mm]	34
BH header pipe diameter	40	[mm]	35
BH header pipe length	40	[m]	36
BH main pipe diameter	250	[mm]	37
BH main pipe length	500	[m]	38
Electricity price	0.7	[SEK/kWh]	39
Maintenance costs	4	[%]	40
DH heat price (for selling, when disch…	0.4	[SEK/kWh]	41
DH heat cost (for buying, when chargi…	-0.14	[SEK/kWh]	42
System life time	20	[years]	43
Discount rate	7	[%]	44

Figur 7. Samtliga inputs i beräkningsexemplet inkl. de enligt i figur 1

STEG 2 OCH 3: PRELIMINÄR DESIGN

Nu när steg 1 (inputs) är gjort blir nästa steg att kontrollera att inga felaktiga uppgifter har angivits (t.ex. decimaltecken, siffror utanför verktygets arbetsområde). Är meddelandet "Inputs OK" i message window så är det OK att gå vidare till steg 3 (Design BTES system) och klicka på "Run Design". Resultatet av steg 3 visas i message window enligt Figur 8.

```
From section 3 - "Design BTES System":
- Designing BTES system, please wait...
- BTES system designed successfully.
---- Preliminary results from the design process:
------- Heat exchanger size (UA value): 4068.95 [kW/K]
------- Number of boreholes: 981 [-]
------- Ground surface area required: 21236.23 [m^2]
------- Max total mass flow through storage: 327 [Kg/s]
------- Heat pumps in series: 4 [-]
------- HP heating capacity: 7.8222 [MWth]
------- Total HP heating capacity: 31.2889 [MWth]
------- HP COP (as defined by user): 5 [-]
------- Discharge power: 30 [MWth]
```

Figur 8. Message window efter steg 3. Systemets preliminära design enligt programmets steady state beräkningen.

Figur 8 visar att borrhålslagret med de ställda inputs består av 981 borrhål, att lagret ockuperar en yta på ca 21 000 kvm och behöver ha med 4st vätska-vätska värmepumpar med värmekapacitet 7,8 MW var. En viktig fråga i detta skede är huruvida den preliminära ytan finns tillgänglig eller om lagrets storlek måste anpassas rent geometrisk.

Nästa steg blir att kontrollera hur lagret presterar både tekniskt och ekonomiskt, steg 4.

STEG 4: PRESTANDA

I Steg 4 utför beräkningsverktyget en dynamisk simulering för att kontrollera hur lagret beter sig under simuleringstiden (i detta fall 5 år). Utförs detta steg framgångsrikt ser meddelandet i message window enligt Figur 9.

```
From section 4 - "Evaluate Performance":
- Launching TRNSYS simulation, please wait...
- Preparing for TRNSYS
- Running TRNSYS model
- TRNSYS simulation finished
- Post-processing data from TRNSYS simulation
- Preparing plots
---- FULL SIMULATION FINISHED SUCCESSFULLY ----
You can click on the buttons in section "5. See Results"
```

Figur 9. Meddelande i message window efter steg 4.

Samtliga resulterande siffror finns i resultatmappen som öppnas via separat knapp i Steg 5. Resultatet i detta fall visas i Tabell 1. Utdrag från utdatafil, resultat (kolumn B i sheet summary).

Ur detta hypotetiska fall framgår det att anläggningen kräver en investeringskostnad på ca **181 MSEK** och har ett nuvärde lika med **571 MSEK**. Lagret har i sin tur en exergi och energiprestanda lika med **52,9%** respektive **86,8%**, och systemets säsongsverkningsgrad är **6,8**. Andra nyckeltal sammanfattas i Tabell 1. Observera i Tabell 1 att invensteringskostnaden för värmepumparna är ca 90

MSEK. Denna investering utgår om man avser att använda lagret utan värmepump. Det samma gäller driftkostnaden för elanvändningen i kompressorn (OPEX_comp) samt energivärden Etot cond och Etot comp.

Tabell 1. Utdrag från utdatafil, resultat (kolumn B i sheet summary)

Parameter	Values	Units
Number of boreholes	981,0	[-]
Ground surface area required	21236,2	[m2]
Max tot mass flow through storage	327,0	[kg/s]
Heat exchanger size (UA value)	4069,0	[kW/K]
Heat pumps in series	4,0	[-]
Heat pump heating capacity	7,8	[MWth]
Total HP heating capacity	31,3	[MWth]
Total CAPEX	180,8	[M SEK]
Boreholes CAPEX	85,1	[M SEK]
Heat exchanger CAPEX	5,7	[M SEK]
Heat pump CAPEX	90,0	[M SEK]
OPEX_tot_avg	2,3	[M SEK]
OPEX_el_avg	19,4	[M SEK]
OPEX_charge_avg	-24,4	[M SEK]
Etot_charg	3481,4	[GWh]
Etot_disch	2753,2	[GWh]
Etot_cond	3750,0	[GWh]
Etot_comp	500,1	[GWh]
Etot_pump	53,8	[GWh]
Profit_avg	72,8	[M SEK]
NPV	571,0	[M SEK]
Sto_eff	86,8	[%]
SPF	6,8	[-]
Exergy_eff	52,9	[%]

I samma utdatafil i steg 5 hittar användaren timdata för den simulerade perioden (sheet "*hourly results*"). Effekter för lagrets laddning (charg_pow_MW) och urladdning (Discharg_Pow_MW) visas i orange respektive mörkgrön i Figur 10 nedan. Den senare representerar den effekten som lagret levererar utan värmepump, som i sin tur är samma som HP_EvapPower_MW under urladdningsperioderna.

Med datan i Figur 10 kan användaren konstatera att lagret uppfyller kravet med att leverera **30 MW** under varje urladdnings säsong. Ett annat vanligt krav att ställa mot ett borrhålslager är temperaturen som användaren önskar hämta upp från lagret under urladdningen, som enligt inputs i Figur 7 är **40 C**. (se i Figur 11, i orange färg. Denna temperatur är den samma som går in i värmepumpens förångare).
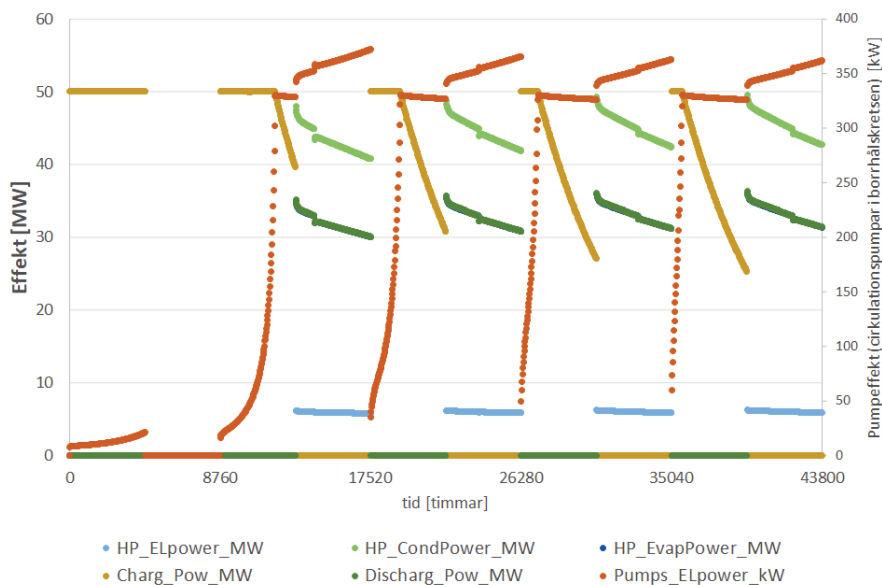
Figur 10. Resulterande effekter
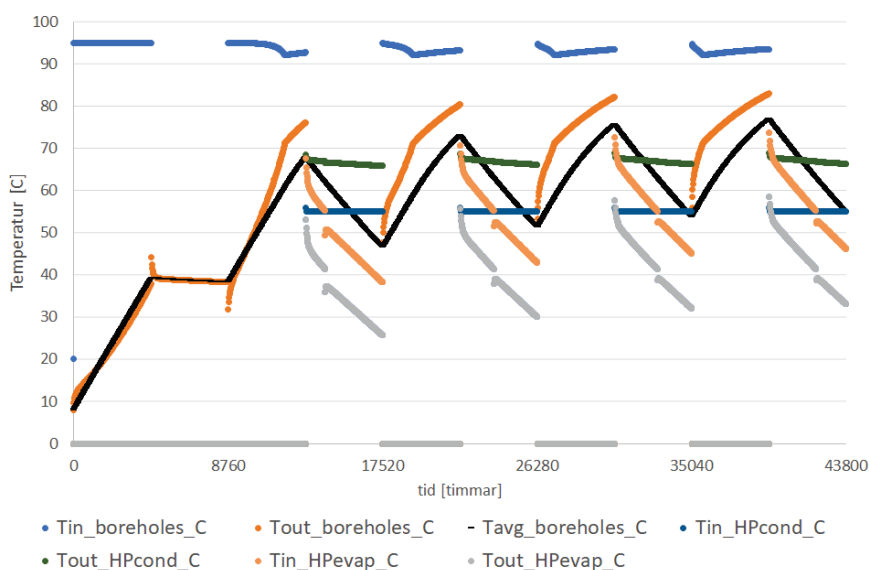
Figur 11. Resulterande temperaturer

STEG 5: OPTIMERING

Om inte alla inputs till beräkningen måste hållas fast kan resultaten ovan optimeras med hjälp av optimeringskartorna som tillhandahålls tillsammans med verktyget. Ett första steg kan vara att grafiskt hitta en kurva för exergi vs nuvärde för urladdningsfallet vid 30 MW och 40 C, dvs en interpolering mellan den gröna och den blåa kurvan i Figur 12. Den blå streckade kurvan indikerar att det borde gå att hitta en systemlösning med nuvärde mellan ca 200 och 400 MSEK och exergiprestanda mellan 54 och 60%, istället för 571 MSEK respektive 53% enligt

resultatet ovan. För att uppnå detta behöver inputparametrarna kombineras på olika sätt.
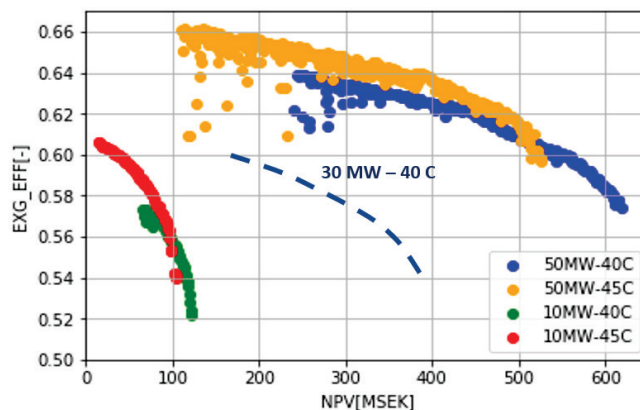
Figur 12. Grafisk interpolering av en paretofront för exergi vs NPV, urladdning 30 MW och 40C

Optimeringskartorna visar hur olika parametrar påverkar nuvärdet och exergin. Vissa parametrar har ingen påverkan medan andra en stor påverkan.

Är investeringsbudgeten till exempel av intresse så kan användaren utnyttja optimeringsdiagrammet för CAPEX (Figur 13) och med hjälp av den interpolerade kurvan för 30 MW och 40C som gäller i just detta fall konstatera att investeringskostnaden för anläggningen är faktiskt cirka 200 MSEK.

På motsvarande sätt kan ett antal olika optimeringsdiagram komma till hjälp så att användaren får ledtrådar om hur en mer optimal design kan erhållas. Inputparametrarna justeras successivt och när denna den optimala designen har hittats kan en dynamisk simulering göras på nytt, för att erhålla ny timdata för samtliga variabler under hela simuleringsperioden.
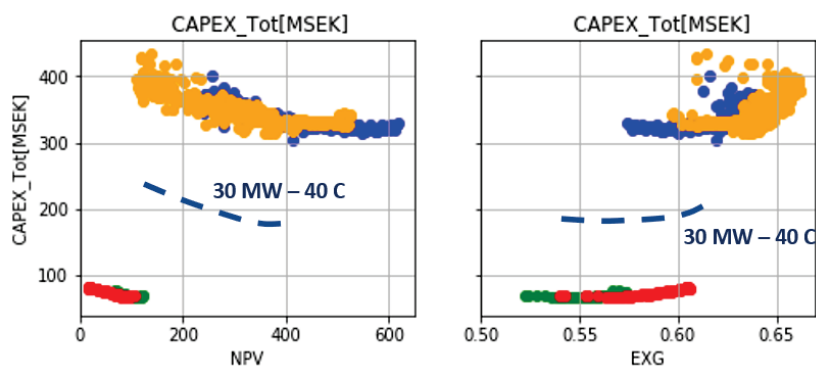
Figur 13. Grafisk interpolering för CAPEX, urladdning 30 MW och 40C

För att jobba vidare med optimeringen kan användaren iterera manuellt göra en känslighetsanalys. Beroende på vilka parametrar man varierar kan olika optimeringskartor komma till nytta vid valet av värden som känslighetsanalysen baseras på.

STEG 6: GRUNDVATTENFLÖDE (SEPARAT VERKTYG)

Antar man att den optimala designen i detta fall är den som beskrivs ovan så kan användaren ange ett lager med 327 parallelkopplade borrhålskretsar (981 borrhål med borrhålsanslutningar i serie, 3st per anslutning) och i samband med riskanalyser och beslutgenomgång studera hur det optimala lagret skulle påverkas av ev. grundvattenflöde av olika storlekar. Denna sista del av processen utförs med ett separat verktyg som finns att hämta här: https://gitlab.com/alblaz/BTESGroundWaterSimulator. Energi och exergiprestanda testas då som funktion av olika projektspecifika grundvattenhastigheter, om några. Ett komplett exempel från Braedsturp, Denmark (med andra dimensioner än det som erhållits ovan) presenteras i samma länk samt i slutrapporten.

För att använda denna kod behöver användare installera julia via https://julialang.org/ .
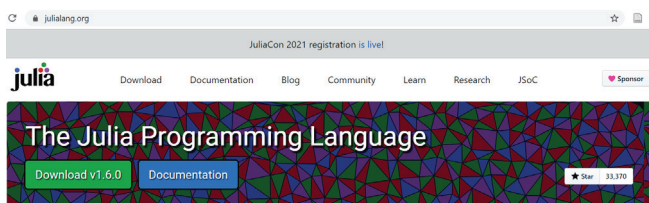
Därefter laddar man ner beräkningsverktyget från gitlabportalen ovan via downloadkanppen längs upp till höger.

Nästa steg blir att installera samtliga packet som verktyget använder, vilket görs via instruktionerna "Initial Set-up", dvs Enter the pkg manager shell mode

```
using the ] key and type following two commands.

(v1.5.4) pkg> activate
```
Och
```
(BTESGroundWaterSimulator) pkg> instantiate
```

Steget **pkg>instantiate** behövs endast den första gången man använder verktyget.

Efter detta är man redo att utföra simuleringar genom att köra koden via

```
julia > include("examples/example1/sim1.jl")
```

Mappstrukturen inom parentesen måste vara densamma som man själv har sparat modellen i. I vissa windowsmiljöer kan det vara nödvändigt att ersätta varje slash "/" med dubbelbakslash "\\", så här:

```
julia > include("examples\\example1\\sim1.jl")
```

Det senare gäller hela mappstrukturen som man avropar från Julia.

Önskar användaren att ändra inputparametrarna och spara beräkningarna med ett annat namn kan en ny mapp och ny simuleringsfil skapas under examples. Till exempel så här

BTESGroundWaterSimulator-master › BTESGroundWaterSimulator-master › examples › example2		
Namn	Senast ändrad	Typ
data	2021-04-20 17:33	Filmapp
results	2021-04-20 17:47	Filmapp
configuration_setup	2021-04-20 16:47	JL-fil
sim2	2021-04-20 16:47	JL-fil

Filen sim2.jl kan öppnas med en textfilläsare och innehåller alla inputparametrar. Och det finns även förklaringar för varje variabel och varje beräkningssteg.

Filen "configuration_setup" visar hur borrhålskonfigurationen kan ritas med XY koordinater och djup. I denna fil kan användaren ange sin projektspecifika geometri. Sedan kan man innanför juliafilen (sim2.jl i detta fall) ange hur borrhålen kopplas med varandra, i serie eller parallellt, under section #4 borehole field configuration.

När användaren är klar med inputsparametrar mm avropas

```
julia > include("examples\\example2\\sim2.jl")
```

och resultatet sparas I mappen "results". Beräkningsexemplet som presenteras i huvudrapportens section 4.1.4 visas hur resultatet presenteras.

PUBLICATION 1 : Performance evaluation of borehole thermal energy storage through energy and exergy analysis

Performance evaluation of borehole thermal energy storage through energy and exergy analysis

Alberto Lazzarotto, Willem Mazzotti Pallard, Mohammad Abuasbeh and José Acuña

KTH, Department of Energy Technology, Brinellvägen 68, 100 44 Stockholm, Sweden

alberto.lazzarotto@energy.kth.se

Keywords: borehole thermal energy storage, performance, exergy analysis

ABSTRACT

The use of densely populated fields of borehole heat exchangers is a viable solution for seasonal thermal energy storage and has great potential to increase the share of renewable energy and reduce the use of fossil fuels. A proper evaluation of borehole storage performance is necessary in order to evaluate benefits of candidate design configurations or to compare borehole storage system with other thermal energy storage options. Performance of borehole heat storage are often presented in literature in terms of energy performance. Another significant performance figure that is considered (although less frequently) is exergy. Exergy has the benefits of taking into account both the quantity of the heat exchanged as well as the temperature at which this heat is exchanged. In this paper we take a first step into this subject and investigate a viable methodology for the analysis of performance of borehole thermal energy storage systems. The method considers as relevant parameters for the analysis energy as well as temperature and exergy. These parameters are evaluated at the interface of the storage, e.g. inlet and outlet quantities, but also within the storage volume. An analytical model based on the line source is utilized to describe the heat transfer within the ground. The model provides the temperature field within the ground volume as a function of time and enables monitoring how the energy stored loses quality, i.e. exergy, as the difference between a given time of interest and the time of injection increases. The analysis proposed aims at breaking down the storage process in the borehole and evaluate how a variety of parameters in the configuration and operation of the system affect the processes of injection, storage and extraction of thermal energy. A set of test cases where a number of design and operational parameters are investigated is presented to illustrate the benefit and insight provided by the analysis.

1. INTRODUCTION

Energy storage will most likely play a crucial role in future, renewable-powered energy systems, due to increased intermittency of production plants, increased interplay between different systems and more decentralized energy prosumption (Chu & Majumdar, 2016; Mohd et al. , 2008;Moriarty & Honnery, 2016; Pickard, 2014). Most of the stored energy is meant for electricity production, mostly through pumped hydro storages that represent about 98% of the total amount of energy stored globally (Aneke and Wang, 2016; Dunn et al., 2011). As for thermal energy storages (TES), they only account for about 1% of the total energy stored (Aneke and Wang, 2016).

It is not surprising that heat is not the preferred form of storage considering that it is, in general, a less useful form of energy: irreversibility in thermodynamic processes usually emerge as heat (e.g. friction). It does not mean, however, that heat is a useless form of energy. Dinçer and Rosen (2010) state that when there is a mismatch between thermal energy supply and demand, e.g. in solar thermal installations, TES is the most direct way to store energy since it avoids unnecessary conversion processes. According to Forman et al. (2016), about half of the global energy production is wasted as heat, more than 60% of which is wasted at temperature below 100°C. Recovering part of this wasted heat would contribute in reducing CO_2 emissions but this would require a match between supply and demand, unless TES are used.

For high-latitude locations, seasonal TES are particularly attractive because there is usually a positive mismatch between supply and demand during summertime while this mismatch is negative wintertime (or vice versa, e.g. for cooling). Because seasonal TES should have large capacities and, thus, large volumes, it is common to find underground seasonal TES. Although it might not be the most efficient solution, the storage media is free and does not take any surface area.

This paper focuses on a common kind of underground TES, the Borehole TES (BTES) – i.e. storage of sensible heat in rock or soil through Borehole Heat Exchangers (BHEs). BTES have large storage capacities and the cost per amount of energy supplied is at the low-end compared to other TES solutions (see Table 3.3 in Dinçer & Rosen, 2011). Gehlin (2016) gives a comprehensive description of the technology providing definitions and a discussion on high temperature (up to 90°C) and low temperature (close to undisturbed ground temperature) BTES systems (Gehlin, 2016) . A rather complete collection of data on existing high temperature storage is provided by Malmberg et al. (2018)and in the report by Kallesøe et al. (2019). Gehlin states that the development of high temperature BTES has decreased after an initial enthusiastic decade in favor of low temperature BTES. However, she also mentions that in recent years there is again a new interest in this technology for seasonal storage of solar heat, industrial waste heat and waste heat from cogeneration plants. This interest is shown also by current research projects such as the EU project Heatstore and the Swedish national program Termiska Energilager (https://www.energiforsk.se/program/termiska-energilager/) which started with the objective of accelerating the theoretical and practical development of the high temperature BTES. This work is part of the latter program and has the objective of investigating performance indicators for borehole energy storage system.

Performance of BTES are often presented in literature in terms of the so called energy efficiency η, which is the ratio between the energy extracted during the discharging season and the energy injected during the charging season. Another figure that is utilized, although less frequently, is the exergy efficiency ψ, which is a dual definition of η in terms of exergy. Exergy has the benefits of taking into account both the quantity of the heat exchanged as well as its ''quality'' which depends on the temperature of the heat. This paper aims at exploring performance indicators for the analysis of high temperature BTES . Six test cases corresponding to

different configurations and system operations are simulated. Figures depending on temperature, energy, and exergy are evaluated at the interface of the storage, e.g. inlet and outlet quantities, but also within the storage volume.

2. METHODOLOGY

This section introduces the model that was implemented to perform borehole storage simulation as well as the performance indicators utilized for the analysis.

2.1 The model

The model used in this study is designed to simulate a borehole storage system operated by circulating a fluid inside an array of BHEs. The array consists of several hydraulic loops connected in parallel such that each loop is provided with the same inlet temperature. The model enables evaluating the performance of BTES systems given the bore field geometry and hydraulic arrangement (Cimmino, 2018; Lazzarotto, 2014). Figure 1 shows the application that is considered in this paper: 8 separate (non-identical) loops are fed in parallel with constant inlet mass flow at 90 °C during the summer and 55 °C during the winter. The borehole configuration and the arrangement studied are the ones of an actual pilot borehole storage (Tordrup et al., 2017). The system is fed from the internal borehole during summer and from the external boreholes during winter. The output temperature and the heat exchanged by the system are not directly imposed and are the result of the specific borehole configuration and operational strategy.
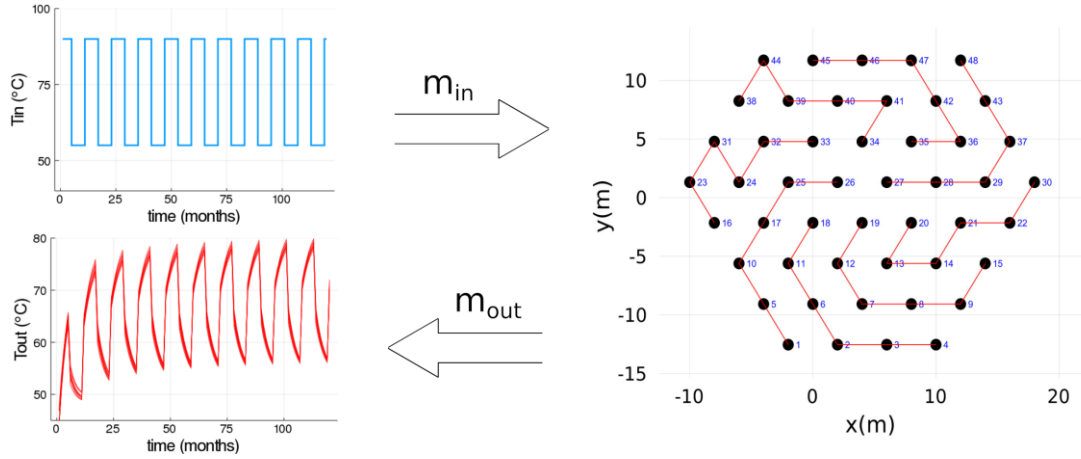

Figure 1: Borehole configuration and operational strategies studied within the paper. The boreholes are fed with mass flow at a temperature Tin(t).

Modeling strategy

In this initial work the ground is modeled as a two dimensional infinite solid by means of infinite line source solution (ILS). The choice of simulating a two dimensional model even though three dimensional models are readily available was made to simplify the methodology employed for the analysis presented in this work which requires to perform numerical integrations in control volumes (section 2.3). As a firststep it was therefore easier to develop the method for two dimensions.

Given a borehole storage with N boreholes the unknowns of the problems are the inlet temperature in the boreholes $T_{in}^{(i)}(t)$, the outlet temperature from the boreholes $T_{out}^{(i)}(t)$, the borehole wall temperature $T_b^{(i)}(t)$ and the power per meter exchanged by each borehole $q_b'^{(i)}(t)$ for a total of 4N unknown at each time step in the simulation. The system can be modeled using a set of 4N linear equations that models the ground, the borehole, the interaction between the ground and the borehole and the topology of the hydraulic network.

Ground Model

$$T_b^{(i)}(t) - \frac{1}{2\pi k_g} \sum_{j=1}^{N} q'^{(j)}(t)\, g(r_{j,i}, t_{\text{step}}) = T_0 + \frac{1}{2\pi k_g} \sum_{k=1}^{N_t-1} \sum_{j=1}^{N} (q'^{(j)}(t_k) - q'^{(j)}(t_{k-1}))\, g(r_{j,i}, t_{N_{t-1}} - t_k) \tag{1}$$

where k_g is the ground thermal conductivity, t is time, $r_{j,i}$ is the distance between borehole i and j, and g is the thermal response factor which, as mentioned above, for the purpose of this paper is modeled using the ILS as showed in the following expression.

$$g(r,t) = \text{ILS}(r,t) = \frac{1}{2}\, E_1\left(\frac{r^2}{4\alpha_g t}\right) \tag{2}$$

where E_1 is the exponential integral and α_g is the thermal diffusivity of the ground. It is worth noting that the term on the right hand side of equation 1 are values that can be computed given the load history of the storage. The equation is written to collect on the left hand side all the unknowns and the relative coefficients and, on the right hand side, the given terms. A similar style in presenting the model equations is adopted below since it provides a good idea of the relative matrix representation which is then implemented to solve the model.

Borehole Model

The borehole has been modeled according to the method introduced by Cimmino (2016). The model is fairly general and can be applied to step-wise constant borehole temperature. In this initial work we consider only the simple case of uniform borehole temperatures. The equation used in this paper is of the following form.

$$a_{\text{in}} T_{\text{in}} + a_{\text{out}} T_{\text{in}} + a_{\text{b}} T_{\text{b}} = 0 \tag{3}$$

For brevity in equation 3 we only report the linear relationship between T_{in}, T_{out} and T_{b}. The formulation for the coefficients a_{in}, a_{out} and a_{b} can be found in the reference article (Cimmino, 2016).

Heat Balance in the borehole

$$\dot{m}\, c_{p_f}\, T_{\text{in}}^{(i)}(t) - \dot{m}\, c_{p_f}\, T_{\text{out}}^{(i)}(t) - q_b'^{(i)}(t)\, H = 0 \tag{4}$$

where H is the length of the boreholes.

Temperature constraint: hydraulic topology

Eq. 4 allows to impose the outlet to a value f(t) while eq 5 allows connecting the outlet of borehole j to the inlet of borehole i. These two constraints enable any possible hydraulic topology for the system.

$$T_{in}^{(i)}(t) = f(t) \tag{5}$$

$$T_{\text{in}}^{(i)} - T_{\text{out}}^{(j)} = 0 \tag{6}$$

Equations 1,3, 4, 5 and 6 can be expressed in matrix form as system of equation $Ax = b$ with 4N equation and 4N unknowns. The system is fairly flexible and we can build several matrices A corresponding to different topology and operation. This enables for instance switching flow direction during operation which may be desirable feature when studying borehole connected in series.

2.3 Performance indicators

The performance of the borehole storage are evaluated both at a system level (inlet-outlet) on a seasonal basis but also within the storage volume at any time t. Performance are evaluated both in terms of energy and exergy. For exergy calculation the temperatures are absolute temperatures expressed in Kelvin and the reference temperature T_0 considered is the undisturbed temperature of the ground equal to 281.15 K.

Seasonal system performance indicators

$$\eta = \frac{Q_d}{Q_c} = \frac{\int_{\tau_c}^{\tau_c + \tau_d} \dot{m} c_p \left(T_{\text{out}}(t) - T_{\text{in}} \right) dt}{\int_0^{\tau_c} \dot{m} c_p \left(T_{\text{in}}(t) - T_{\text{out}} \right) dt} \tag{7}$$

$$\psi = \frac{\text{Ex}_d}{\text{Ex}_c} = \frac{\int_{\tau_c}^{\tau_c + \tau_d} \dot{m} c_p \left[(T_{\text{out}}(t) - T_{\text{in}}(t)) - T_0 \ln\left(\frac{T_{\text{out}}(t)}{T_{\text{in}}(t)}\right) \right] dt}{\int_0^{\tau_c} \dot{m} c_p \left[(T_{\text{in}}(t) - T_{\text{out}}(t)) - T_0 \ln\left(\frac{T_{\text{in}}(t)}{T_{\text{out}}(t)}\right) \right] dt} \tag{8}$$

where Q and Ex stands respectively for heat and exergy, and the pedice 'c' and 'd' stand respectively for charging and discharging.

Storage performance indicator

$$\eta_{\text{storage}}(V,t) = \frac{Q_{\text{stored}}(V,t)}{Q_{\text{exchanged}}(t)} = \frac{\int_V \rho_g c_{p_g} \left(T(\mathbf{x},T) - T_0 \right) dV}{\int_0^t m_f c_{p_f} \left(T_{\text{in}}(t) - T_{\text{out}}(t) \right) dt} \tag{9}$$

$$\psi_{\text{storage}}(V,t) = \frac{\text{Ex}_{\text{stored}}(V,t)}{\text{Ex}_{\text{exchanged}}(t)} = \frac{\int_V \rho c_p \left[(T(\mathbf{x},t) - T_0) - T_0 \ln\left(\frac{T(\mathbf{x},t)}{T_0}\right) \right] dV}{\int_0^t \dot{m} c_p \left[(T_{\text{in}}(t) - T_{\text{out}}(t)) - T_0 \ln\left(\frac{T_{\text{in}}(t)}{T_{\text{out}}(t)}\right) \right] dt} \tag{10}$$

Where Q_{stored} is the energy stored in the storage volume and $Q_{\text{exchanged}}$ is the cumulative energy injected and extracted in to the BTES system. Similar definitions but in terms of exergy applies to $\text{Ex}_{\text{stored}}$ and $\text{Ex}_{\text{exchanged}}$. Since in this paper the model used to simulate the borehole storage is a two dimensional model, the units of Q_{stored} and $\text{Ex}_{\text{stored}}$ are in (MWh/m). For this reason $Q_{\text{exchanged}}(t)$ and $\text{Ex}_{\text{exchanged}}(t)$ needs to be accordingly scaled by the length H of the boreholes. Seasonal parameters are presented in literature in several papers (Kizilkan and Dincer, 2012; Rosen et al., 2004; Rosen and Dincer, 2003; Sliwa and Rosen, 2017) and have been applied to borehole storage systems. The storage indicators have been used to optimize the operation of water tanks (Jack and Wrobel, 2009) but to the authors knowledge have not been used for borehole thermal storage application.

Other figures that are considered in this study are the fluid outlet temperature T_{out} and the mean storage temperature T_{storage}

$$T_{\text{storage}}(V,t) = \frac{\int_V T(\mathbf{x},t) dV}{\int_V dV} \tag{11}$$

2.4 The storage volume

The evaluation of the storage performance requires the calculation of an integral over the storage volume. Unlike other storage systems such as water tanks where the identification of the storage volume is trivial, borehole systems are unbounded. The choice of a control volume for the storage is therefore not trivial and requires some definitions. In order to make a sensible choice for the boundary we considered a volume around the boreholes that contains a percentage $1-\epsilon$ of the overall heat injected after a time τ_d corresponding to the time for the discharge cycle. We picked the discharging time as a reference time because it is the relevant time constant for extracting useful heat from the storage volume.

Lazzarotto et al.

$$\frac{Q_{\text{stored}_{\epsilon,\tau_d}}(V_\epsilon, \tau_d)}{Q_{\text{injected}}(\tau_d)} = 1 - \epsilon \tag{12}$$

For a single borehole case the radius r_ϵ of this region is the one satisfying the following expression.

$$\frac{1}{q'\tau_d} \rho_g c_{p_g} \int_{r_\epsilon}^{+\infty} \frac{q'}{4\pi k_g} E_1\left(\frac{r^2}{4\alpha_g \tau_d}\right) 2\pi r \, dr = \epsilon \tag{13}$$

where E_1 is the Exponential integral function. The value of r_ϵ can be easily computed numerically and is utilized within this paper to provide a reference value to define the storage region containing N sources at location (x_i, y_i) with i=1,..N. The procedure consists in determining the family of points (x,y) with minimum distance from the sources (x_i, y_i) equal to r_ϵ. Such region V_{ϵ_1, τ_d} with unknown $\epsilon_1 \leq \epsilon$ contains the storage volume V_{ϵ, τ_d} and guarantees that at most only a portion ϵ of the heat extracted during the discharging season is coming from the region outside V_{ϵ_1, τ_d}

It is clear that not all the energy/exergy stored in V_{ϵ_1, τ_d} is recoverable. On the other hand such definitions of storage efficiencies measure the capability of the BTES of mantaining the energy injected/extracted in the surrounding of the borehole system at distance from which it can be partly discharged.

The integrals of equation 9 and 10 are finite since they represent the energy and exergy stored in the volume. On the other hand, the line sources are singularities and the evaluation of the integrand function at the source's location returns infinity. This problem is solved by using the fact that the integration point in Gauss quadrature schemes are never at edges of the integration domain. We can therefore build the discretization domain following this rule and make sure that sources are placed on the boundary of elements of the discretization. Once we adopt these precautions we can safely calculate the integrals 9, 10 and 11 using numerical integration routines.

An interesting exercise is the calculation of η_{stored} in the infinite region which provides a verification of the correctness of the implementation of the borehole model (eq. 1) since η_{stored} must be equal to 1, i.e. the energy injected the ground must be stored somewhere in the ground since the model considered is an infinite solid. The integral can be performed by exploiting suitable change of variables such as $x = t/(1-t^2)$ that maps the unbounded domain $(-\infty, +\infty)$ to the finite domain $(-1, +1)$, or $x = a+t/(1-t)$ that maps the unbounded domain $(a, +\infty)$ to the finite domain $(0, +1)$. This test was performed and verified.

Table 1: Properties utilized to define the reference case configuration case 0.

Property	Symbol	Value	Units
borehole radius	r_b	0.0575	m
borehole length	H	100	m
ground conductivity	k_g	3	W/(m K)
ground heat capacity	C_g	$1.875 \cdot 10^6$	J/(m3 K)
grout conductivity	k_b	1.5	W/(m K)
grout heat capacity	C_b	$3.1 \cdot 10^6$	J/(m3 K)
minimum boreholes distance	B	4	m
mass flow rate per loop	$\dot{m}$	0.5	kg/s
density fluid	ρ_f	1000	
specific heat capacity fluid	cp_f	4182	J/(kg K)
arrangement	-	series	-
inlet temperature summer time	$T_{in,s}$	90	°C
inlet temperature winter time	$T_{in,w}$	55	°C
Undisturbed temperature	T_0	8	°C

2.5 Test cases design

The configuration showed in figure 1 was used as a reference case. Table 1 gives an overview of the parameters utilized to model the ground and the boreholes. In the base case configuration, the boreholes are connected in series and, as previously mentioned, they are supplied with a temperature of 90 °C during summer and 55 °C during winter time. A flow of 0.5 kg/s per loop is imposed and circulation goes from the center to the outer region of the boreholes during summer and in the opposite direction during wintertime, i.e. six months each. Simulations are performed with a monthly time step and for a time horizon of ten years. Modifications of all the properties provided in table 1 can be applied to compare the performance indicators presented for various a large array of configurations. In this paper, as shown in table 2, only grout thermal conductivity, mass flow rate and borehole arrangement (parallel or series) were varied in order to illustrate the method.

Table 2: Definition of five case studies obtained by modifying the properties arrangement, grout thermal conductivity and mass flow rate per borehole. The underlined properties highlighted in red are the properties that have been changed compared to the reference case.

	arrangement	k_b (W/(mK))	$\dot{m}$ (kg/s)
case 0	series	1.5	0.5
case 1	parallel	1.5	0.5
case 2	series	2.5	0.5
case 3	parallel	2.5	0.5
case 4	series	2.5	1
case 5	parallel,s	2.5	1

3. RESULTS AND DISCUSSION

3.1 Temperatures analysis

The model described in section 2 was used to obtain the solutions for the temperatures T_i, T_o and T_b, and for the heat rates q_b' for the six test cases. These results (figures 2-7) are displayed for a set of borehole located along a series connection in the base configuration. A color code is utilized to distinguish each individual borehole. For borehole in series (figure 2), the inlet temperatures T_i (solid thick lines) during summer time decrease from the highest value (equal to 90°C) of the innermost borehole to the lowest value of the outermost borehole. The outlet temperature T_o (thin line) can be distinguished only for the last borehole in the loop since is the only one in which the outlet temperature does not coincide with the inlet temperature of the previous borehole in the chain. For borehole in parallel (figure 3) all the inlet temperatures T_i coincide (and only one of them can be displayed) but we can appreciate each single outlet temperature T_o (thin lines). The borehole temperatures T_b are displayed using a scatter plot. By comparing the temperature plots for series and parallel we can notice how the series configuration induces greater radial stratification in the BTES temperatures. Regarding heat rates, a few observations can be done. First of all, the power exchanged for series arrangement is significantly lower when compared to the relative parallel cases. In parallel arrangement the heat rate during heat injection is for the most part exchanged by the outermost boreholes. While for the series case, the heat rate during heat injection is initially mostly exchanged in the center and decreases with time until the largest portion of heat is rejected to the outermost boreholes. Table 3 shows that for the cases investigated the yearly mean extraction temperature is up to 4.5 °C higher for borehole connected in series compared to borehole in parallel. These values are much larger when we consider the monthly values (figure 8b). The table also shows that the mean storage temperature is up to 2 °C higher for parallel connections. This result is due to the larger amount of net power exchanged with these configurations. The improvement in grouting material in cases 3 and 4 results in slightly higher outlet temperatures. On the other hand the increase in flow reduces the outlet temperature during extraction but at the same time increases up to 1.5°C the average storage temperature since the net heat exchanged is increased. For the calculation of the mean storage temperature (equation 11) we used the procedure described in section 2.4. We considered ϵ equal to 0.01, a discharging time τ_d of 6 months and solved equation 13. The solution yields an r_ϵ of 17.54 m which was utilized to build the domain $V_{\epsilon 1, \tau d}$. Figure 8a displays the domain area (~2954.27 m^2) and the discretization utilized for the numerical integration procedure.
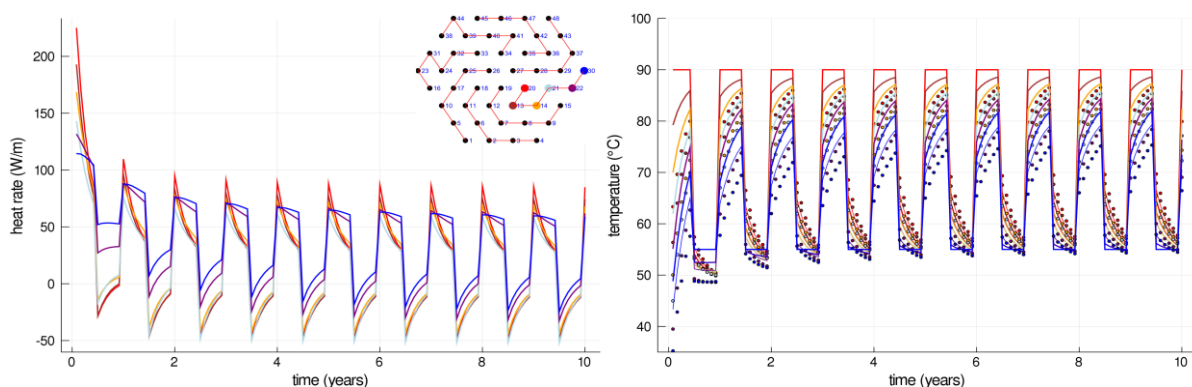
Figure 2: heat rate and temperature plots for case 0. A bore field map is used to display the color code used for displaying results of heat rate and temperature for selected boreholes. In the temperature plot, inlet temperatures T_i are displayed with thick solid lines, outlet temperature T_o with thin solid lines and borehole temperatures T_b using a scatter plot.

Figure 3: heat rate and temperature plots for case 1.

Figure 4: heat rate and temperature plots for case 2.

Figure 5: heat rate and temperature plots for case 3.

Figure 6: heat rate and temperature plots for case 4.

Figure 7: heat rate and temperature plots for case 5.

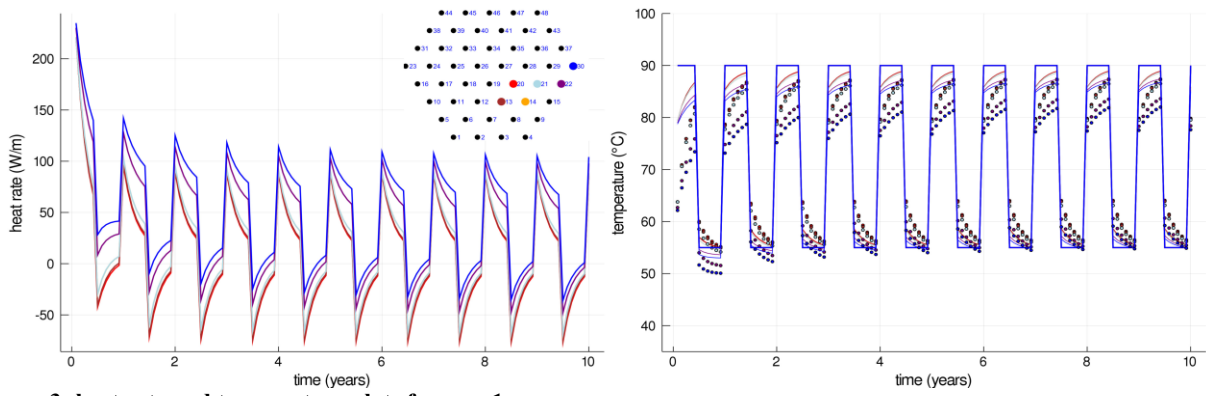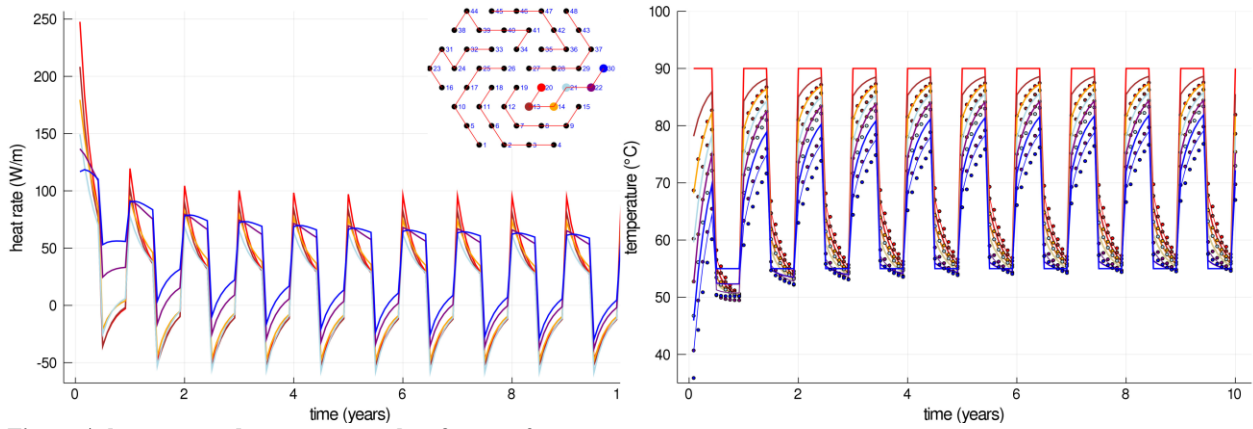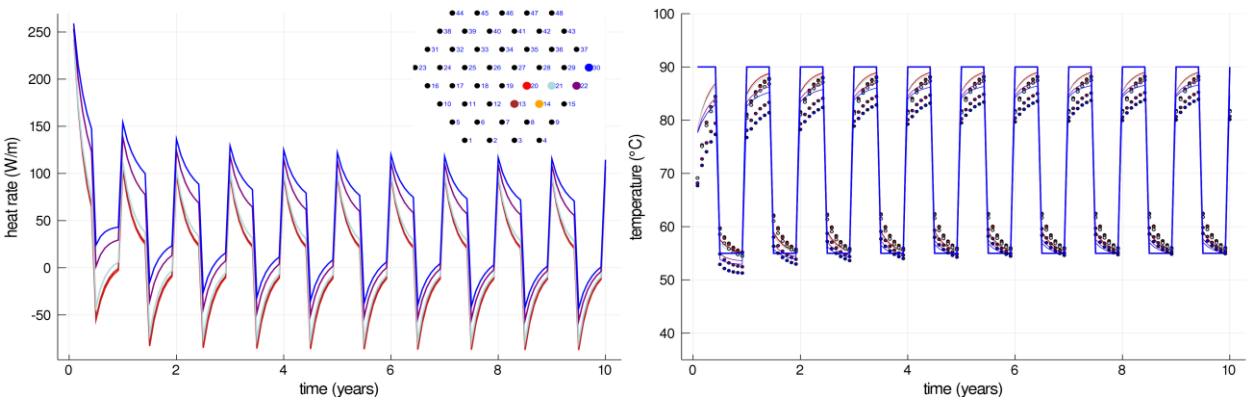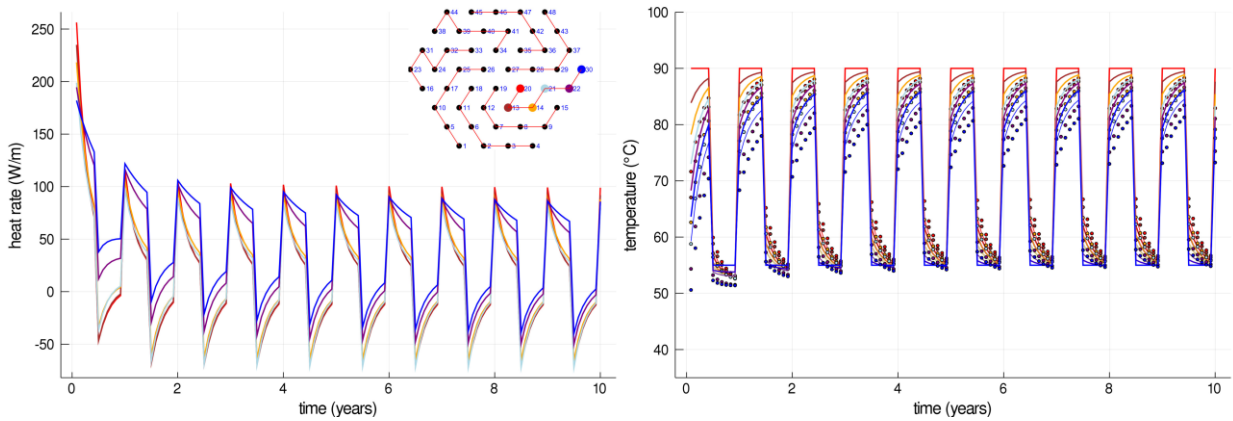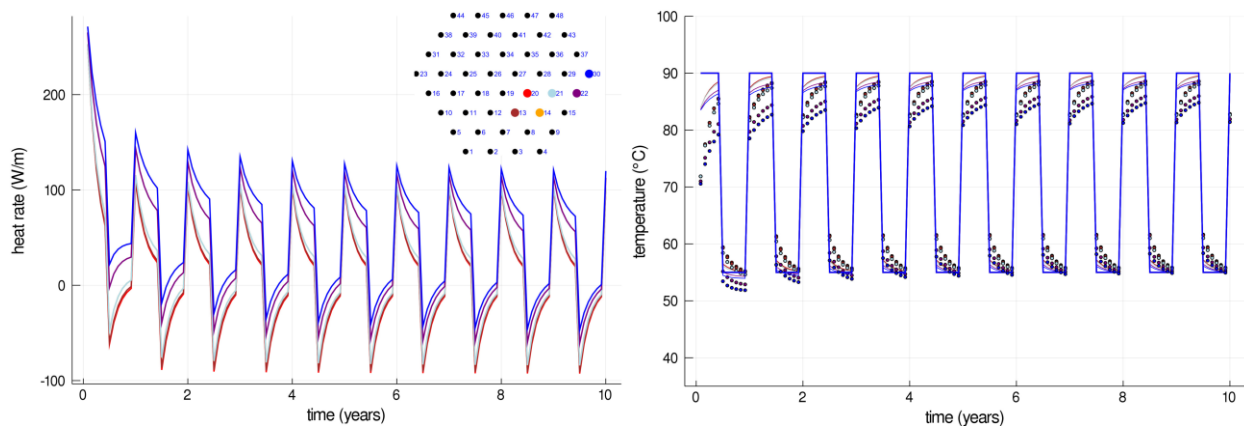**Table 3: yearly mean outlet temperatures during injection and extraction and yearly mean temperature of the storage, evaluated after 10 year of operation.**

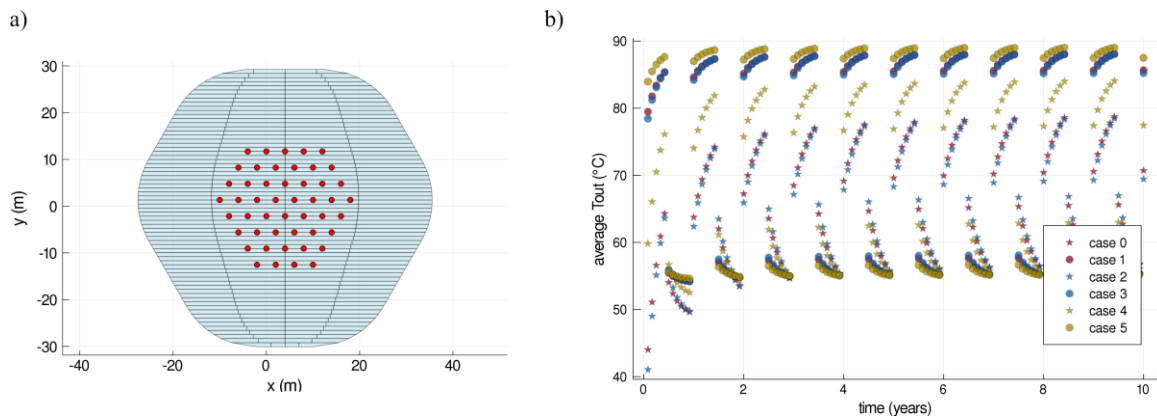| case	$\bar{T}_{out,inj}^{(year10)}$(°C)	$\bar{T}_{out,ext}^{(year10)}$(°C)	$\bar{T}_{storage}^{(year10)}$(°C)
0	75.3	60.3	45.1
1	87.1	56.2	47.1
2	74.6	60.9	45.5
3	86.9	56.4	47.6
4	81.4	58.7	46.8
5	88.4	55.7	47.9

Figure 8: a) Storage domain $V\epsilon_{1,\tau_d}$ obtained considering ϵ equal to 0.01.The plot show also the discretization utilized for the numerical the integrations evaluated on $V\epsilon_{1,\tau_d}$.9. b) mean outlet temperatures from the loops for each of the study cases.

3.2 Energy analysis

Energy flows injected and extracted from the BTES were calculated along with the energy stored in the BTES domain. Efficiencies were calculated as described in section 2.3. Table 4 and 5 show the values obtained for a number of relevant quantities after 10 years of operation for the 6 study cases investigated.

The results show that under the considered operational strategy (constant mass flow rate per branch and constrained input temperature), systems in parallel arrangement can extract and inject a significantly higher amount of heat than the series arrangement. The series arrangement is supplied with 1/6 of the mass flow and in order to achieve the same heat exchange would have to reach a temperature difference between inlet and outlet of the chain equal to 6 time the ΔT in a single borehole for the parallel arrangement case. This condition does not occur for the simulated cases. As seen in section 3.2, the increased extraction obtained with parallel arrangement comes at the cost of a lower extraction temperature. Improvement in the grouting material is beneficial and can highly improve the energy extracted. Further increase in the extraction/injection performance can be achieved by increasing the flow rate.

The difference in the net heat exchanged between the two arrangements is still in favor of parallel but it is less pronounced compared to the difference in extraction rate. As a consequence, the difference in heat stored within the storage volume is relatively low for the

6 cases considered (figure 9). As seen in section 3.1 this difference corresponds to a variation of around 2 °C in the mean temperature of the storage volume.

Figure 10 shows the seasonal efficiency and the storage efficiencies as a function of time. The first figure measure the performance in exchanging heat with the storage while the second figure assess the performance of the storage in maintaining the heat within the storage volume. The two plots shows opposite trends. While the efficiency η increases in time, the efficiency $\eta_{V\epsilon}$ decreases in time. This fact is depicted in figure 11. As time increases the temperature within the borehole storage increases easing the process of extracting energy at high temperature. On the other hand, more and more energy diffuses across the BTES boundary and therefore is not recoverable under the current operation.

Another observation that can be done by looking at Figure 10 is that there is a significant gap in seasonal efficiencies between the various solutions investigated. The gap in energy efficiency is readily explained by the inability of the series connected borehole to exchange as much energy as the parallel configurations. Increasing the flow by a factor 2 helps mitigate this issue and reduce this gap.

Table 4: Results of energy analysis evaluated after 10 year of operation.

case	$Q_{in}^{(year10)}/H$ (MWh/m)	$Q_{out}^{(year10)}/H$ (MWh/m)	$Q_{exchanged}^{(tot)}/H$ (MWh/m)	$Q_{stored, V\epsilon1}$ (MWh/m)	$Q_{stored, V\infty}$ (MWh/m)	$\eta^{(year 10)}$	$\eta_{stored, V\epsilon1}$	$H_{stored, V\epsilon\infty}$
0	10.765	3.924	104.627	55.560	104.627	0.364	0.531	1
1	12.685	5.527	111.930	58.568	111.930	0.436	0.523	1
2	11.244	4.363	105.852	56.051	105.852	0.388	0.530	1
3	13.392	6.172	113.697	59.292	113.697	0.461	0.521	1
4	12.552	5.480	110.459	57.944	110.459	0.437	0.525	1
5	13.732	6.483	114.525	59.635	114.525	0.472	0.521	1

Table 5: Results of energy in terms of percentage change compare to reference case 0

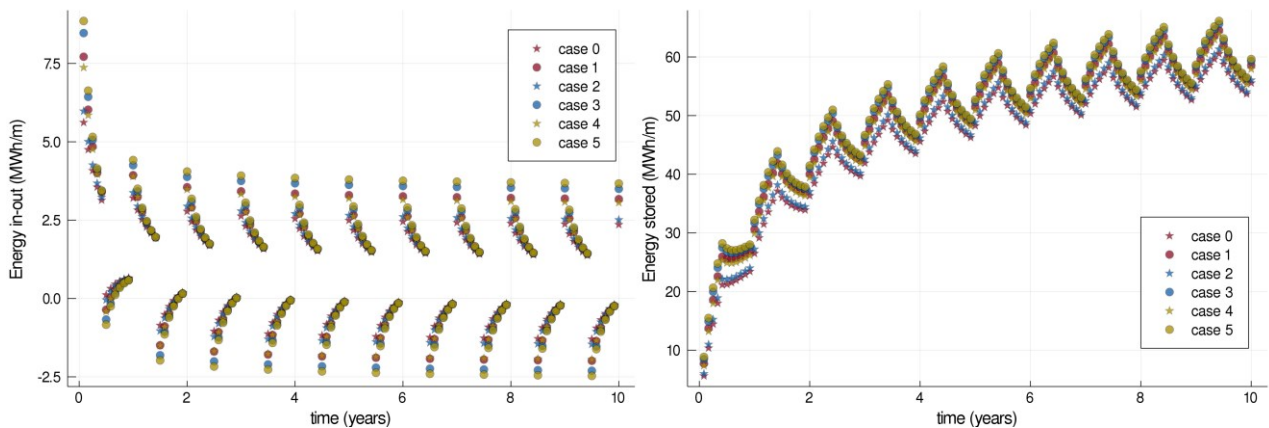| case	$Q_{in}^{(year10)}/H$	$Q_{out}^{(year 10)}/H$	$Q_{exchanged}^{(tot)}/H$	$Q_{stored, V\epsilon1}$	$Q_{stored, V\infty}$	$\eta^{(year 10)}$	$\eta_{stored, V\epsilon1}$	$\eta_{stored, V\epsilon\infty}$
1	+17.83	+40.85	+6.97	+5.41	+6.97	+19.53	-1.46	+0
2	+4.45	+11.19	+1.17	+0.88	+1.17	+6.45	-0.28	+0
3	+24.40	+57.28	+8.66	+ 6.71	+8.66	+26.42	-1.79	+0
4	+16.59	+39.67	+ 5.57	+4.29	+5.57	+19.78	-1.21	+0
5	+27.56	+65.22	+9.46	+7.33	+9.46	+29.51	-1.94	+0

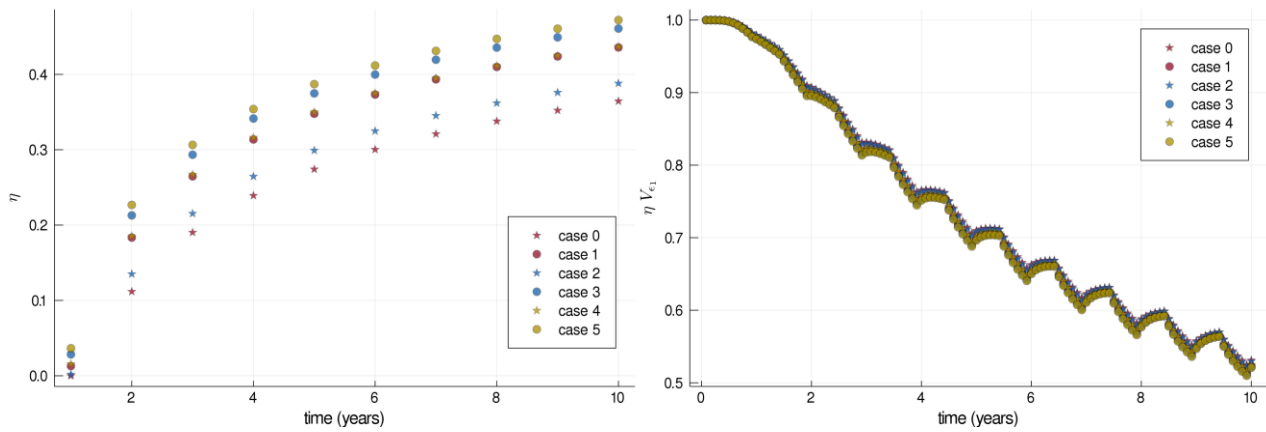**Figure 9: Energy injected and extracted and energy stored within the control volume $V\epsilon1$.**

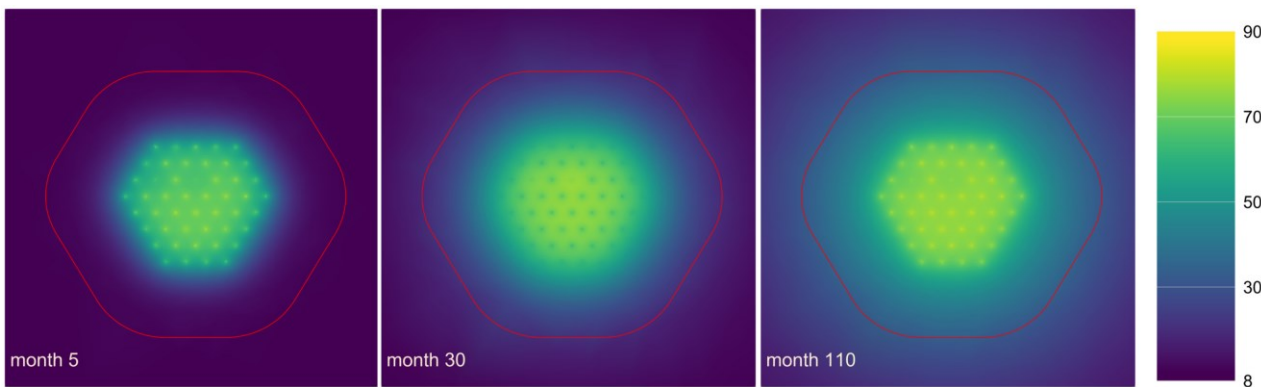**Figure 10: Seasonal energy efficiency η and storage energy efficiency η$_{V\epsilon 1}$.**

Figure 11: Evolution of the temperature field (in °C) during the operation of the BTES. The red line is the borehole storage boundary considering that maximum 1% of the heat outside this region can be recovered by the boreholes under the current operation.

3.3 Exergy analysis

Analogous parameters to the ones just presented in section 3.2 were calculated also in terms of exergy. Table 6 and 7 show the values obtained for each of the relevant quantities after 10 years of operation in the various study cases investigated. Similarly to what already observed in the energy analysis section, the exergy extracted in the BTES is significantly larger for systems in parallel arrangement with comparable mass flow rate per branch. Improvement in the heat exchanger and increase in flow increase these figures.

Regarding exergy efficiencies, Figure 13 shows that the spread in the values of seasonal exergy efficiencies in the different cases is much lower compared to the spread observed in figure 10 for energy efficiencies. This result reflect the fact that although the series BTES exchanges a lower amount of power compared to the parallel BTES, it injects this heat at a lower temperature and extract it at a higher temperature exploiting the stratification in the storage.

Another observation that can be done is that the exergy efficiency of the storage shows more significant variations compared to the energy efficiency of the storage which was almost indistinguishable between the different cases. The configurations connected in parallel yields a ψ$_{stored, V\epsilon 1}$ that is around 10% lower compared to series configuration. This reflects the fact that injection of higher temperature heat in the outer boreholes results in higher exergy losses and that the better stratification obtained in the storage contribute in reducing exergy destruction. This cannot be observed in the energy losses η$_{V\epsilon 1}$.which give very similar values for all the configurations.

Figure14 summarize the results for both seasonal efficiencies and storage efficiencies at 10th year of operation. The figure clearly shows that higher values of η do not necessarily corresponds to lower losses from the storage volume. In fact the configuration yielding the lowest seasonal energy and exergy efficiencies is also the one retaining the highest exergy storage efficiency ψ$_{stored, V\epsilon 1}$. This example shows how using several parameters to analyze and compare different BTES configurations can improve the understanding of the system and provide insight to improve the design

Table 5: Results of exergy analysis evaluated after 10 year of operation.

case	$Ex_{in}^{(year10)}/H$ (MWh/m)	$Ex_{out}^{(year10)}/H$ (MWh/m)	$Ex_{exchanged}^{(tot)}/H$ (MWh/m)	$Ex_{stored, Vc1}$ (MWh/m)	$Ex_{stored, V\infty}$ (MWh/m)	$\psi^{(year\ 10)}$	$\psi_{stored, Vc1}$	$\psi_{stored, V\infty}$
0	2.251	0.598	22.572	3.592	4.406	0.266	0.159	0.195
1	2.822	0.804	27.864	3.947	4.895	0.285	0.142	0.176
2	2.341	0.670	22.858	3.650	4.486	0.286	0.160	0.196
3	2.976	0.901	28.676	4.038	5.020	0.303	0.141	0.175
4	2.709	0.822	26.020	3.875	4.795	0.303	0.149	0.184
5	3.075	0.938	29.539	4.083	5.079	0.305	0.138	0.172

Table 6: Results of exergy analysis in terms of percentage change compare to reference case 0.

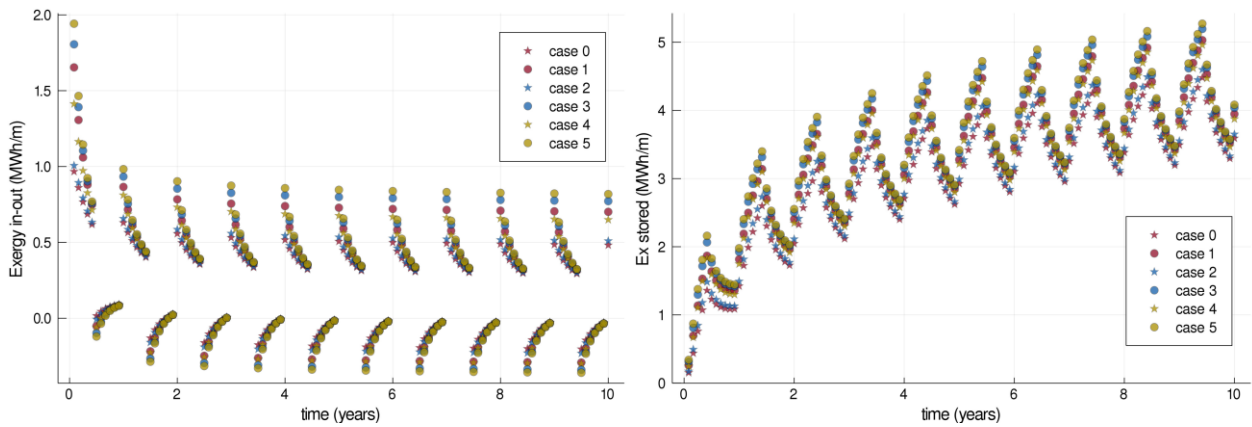| case	$Ex_{in}^{(year10)}/H$	$Ex_{out}^{(year10)}$	$Ex_{exchanged}^{(tot)}/H$	$Ex_{stored, Vc1}$	$Ex_{stored, V\infty}$	$\psi^{(year\ 10)}$	$\psi_{stored, Vc1}$	$\psi_{stored, V\infty}$
1	+ 25.37	+34.57	+23.44	+9.88	+11.09	+7.33	-10.98	-10.0
2	+ 4.01	+12.01	+1.26	+1.62	+1.81	+7.68	+0.35	-0.54
3	+32.20	+50.64	+27.04	+12.43	+13.92	+13.94	-11.50	-10.34
4	+20.36	+37.53	+15.27	+7.87	+8.82	+14.26	-6.42	-5.60
5	+36.62	+56.88	+30.86	+13.66	+15.28	+14.82	-13.14	-11.9

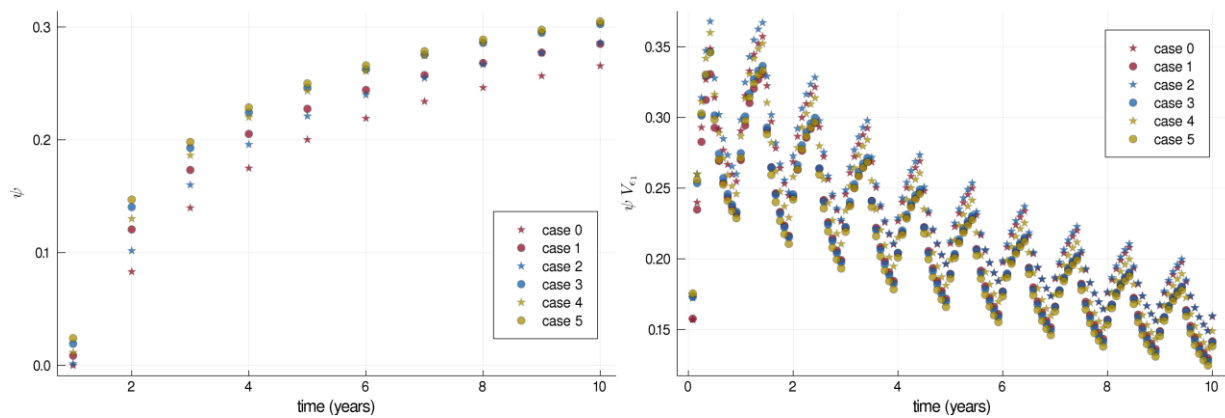**Figure 12: Exergy injected and extracted and exergy stored within the control volume Vc1.**

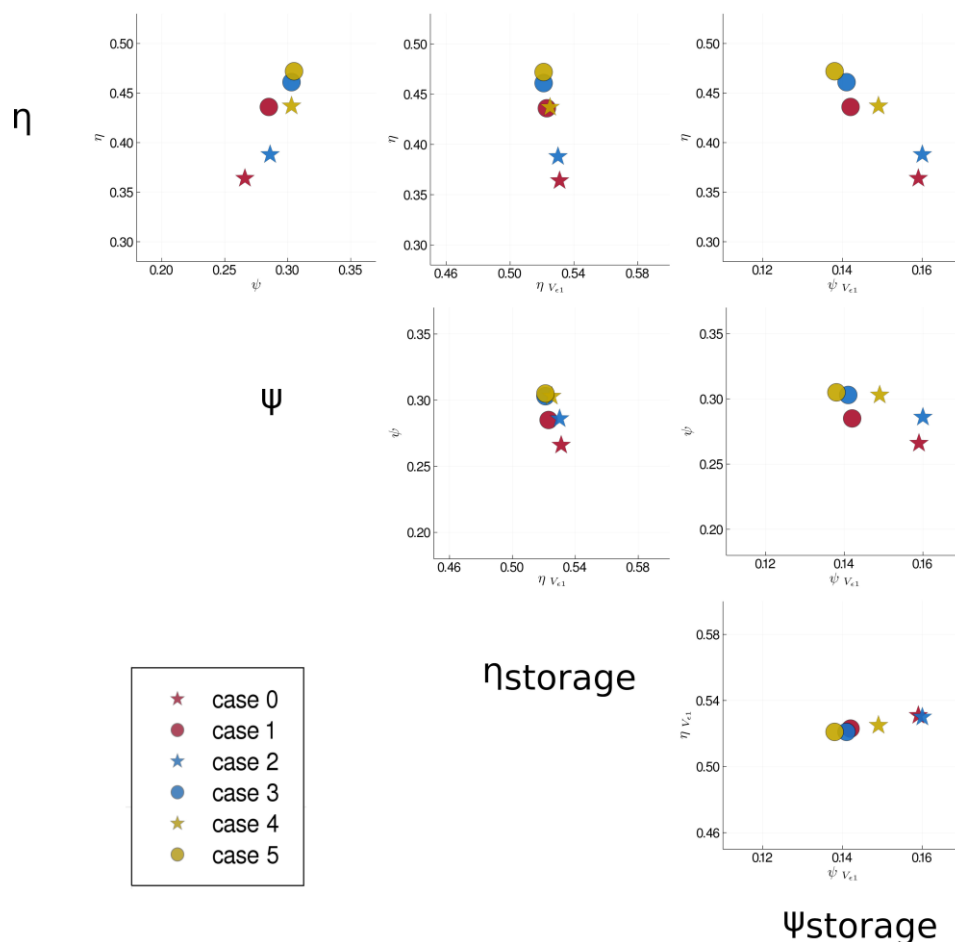**Figure 13: Seasonal exergy efficiency η and storage exergy efficiency ηVc1.**

Figure 14: Parameters η, ψ, η$_{Vc1}$, ψ $_{Vc1}$, for the 6 study cases at the 10th year of operation.

3.4 Limitations of the current approach

The results showed in this paper are calculated using the ILS solution to model the ground. This approach eases the process of numerical integration which was necessary to compute some of the performance indicators investigated in this paper. On the other hand, the ILS solution is known to present a significant deviation in the long term thermal behavior compared to three dimensional models such as the Finite Line Source, since it does not account for heat transfer in the axial direction. For this reasons the results shown in this paper should not be taken as absolute figures of the actual behavior of the system. Instead they should be seen as qualitative results that are used to display the potential use of the considered indicators to evaluate performance of the system but also to better understand its behavior.

4. CONCLUSIONS

The comparison of BTES systems with different configurations and different operating conditions is a non-trivial problem. The seasonal energy efficiency η is the most utilized parameters for this task. Although η is indeed a very important parameter, it is not sufficient to fully characterize the system operation and performance.

A first step into investigating a viable methodology for performance analysis of high temperature BTES systems has been presented in this paper. We explored the use of figures based on temperature, energy, and exergy and we evaluated these parameters as inlet and outlet quantities but also within the storage volume.

In order to test this approach, a BTES model based on classical analytical solution was developed. along with methods to compute energy stored, exergy stored in the ground storage control volume.

The method was illustrated with the help of 5 study cases to one reference case where the boreholes are connected in series and each borehole loop uses constant mass flow rate, with fluid circulation going from the center to the outer region during injection and in the opposite direction during extraction (injection and extraction temperatures of 90 °C and 55 °C, respectively). The reference temperature was chosen to be equal to the undisturbed ground level and control volume around the boreholes was chosen in such a way that that it contains a percentage of the overall heat injected after a time corresponding to the time for the discharge cycle. The borehole arrangement (series/parallel) were varied and mass flow rate and grout thermal conductivity were increased in the study cases.

Lazzarotto et al.

The study cases investigated helped highlighting the richness of the system behavior and how a single parameter can hardly fully characterize the performance of the system.

5. ACKNOWLEDGMENTS

REFERENCES

Aneke, M.: Wang, M. Energy storage technologies and real life applications – A state of the art review. *Applied Energy* **179**, (2016) 350–377.

Chu, S., Majumdar, A., 2012. Opportunities and challenges for a sustainable energy future. Nature 488, 294–303. https://doi.org/10.1038/nature11475

Cimmino, M.: G-functions for bore fields with mixed parallel and series connections considering axial fluid temperature variations, in: Proceedings of the IGSHPA Research Track (2018).

Cimmino, M.: Fluid and borehole wall temperature profiles in vertical geothermal boreholes with multiple U-tubes. *Renewable Energy* **96**, Part A, (2016), 137–147 .

Dincer, I., Rosen, M.: Thermal Energy Storage: Systems and Applications, 2nd ed. Wiley (2010).

Dunn, B., Kamath, H., Tarascon, J.-M., 2011. Electrical Energy Storage for the Grid: A Battery of Choices. Science 334, 928–935. https://doi.org/10.1126/science.1212741

Gehlin, S: Borehole thermal energy storage, in: Rees, S.J. (Ed.), Advances in Ground-Source Heat Pump Systems. Woodhead Publishing, (2016) pp. 295–327.

Jack, M.W., Wrobel, J., 2009. Thermodynamic optimization of a stratified thermal storage device. *Applied Thermal Engineering* **29**, (2009), 2344–2349.

Kallesøe, A.J. et al: HEATSTORE Underground Thermal Energy Storage (UTES) – state-of-the-art, example cases and lessons learned (2019).

Kizilkan, O., Dincer, I.:. Exergy analysis of borehole thermal energy storage system for building cooling applications. *Energy and Buildings* **49**, (2012), 568–574.

Lazzarotto, A.: A network-based methodology for the simulation of borehole heat storage systems. *Renewable Energy* **62**, (2014), 265–275.

Malmberg, M., Mazzotti, W., Acuña, J., Lindståhl, H., Lazzarotto, A: High temperature borehole thermal energy storage - A case study, in: Proceedings of the IGSHPA Research Track (2018).

Mohd, A., Ortjohann, E., Schmelter, A., Hamsic, N., Morton, D., 2008. Challenges in integrating distributed Energy storage systems into future smart grid, in: 2008 IEEE International Symposium on Industrial Electronics. Presented at the 2008 IEEE International Symposium on Industrial Electronics, pp. 1627–1632. https://doi.org/10.1109/ISIE.2008.4676896

Moriarty, P., Honnery, D., 2016. Can renewable energy power the future? Energy Policy 93, 3–7. https://doi.org/10.1016/j.enpol.2016.02.051

Pickard, W.F., 2014. Smart Grids Versus the Achilles' Heel of Renewable Energy: Can the Needed Storage Infrastructure Be Constructed Before the Fossil Fuel Runs Out? Proc. IEEE 102, 1094–1105. https://doi.org/10.1109/JPROC.2014.2316359

Rosen, M.A., Dincer, I.: 2003. Exergy methods for assessing and comparing thermal storage systems. *International Journal of Energy Research* **27**, (2003) 415–430

Rosen, M.A., Tang, R., Dincer, I.: 2004. Effect of stratification on energy and exergy capacities in thermal storage systems. International Journal of Energy Research **28**, (2004) 177–193.

Sliwa, T., Rosen, M.A.:. Efficiency analysis of borehole heat exchangers as grout varies via thermal response test simulations. Geothermics 69, 132–138. (2017).

Tordrup, K.W., Poulsen, S.E., Bjørn, H.: An improved method for upscaling borehole thermal energy storage using inverse finite element modelling. Renewable Energy 105, 13–21. (2017).

PUBLICATION 2 : Performance Evaluation of a High Temperature Borehole Thermal Energy Storage Under Influence of Groundwater Flow

Master of Science Thesis

Department of Energy Technology

KTH 2020

**Performance Evaluation of a High Temperature
Borehole Thermal Energy Storage Under Influence of
Groundwater Flow**

TRITA-ITM-EX 2020:617

Max Hesselbrandt

Approved	Examiner	Supervisor
	Björn Palm	Alberto Lazzarotto
	Commisioner	Contact person
	Bengt Dahlgren AB	José Acuña

Abstract

Recent years have seen a growing interest in large-scale high-temperature borehole thermal energy storage (HT-BTES) as a means to store industrial waste heat and solar energy between the seasons. A profound understanding and characterization of the thermal and hydraulic processes involved in such systems is required for the optimal design as well as for environmental assessments of the storage.

In this work, the importance of groundwater flow effects on the thermal performance of HT-BTES has been studied. The current research status on groundwater flow and transport modeling techniques applied in the field of shallow geothermal energy as well as in other geosciences disciplines has been reviewed. A finite element heat conduction model of an existing HT-BTES located in dry heterogeneous soil has been developed and validated against operational and monitoring data. The heat conduction model provided a basis by which to compare the behaviour and performance of the storage under influence of groundwater flow. Numerical experiments were conducted considering both pure heat conduction as well as different scenarios accounting for groundwater flow. A performance evaluation study based on key performance indicators in terms of energy and exergy efficiencies has been carried out to quantify the impact of groundwater flow on the amount and quality of the heat being stored and exchanged. The analysis shows that the presence of groundwater flow is in general detrimental to the energy and exergy performance of the HT-BTES. The results indicate, however, that small groundwater flow rates also can have a slight positive effect on seasonal energy and exergy efficiencies as compared to case of pure conduction. Further studies are though needed where a wider range of time scales, BHE designs, operation conditions and subsurface conditions are adressed.

From the inherent uncertainties associated with subsurface flow and transport processes it follows that general guidelines on how and under what conditions groundwater flow may have impact on BTES design and performance are difficult to provide. The characteristics of these processes in porous, and particularly fractured, media are often very site-specific and scale dependent, making it a challenging task to select and use an appropriate modeling approach that can capture all relevant features of the problem. To face this challenge, various modeling approaches, typically based on deterministic and stochastic continuum or discrete fracture network concepts, have been developed within the field of subsurface flow and transport modeling. To widen the modeling framework typically employed in shallow geothermal energy applications, their applicability also in the context of BTES modeling could be explored.

Sammanfattning

Intresset för säsongslagring av industriell överskottsvärme och solenergi genom högtemperaturborrhålslager (HT-BTES) har på senare år ökat. För att möjliggöra en optimal design av dessa system, samt för att bedöma deras inverkan på omgivande miljö, krävs djupgående förståelse och karaktärisering av de kopplade termiska och hydrauliska processer som påverkar lagret.

I detta arbete har grundvattenflödets inverkan på högtemperaturlagers termiska prestanda behandlats. Nuvarande kunskapsläge inom modellering av grundvattenflödes- och transportprocesser i porösa och sprickiga medier har granskats, liksom dess användning inom geoenergi och andra geovetenskapliga områden. En värmeledningsmodell av ett befintligt HT-BTES i torr, heterogen jord har utvecklats genom finita elementmetoden och validerats mot mätdata. Värmeledningsmodellen tillämpades som referens för jämförelse med utökade modeller i vilka inverkan av grundvattenströmning beaktats genom kopplade hydro-termiska beräkningar. En utvärdering av lagrets prestanda med avseende på nyckelindikatorer i form av energi- och exergiverkningsgrad har utförts för att kvantifiera inverkan av grundvattenflödet på mängden och kvaliteten av den värme som överförs och lagras genom borrhålslagret. Resultaten visar att förekomsten av grundvattenströmningar genom lagret generellt har en negativ inverkan på dess energi- och exergiverkningsgrad. Däremot finns det i resultaten indikationer om att låga grundvattenflöden även kan bidra till en svagt positiv effekt jämfört med fallet med ren värmeledning. Vidare och mer omfattande studier bör dock utföras där längre tidsskalor samt en större uppsättning lagerdimensioner, driftscenarion, och markförhållanden beaktas.

Till följd av att det kring strömnings- och transportprocesser i mark alltid råder inneboende osäkerheter är det svårt att upprätta generella riktlinjer kring hur och under vilka omständigheter ett grundvattenflöde kan ha inverkan på ett borrhålslagers design och prestanda. Typiskt för dessa processer i porösa och i synnerhet sprickiga medier är att de är mycket platsspecifika och skalberoende, vilket medför utmaningar vid valet av ett lämpligt modellkoncept för att beskriva dem med erfoderlig precision. Detta har lett till att ett stort antal modelleringskoncept har utvecklats och prövats för detta ändamål, vilka främst baseras på antaganden om deterministiska eller stokastiska kontinuum och diskreta spricknätverk. Tillämpbarheten av dessa modellkoncept även för modellering av HT-BTES bör undersökas och utvärderas för att möjliggöra analys av borrhålslager under inverkan av komplexa strömningsförhållanden.

Acknowledgement

Table of Contents

1 Introduction

1.1 Background

Increasing concerns on climate change and energy shortage has given rise to a growing attention towards high-performance energy technologies that harness energy sources in a sustainable manner. Waste heat recovery and thermal energy storage systems have been identified as key enablers for meeting climate neutrality targets and expanding the use of renewable energy resources (Bianchi et al., 2019; Wheatcroft et al., 2020). In climate regions where large seasonal temperature variations prevail, borehole thermal energy storage (BTES) is a promising means for meeting temporal mismatches between energy availability and demand. BTES systems consist of an array of vertical closed or open loop borehole heat exchangers (BHE) inserted into the ground. In the non-heating season months, energy from solar thermal collectors, industrial waste heat or other sources is transferred to the boreholes and stored as sensible heat in the surrounding soil or rock mass. The storage can be discharged whenever the heating demand increases, thus balancing the seasonal phase difference between energy demand and supply.

Sustainable design and operation of single and multiple BHEs has been an integral aspect in research and development of BTES technology and other types of shallow geothermal systems. Both theoretical and experimental investigations have been carried out to study reliability and long-term behavior of thermally interacting BHEs (Rybach and Eugster, 2010; Rybach and Mongillo, 2006; Signorelli et al., 2005). Major efforts have involved the development of modeling techniques for predicting and analyzing the thermal processes ocurring inside the borehole and in the surrounding ground (Eskilson, 1987; Hellström, 1991; Zeng et al., 2002). Accurate prediction of both short-term and long-term BHE fluid temperatures is crucial to the design and evalutation of BHE systems. Most existing design tools (ASHRAE, 2015; BLOCON, 2017; Pahud et al., 1996) are based on semi-analytical models for solving the spatiotemporal temperature response to a thermal load on the ground with different combinations of borehole geometries and field configurations. These tools benefit from quick calculation times, which drastically shortens the iterative process of determining appropriate dimensions of the BTES system. The mathematical models used do however rely on simplifying assumptions, viz., that the heat is transferred only by pure conduction in a homogeneous and isotropic medium (Spitler and Bernier, 2016). Consequently, any effects of groundwater flow in porous media or through fractured rock are assumed to be negligible.

Several authors have questioned the validity of these assumptions. (Chiasson et al., 2000), (Sutton et al., 2003) and (Diao et al., 2004) reported that the presence of groundwater flow may have non-negligible or significant impact on the ground resistance compared to a case of pure conductive heat transfer. Given the objective of maintaining the temperature anomalies within the storage volume as large as possible at all times, any process of heat transport across the storage boundaries will contribute to heat losses from the system and can thus have detrimental effects on the performance. Since many BTES systems rely on designs and operation strategies that are intended to promote thermal stratification inside the storage, additional heat transport due to advection may also act to smooth out temperature gradients and thus cause exergy destruction. Hence, neglecting the influence of groundwater flow in the design process may result in conservative or inadequate solutions (Spitler and Bernier, 2016; Zhang et al., 2015), and BTES systems may be negatively impacted by groundwater advection (Banks, 2015; Nguyen et al., 2017).

To date there is a paucity of literature on groundwater effects on BTES system performance (Angelotti et al., 2014). Further investigation is required to provide guidance on understanding subsurface heat transport processes in BTES applications. In addition, no consistent framework has yet been established to provide a methodology for analyzing and comparing thermal performance of BTES systems that are subjected to different subsurface and operating conditions (Lazzarotto et al., 2020). Hence, further efforts need to be undertaken in planning, design, and operation of BTES systems, including development of in-situ characterization and modeling techniques, performance optimization tools and system monitoring practices and procedures. Development of accurate simulation models and detailed energy and exergy analyses of the storage could help to improve performance and bring down uncertainties surrounding decisions about investment and implementation of BTES technologies.

1.2 Aims and objectives

This study sets out evaluate the importance of groundwater advection on the on the energy and exergy thermal performance of a high-temperature BTES. The study aims to investigate the contribution of advective heat transport to the overall heat flow and temperature degradation within and across the storage medium.

The main objectives of this work are to

1. Carry out a literature review on current research status on groundwater effects on BTES systems, and methods used in different research fields and engineering applications for modeling coupled hydro-thermal subsurface processes in various hydrogeological environments.

2. Develop and implement appropriate tools for numerical modeling of series-connected borehole heat exchanger arrays, to enable simulation of thermally stratified BTES systems with variable flow-direction control.

3. Develop a numerical 3D finite element-based pure-conduction model of an existing high-temperature BTES (HT-BTES) system located above the groundwater table and perform a model validation study using monitored operational data and ground temperature measurements. The pure-conduction model serves the purpose of validating the tool described in 2) and providing a reference scenario for comparison of thermal performance in this study.

4. Develop an extended coupled hydro-thermal model based on the reference scenario model and perform numerical experiments of the HT-BTES system accounting for heat advection, by imposing hypothetical hydraulic conditions in a saturated, confined, multi-layered porous medium.

5. Collect, define, and implement appropriate performance indicators and perform an energy and exergy thermal performance analysis based on the simulations of pure-conduction and coupled hydro-thermal models of the BTES system.

2 Literature review

In this section, a review on advective heat transport and groundwater effects in BTES and shallow geothermal applications is provided. An insight is developed into current modeling techniques and design concepts and practices in BTES development. Also given is a review of concepts and techniques for modeling of groundwater flow and heat transport employed in other related fields, such as groundwater resources management, nuclear waste disposal, and deep geothermal energy exploition.

Accurate modeling and simulation of borehole heat exchangers has been a challenging task because of the vastly varying spatial and temporal scale perspectives of the heat transport processes involved. Simulating the exchange of heat between the heat carrier fluid with the surrounding ground involves solving a local heat transport problem along an extremely slender borehole, and coupling the solution to a global problem that considers thermal processes occuring in the ground due to a single or multiple interactive BHEs. The temporal scale of these processes ranges from seconds to years, making it difficult to catch all relevant features of the processes within a single simulation model. In addition, other parameters such as groundwater movements, phase change conditions and non-uniform ground temperature distribution due to surface effects, geothermal heat flow, ground heterogeneity etc. may add complexity to the heat transport problem under consideration.

During the last decades, research on BHE modeling has mainly focused on numerical, analytical, or semi-analytical approaches for analyzing local thermal processes inside the borehole and pure conduction heat transfer processes in homogeneous and isotropic ground. Early contributions include the work by Eskilson (Eskilson, 1987; Eskilson and Claesson, 1988), who introduced the concept of g-functions to model the thermal response of single or multiple interactive BHEs, and (Hellström, 1991) who developed the duct storage model (DST) for simulating thermal processes inside heat storages consisting of uniformly placed BHEs or pile heat exchangers. (Semi-) analytical BHE modeling approaches have also been widely studied and applied to approximate the BHEs as infinite line (Carslaw and Jaeger, 1959; Ingersoll et al., 1954), finite line (Cimmino et al., 2013; Lamarche and Beauchamp, 2007; Zeng et al., 2002) or cylindrical heat sources (Bernier, 2001).

While heat conduction models have been thoroughly investigated and established in design tools used for both academic and commercial purposes (Zhang et al., 2018), approaches to model advection-diffusion based heat transport processes have received far less attention in research in ground source heat pump (GSHP) and BTES technologies (Banks, 2015). In recent years, however, a growing interest has developed in groundwater effects on GSHP and BTES thermal performance and related subjects. Noteworthy studies dealing with analytical modeling of coupled groundwater flow and heat transfer in porous media are (Sutton et al., 2003) and (Diao et al., 2004), who developed ground resistance models based on the moving infinite line source (MILS) solution to the advection-diffusion equation. (Molina-Giraldo et al., 2011b) further developed the MILS theory by introducing a solution to the moving finite line source (MFLS) problem to account for axial effects and constant surface temperature, and (Katsura et al., 2020) derived an approximate solution of the moving infinite cylinder source model. (Molina-Giraldo et al., 2011a) and (Chiasson and O'Connell, 2011) also considered the effect of thermal dispersion upon advective and conductive heat transport. All these models presume simplified conditions such as homogeneous and isotropic ground material properties, uniform and steady groundwater flow, and constant ground surface temperature. However, recently developed analytical models have made it possible to account also for spatial and temporal variations in ground surface temperature (Rivera et al., 2015), and non-uniform groundwater flow in vertically-layered porous media (Hu, 2017).

Numerical models based on finite volume, finite element and finite difference methods have been proposed to better represent actual surface and subsurface conditions, or for enabling investigation of the effects of other groundwater related transport phenomena on shallow geoethermal systems (e.g. unsaturated moisture migration, freezing and thawing processes etc.). Several numerical parameter studies have been carried out to investigate the effects of groundwater flow on BHE systems with different field configurations and orientations, flow velocities, material properties, heat loading conditions etc., most of them assuming uniform 3D flow under homogeneous and isotropic ground conditions (Angelotti et al., 2014; Catolico et

al., 2016; Choi et al., 2013; Dehkordi et al., 2015b; S. Emad Dehkordi and Schincariol, 2014; Nguyen et al., 2017; Yang et al., 2013). Quite a few studies have considered heterogeneous ground conditions or groundwater flow occuring along discrete pathways; (Nguyen et al., 2015) and (Gehlin and Hellström, 2003) studied thermal impacts of groundwater flow on BHEs in heterogeneous fractured domains represented as equivalent porous media. (Gehlin and Hellström, 2003) also performed simulations considering the effect of a single, discrete fracture, and a similar approach was adopted by (Dehkordi et al., 2015a) to study the effect of multiple vertical discontinuities forming a discrete, interconnected fracture system. (Diersch and Bauer, 2014) performed numerical experiments with a BTES system in stratified soil to investigate the influence of groundwater flow on the storage efficiency, and (Luo et al., 2014) performed a comparative analysis of advection effects on thermal exchange rates in BHEs inserted in homogeneous and layered heterogeneous ground, respectively.

In general, conclusions reported in the literature show an agreement that occurence of groundwater movements can be both beneficial and detrimental to GSHP and BTES thermal performance, and that this is substantially determined by the intented mode of operation of the system. For systems operating dominantly in heat extraction or injection mode, heat advection effects are considered to have positive impact because of the tendency to reduce near-borehole temperature anomalies induced during operation. In contrast, regarding systems designed for heat storage (i.e., BTES systems), moving groundwater may carry stored heat away from the storage site, thus introducing additional losses resulting in impairment of performance. This is particularly true for HT-BTES systems, which operate at fairly elevated temperatures with respect to undisturbed subsurface temperatures. Also, under specific conditions, BTES performance may be further influenced by heat losses caused by moisture migration in the vadose zone or density-driven groundwater movements (Catolico et al., 2016; Moradi et al., 2015).

In their comprehensive review on groundwater aspects in GSHP system development, (S.E. Dehkordi and Schincariol, 2014) pointed out the lack of consideration of flow and heat advection processes given in current guidelines, regulations, and design practises concerning especially closed-loop systems. Indeed, only a few cases can be found in the literature where in-situ hydrogeological conditions have been thoroughly mapped and considered in design, operation and monitoring of existing or planned closed-loop shallow geothermal systems. Of these, most are medium to large scale or pilot BTES plants, some examples being the Crailsheim BTES (Bauer et al., 2009; Mielke et al., 2014) and Paskov BTES (Grycz et al., 2014; Rapantova et al., 2016). Besides the fact that candidate sites for implementing BTES systems are likely to be selected because of suitable hydrogeological characteristics, e.g. no or moderate occurrence of groundwater or hydraulic gradients (see for example (Lanini et al., 2014; Nordell et al., 2016; Nußbicker et al., 2003)), other possible reasons that can be brought up to explain why groundwater effects have been neglected or simplified in BTES development include lack of integration between geosciences and HVAC disciplines (S.E. Dehkordi and Schincariol, 2014) and that extensive, multidisciplinary field investigation campaigns, although necessary for optimal technical design (Luo et al., 2016), may entail high costs.

A related hurdle is that inherent compositional and spatial diversity of subsurface conditions commonly causes large variations in groundwater flow characteristics in different scales and domains, which creates difficulties in providing guidelines on, for example, critical threshold flow rates for which both advective and diffusive heat transport may be of significance. Existing attempts to provide such guidelines (Angelotti et al., 2014; Banks, 2015; Molina-Giraldo et al., 2011a) are based on assumptions of uniform groundwater flow, thus neglecting possible impacts of ground heterogeneity and anisotropy. This issue has also been addressed concerning guidelines applicable for aquifer thermal energy storage (ATES) design (Sommer et al., 2013). It is worth mentioning that values of physical properties (expressed in terms of thermal diffusivity) that govern the rate of heat conduction typically vary over a range of ~1 order of magnitude in saturated ground (Andújar Márquez et al., 2016), whereas the corresponding parameter in groundwater flow analogy (hydraulic diffusivity) can take values that span over an extreme range of orders of magnitude (Pacheco, 2013). It has also been shown that these heterogeneities appear at a wide range of spatial scales, e.g. from microscopic pore scale to macroscopic aquifer scale (Le Borgne et al., 2004; Wheatcraft and Tyler, 1988). In this context, one might raise the question whether an assumption of homogeneous and isotropic ground is applicable and adequate to meet the requirements on accuracy in modeling, design, and analysis of

monitoring data in BTES applications. If not, what spatial scale and complexity level should be considered when approaching the problem, and what is the importance of the specific geological and hydrogeological characteristics of the subsurface media?

In hydrogeology, the scale-effect problem has been a topic of discussion for many years (Berkowitz, 2002; Neuman, 1990). Various studies have reported that hydraulic properties investigated in field or laboratory appear to be functions of the scale of the test or measurement (Maréchal et al., 2004; Rovey, 1994). According to (Nastev et al., 2004), this effect can be attributed to a combination of factors, including ground heterogeneity as well as the scale and spatial repartition of the measurements.

In the field of groundwater flow and subsurface transport modeling, a wide variety of modeling approaches and conceptual models has been developed and adopted to face the challenges related to scale effects, heterogeneity, and preferential flow in porous and fractured media (Bear and Cheng, 2010; Berre et al., 2018; Konikow, 2011). Considering that many problems involve investigation of large domains at e.g., aquifer or regional scale levels, continuum approaches have been widely used for this purpose. Because most subsurface flow and transport processes involve multiple phases, i.e., solids, liquids, and gases, that exchange mass, momentum and energy, describing and solving the coupled flow and transport problem at a microscopic level would require knowledge about the exact geometry of the phase interfaces and ability to measure quantities or determine model parameters within each of the phases. Instead, these complex issues can be circumvented by regarding the problem at a macroscopic level where the properties and behaviour of the different phases at the microscopic level are spatially averaged and assigned to every point of the porous medium domain, which thus can be treated as a single continuum or multiple continua representating each phase (Bear et al., 1993).

In his well-known book on groundwater hydraulics, (Bear, 1972) described the characteristics of porous media and introduced the concept of a representative elementary volume (REV) in soil hydrology. The existence of a REV is a fundamental assumption of continuum mechanics. In the averaging procedure used for transforming quantities and variables from microscopic to macroscopic scale, the REV describes the minimum volume, or range of volumes, for which the averaged quantities are independent of the size of the averaging volume. The porous medium can be inhomogeneous on scales larger than the minimum REV scale, and some systems may contain multiple REV scales. However, if a REV cannot be found within a given domain, the domain cannot be treated as a porous medium and the continuum assumption is not valid.

A continuum approach can in certain cases be justified also for the modeling of flow and transport in fractured rock, for example if the fracture system consists of a dense network of well-interconnected fractures. In continuum models, the fractures within the formation are represented implicitly without making any geometric distinction between the fractures and the rock matrix. Many fractured rock environments do not, however, possess any homogenization scale due to the lack of scale separation in the fracture network (Berre et al., 2018). In such situations, the continuum assumption is not applicable and a discrete fracture network (DFN) approach where fractures are represented explicitly may be required to accurately capture the flow and transport dynamics in the fractured rock.

Historically, typical applications of conceptual and numerical fluid flow and transport models in fractured rock have involved simulation of nuclear waste disposals (Joyce et al., 2014; Selroos et al., 2002), petroleum reservoir exploitation (Pruess, 1985), deep enhanced geothermal energy systems (Jacquey, 2017; Kalinina et al., 2012) and underground structuring (Chen, 2010; Karimzade et al., 2017). The complex nature of flow and transport in fractured media has led to the development of numerous characterization and modeling approaches, most of which are based on either one or a combination of the above-mentioned continuum or discrete fracture network concepts. In either case a deterministic or stochastic framework can be used to describe the fracture characteristics. Extensive reviews on the topic are given by (Berkowitz, 2002) and (Neuman, 2005), and more detailed information is given by (Bear et al., 1993), (Dietrich et al., 2005), (U.S. National Committee for Rock Mechanics, 1996), and (Adler, 1999).

3 Methodology

The methodology employed in this study for examining groundwater flow effects on BTES system thermal performance is introduced in this section. An approch based on numerical experiments of a HT-BTES system in porous media is followed, for which the commercial finite element code FEFLOW 7.1 (an acronym of Finite Element subsurface FLOW simulation system) was selected for coupled flow and heat transport modeling and simulations (Diersch, 2014). Finite element methods, although computationally expensive, have proven to be effective and accurate in modeling borehole heat exchanger systems (Diersch et al., 2011a; Ozudogru et al., 2015). To circumvent the need for fully discretizing the geometry of the BHEs within the finite element grid, various numerical and analytical approaches have been proposed for modeling local flow and thermal processes within the borehole (Al-Khoury et al., 2005; Al-Khoury and Bonnier, 2006; Eskilson and Claesson, 1988). The local problem can be linked to the global problem by 1D finite element representations of the BHE coupled to the 3D porous medium discretization. Based on the models provided by (Al-Khoury et al., 2005) and (Eskilson and Claesson, 1988), further extensions to support different BHE configurations (e.g. double U-pipe and coaxial pipe BHE) have been developed by (Bauer D. et al., 2011) and (Diersch et al., 2011b) and adapted to the FEFLOW simulator. Because of the combination of wide, accurate and computionally efficient BHE modeling techniques with detailed 3D analysis capabilities of coupled subsurface hydro-thermal processes, FEFLOW was deemed to be a suitable code for assessing groundwater impacts on BTES systems.

The procedure of the numerical experiments conducted in this study is summarized below and detailed in the following subsections. The methodology comprised six main stages:

1) A dataset comprising ~5 years of operational and monitoring data from an actual pilot HT-BTES plant located in Brædstrup, Denmark, was analyzed and preprocessed following the approach by (K. W. Tordrup et al., 2017), who performed an inverse modeling study of the Brædstrup BTES based on the initial two years of operation.

2) A plug-in for enabling simulation of series-connected BHEs with flow direction control was developed using the C++ programming language with the APIs available for FEFLOW. Not only is it required to consider actual operation conditions of the Brædstrup storage, but flow direction control is generally an important aspect in BTES design for maintaining horizontal temperature stratification in the storage to improve exergetic performance (Dincer and Rosen, 2007). Taking it into consideration is thus essential in BTES thermal performance assessment and analysis.

3) A 3D pure-conduction finite element model of the Brædstrup BTES was developed, for which the subsurface thermal properties inferred by (K. W. Tordrup et al., 2017) and time-aggregated operational data were taken as model inputs. The pure-conduction model served two purposes: partly for validating the plug-in tool described above, and partly for providing a validated simulation scenario in which the Darcy flux is known to be zero throughout the model. Since the storage is actually located well above the phreatic surface (K. W. Tordrup et al., 2017), no heat transport mechanisms other than conduction are likely to have significant impact on the thermal distribution close and within the storage domain, with the only possible exceptions being unsaturated moisture flow, advective infiltration in unsaturated seepage zones or local advection in small, perched aquifers. These site characteristics, in combination with extensive monitoring data comprising subsurface temperature measurements availabe, constitute a unique opportunity for characterizing the exergetic behaviour of a HT-BTES under ideal (i.e. well known) conditions.

4) The pure-conduction finite element model was extended to include heat advection by defining a hypothetical confined groundwater system within the model domain. This was accomplished by specifying steady Dirichlet boundary conditions on opposite (upstream-downstream) borders of the domain, thus imposing a uniform hydraulic gradient across the storage site. Also, hydraulic properties based on typical values taken from literature (Heath, 1983) were attributed to the model to represent the multi-layered soil composed of unconsolidated sediments present at the Brædstrup storage site.

5) Steady-flow, transient-transport simulations of the coupled hydro-thermal model were performed with varying hydraulic gradient. The BHE boundary conditions (fixed inlet temperature and flow rate) imposed

in the simulation of the pure-conduction model were applied also in these simulations, hence the unknown time-dependent parameters describing the outlet temperature of the heat carrier fluid and the temperature field throughout the domain were obtained as a function of hydraulic gradient.

6) Suitable simulation results for evaluating energy and exergy performances of the HT-BTES were gathered from all of the simulation runs, including the simulation of the pure-conduction model as a contrasting reference to the cases affected by heat advection. Following an approach similar to the one suggested by (Lazzarotto et al., 2020), energy and exergy efficiencies evaluated both at a system level (with respect to inlet and outlet energy/exergy flows) as well as within the storage were selected as Key Performance Indicators (KPIs).

3.1 Description of the Brædstrup pilot BTES plant

The Brædstrup pilot HT-BTES was implemented in 2011-2012 as part of a local district heating facility comprising combined heat and power gas turbines, electrical and gas boilers, solar thermal collectors, and hot water storage tanks. During summer, excess heat produced by the solar thermal collectors is transferred to and stored in the BTES. The BTES is discharged during non-productive times by means of a heat pump coupled to the storage.

A detailed description of the Brædstrup BTES and the subsurface geological and thermal settings at the storage site is given by (K. W. Tordrup et al., 2017) and (Sørensen et al., 2013). In Figure 1 an overview of the system is shown, including information on the lithology of the unconsolidated Quaternary glacial deposits in the area, configurations and dimensions of BHEs and observation wells, as well as the bore field arrangement.

The storage system consists of 48 grouted double U-pipe BHEs inserted to a depth of 45 m beneath two top layers of covering soil material and mussel shell insulation, each with a thickness of 0.5 m. As indicated in Figure 1, the soils at the site consist of alternating strata dominated by clay till, silt, sand and gravel. Measured water content levels (2-8% in the sand deposits) indicate that the soil is relatively dry. During drilling of the boreholes, water seepage was however encountered in the upper clay till layer (-3 to –9 m) and at a depth slightly beneath borehole bottom (-49 m), but these findings were probably due to temporary occurrence of snowmelt water or perched water (Sørensen et al., 2013). Instead, water levels monitored in some neighboring wells indicate that the groundwater table in the area is located at a depth of around 65-70 m ("GEUS," n.d.; K. W. Tordrup et al., 2017). That is, the borehole bottoms are located well above the groundwater table and hence dry-unsaturated conditions are likely to prevail in most points within the storage.

The heat exchanger boreholes are drilled 3 m apart in a hexagonal grid system. Since two single U-pipes are insert in each borehole, the system contains a total of 96 borehole loops that can be arbitrarily interconnected in series or parallel with a great variety of possible configurations. In this case, the U-pipes are arranged in 16 different arrays. As seen in Figure 1, the BHE arrays can be grouped into two different configurations, so that each contains one U-pipe per borehole. Hence, the two U-pipes installed within the same borehole are connected to separate arrays, each of which containing six series-connected loops ordered from the center to the periphery of the storage. When the storage is operated in charging mode, the heat carrier fluid flow is directed from the center, and in the opposite direction under discharging operation. These specific array arrangements combined with the flow-switching operation strategy serve the purpose of creating horizontal thermal stratification within the storage to improve temperature retention during the storing cycle.

In addition to the heat exchanger boreholes, five observation wells have been installed at different locations within (T1, T2, T3, T5) and outside (T4) the storage as shown in Figure 1. In each of the observation wells, temperature sensors for measuring soil temperature variations have been inserted at 20 fixed depth levels ranging from 0 m to -59 m beneath the insulation layer.
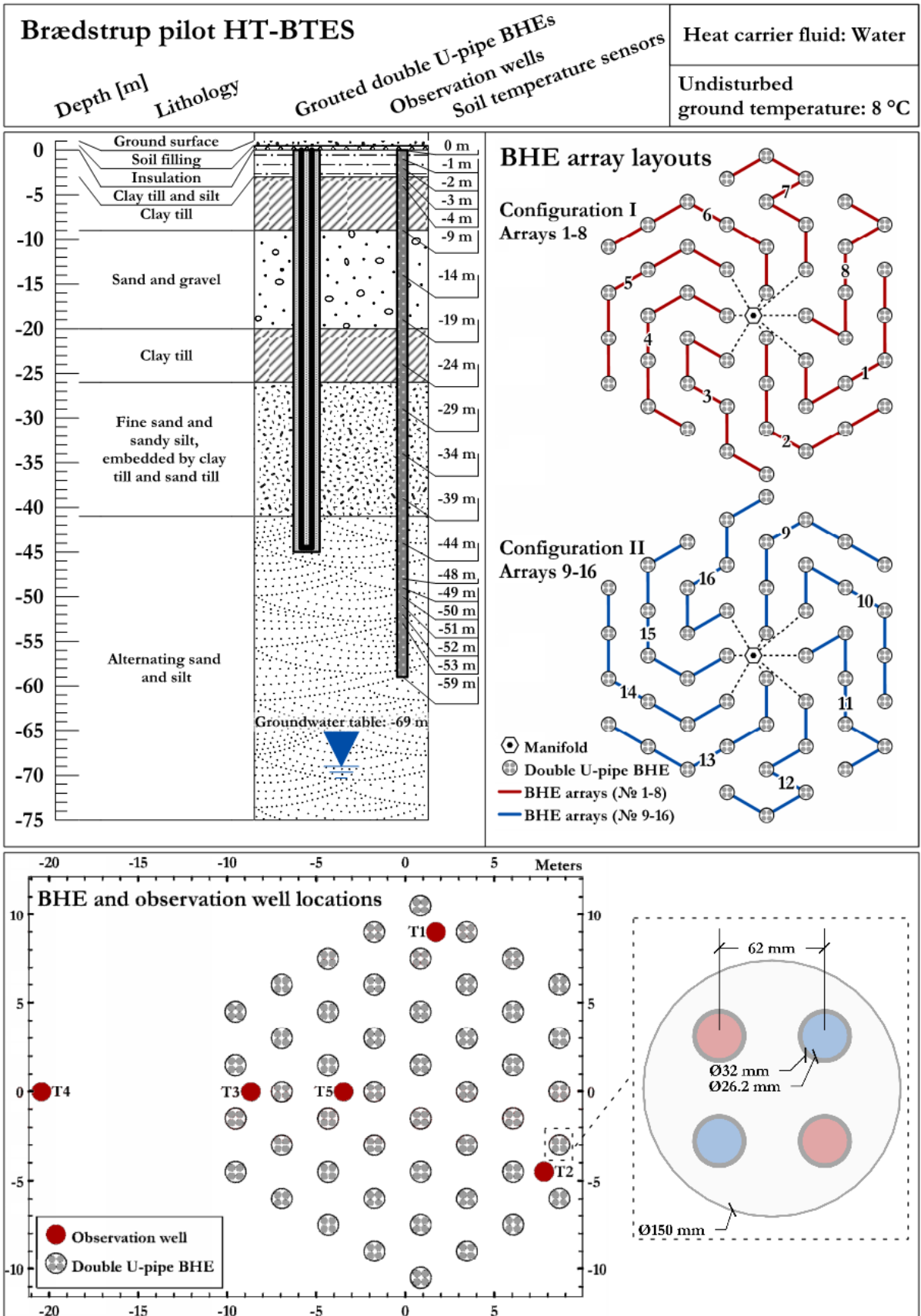
Figure 1. Overview of the Brædstrup BTES design.

3.2 Pre-processing of operational and monitoring data

The Brædstrup district heating facility has been studied on a system level by (Karl Woldum Tordrup et al., 2017), who developed a TRNSYS model of the system. Inverse modelling applied to one year of operational data was used to infer key parameters of each of the individual system components. (Tordrup et al., 2016) and (K. W. Tordrup et al., 2017) also performed detailed component level analyses of the BTES, with the objective of determining thermal properties of the heterogeneous soil strata at the storage site. A finite element model of the BTES was developed, and heat capacities and thermal conductivities were inferred by calibrating the model using operational data and distributed subsurface temperature measurements collected during the first 310 days of operation. Simulations during the following 200 days of operation (510 days in total) showed good agreement with observations of subsurface temperatures and heat extraction and injection rates.

In the present study, a larger dataset comprising 1683 days (2012-05-22 to 2016-12-31) of operational (flow rate and temperatures at BTES inlet and outlet) and subsurface temperature monitoring data has been utilized. The operational and monitoring data was used for 1) defining transient BHE BCs used as input to finite element simulation models, i.e. flow rate, inlet temperature and operation mode, as described in section 3.4, and for 2) comparisons of simulated and observed soil temperatures and return temperatures. The objective of the pre-processing procedure was to 1) identify and eliminate erroneous data, and fill in missing data, and 2) time-aggregate high-resolution data to lower resolution data, mainly for reducing the computational effort needed when performing simulations with transient BCs that swiftly vary with time.

The pre-processing procudure essentially follows the approach given in (K. W. Tordrup et al., 2017) to obtain low resolution aggregated values of soil temperatures, BTES forward/return temperatures and volumetric flow rate, with some exceptions. First, the heat carrier fluid temperature data used are the temperatures of the mixed flow at the BTES inlet and outlet, in contrast to (K. W. Tordrup et al., 2017) who considered the inlet/outlet of each individual BHE array for deriving aggregated flow rate and temperature time series. This is because a large portion of the BHE array temperature records was missing in the larger data set. Also, the data was aggregated from 5-min to 72-h resolution in the present study, as compared to 1-h to 24-h resolution in the previous study.

Before time-averaging, the high-resolution data was inspected to identify possible outliers and erroneous measurement points. For filtering the data containing forward temperature, return temperature and flow rate measurements, outlier thresholds were manually selected based on visualizations of time-ordered data as well as empirical cumulative distribution functions calculated for each vector of measurement points. The selected intervals were [0 °C, 85 °C] (forward temperature), [0 °C, 70 °C] (return temperature) and (0 m³/h, 30.5 m³/h] (flow rate). Data points outside these intervals as well as missing data points were replaced by interpolated values.

An energy conservation equation was set up to determine flow rate values in the low-resolution domain, according to Eq. 1 (K. W. Tordrup et al., 2017):

$$\dot{V}_l = \frac{1}{(T_{f,l} - T_{r,l})\Delta t} \int\limits_{t}^{t+\Delta t} \dot{V}_h(T_{f,h} - T_{r,h})\, dt \tag{1}$$

where $\dot{V}_l$ is the volumetric flow rate, $T_{f,l}$ is the forward temperature and $T_{r,l}$ is the return temperature aggregated over a timestep Δt with length 72 h, and $\dot{V}_h$, $T_{f,h}$ and $T_{r,h}$ are the corresponding parameters in the high-resolution domain. Aggregated values of flow rate resulting in <0.1 m³/h were set to zero, because the numerical solver occasionally exhibits unstable behavior when very low heat carrier flow rates are imposed. The aggregated time series of forward temperature, return temperature and flow rate are shown in Figure 2. Also shown in the figure is the net amount of energy injected into the ground calculated from the flow rate and the inlet-outlet temperature difference, assuming a volumetric heat capacity of the heat carrier fluid equal to 4.19 MJ/m⁻³/K⁻¹.
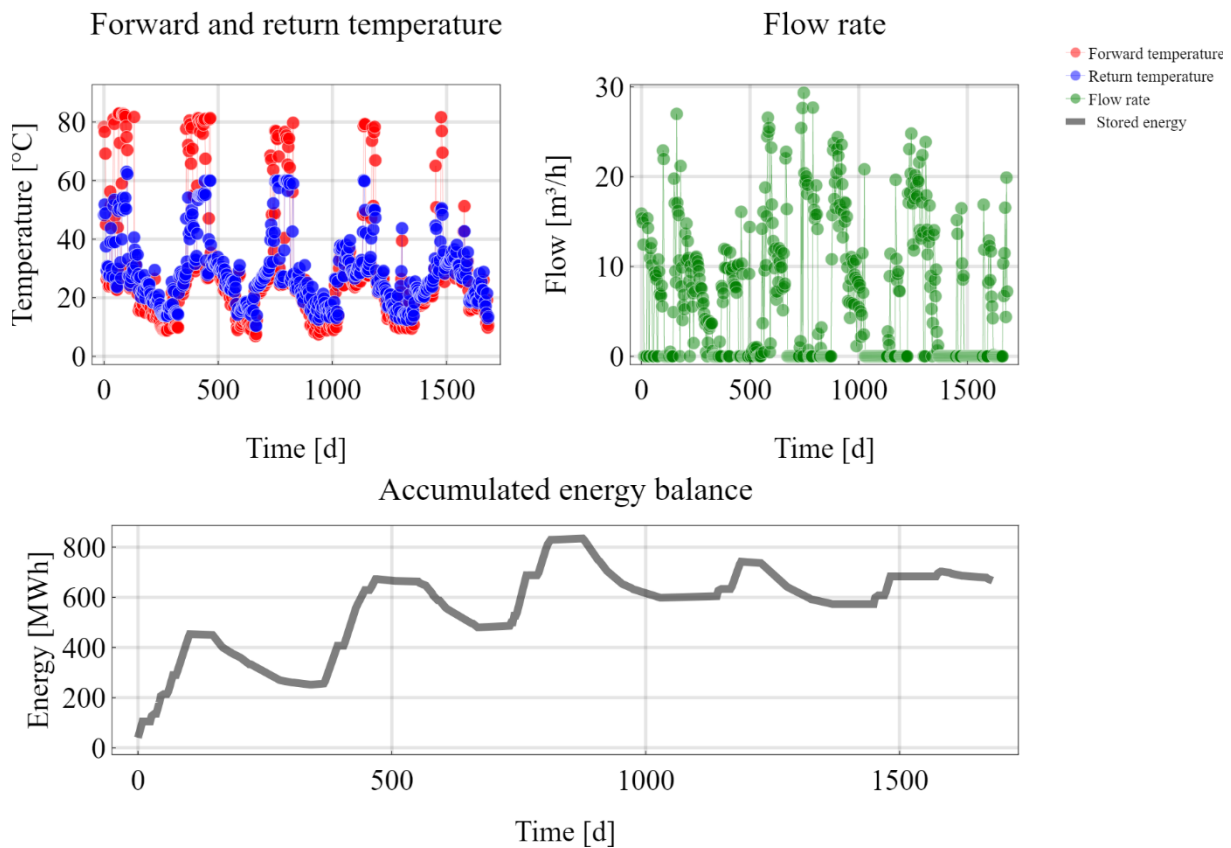
Figure 2. Top: Aggregated time series (72-h resolution) of total flow rate and BTES inlet and outlet temperatures. Bottom: Accumulated energy balance during the first 1683 days of operation.

Soil temperature records from observation wells T1-T5 were inspected visually and aggregated to 24-h resolution. Among a total of 100 time series records, 13 were omitted either because of the measurement data being erroneous or the temperature probes being located close to or on the boundary of the domain of interest (T1 at 0 m; T2 at 0 m, 34 m, 48 m; T3 at 0 m; T4 at depths 0 m, 1 m, 2 m, 3 m, 4 m, 34 m, T5 at 0 m, 44 m). The selection procedure is not further elaborated here since the soil temperature measurements were only used for visual comparison with computed soil temperatures at corresponding model points.

3.3 Plugin development for BTES system operation control

The concept of designing BTES systems using arrays of series-connected BHEs with flow-reversal capability has been adopted in several HT-BTES implementations, in addition to the Brædstrup storage (Catolico et al., 2016; Nordell, 1994; Rapantova et al., 2016). Although FEFLOW provides a built-in tool for modeling interconnected BHEs, it is not capable of modeling BHE arrays with reverse-flow operation (as of version 7.3). A plugin has therefore been developed to allow for simulations of actual operation conditions of the Brædstrup BTES and other systems with similar design and operation strategy. The plugin was developed using C++ with the FEFLOW APIs, which enable reading or modification of model parameters during simulation run-time.

Using the plugin, an arbitrary number of parallel arrays of series-connected BHEs can be defined by grouping and sorting the BHEs on the basis of an array ID and an ascending number that specificies the linking order of a borehole within an array. The lowest-order BHE within the array (e.g., № 11 in Figure 3) constitutes the array inlet during charging, and vice versa during the discharging period.
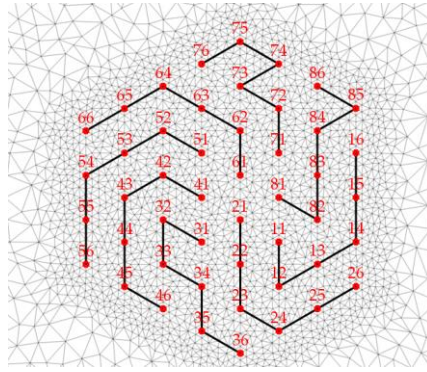
Figure 3. ID convention for defining BHE arrays and their connectivity.

The plugin controls the BHE array operation by taking three time-series as user input: 1) mode of operation (charging/inactive/discharging), 2) total flow rate and 3) inlet temperature to the storage. Before each time step or iteration, the flow rate and inlet temperature at current time are set as boundary conditions at the inlet of the first BHE of the array, according to the mode of operation. The flow is assumed to be uniformly distributed between the BHE arrays.

Since the inlet temperature at the remaining BHE inlets are unknown (and the matrix equation system representing the processes within the BHEs being inaccessible through the API), the resulting BHE outlet temperatures obtained in the previous time step or iteration are set as inflow temperature for the next BHE in the array at next time step. The number of iterations per time step may be restricted to reduce simulation time. One should though keep in mind that errors may be introduced in case rapid changes in boundary conditions or primary variable (temperature) occur, and if the time-step sizes are not sufficiently small. However, as will be shown in section 4.1, the thermal behaviour of the BHE array can be approximated quite accurately (in long-term analysis) by using automatic time-stepping control in combination with low-resolution BHE inlet boundary conditions during simulation. Further development is required for enabling analysis of short-term effects to accurately reproduce the full dynamics of series-connected BHEs.

Future improvement of the plugin will enable specifying individual boundary conditions for specific BHE arrays, as well as defining other BC options than the inlet temperature type (e.g., power and temperature difference), which would allow for detailed studies on optimization of BTES operation strategies and BHE array design. The source code will be published on https://github.com/MaxHesselbrandt/BTESrevFlow.

3.4 Pure-conduction finite element model development

To investigate thermal performance of a HT-BTES unaffected by groundwater flow, a pure-heat conduction model of the Brædstrup BTES has been developed and simulated using actual operational data (see section 3.2) as input. In combination with extensive measurement data available, the subsurface characteristics at the storage site appear to constitute favorable conditions for purposes of validation and performance analyses. Due to the storage being situated in the vadose zone well above the regional groundwater table, there is less probability that other transport mechanisms than conduction may significantly contribute to the subsurface temperature distribution observed during operation. Hence, less uncertainties exist in subsurface characterization when attempting to reproduce the thermal behaviour of the storage by means of simulation models. If a pure-conduction model proves to sufficiently estimate the observed data, the effect of groundwater flow on the subsurface thermal regime may be readily quantified by direct comparisons between the conduction model and hypothetical advective-transport models. The latter would also give an insight on how the real system would have performed under the influence of groundwater flow.

Another objective of the pure-conduction model was to validate that the FEFLOW plugin tool described in section 3.3 is capable of capturing the long-term behaviour of BHE arrays in an accurate manner. Besides being important for predicting heat exchange rates for the BTES system, an accurate representation of the temperature distribution close to the boreholes is crucial for understanding groundwater effects on storage stratification and factors affecting exergy destruction within the storage.

At the Brædstrup storage site dry-unsaturated conditions prevail, meaning that transient heat transport in the soil is either handled by the 3D heat conduction equation (Carslaw and Jaeger, 1959) or by differential equations describing coupled unsaturated flow and heat transport phenomena, e.g. (DHI-WASY, 2009). It is assumed here that heat transport occurs only by thermal conduction. However, for convenience, throughout this study the model domain is treated as a confined, saturated porous medium with bulk thermal properties equivalent to that of a dry medium. This way, the pure-conduction model can be extended to also account for heat advection only by imposing non-zero hydraulic boundary conditions onto the model domain. This means that the medium is assumed to have porosities saturated by groundwater, described by the volume fraction ε. The conservation equation of thermal energy in a saturated porous medium g, consisting of a solid phase s and a fluid phase f, reads as (Diersch et al., 2011b)

$$\frac{\partial}{\partial t}\left\{[\varepsilon\rho^f c^f + (1-\varepsilon)\rho^s c^s]T_g\right\} + \nabla\cdot\left(\rho^f c^f \boldsymbol{q}T_g\right) - \nabla\cdot(\boldsymbol{\Lambda}\cdot\nabla T_g) = Q, \tag{2}$$

where $\boldsymbol{q}$ is the flux expressed by Darcy's law, ρ and c are the density and specific heat capacity of the phases (indicated by their respective superscript), T_g is the temperature of the saturated medium, Q is a heat sink/source term (e.g., due to a BHE), and $\boldsymbol{\Lambda}$ is the tensor of thermal hydrodynamic dispersion written as

$$\boldsymbol{\Lambda} = \left[\varepsilon\lambda^f + (1-\varepsilon)\lambda^s\right]\boldsymbol{I} + \rho^f c^f[\alpha_T\|\boldsymbol{q}\|]\boldsymbol{I} + (\alpha_L - \alpha_T)\frac{\boldsymbol{q}\otimes\boldsymbol{q}}{\|\boldsymbol{q}\|}. \tag{3}$$

In Eq. 3, α_L and α_T are the longitudinal and transverse thermodispersivities, respectively, λ is the thermal conductivity, and $\boldsymbol{I}$ is the identity matrix. In the case of pure conduction, $\boldsymbol{q}$ is a zero vector, thus Eq. 2 reduces to the heat conduction equation

$$(\rho c)_g\frac{\partial T_g}{\partial t} - \nabla\cdot(\boldsymbol{\lambda}\cdot\nabla T_g) = Q, \tag{4}$$

where $(\rho c)_g = \varepsilon\rho^f c^f + (1-\varepsilon)\rho^s c^s$ is the bulk volumetric heat capacity and $\boldsymbol{\lambda} = \lambda_g\boldsymbol{I} = \left[\varepsilon\lambda^f + (1-\varepsilon)\lambda^s\right]\boldsymbol{I}$ is the bulk thermal conductivity of the porous medium.

For solving the heat conduction problem, the finite element method has been applied using FEFLOW 7.1 for mesh construction, modeling, and simulation. The model domain consists of a rectangular prism with dimension of 600 m × 200 m × 80 m. Even though a rather uniform temperature field is expected to evolve around the BHEs in the case of conductive heat transfer, the domain is elongated along the x-axis to capture downstream temperature dynamics in simulations of the extended model where groundwater flow is assumed (see section 3.5). The domain was discretized by first constructing a 2D unstructured mesh using a triangulation code which is capable of generating exact Delaunay triangulations (Shewchuk, 1996). The 3D mesh structure was set up by extruding the 2D mesh along the depth direction (z-axis) to create a vertically structured grid partitioned into 61 plane layers of triangular prismatic elements, with thicknesses of 1 m for layers in the depth interval 0-59 m and between 1 m to 4.2 m at larger depths. The discretization procedure resulted in a 3D mesh consisting of 1 018 029 elements.

In FEFLOW, BHEs are modeled as 1D representations of the real geometry of the piping material and borehole filling (see for details (DHI-WASY, 2010; Diersch et al., 2011b) by imposing BHE BCs on nodes linked along vertical edges of the discretization. The horizontal 2D mesh was locally refined in the interspace region between the BHE nodes, as well as the area surrounding the BTES with emphasis on the downstream region where the thermal front migrates in the presence of groundwater movements. Specifically, the mesh around the BHEs is designed in such that an ideal spacing between the BHE nodes and respective surrounding nodes is applied to attain highest numerical accuracy, for reasons elaborated by (Diersch et al., 2011a). The mesh in the surrounding of the BHE nodes is shown in an overview of the model discretization in Figure 4, where the positions of the BHE representations are also indicated (linked in accordance with Configuration I shown in Figure 1).
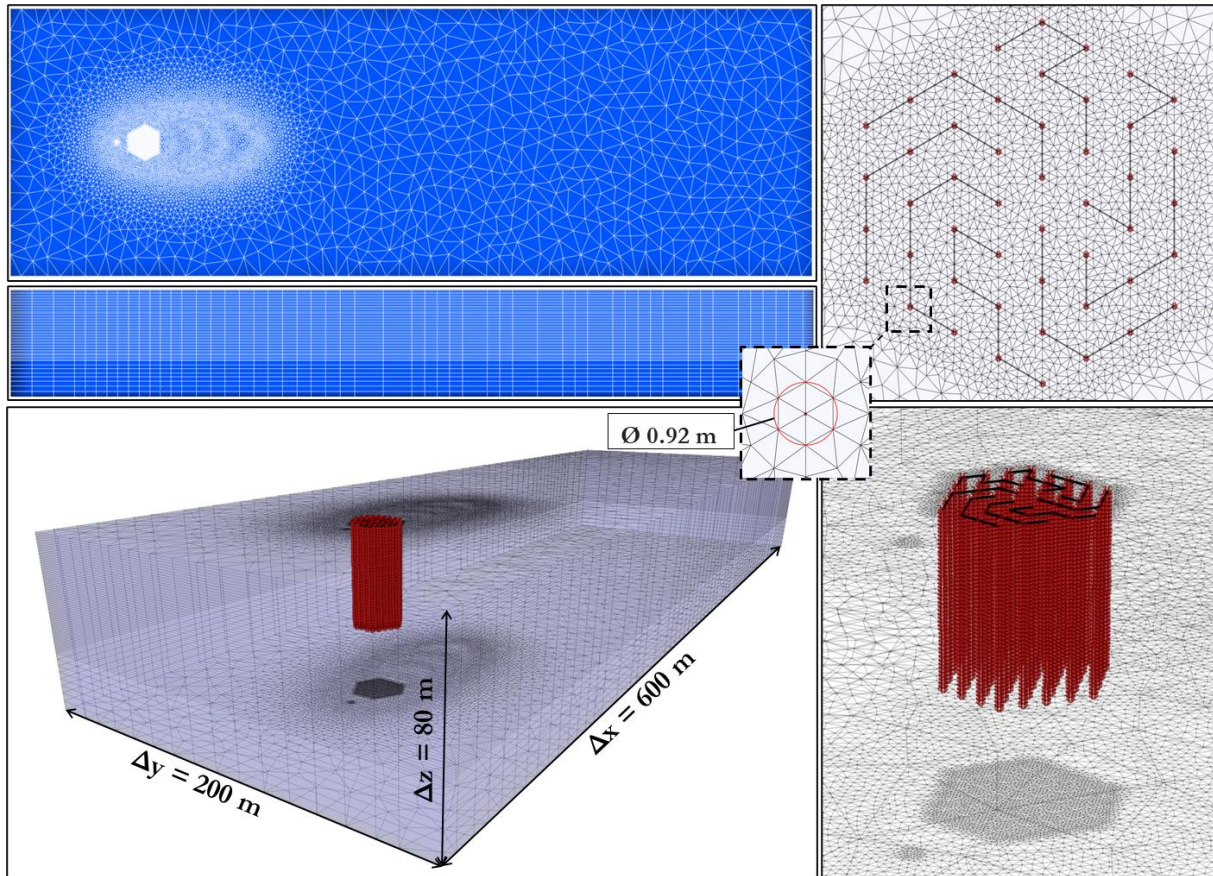
Figure 4. Overview of the model discretization.

The BHE BCs extend from the top of the model ($z = 0$ m) down to a depth of 45 m. The layers of heat insulation and soil fill located above the BTES at the actual site are not included in the model. Instead, the top boundary as well as the lateral and bottom boundaries are assumed to be adiabatic and thus no thermal interaction with the ground surface is accounted for. Consequently, all heat flow across the model boundaries occurs through the BHEs. Based on soil temperature measurements recorded before operation of the Brædstrup storage was initiated, an initial condition T_0 of 8 °C was set throughout the model domain.

Model parameters describing the bulk thermal properties of the vertically-layered porous media are obtained from (K. W. Tordrup et al., 2017). In their study, estimates of bulk thermal conductivity and volumetric heat capacity values for six different geological layers were inferred by inverse modeling of observed operational and soil temperature data. They found that the energy balance prediction ability of the model was improved when accounting for soil heterogeneity, in comparison with simulations of a model assuming homogeneous soil properties based on the the results of a standard thermal response test performed at the Brædstrup storage site. Since the double U-pipes in each BHE cannot be handled separately in FEFLOW, each of the two BHE array configurations of the storage (shown in Figure 1) cannot be represented correctly within the same model. Therefore, (K. W. Tordrup et al., 2017) carried out two parameter analyses for each of the configurations, assuming that both U-pipes within each borehole were identically linked to the U-pipes in previous and next BHEs in the array. The final parameter estimates were taken as the average of the estimates obtained from respective analysis.

In the present study only Configuration I has been considered, and the corresponding bulk material parameter estimates presented by (K. W. Tordrup et al., 2017) were adopted in the model, see Table 1. A porosity of 0.2 m³/m³ was assumed for all layers, and the material properties for each phase were accordingly adjusted and assigned to the model so that input parameters equivalent to the bulk property values were set (see Eq. 2 and Eq. 3). For the numerical solution of the heat conduction problem, isotropic conditions are assumed.

Table 1. Material properties of the vertically layered subdomains within the model.

Formation	Extent from top boundary [m]	Porosity [m³/m³]	Thermal conductivity [W/m/K]			Volumetric heat capacity [MJ/m³/K]		
		ε	λ^f	λ^s	λ_g[1]	$\rho^f c^f$	$\rho^s c^s$	$(\rho c)_g$[1]
Clay till and silt	0-3	0.2	0.6	2.68	**2.26**	4.18	1.51	**2.04**
Clay till	3-9	0.2	0.6	1.61	**1.41**	4.18	1.79	**2.27**
Sand and gravel	9-20	0.2	0.6	1.84	**1.59**	4.18	1.06	**1.68**
Clay till	20-26	0.2	0.6	1.70	**1.48**	4.18	1.68	**2.18**
Fine sand and sandy silt, embedded by clay till and sand till	26-41	0.2	0.6	2.05	**1.76**	4.18	1.39	**1.95**
Alternating sand and silt	41-80	0.2	0.6	2.86	**2.41**	4.18	1.24	**1.83**

[1] (K. W. Tordrup et al., 2017)

The BHE heat transfer problem was considered using the parameters and settings listed in Table 2. Further information on the geometric relations of the double U-pipe BHEs is given in subsection 3.1.

Table 2. Details on parameter settings used for local BHE problem.

Parameter	Value	Unit
№ of BHEs	48	[-]
№ of BHE arrays	8	[-]
BHE array configuration	I[*]	[-]
BHE length	45	[m]
BHE diameter	0.15	[m]
Volumetric flow rate	Transient[**]	[m³]
Inlet temperature BC	Transient[**]	[°C]
Flow direction of heat carrier fluid	Transient[**]	[-]
Pipe configuration	2U	-
Shank spacing	0.062	[m]
U-pipe outer diameter	0.032	[m]
U-pipe wall thickness	0.0029	[m]
U-pipe thermal conductivity	0.42	[W/m/K]
Grout thermal conductivity	1.44	[W/m/K]
Heat carrier fluid	Water	[-]
Volumetric heat capacity of heat carrier fluid	4.19	[MJ/m³/K]
Thermal conductivity of heat carrier fluid	0.614	[W/m/K]
Dynamic viscosity of heat carrier fluid	7.97e-4	[kg/m/s]
Density of heat carrier fluid	996	[kg/m³]
BHE thermal resistance	Calculated[***]	[-]
Computational method	Quasi-stationary analytical (Eskilson-Claesson)[****]	[-]

[*] See section 3.1/Figure 1.

[**] See section 3.2 and 3.3.

[***] (DHI-WASY, 2010)

[****] (Eskilson and Claesson, 1988)

The simulation parameters used are shown in Table 3. A simulation of 1683 days was performed, equal to the duration of the observed data series available after operation start (see subsection 3.2).

Table 3. Parameters and conditions used for the simulation.

Parameter	Value	Unit
Simulation time period	1683	[d]
Time step control	Automatic	[-]
Initial time step length	1e-6	[d]
Predictor-corrector scheme	Forward Adams-Bashforth / Backward Trapezoid	[-]
Maximum iterations per time step	1	[-]
Error tolerance (Euclidian L^2 norm)	1e-4	[-]

3.5 Coupled hydro-thermal modeling

The pure conduction model described in section 3.4 was extended to investigate the influence of groundwater flow on the performance of the BTES. For this purpose, a hypothetical groundwater system has been considered assuming steady-flow, transient-transport in a confined, saturated porous medium. Based on the vadose zone lithological profile at the Brædstrup storage site, hydraulic properties and thermodispersivity were attributed to the model layers using typical values from literature. As can be seen in Figure 5, first-type boundary conditions were fixed on upstream and downstream lateral boundaries to impose a uniform hydraulic gradient across the domain, whilst impermeable boundaries were imposed on the remaining boundaries. The solution of the problem is a steady heterogeneous flow field that can be coupled to the heat transport problem according to Eq. 2 in subsection 3.4.
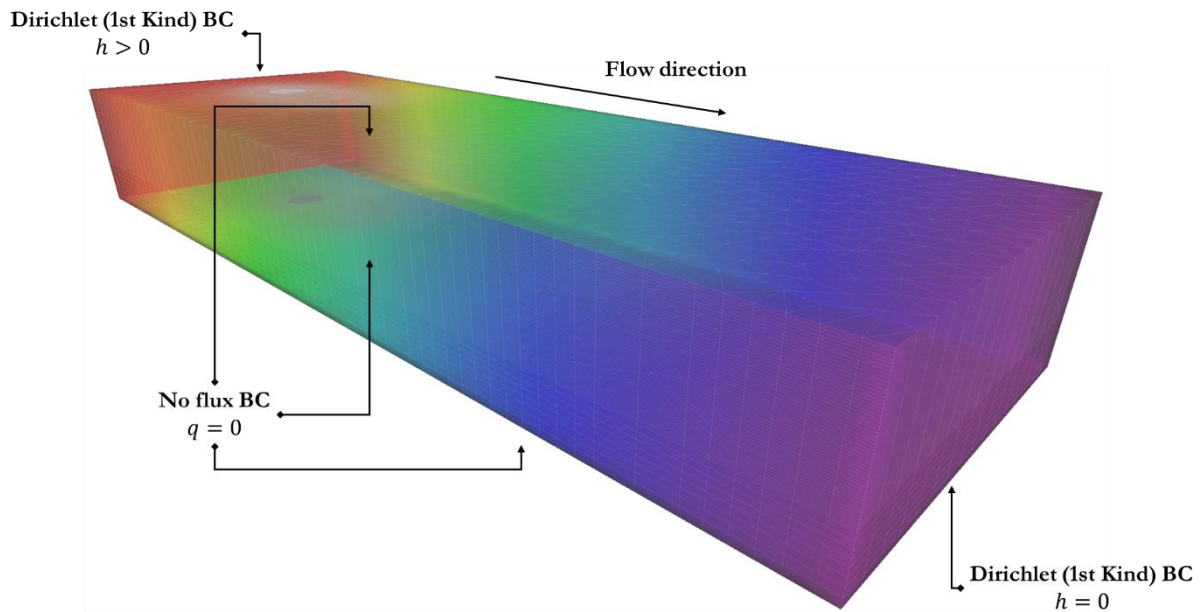
Figure 5. Hydraulic boundary conditions applied to the coupled hydro-thermal model.

Soil characterization performed at the storage site showed the presence of layered sequences of primarily clay till, silt, sand, and gravel (Sørensen et al., 2013). Under saturated conditions, the hydraulic characteristics of these soil types may vary greatly depending on composition and geometrical properties. Fine-grained clayey materials have typically high porosity but low permeability, whereas the intergranular pore spaces in coarser-grained sand and gravel materials permit water to flow relatively freely thus contributing to higher permeability. To the geological layers considered in the pure-conduction model, hydraulic conductivities (assuming isotropic conditions) were attributed based on typical values found in the literature, e.g. (Heath,

1983; Lakshmanan, 2011). As shown in Figure 6, the groundwater flow model consists of three zones with relatively high hydraulic conductivity and three low-transmissivity zones representing the sandy and clayey layers, respectively. Dispersivity of the soil were assumed to be 5 m in the longitudinal direction and 0.5 m in the transverse direction for all layers.
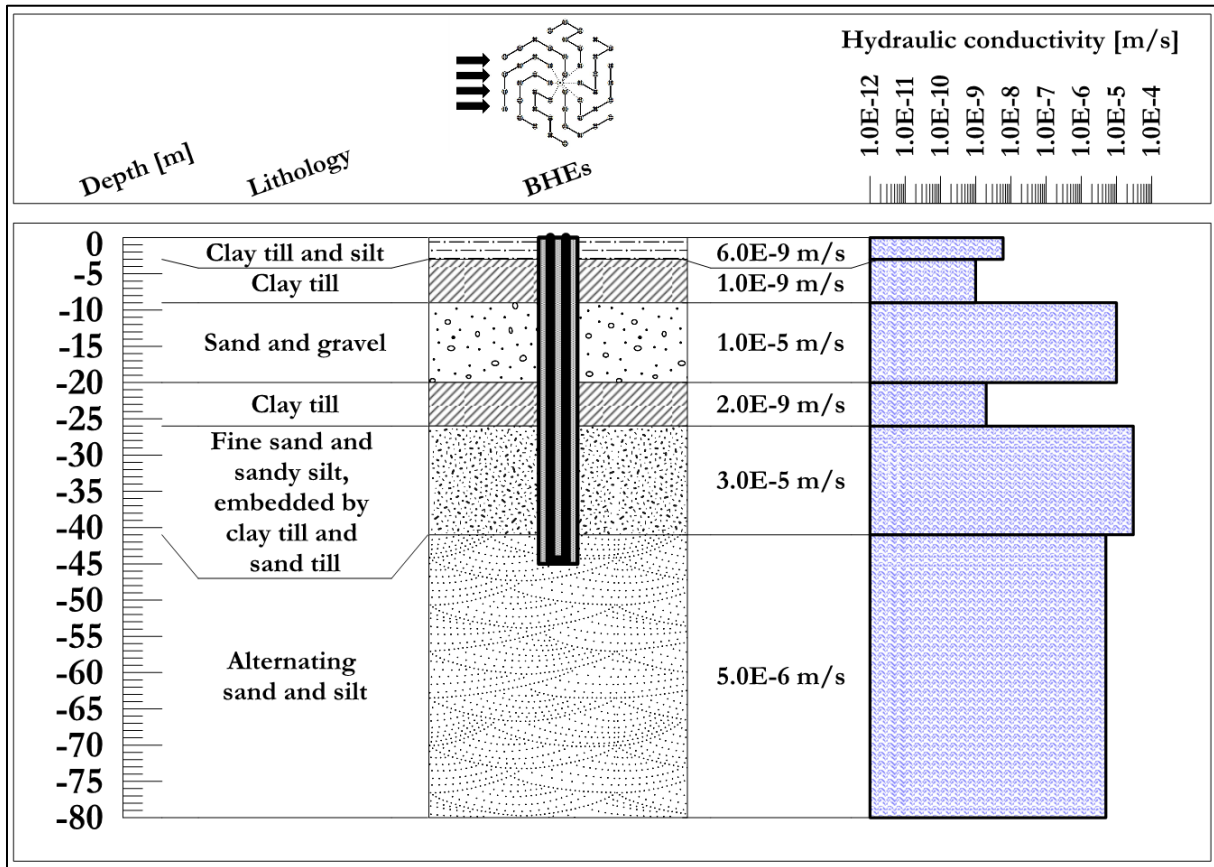

Figure 6. Hydraulic properties of the layered soil.

With a fixed hydraulic head of 0 m set on the downstream boundary nodes, five rounds of simulations were performed (including the pure-conduction base scenario) where the hydraulic head set on the upstream boundary nodes was altered to observe the effect of different hydraulic gradients across the model domain, see Table 4. For each of the simulations, all other material properties, boundary conditions and simulation parameters were maintained equal to those used in the simulation of the pure-conduction scenario described in section 3.4.

Table 4. Summary of scenarios for model simulation.

Scenario №	Upstream hydraulic head BC [m]	Downstream hydraulic head BC [m]	Hydraulic gradient [%]
1	0	0	0
2	1	0	-0.17
3	5	0	-0.83
4	7	0	-1.17
5	10	0	-1.67

3.6 Energy and exergy performance evaluation

In literature, BTES system performance is commonly assessed and quantified with respect to a ratio representing the amount of thermal energy injected to versus extracted from the BTES during a storing cycle, e.g., (Bauer et al., 2009; Nilsson, 2020; Nußbicker et al., 2003). Common names are storage efficiency,

energy efficiency or utilization ratio. As pointed out by (Dincer and Rosen, 2007), assessing the storage performance only by energy analysis has some shortages associated with loss of information on availability and quality of the heat being stored and discharged. They emphasized the importance of exergy analysis as a complement to energy analysis for assessing, comparing, and improving thermal energy storage performance. Exergy analysis has been applied in a few studies of BTES and GSHP systems (Hepbasli, 2005; Kizilkan and Dincer, 2012; Ozgener et al., 2005; Sharqawy et al., 2009), but has not been established as a standard method in shallow geothermal system design.

In this study, an approach based on the work by (Lazzarotto et al., 2020) has been implemented for assessment of BTES system energy and exergy performance. In their paper, relevant parameters for energy analysis as well as exergy and temperature analysis were formulated and evaluated at storage boundaries, i.e., at inlet and outlet but also with respect to a subsurface interface between the storage volume and surrounding ground. A 2D analytical BHE model based on the infinite line source was utilized to demonstrate their approach.

Performance indicators for quantifying system as well as storage energy and exergy efficiencies used by (Lazzarotto et al., 2020) are defined as follows:

Seasonal system performance indicators	$$\eta_{Q,system} = \frac{Q_d}{Q_c} = \frac{\int_{\tau_c}^{\tau_c+\tau_d} \dot{m}(t)c_p\left[T_r(t) - T_f(t)\right]dt}{\int_{0}^{\tau_c} \dot{m}(t)c_p\left[T_f(t) - T_r(t)\right]dt}$$	(5)
	$$\psi_{Ex,system} = \frac{Ex_d}{Ex_c} = \frac{\int_{\tau_c}^{\tau_c+\tau_d} \dot{m}(t)c_p\left\{\left[T_r(t) - T_f(t)\right] - T_0 \ln\frac{T_r(t)}{T_f(t)}\right\}dt}{\int_{0}^{\tau_c} \dot{m}(t)c_p\left\{\left[T_f(t) - T_r(t)\right] - T_0 \ln\frac{T_f(t)}{T_r(t)}\right\}dt}$$	(6)

Storage performance indicators	$$\eta_{Q,storage}(\Omega, t) = \frac{Q_{stored}(\Omega, t)}{Q_{exchanged}(t)} = \frac{\int_{\Omega} \left(\rho(\boldsymbol{x})c_p(\boldsymbol{x})\right)_g [T(\boldsymbol{x},t) - T_0(t)]\, d\Omega}{\int_{0}^{t} \dot{m}c_p[T_f(t) - T_r(t)]\, dt}$$	(7)
$$\psi_{Ex,storage}(\Omega, t) = \frac{Ex_{stored}(\Omega, t)}{Ex_{exchanged}(t)} = \frac{\int_{\Omega} \left(\rho(\boldsymbol{x})c_p(\boldsymbol{x})\right)_g \left\{[T(\boldsymbol{x},t) - T_0(t)] - T_0\ln\frac{T(\boldsymbol{x},t)}{T_0}\right\}d\Omega}{\int_{0}^{t} \dot{m}c_p\left\{[T_f(t) - T_r(t)] - T_0\ln\frac{T_f(t)}{T_r(t)}\right\}dt}$$		(8)

Description of parameters in Eq. 5 to Eq. 8 is given below. It should be noted that the unit for temperature in Eq. 6 and Eq. 8 is Kelvin.

Q	Thermal energy	Ex	Thermal exergy	c_p	Heat carrier specific heat capacity	Subscripts			
τ	Time duration	$\dot{m}$	Heat carrier mass flow rate	Ω	Storage domain/volume	c	Charging	d	Discharging
T	Temperature	$(\rho c_p)_g$	Ground volumetric heat capacity			f	Forward	r	Return
$\boldsymbol{x}$	Spatial coordinate	T_0	Reference temperature						

As can be understood from Eq. 5-Eq. 8, theory and methods of energy and exergy analyses are similar, with a few differences. In Eq. 6 and Eq. 8, the temperature of the heat exchange as well as the quality of the heat being stored is reflected by the introduction of a reference temperature T_0, as is further described by (Dincer and Rosen, 2007) in their elaborate review on exergy storage. In this study, the undisturbed ground temperature of 8 °C (281.15 K) was chosen as reference temperature for evaluation of the exergy performance indicators.

By introducing the volume of the storage domain Ω in Eq. 7 and Eq. 8, it is possible to reflect the amount of heat and exergy being lost (or destroyed, from an exergy perspective) to the ambient ground in relation to the amount being stored and recovered. However, a BTES has intuitively no bottom or lateral boundaries, hence the storage domain is indefinite. (Lazzarotto et al., 2020) get around this issue by defining the storage domain as a volume (or area in 2D problems) containing a certain portion $(1 - \epsilon)$ of the total amount of energy in the ground after a characteristic time τ of heat injection:

$$Q_{stored,\epsilon,\tau}\left(\Omega_{\epsilon,\tau}, \tau\right) = (1 - \epsilon)Q_{injected}(\tau) \tag{9}$$

This definition is not trivial because the subsurface temperature field is dependent on the ground thermal characteristics as well as the boundary conditions assumed in the heat transfer model. Specifically, in this study, due to variations in groundwater flow field no consistent solution to Eq. 9 can be found that represents the storage domain in all scenarios described in section 3.5. This concern was circumvented, however, by choosing the model setup used for simulation of the pure conduction scenario for defining the storage domain. Calculating the temperature distribution based on pure conduction heat transfer is a sensible choice because it provides possibility to characterize the additional effect of advection on heat flow rates across the storage boundaries.

A discrete approximate approach to the analytical one suggested by (Lazzarotto et al., 2020) was used to define the storage domain $\Omega_{\epsilon,\tau}$. Instead of imposing a transient temperature BC on the BHE array inlets, a constant heat injection power BC were set to each individual BHE for a simulation time duration τ of 180 days. Applying a fraction ϵ of 0.01, the boundary Γ of the storage domain $\Omega_{\epsilon,\tau}$ was determined by finding an approximate minimum of the objective function f_{τ,q_Γ} with respect to the energy density q_Γ at Γ (using T_0 as reference temperature):

$$f_{\tau,q_\Gamma} = (1 - \epsilon)Q_{injected,\tau} - \sum_{i \in N} V_i q_i \tag{10}$$

where N is a set of finite elements within the model domain, with energy density q that fulfils the condition $q \geq q_\Gamma$ at time τ. Thus, Γ represents the boundary that encloses the elements in the set N corresponding to the minimum of f_{τ,q_Γ}. The storage domain $\Omega_{\epsilon,\tau}$ is shown in Figure 7.
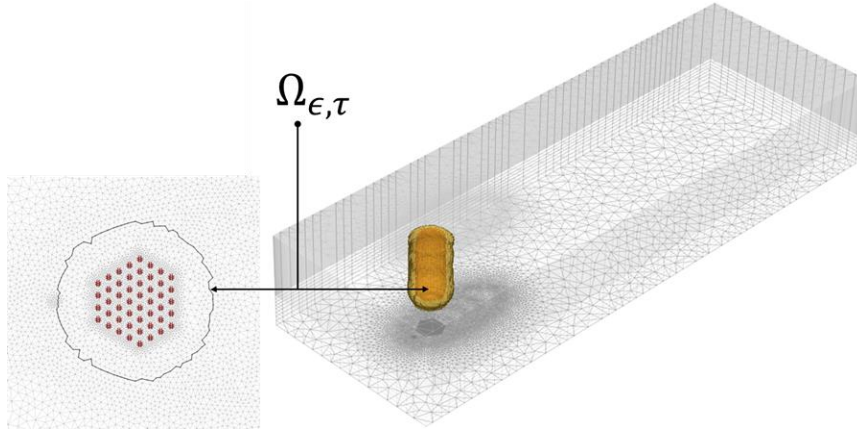
Figure 7. Storage domain $\Omega_{\epsilon,\tau}$ evaluated at time $\tau = 180$ days for $\epsilon = 0.01$.

Based on the storage domain $\Omega_{\epsilon,\tau}$, the average storage temperature $\bar{T}_{storage}$ can be estimated by the expression

$$\bar{T}_{storage}(t) = T_0 + \frac{\sum_{i \in \Omega_{\epsilon,\tau}} V_i q_i(t)}{\sum_{i \in \Omega_{\epsilon,\tau}}\left(V \rho c_p\right)_i} \tag{11}$$

The system and storage performance indicators presented in Eq. 5-Eq. 8 and Eq. 11 were evaluated for each of the simulation scenarios summarized in Table 4 (section 3.5). In addition, the simulation results were analyzed qualitatively for characterization of mechanisms contributing to heat losses and exergy destruction

during the storage cycle. For defining the integration limits in Eq. 5 - Eq. 6, charging and discharging periods as shown in Table 5 have been considered.

Table 5. Charging and discharging periods.

	Storing cycle 1	Storing cycle 2	Storing cycle 3	Storing cycle 4
Charging period [d]	0-105	370-467	730-828	1137-1189
Discharging period [d]	106-369	468-729	829-1136	1190-1452

4 Results

The results from the simulations of the pure conduction and coupled groundwater flow and heat transport scenarios described in subsections 3.4 and 3.5 are presented in this section. In section 4.1 the outcome of the validation study is presented, which was performed with respect to observed operational and soil temperature measurement data from the Brædstrup HT-BTES to assess the accuracy of the pure conduction model in combination with the plugin tool for BHE array modeling developed within this work (section 3.3). In section 4.2, results are presented for the simulations concerning groundwater advection as well as pure conduction scenarios, in terms of the performance indicators detailed in section 3.6. A qualitative assessment of the importance of groundwater flow on heat loss and exergy destruction events occurring during the storing cycles is given in section 4.3.

4.1 Validation study

The pure conduction model was simulated using aggregated input time series of flow rate, inlet temperature and flow direction (section 3.2) based on real operational data of the Brædstrup storage, considering a time period from 2012-05-22 (start of operation) to 2016-12-31. In Figure 8, computed values of net amount of injected heat, average heat load as well as return temperatures are shown with corresponding observed quantities. All values are aggregated to 72 h resolution, as is the resolution of input time series.
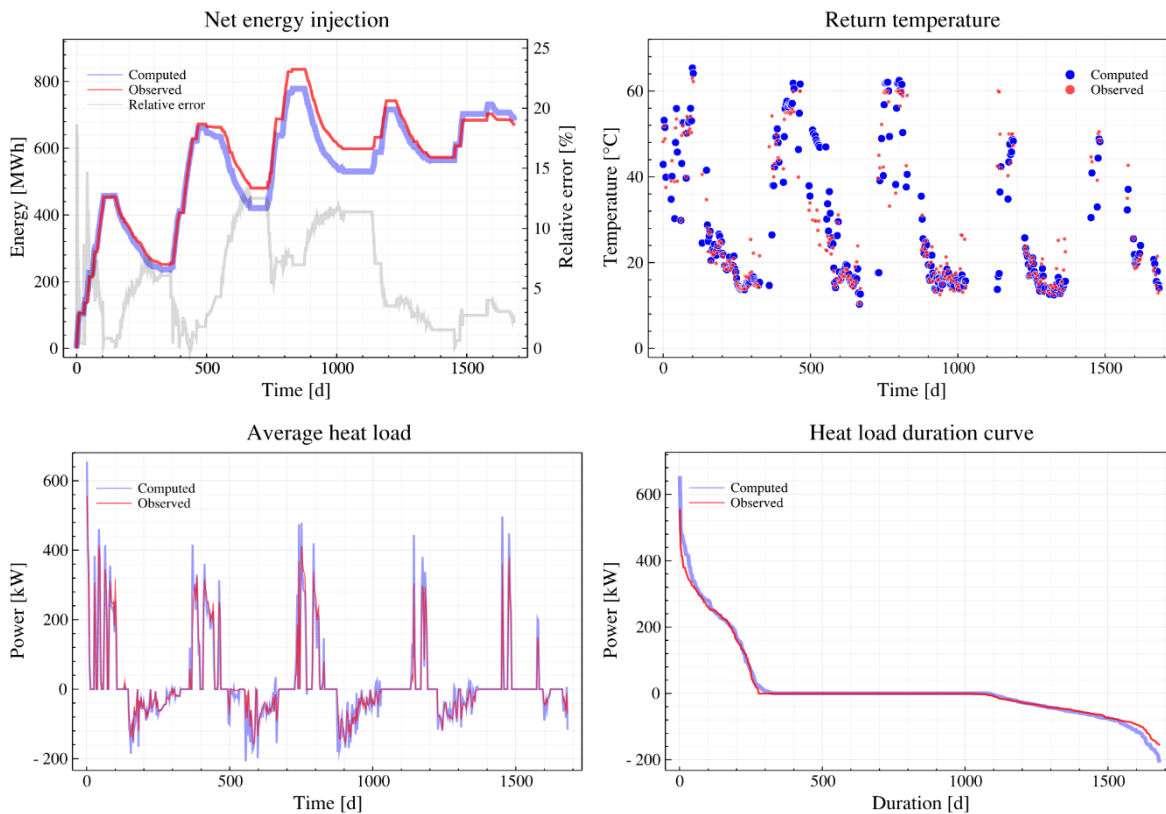

Figure 8. Time series of computed and observed quantities aggregated to a resolution of 72 h. Top, left to right: 1. Net amount of thermal energy injected into the storage. 2. BTES (mixed flow) return temperature. Bottom, left to right: 1. Average heat load on the BTES. 2. Average heat load duration curve.

As can be seen in Figure 8 (top, left), computed values of net injected heat show good agreement with observed data, particularly at times during the first charging period but also during the second charging period. Some divergence can be observed during the first discharging season, which is a tendency that reappears also for subsequent discharging periods. This tendency was also observed by (K. W. Tordrup et al., 2017), who suggest that the deviation may be due to the BHE model used (Eskilson and Claesson, 1988) being inaccurate for highly transient loading conditions, as it assumes quasi-stationary behaviour of the BHE. Consequently, simulated BTES outlet temperatures will deviate from real values. Such an example can be seen in Figure 8 (top, right) during the second discharge period, where overestimations in computed

return temperatures introduce an offset of about 55 MWh during the subsequent storing cycle. Considering such tendency in combination with the approximate method used for linking the BHE outlets/inlets in the BHE array modeling plugin, care must be taken when applying the tool for short-term problems. However, as indicated by the relative error indicator shown in the energy chart (top, left), the deviation decreases during the fourth storing cycle and the relative error reduces to around 2% (682 MWh computed vs 668 MWh observed net energy injection into the storage) at the final time step of the simulation. In Table 6, a summary of other basic measures of errors between computed and observed data is presented.

Table 6. Basic measures of errors between computed and observed data.

	Net injected energy [MWh]	Power [kW]	Return temperature [°C]
RMSE	40	29	7
Maximum absolute error	77	250	43.3
Max. (computed/observed)	778/836	655/556	65.4/63.0
Min. (computed/observed)	0/0	-208/-156	10.3/10.4

For assessing the soil temperature prediction ability of the pure conduction model, temperature simulation results were recorded at 3D locations corresponding to those of the actual temperature probes inserted in observation wells T1-T5 (see Figure 1 in section 3.1) and evaluated by visual comparison with observed data. Observation wells T1, T2, T3 and T5 are located inside the external circumference of the bore field, whereas T4 is located at ~11 m from the bore field periphery. Time series records of computed and observed soil temperatures at 15 different points are shown in Figure 9. Here, three depths for each of the observation wells have been randomly selected to reflect the overall tendencies of the model prediction capabilities.

Computed temperatures generally agree well with observed soil temperature data. However, the model seems to overestimate near-surface soil temperatures, especially during times when the BTES system is inactive (e.g., T2 at 3 m and 4 m; T3 at 1 m; T5 at 2 m), which is possibly due the assumption of adiabatic ground surface at the top boundary of the model domain. Outside the bore field and beneath the BHEs, the model generally fails to accurately capture the dynamics of the soil temperature pulses occurring during the storing cycles (e.g., T3 at 50 m; T4 at 9 m; T5 at 51 m), although temporal-averaged time series of the temperature data would show reasonable accuracy. Inside the bore field, at intermediate depths relative the length of the BHEs (e.g., T1 at 19 m; T2 at 24 m; T3 at 14 m), very good agreement can be observed between computed and observed data considering the high and rapid variations in temperature levels occurring over the course of a storing cycle. It can be seen that the model is also capable of capturing thermal stratification within the storage by noting that the highest computed and observed overall temperature levels are reached in T5 (T5 at 2 m and 9 m in Figure 9), which is the innermost of the five observation wells in relation to the storage center.
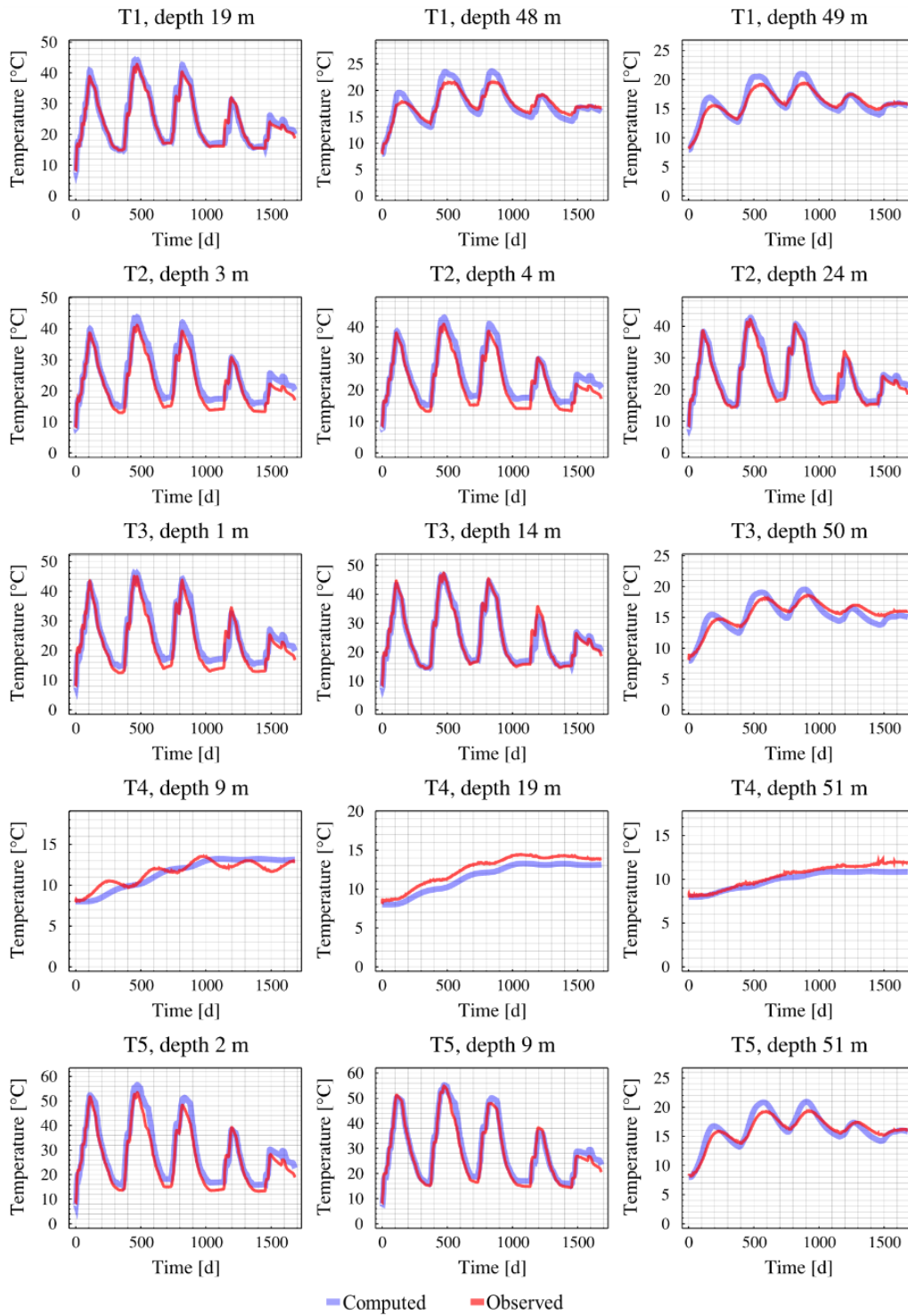
Figure 9. Time series records of computed and observed soil temperatures at 15 different points.

4.2 Energy and exergy performance indicators

Storage performance and system seasonal performance were evaluated in terms of energy and exergy efficiency in accordance with the definitions given in section 3.6. Figure 10 shows the results in terms of seasonal system performance indicators. First, a note must be made on the seasonal development of the indicator values. Comparisons between different storing cycles must be made with caution since the flow rate and BTES forward temperature vary over the seasons, which has direct impact on the amounts of energy and exergy exchanged during each cycle. However, it can be seen that scenarios concerning pure conduction (S1) and hydraulic head difference of 1 m across the model domain (S2) show quite similar performance in seasonal energy exchange and efficiency for each storing cycle. During the fourth storing cycle, S2 even performs slightly better than S1 in terms of energy efficiency. This may be attributed to enhanced heat transport within the storage due the groundwater movements, and similar tendency was observed by (Bauer et al., 2009) in their study on the performance of a high temperature BTES. For the scenarios concerning higher hydraulic head differences (S3, S4, S5), detrimental effects on the storage energy efficiency become evident as their indicator values decreases with increasing hydraulic head for each cycle of operation. It can also be observed that higher groundwater flow rates consistently tend to contribute to higher charged energy and less discharged energy amounts.
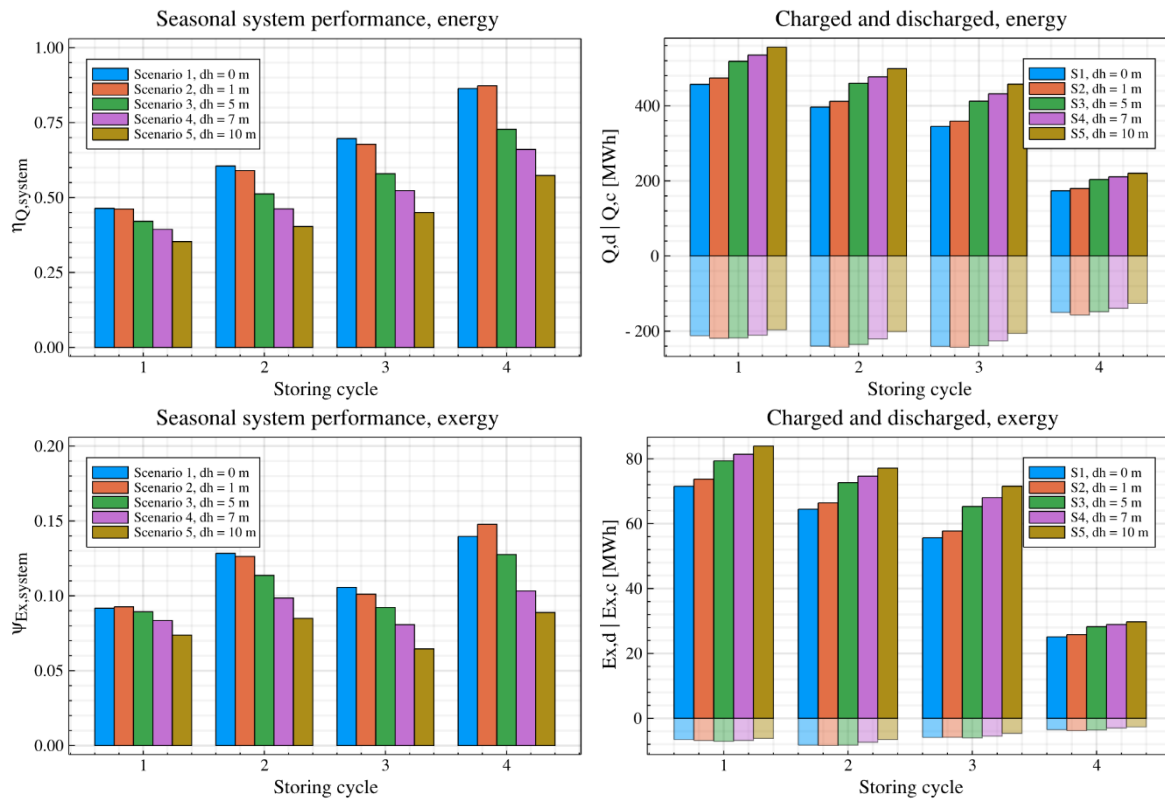
Figure 10. Left: Seasonal energy efficiency ($\eta_{Q,system}$) and seasonal exergy efficiency ($\psi_{Ex,system}$) computed for the first four storing cycles.

Similar trends can be distinguished concerning seasonal exergy efficiencies shown in Figure 10 (bottom charts). However, during the second storing cycle all exergy efficiency indicator values of each scenario differ positively from those evaluated during first and third storing cycle. This is an effect caused by initially high estimated return temperatures during discharge, which is clarified in Figure 11 (top), showing forward and return temperatures for all scenarios during the charging and discharging periods. It is worth to note that return temperatures during this period tend to be overestimated as compared to observed data (see

section 4.1), although the figures depicted here only consider modeled scenarios with identical conditions besides the hydraulic head value imposed on the upstream boundary.
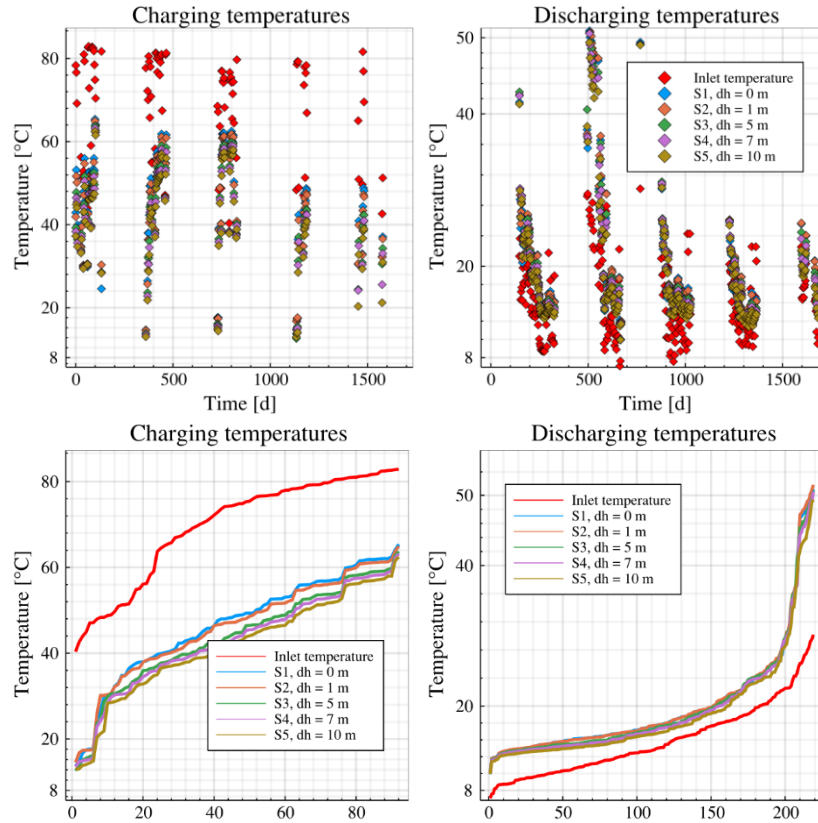
Figure 11. Top, left to right: 1. Charging temperatures vs. operation time. 2. Discharging temperatures vs. operation time. Bottom, left to right: 1. Duration curves for inlet and outlet temperatures during charging operation. 2. Duration curves for inlet and outlet temperatures during discharging operation.

Another observation from Figure 10 is that charged amounts of exergy tend to deviate more than discharged exergy amounts when comparing the scenarios for single storing cycles. For clarity, charging and discharging temperatures are presented sorted in ascending order in Figure 11 (bottom), where the horizontal axes represent the number of data points with 72-h resolution. While there is a clear difference in overall charging return temperature levels between the scenarios, less deviation can be observed between the sorted values of discharging return temperature. This is an indication that groundwater flow tends to enhance exergy exchange during charging, but it is not the dominating mechanism of degradation of the temperature build-up within the storage after charging ends, for the specific groundwater flow rates, storage design and operation conditions considered.

This is further shown by observing storage energy and exergy performance indicators seen in Figure 12. Apparently, differences between the scenarios tend to be more pronounced when regarding energy storage performance. It is seen that groundwater flow has a clear effect on the net amount of energy injected into the ground, which is primarily driven by enhanced exchange rates during charging, and less importantly by differences in discharging heat rates. For the initial storing cycles, higher or similar amounts of energy are stored within the storage when comparing groundwater flow scenarios with the pure conduction case, indicating that additional heat flow across storage boundaries induced by advection is rather balanced with the additional heat injection. This tendency does however decline as time develops, and at the final time step the largest amounts of stored energy are observed for the scenarios considering no (S1) or low (S2) groundwater flow velocities, although these scenarios show the lowest amounts of net energy injected. Consequently, as the increase of groundwater velocity, storage energy efficiencies are decreasing after a

certain time. At the end of the simulation period, the storage energy efficiency for the case of highest velocity (S5) is 18%, as compared to 45% in case of pure conduction (S1).
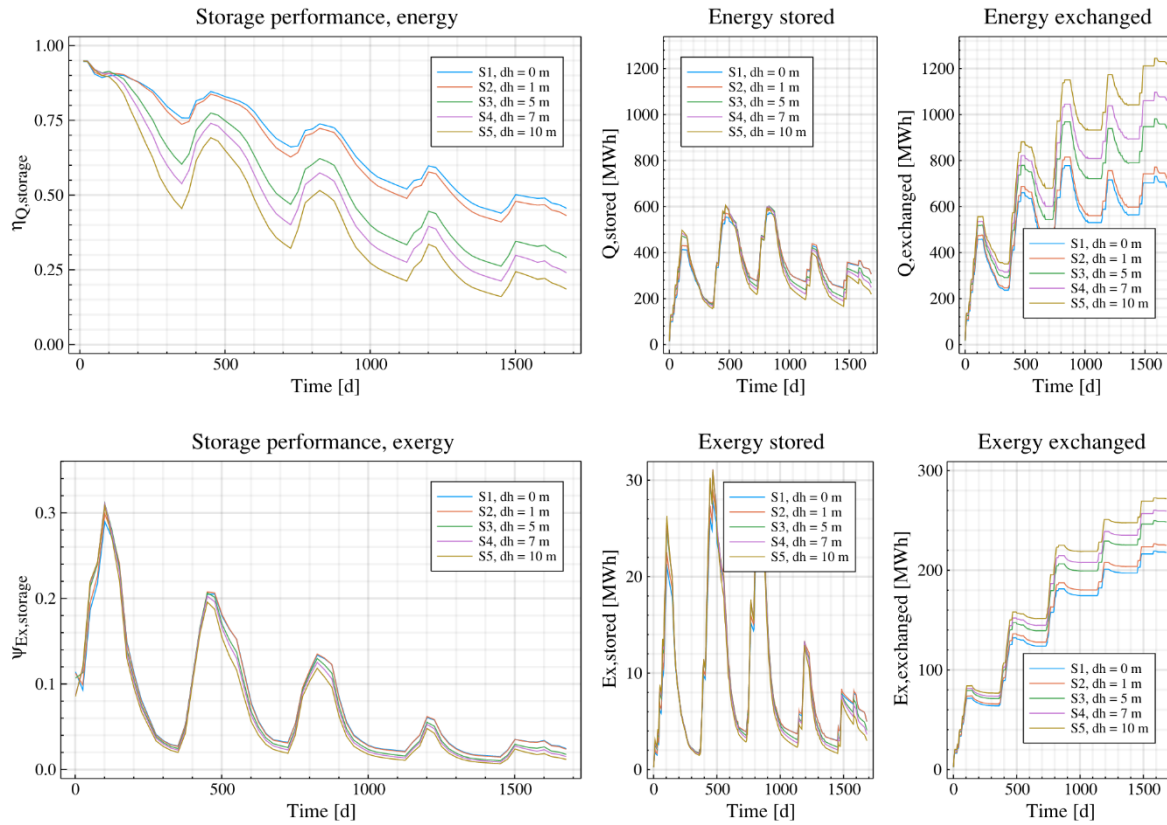

Figure 12. Storage energy efficiency ($\eta_{Q,storage}$) and storage exergy efficiency ($\psi_{Ex,storage}$).

By comparing the plots showing energy and exergy storage efficiencies in Figure 12, it appears that the exergy indicator is less sensitive to groundwater flow rate than the energy indicator. Again, as in the case of energy exchange, it is evident that groundwater flow promotes exergy transfer during charging. It can also be seen that the amount of exergy extracted from the storage is rather low and equal for all scenarios, but this tendency is not reflected by the figure representing the amount of exergy stored in the storage volume, which still shows large fluctuations between charging and discharging periods as a result of exergy losses and destruction. For example, at the end of the initial charging period around 70% of the exergy injected into the storage was already lost or destroyed in all scenarios. During the subsequent discharging period, only around 6 MWh of exergy was extracted, while the amount of exergy stored dropped from between 20-24 MWh to less than 2 MWh at the end of the storing cycle irrespective of groundwater flow rate. Hence, there is a single or combination of mechanism that causes large exergy loss and destruction rates within the storage volume, and the exergy storage performance is accordingly poor. Although it can be seen after a couple of storage cycles that lower groundwater flow velocities contribute to somewhat higher exergy storage efficiency, it is not of main importance for the overall performance. It should, however, be noted that the effect of groundwater flow on exergy performance could be more prominent under other operation and subsurface conditions than the ones set out in this study.

As can be understood from the definitions of the storage energy and exergy performance indicators (section 3.6), exergy analysis is capable of reflecting the quality of the heat being injected, stored and extracted, which is in contrast to energy analysis that only considers quantity. In the case of the Brædstrup HT-BTES, the system is operated using rather high charging temperatures (i.e. high quality heat), while heat is discharged at temperatures relatively close to the reference environment (undisturbed ground) temperature (Figure 11). Under such conditions energy extraction is promoted and the storage temperatures will be kept at moderate levels (see Figure 13), but the exergy performance will be penalized.
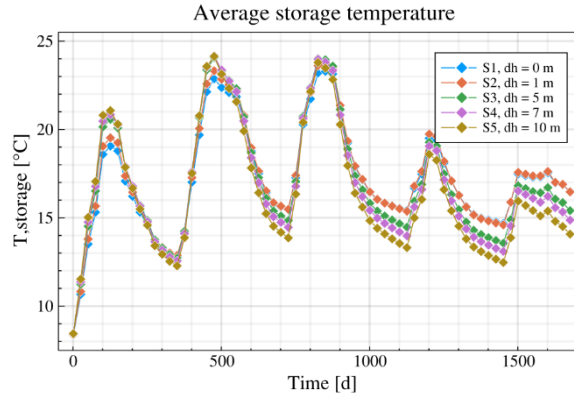
Figure 13. Average soil temperature inside the storage domain.

In this view, an alternate operation strategy could for example be to use the high quality heat for short-term storage purposes and use lower quality heat to balance a combined heat and cold storage operating alternately above and below the temperature of the undisturbed ground. Otherwise, the high quality heat could be used to maximize the temperature build-up within the storage, in combination with energy extraction rate control with respect to a threshold discharge temperature that enables the heat to be recovered possibly without the use of heat pumps. In the latter case, the effect of groundwater flow on exergy storage would probably be relatively more prominent because of cold groundwater is advected into the storage region and contributes to temperature degradation by mixing and disturbance of stratification. For a storage operating under balanced conditions at temperature levels close to the undisturbed ground temperature, this effect is expected to be minor.

4.3 Energy losses and exergy destruction

Temperature fields obtained from the simulations were visualized to provide a qualitative insight on groundwater impacts on storage thermal performance. For this purpose, the scenarios concerning minimum (S1) and maximum (S5) groundwater velocity were considered to demonstrate the contrast between pure conduction and advection-influenced conditions. The relative importance of advective to conductive heat transport can be expressed by a dimensionless parameter called the Péclet number, which characterizes the ratio of the heat advection rate caused by groundwater movements to the rate of temperature gradient driven heat conduction:

$$Pe = \frac{Lq}{\alpha} \tag{12}$$

where L is a characteristic length, here the borehole length, q is the Darcy flux and α is the thermal diffusivity of the porous medium. As shown in Figure 14, the Darcy flux varies greatly over low- and high-permeability layers for the groundwater flow scenarios, and the Péclet number is varying accordingly. For Péclet numbers greater than 1, advective transport dominates over conductive effects. This is true in the depth intervals of 9-20 m and 26-80 m for all flow scenarios except S2, where Péclet numbers larger than unity are reached only in the interval of 26-41 m. In the low-permeability zones Péclet numbers are several orders of magnitude smaller than 1, thus a conduction-dominated thermal regime prevails in these layers.
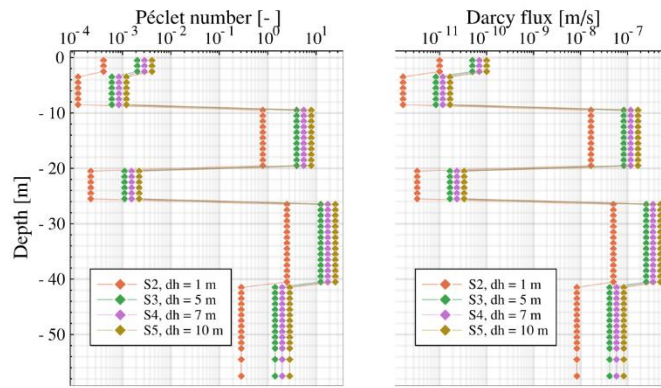
Figure 14. Variation of Péclet number and Darcy flux with depth.

For scenario S5, Péclet numbers in the range between 1.2E-3 and 2.5E+1 are obtained, corresponding to Darcy flux rates between 1.7E-11 m/s (1.44E-4 cm/d) and 5.0E-7 m/s (4.3 cm/d). Considering these rates relative to the spatial and temporal scale of the storage and the storing cycles, respectively, only flux rates having similar magnitudes as the latter are expected to be high enough to have visible impact on the temperature distribution over the course of a storage cycle. In Figure 14, cross-section views of the storage visualizing the evolution of the temperature distribution (described by combined continuous temperature and isotherms plots) during the initial storing cycle for scenarios S1 (pure conduction) and S5 (maximum hydraulic gradient) are shown.

The times considered here correspond to the end of the charging period (105 d), 12 days ahead of discharging start (135 d), 3 days after discharging start (150 d), and subsequent times (201 d, 249 d) until end of the initial discharging period (369 d). The storage domain is indicated as a fixed line surrounding the BHEs. Indeed, groundwater flow effects on the thermal distribution can be observed within the high-permeability zones already at the end of the charging period. These effects appear as thermal plumes that develop in the downstream direction of the flow. It can also be seen that the thermal distributions within the low-permeability zones are initially similar for both scenarios. The storage in both scenarios exhibits temperatures equal to or larger than 54 °C at the center regions, but this high temperature field is considerably more developed in the groundwater flow scenario due to heat transfer enhancement effects. Some tendency of the high temperature field being displaced in the direction of the groundwater flow can be observed, although the highest thermal energy density still is concentrated close to the storage center. The visualizations comply well with the quantitative results presented in section 4.2, where stored amounts of energy and exergy as well as average storage temperature are shown to be at highest levels for the case of maximum flow rate at the end of the initial charging period.

At time 135 d, the storage is in inactive operation mode before discharging starts at time 147 d, hence any changes in storage energy or exergy content are due to subsurface losses or destruction. Comparing the temperature fields at 105 d and 135 d clearly shows that a main part of the region containing high quality heat (≥ 54 °C) have been degraded in both scenarios. The rapid rate of temperature loss also in scenario S1 indicates that heat conduction is a significant source of exergy destruction during this phase. Advective effects on the center region temperature field also become more prominent. A clear disturbance of the temperature field particularly in the lower high-permeability layer can be observed, which results in locally lower ground temperatures close to the BHEs located in the upstream region of the storage, and vice versa in the downstream region. While no substantial heat flow across the storage boundaries can be seen in the pure conduction scenario, temperatures up to around 28 °C occur outside the storage domain at time 135 d.

The plots showing temperature fields at consequent times (150-369 d) represent the development of the thermal process occurring during discharge. The presence of BHEs is indicated by slender vertical low temperature regions inside the storage. Shortly after discharging starts (150 d), clear horizontal stratification and uniformly distributed thermal gradients can be distinguished in the pure conduction scenario, which enable efficient use of the series connected BHEs.

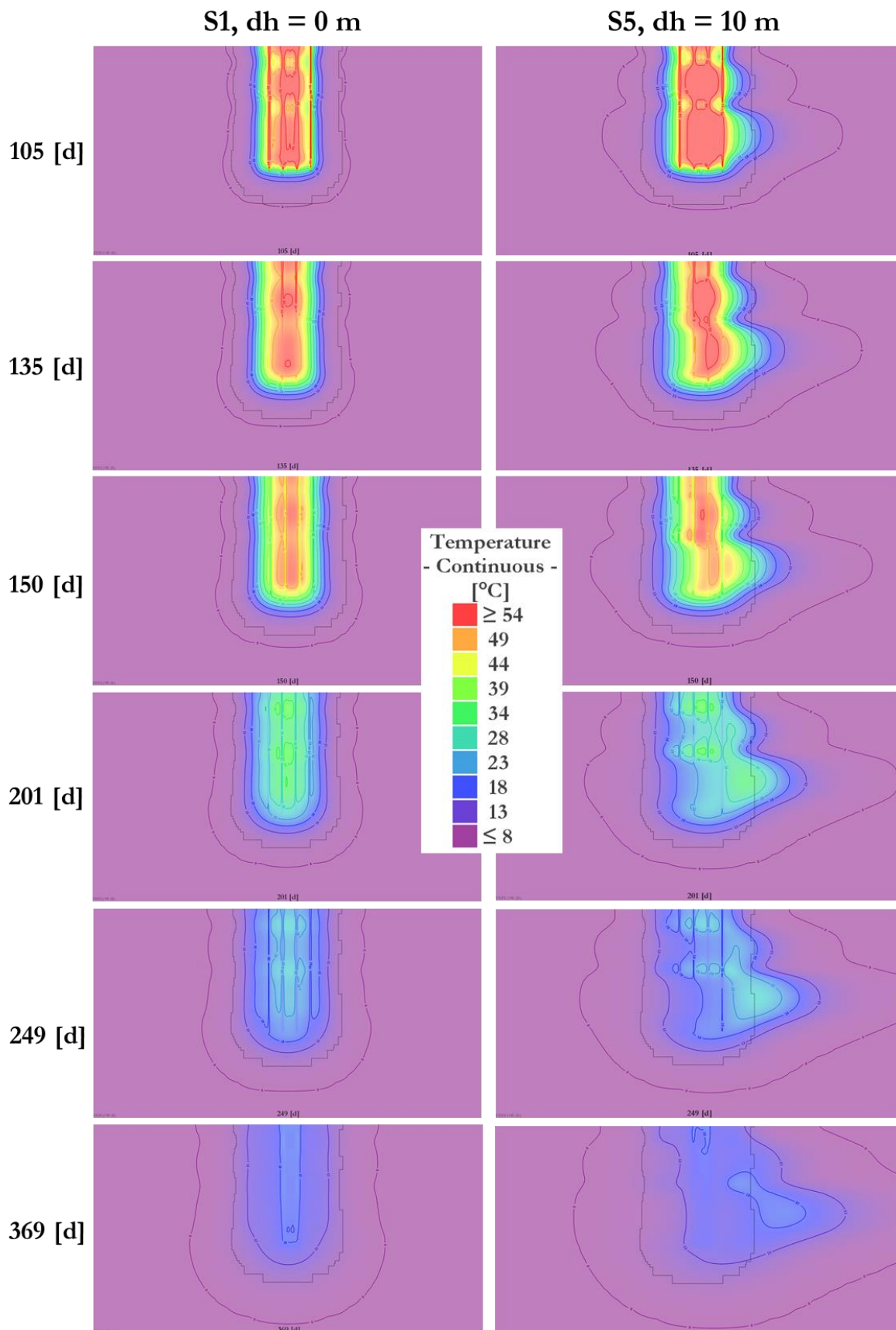*Figure 15. Cross-section views of the storage showing the evolution of the temperature distribution during the initial storing cycle for Scenario 1 (pure conduction) and Scenario 5 (maximum hydraulic gradient).*

This is not the case in the groundwater flow scenario, where a distorted and, locally, a slightly layered temperature distribution has been induced. A possible consequence of this effect might be, for example,

that the heat carrier fluid extracts heat in one region of the storage domain and re-injects it into another region at lower temperature. Depending on storage temperature distribution and BHE array arrangement, this could possibly even result in net energy injection into the storage through some of the BHE arrays, contrary to the intended discharging operation.

During remaining times (201-369 d), the temperature build-up within the storage continues to degrade. At final time, it can be clearly seen that large amounts of heat have been lost to the ambient ground in the groundwater flow scenario. The heat that has been advected downstream the storage region cannot be recovered. As shown in section 4.2 (Figure 12), only ~45% of the net injected heat remains within the storage domain at the end of the first storing cycle, as compared to ~75% in case of the pure conduction scenario.

Another view of the storage at identical times as those considered above is shown in Figure 15. Here, horizontal temperature fields at a depth of 35 m are shown in relation to BHE locations and BHE array arrangement, allowing for better demonstration of the importance of thermal stratification within the storage. As can be seen at time 150 d, a drift of the high temperature region originating from the storage center can be identified in the groundwater flow scenario. Because of the advection movement, only a single (out of eight) array outlet borehole intersects with the region defined by the maximum isotherm shown (49 °C) at this depth. At the subsequent time point, the maximum isotherm has decreased to 28 °C, and the region within this contour is completely located outside the bore field perimeter. This implies that no efficient storage operation and use of the heat injected can be accomplished under these conditions, with the specific borehole arrangement considered.

S1, dh = 0 m, z = -35 m **S5, dh = 10 m, z = -35 m**

105 [d]

135 [d]

150 [d]

Temperature
- Continuous -
[°C]

≥ 54
49
44
39
34
28
23
18
13
≤ 8

201 [d]

249 [d]

369 [d]

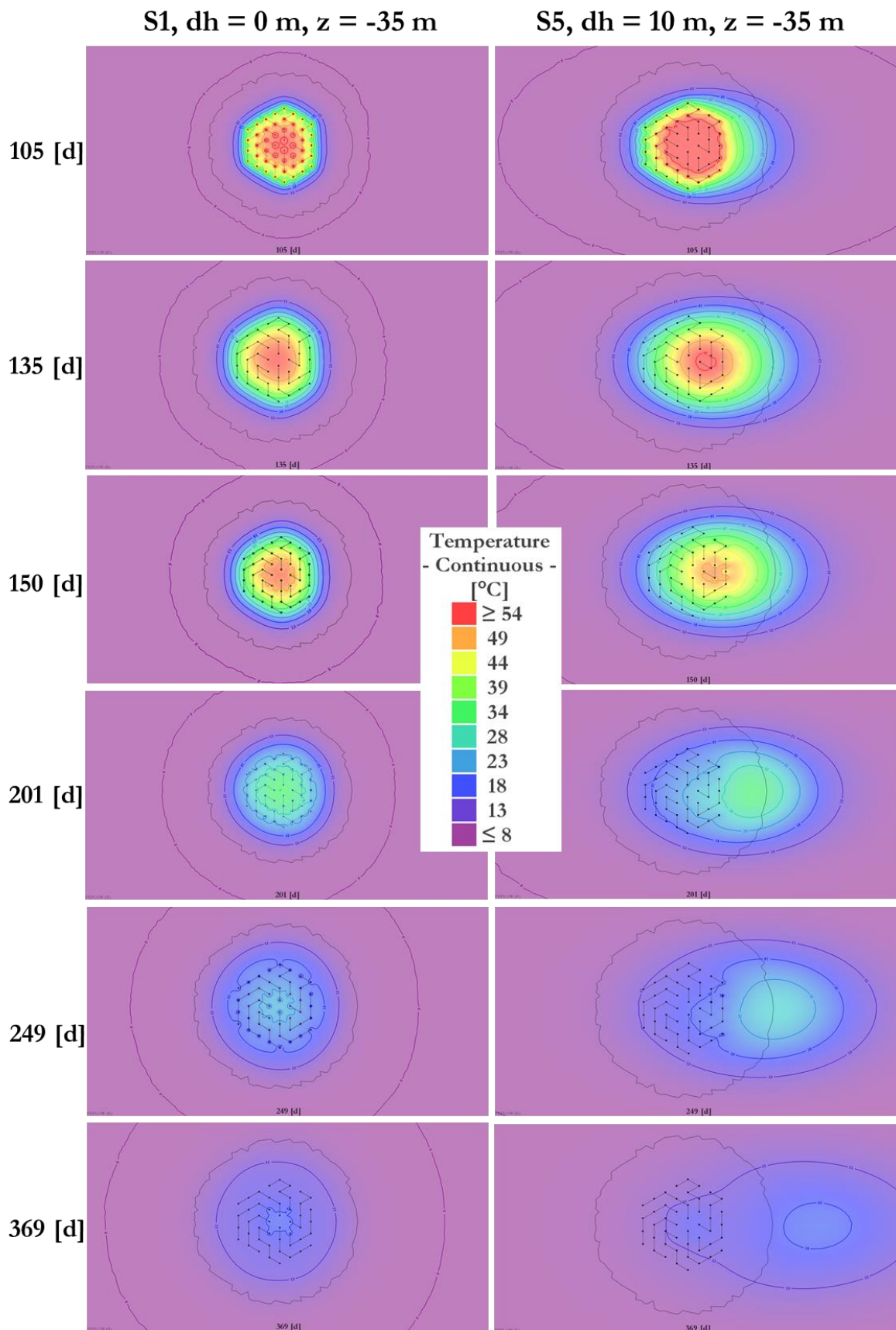*Figure 16. Top views of the storage at z = -35 m showing the horizontal temperature distribution development during the initial storing cycle for Scenario 1 (pure conduction) and Scenario 5 (maximum hydraulic gradient).*

5 Discussion

Development of efficient borehole thermal storage systems requires profound understanding of the subsurface thermal and hydraulic processes involved, as well as of the importance of proper operation strategies and BHE designs. Detailed and accurate coupled hydro-thermal modeling of subsurface processes could greatly help to gain insight into BTES thermal behavior under different ground conditions. Coupling between models of the BTES and other components within an energy system would also allow for advanced prediction and optimization procedures to be implemented in system design and operation.

Modeling of coupled subsurface processes is however associated with many challenges, which bring considerable difficulties to BTES thermal analysis. Among them, ground heterogeneity, anisotropy and scale effects can particularly be sources of difficulties in characterizing ground conditions and accurate modeling of subsurface thermal distribution in BTES systems. This is particularly true in fractured hard rock environments, where the fluid flow behavior commonly is significantly affected by intrinsic variety of fracture network characteristics at different spatial scales. Increasing development of underground infrastructure as well as conflicting interests in subsurface resources, especially in urban areas, are also factors likely to add complexity to the problem. Not only could groundwater aspects be of importance for BTES design and performance, but they could also be of significance regarding BTES thermal and chemical impacts on the surrounding environment, which may be more sensitive to groundwater movements than the storage itself. Hence, there is a need for gaining a deeper understanding of how BTES and groundwater systems interact, and what possible impacts that could follow in different environments.

Although groundwater aspects have received relatively little attention in research in closed-loop shallow geothermal systems, concepts of groundwater flow and subsurface transport processes have been extensively studied within the field of hydrogeology and other geosciences disciplines during the last decades. Significant advancements have been made in understanding these processes for a wide variety of hydrogeological conditions. Approaches for dealing with even extreme heterogeneity and anisotropy (e.g., in the case of fractured hard rock) have been developed, driven among other by extensive research programs on nuclear waste disposal in deep rock repositories.

Although being applicable to other problems, e.g., thermal storage in shallow fractured rock, assessment of what approach is best suited for the specific application, the spatiotemporal scale of the problem, the ground characteristics, and the level of accuracy and detail required is not trivial. First, there is a paucity of experimental data regarding BTES subsurface temperatures in general, and particularly from systems in groundwater rich areas or in fractured rock. Second, adoption of modeling approaches employed for other engineering applications and research disciplines (e.g., enhanced geothermal systems, CO_2 sequestration, waste disposal etc.) must be done with care, since the spatial or temporal scale or other aspects of the processes involved could be fundamentally different. Third, the characteristics of a flow and transport problem are often very site-specific, and the validity of a specific modeling approach must be assessed within that context. For example, employing the classical continuum modeling approach to study flow and transport processes within a granular porous material is most often a reasonable choice, while in a fractured rock mass for which a representative elementary volume cannot be found it would not be meaningful. Instead the actual geometry of the water-bearing features must be considered to some extent (see, e.g., (Shapiro, 1987)). Validation and applicability assessment of conceptual or mathematical modeling approaches available is thus not straightforward, and a generic answer to the question of what approach that is best suited for handling flow and heat transport processes in BTES systems cannot be given. An elaboration on these issues is given by (Tsang, 1990).

To make further advancement in understanding coupled hydro-thermal processes in BTES applications, efforts related to the issues discussed above should be made. A key contribution could come from experimental data, which requires further implementation of pilot or full-scale BTES projects with focus on designing data acquisition systems that are well suited for monitoring subsurface hydraulic and thermal processes during operation. This also includes development of in-situ investigation methods for combined characterization of hydrogeological and thermal ground conditions (see, e.g., (Klepikova, 2013)), that are capable of capturing characteristics at all scales relevant to the problem. Moreover, a comprehensive review

and comparison of concepts and methods used to study groundwater flow and transport processes in porous and fractured media (in particular) could be carried out, and their applicability in the context of BTES modeling could be assessed. Both implicit as well as explicit conceptual and numerical models for representing fractured porous media (Berkowitz, 2002; Berre et al., 2018) should be employed and compared. Detailed analysis would provide deeper intuitive and computational understanding of how observations made of in-situ hydraulic and geometric fracture characteristics translate to predictive ability. That is, to gain an understanding of at what critical level of fracturing etc. advection effects might become significant to BTES thermal performance. Also, detailed modelling using explicit conceptualizations of water-bearing features can be an effective approach for assessing the accuracy and applicability of less computationally demanding implicit models (see, e.g., (Chen et al., 2017)).

Besides the importance of accurately considering the hydro-thermal processes occurring in the ground, a detailed and realistic representation of the ground-coupled heat exchanger system is required to enable precise evaluation and optimization of the thermal performance of the BTES. The great variability in possible BHE arrangements and operation strategies, associated with the objective of maintaining thermal stratification within a HT-BTES, entails more modeling complexity when compared to ordinary parallel-connection arrangements that are frequently used in low-temperature systems. The FEFLOW plugin tool developed within this work (Section 3.3) allows for modelling of any number of arbitrarily interconnected BHEs. Currently, the plugin supports boundary conditions with equal array inlet temperature and flow rate, and variable flow direction according to user-defined control rules. Further efforts can be made to extend the modeling capabilities by implementing support for other types of BHE boundary conditions as well as coupling with dynamic energy simulation codes such as TRNSYS or Modelica-based software to model the interaction between the BTES and other components within the energy system.

In the validation study (Section 4.1), it was found that the pure conduction model could fairly accurately reproduce observed BHE heat exchange rates as well as depth-distributed soil temperatures measured at different locations throughout the Brædstrup storage. Hence, the FEFLOW plugin proved to be a useful tool for predicting the thermal behavior of the BHEs and capturing the thermal dynamics of the storage, including the thermal stratification that is built up due to the series-connection BHE arrangement used in the BTES design. These are important features for evaluating the thermal performance of the BTES and thus, their accurate prediction gives the possibility to optimize the design and operation of the storage with regards to for example energy or exergy efficiency. However, it must be emphasized that the plugin has shown to be valid only for this specific model, and hence further validation with other BHE geometries, series arrangements, input data time resolutions etc. is required. A limitation of the numerical approach employed in this study is that the computational burden of the calculation can be very high compared to analytical methods, especially in cases when high temporal resolution of boundary conditions or dependent variables is required. A temporal resolution in the order of days, as was applied in this study, can be adequate for capturing the thermal dynamics of the ground, but for predicting the short-term behavior of the BHEs it is not suitable. Substantial computational effort can however be saved by the use of the quasi-stationary analytical BHE model by (Eskilson and Claesson, 1988) available in FEFLOW. It comprises a reasonable compromise between computational efficiency and accuracy, and has shown to be a good alternative to numerical 1D BHE models as well as fully discretized 3D solutions for processes occurring at temporal scales larger than a few hours (DHI-WASY, 2010). Because of the assumption of local steady-state conditions inside the BHEs, care must though be taken if the actual short-term loading conditions are highly transient. This was the case especially during the discharge periods, which consequently contributed to deviations between observed and computed BHE temperatures. These tendencies were also reported by (K. W. Tordrup et al., 2017).

Overall, however, the agreement between computed and observed heat exchange rates and subsurface temperature is fairly satisfactory. The temperature fields obtained from the simulation of the pure conduction model can therefore be considered to be suitable for analyzing the thermal behavior of the real storage, as well as for comparisons with simulation results obtained from other models accounting for alternative hypothetical loading or ground conditions. In this work, the pure conduction model served the purpose of providing a reference scenario for evaluating how the storage performance depends on

groundwater flow under equal charging and discharging (flow and inlet temperature) conditions. Although a simple, hypothetical representation of a real groundwater system, the coupled hydro-thermal model features some characteristics that may be encountered in many hydrogeological environments. For example, vertical soil heterogeneity was accounted for by assigning a hydraulic conductivity value to each of the geological layers that were identified by (K. W. Tordrup et al., 2017). The presence of highly conductive as well as low-permeability adjacent sublayers creates an extremely heterogeneous environment where both conduction and advection dominated heat transport regions may exist if a hydraulic gradient is present (Figure 14). The variability in thermal regimes between these regions suggests that considering solely heat conduction or assuming homogeneous medium, which are common assumptions in design of closed-loop shallow geothermal systems, may in some cases be insufficient to provide a good representation of the processes that occur in the actual system. Therefore, when investigating a potential storage site or designing the borefield, it is of importance to consider the site-specific conditions and collect appropriate information to assess the validity and applicability of these assumptions.

By extending the performance evaluation analysis beyond the boundaries at the BHE inlets and outlets, it is possible to compare quantitatively how different subsurface characteristics affect the storage capacity and the temperature regime inside the storage. There are some limitations associated with the conventional seasonal energy efficiency/utilization ratio indicator that is frequently used in the literature to assess the performance of BTES systems. To evaluate this performance figure, the storage is essentially treated as a black-box system without considering neither how energy is lost nor how it is charged and discharged. For example, it is possible to achieve a seasonal energy ratio of 1 if heat is discharged at temperatures lower than that of the undisturbed ground (e.g., in the case of BHEs coupled to a heat pump), but the discharge rate of the same storage could also be restricted due to temperature mismatches if the system is directly coupled to the heat sink. Also, no information is provided on how the injected heat is distributed in the ground, e.g., whether it is still available in the vicinity of the BHEs or has been lost to the ambient. Overall, the sole consideration of energy efficiency cannot be deemed sufficient for evaluation of BTES system thermal performance since it does not adequately address concerns about the thermal processes occuring within the storage. Neither does it explicitly account for the temperature at which heat is injected, stored and extracted. Therefore, by introducing the concepts of exergy and storage efficiency in the analysis, a better characterization of the system and storage performances can be achieved. The four indicators employed in this study depict the energy and exergy performance at the system level (based on inlet/outlet quantities) as well as at the storage level (based on inlet/outlet and subsurface quantities). Although each of the indicators alone cannot capture all factors relevant for assessing the thermal performance of the storage system, together they complement each other and provide a rational and comprehensive basis for BTES performance evaluation. However, while the seasonal system indicators have been fairly established in the literature (e.g., (Kizilkan and Dincer, 2012; Rezaie et al., 2015)), the storage indicators were recently introduced by (Lazzarotto et al., 2020) and are rather novel in BTES applications. Since evaluation of the latter indicators depend on a parameter representing the storage volume, a viable definition and consistent application thereof is required to facilitate comparison of storage performance across studies dealing with different BTES designs and subsurface conditions. Defining the storage volume is not straightforward due to the ambiguity of the lateral and lower boundaries of the storage. In (Lazzarotto et al., 2020) as well as in the present work, the storage volume was defined by identifying a subdomain containing a certain portion of the total amount of heat injected after a characteristic time (see Section 3.6). This approach is not ideal for assessing and comparing storages that are situated in environments with substantially different conditions. If the storage domain is defined using the actual heat distribution it will also reflect and depend on factors contributing to losses and will thus contain a large amount of non-recoverable heat. Considering that the purpose of the storage performance indicator is to quantify the ability of the storage to maintain the injected heat within the storage volume, the limitations of this definition become apparent. Therefore, future work may study how the selection of storage volume affects the storage performance indicator values, and whether other approaches to defining the storage volume might be better suited. For example, a definition of the storage volume based on the geometric characteristics of the BTES can be considered, as is done, e.g., in the DST model (Chapuis and Bernier, 2009). Extending the energy and exergy analyses by considering also smaller subdomains within the storage could help to improve the understanding of the

thermal behavior of the BTES. Likewise, refining the resolution of the analysis at the system level (e.g., by evaluating the performance of individual BHE arrays) may also help to provide better insight in the functioning of the system and to identify sources of inefficiencies throughout the storing cycles.

From the energy and exergy analyses, it was found that groundwater flow has in general negative impact on the BTES thermal performance, which tends to decrease with higher flow rate. This finding is in agreement with most studies that have investigated groundwater flow effects on BTES systems (Catolico et al., 2016; Diersch and Bauer, 2014; Nguyen et al., 2017). A few exceptions to this trend could however be observed. For example, for the case of the smallest non-zero hydraulic gradient considered, it was found that the BTES seasonal energy and exergy efficiencies occasionally were slightly higher when compared to the case of pure conduction. This can possibly be attributed to enhanced heat transfer induced by the groundwater movement. It is, however, likely that after a time longer than the simulation time considered, consistently negative effects of groundwater flow can become apparent also in this scenario. To gain a more thorough understanding of the influence of groundwater flow, parametric analysis considering larger time scales and different ranges of groundwater flow rates as well as charging and discharging temperature levels is recommended. For this purpose, rather than computationally demanding numerical methods, analytical models could provide a suitable means to generate the extensive simulation data required for the analysis.

6 Conclusions and recommendations for future research

The assumption of pure conduction heat transfer in a homogeneous and isotropic medium has traditionally been a standard assumption in the field of modeling and design of borehole heat exchangers for shallow geothermal applications, although such ideal conditions are rare in actual subsurface environments. With the growing interest in large-scale HT-BTES systems, adequate practises for characterizing and accounting for the geological and hydrogeological conditions at the storage site are required for successful design and performance evaluation of the system, as well as for assessing the impact of the BTES on the surrounding environment.

Because of the compositional and spatial diversity of hydrogeological conditions found at different scales and sites, there is no universally valid approach for characterizing and modeling subsurface flow and transport processes. Recent and ongoing research on coupled subsurface hydro-thermal processes in porous and fractured media has provided a robust and comprehensive framework for modeling complex flow and transport processes in a wide variety of hydrogeological settings to face this challange. These modeling concepts, typically based on deterministic and stochastic continuum or DFN approaches, have now become become well-established in hydrogeologic practice. Future exploration of their applicability also in the context of BTES modeling could provide a basis for more accurate prediction of the subsurface temperatures within the storage.

It follows from the site-specific nature of any groundwater flow and transport problem that general guidelines on groundwater effects on BTES design and performance are difficult to provide. Instead, an individual assessment is typically required for each case, and a numerical approach to the study of actual coupled flow and transport problems is usually needed. In this work, a FEM pure heat conduction model has been applied to simulate the operation of an existing HT-BTES located in dry heterogeneous soil. To replicate the actual BTES operation, a FEFLOW plugin tool for enabling control of flow direction through series-connected BHEs has been developed and validated against operational and monitoring data. The plugin tool was shown to be capable of accurately predicting the long-term thermal dynamics of the BHEs and the storage medium. However, further evaluation is required for assessing its applicability for shorter-term problems.

The validated pure conduction model provided a benchmark by which to compare the behaviour of the BTES under influence of groundwater flow. Numerical experiments were conducted by assuming a hypothetical groundwater flow system within the model domain. The simulations demonstrate that the thermal behaviour of a BTES in a conduction-dominated environment is fundamentally different from that in an advection-dominated environment. In the pre-investigation and design process for HT-BTES systems, appropriate and sufficient information should therefore be collected to assess the validity and applicability of assuming either conduction or combined conduction-advection heat transport in the ground.

Based on KPIs in terms of energy and exergy efficiencies evaluated at a system as well as a storage level, a performance evaluation study has been carried out to quantify how the occurrence of groundwater flow affect the amount and quality of the heat being stored and exchanged. Adding exergy next to conventional performance figures based on energy efficiency may contribute to a more comprehensive understanding of the thermal behaviour and performance of the BTES system as it can reflect the energy usability under different operation conditions and allow for identifying sources of inefficiencies throughout the storing cycles. Based on the performance evaluation study, it was shown that high groundwater flow rates are in general detrimental to the performance in terms of seasonal system energy and exergy efficiency, as well storage energy efficiency. The results indicate, however, that small groundwater flow rates can have a slight positive effect on the system level performance due to enhanced heat transport driven by advection. Advective effects on storage exergy performance were found to be less pronounced, which could be an effect of other major mechanisms contributing to temperature degradation under investigated conditions.

Future studies are called for to further evaluate HT-BTES performance under a wider range of time scales, BHE designs, operation conditions and subsurface conditions. A numerical approach as is used in this work can be applied for simulations with a high level of detail and accuracy, although this comes with a high

computational burden. Therefore, it is recommended to explore the use of analytical methods for conducting extensive parametric studies.

Bibliography

Adler, P.M., 1999. Fractures and Fracture Networks, Theory and Applications of Transport in Porous Media, 15. Springer Netherlands, Dordrecht.

Al-Khoury, R., Bonnier, P.G., 2006. Efficient finite element formulation for geothermal heating systems. Part II: transient. International Journal for Numerical Methods in Engineering 67, 725–745. https://doi.org/10.1002/nme.1662

Al-Khoury, R., Bonnier, P.G., Brinkgreve, R.B.J., 2005. Efficient finite element formulation for geothermal heating systems. Part I: steady state. International Journal for Numerical Methods in Engineering 63, 988–1013. https://doi.org/10.1002/nme.1313

Andújar Márquez, J.M., Martínez Bohórquez, M.Á., Gómez Melgar, S., 2016. Ground Thermal Diffusivity Calculation by Direct Soil Temperature Measurement. Application to very Low Enthalpy Geothermal Energy Systems. Sensors (Basel) 16. https://doi.org/10.3390/s16030306

Angelotti, A., Alberti, L., La Licata, I., Antelmi, M., 2014. Energy performance and thermal impact of a Borehole Heat Exchanger in a sandy aquifer: Influence of the groundwater velocity. Energy Conversion and Management 77, 700–708. https://doi.org/10.1016/j.enconman.2013.10.018

ASHRAE, 2015. 34. Geothermal Energy, in: 2015 ASHRAE Handbook - Heating, Ventilating, and Air-Conditioning Applications. American Society of Heating Refrigerating and Air-Conditioning Engineers, Inc.

Banks, D., 2015. A review of the importance of regional groundwater advection for ground heat exchange. Environ Earth Sci 73, 2555–2565. https://doi.org/10.1007/s12665-014-3377-4

Bauer D., Heidemann W., Müller-Steinhagen H., Diersch H.-J. G., 2011. Thermal resistance and capacity models for borehole heat exchangers. International Journal of Energy Research 35, 312–320. https://doi.org/10.1002/er.1689

Bauer, D., Heidemann, W., Müller-Steinhagen, H., G Diersch, H.-J., 2009. MODELLING AND SIMULATION OF GROUNDWATER INFLUENCE ON BOREHOLE THERMAL ENERGY STORES, in: Proceedings of Effstock, the 11th International Conference on Thermal Energy Storage. Stockholm, Sweden.

Bear, J., 1972. Dynamics of Fluids in Porous Media. Dover Publications, New York.

Bear, J., Tsang, C.F., de Marsily, G., 1993. Flow and contaminant transport in fractured rocks. Academic Press, San Diego, CA United States.

Bear, J.J., Cheng, H.-D.A., 2010. Modeling Groundwater Flow and Contaminant Transport, Theory and Applications of Transport in Porous Media. Springer, Dordrecht. https://doi.org/10.1007/978-1-4020-6682-5_1

Berkowitz, B., 2002. Characterizing flow and transport in fractured geological media: A review. Advances in Water Resources 25, 861–884. https://doi.org/10.1016/S0309-1708(02)00042-8

Bernier, M.A., 2001. Ground-coupled heat pump system simulation. ASHRAE Transactions 107, 605–616.

Berre, I., Doster, F., Keilegavlen, E., 2018. Flow in Fractured Porous Media: A Review of Conceptual Models and Discretization Approaches. Transp Porous Med. https://doi.org/10.1007/s11242-018-1171-6

Bianchi, G., Panayiotou, G.P., Aresti, L., Kalogirou, S.A., Florides, G.A., Tsamos, K., Tassou, S.A., Christodoulides, P., 2019. Estimating the waste heat recovery in the European Union Industry. Energ. Ecol. Environ. 4, 211–221. https://doi.org/10.1007/s40974-019-00132-7

BLOCON, 2017. EED version 4.

Carslaw, H.S., Jaeger, J.C., 1959. Conduction of Heat In Solids. Oxford science publications, Oxford.

Catolico, N., Ge, S., McCartney, J.S., 2016. Numerical Modeling of a Soil-Borehole Thermal Energy Storage System 15. https://doi.org/10.2136/vzj2015.05.0078

Chapuis, S., Bernier, M., 2009. Seasonal Storage of Solar Energy in Borehole Heat Exchangers. Presented at the Eleventh International IBPSA Conference, Glasgow, Scotland, pp. 599–606.

Chen, R., 2010. Groundwater inflow into rock tunnels (thesis).

Chen, T., Clauser, C., Marquart, G., 2017. Efficiency and accuracy of equivalent fracture models for predicting fractured geothermal reservoirs: the influence of fracture network patterns. Energy Procedia 125, 318–326. https://doi.org/10.1016/j.egypro.2017.08.206

Chiasson, A., O'Connell, A., 2011. New analytical solution for sizing vertical borehole ground heat exchangers in environments with significant groundwater flow: Parameter estimation from thermal response test data. HVAC&R Research 17, 1000–1011. https://doi.org/10.1080/10789669.2011.609926

Chiasson, A.C., Rees, S.J., Spitler, J.D., 2000. A Preliminary Assessment Of The Effects Of Ground-Water Flow On Closed-Loop Ground-Source Heat Pump Systems. ASHRAE Transactions 106, 380–393.

Choi, J.C., Park, J., Lee, S.R., 2013. Numerical evaluation of the effects of groundwater flow on borehole heat exchanger arrays. Renewable Energy 52, 230–240. https://doi.org/10.1016/j.renene.2012.10.028

Cimmino, M., Bernier, M., Adams, F., 2013. A contribution towards the determination of g-functions using the finite line source. Applied Thermal Engineering 51, 401–412. https://doi.org/10.1016/j.applthermaleng.2012.07.044

Dehkordi, S.E., Olofsson, B., Schincariol, R.A., 2015a. Effect of groundwater flow in vertical and horizontal fractures on borehole heat exchanger temperatures. Bull Eng Geol Environ 74, 479–491. https://doi.org/10.1007/s10064-014-0626-4

Dehkordi, S. Emad, Schincariol, R.A., 2014. Effect of thermal-hydrogeological and borehole heat exchanger properties on performance and impact of vertical closed-loop geothermal heat pump systems. Hydrogeol J 22, 189–203. https://doi.org/10.1007/s10040-013-1060-6

Dehkordi, S.E., Schincariol, R.A., 2014. Guidelines and the design approach for vertical geothermal heat pump systems: current status and perspective. Can. Geotech. J. 51, 647–662. https://doi.org/10.1139/cgj-2012-0205

Dehkordi, S.E., Schincariol, R.A., Olofsson, B., 2015b. Impact of Groundwater Flow and Energy Load on Multiple Borehole Heat Exchangers. Groundwater 53, 558–571. https://doi.org/10.1111/gwat.12256

DHI-WASY, 2010. FEFLOW White Papers Vol. 5.

DHI-WASY, 2009. FEFLOW White Papers Vol. I.

Diao, N., Li, Q., Fang, Z., 2004. Heat transfer in ground heat exchangers with groundwater advection. International Journal of Thermal Sciences 43, 1203–1211. https://doi.org/10.1016/j.ijthermalsci.2004.04.009

Diersch, H.-J.G., 2014. FEFLOW Finite Element Modeling of Flow, Mass and Heat Transport in Porous and Fractured Media. Springer Berlin Heidelberg, Berlin, Heidelberg.

Diersch, H.-J.G., Bauer, D., 2014. Analysis, modeling and simulation of underground thermal energy storage (UTES) systems. Elsevier Inc.

Diersch, H.-J.G., Bauer, D., Heidemann, W., Rühaak, W., Schätzl, P., 2011a. Finite element modeling of borehole heat exchanger systems: Part 2. Numerical simulation. Computers & Geosciences 37, 1136–1147. https://doi.org/10.1016/j.cageo.2010.08.002

Diersch, H.-J.G., Bauer, D., Heidemann, W., Rühaak, W., Schätzl, P., 2011b. Finite element modeling of borehole heat exchanger systems: Part 1. Fundamentals. Computers & Geosciences 37, 1122–1135. https://doi.org/10.1016/j.cageo.2010.08.003

Dietrich, P., Helmig, R., Sauter, M., Hötzl, H., Köngeter, J., Teutsch, G. (Eds.), 2005. Flow and Transport in Fractured Porous Media. Springer-Verlag, Berlin/Heidelberg. https://doi.org/10.1007/b138453

Dincer, I., Rosen, M.A., 2007. Chapter 9 - EXERGY ANALYSIS OF THERMAL ENERGY STORAGE SYSTEMS, in: Dincer, I., Rosen, M.A. (Eds.), EXERGY. Elsevier, Amsterdam, pp. 127–162. https://doi.org/10.1016/B978-008044529-8.50012-4

Eskilson, P., 1987. Thermal analysis of heat extraction boreholes. Department of Mathematical Physics, University of Lund, Lund, Sweden.

Eskilson, P., Claesson, J., 1988. Simulation Model for Thermally Interacting Heat Extraction Boreholes. Numerical Heat Transfer 13, 149–165. https://doi.org/10.1080/10407788808913609

Gehlin, S.E.A., Hellström, G., 2003. Influence on thermal response test by groundwater flow in vertical fractures in hard rock. Renewable Energy 28, 2221–2238. https://doi.org/10.1016/S0960-1481(03)00128-9

GEUS [WWW Document], n.d. URL http://www.geus.dk/ (accessed 12.4.20).

Grycz, D., Hemza, P., Rozehnal, Z., 2014. Charging of the Experimental High Temperature BTES Via CHP Unit - Early Results. Energy Procedia, Proceedings of the 2nd International Conference on Solar Heating and Cooling for Buildings and Industry (SHC 2013) 48, 355–360. https://doi.org/10.1016/j.egypro.2014.02.041

Heath, R.C., 1983. Basic ground-water hydrology. USGeological Survey ;--For sale by Distribution Branch, Text Products Section, USGeological Survey,.

Hellström, G., 1991. Ground heat storage : thermal analyses of duct storage systems.

Hepbasli, A., 2005. Thermodynamic analysis of a ground-source heat pump system for district heating. International Journal of Energy Research 29, 671–687. https://doi.org/10.1002/er.1099

Hu, J., 2017. An improved analytical model for vertical borehole ground heat exchanger with multiple-layer substrates and groundwater flow. Applied Energy 202, 537–549. https://doi.org/10.1016/j.apenergy.2017.05.152

Ingersoll, L.R., Zobel, O.J., Ingersoll, A.C., 1954. Heat Conduction With Engineering, Geological, and Other Applications, Revised edition. ed. University of Wisconsin Press.

Jacquey, A.B., 2017. Coupled Thermo-Hydro-Mechanical Processes in Geothermal Reservoirs:

Joyce, S., Hartley, L., Applegate, D., Hoek, J., Jackson, P., 2014. Multi-scale groundwater flow modeling during temperate climate conditions for the safety assessment of the proposed high-level nuclear waste repository site at Forsmark, Sweden. Hydrogeol J 22, 1233–1249. https://doi.org/10.1007/s10040-014-1165-6

Kalinina, E., McKenna, S.A., Klise, K.A., Hadgu, T., Lowry, T.S., 2012. Incorporating Complex Three-Dimensional Fracture Networks Into Geothermal Reservoir Simulation. GRC Transactions 36, 6.

Karimzade, E., Sharifzadeh, M., Zarei, H.R., Shahriar, K., Cheraghi Seifabad, M., 2017. Prediction of water inflow into underground excavations in fractured rocks using a 3D discrete fracture network (DFN) model. Arab J Geosci 10, 206. https://doi.org/10.1007/s12517-017-2987-z

Katsura, T., Shoji, Y., Sakata, Y., Nagano, K., 2020. Method for calculation of ground temperature in scenario involving multiple ground heat exchangers considering groundwater advection. Energy and Buildings 220, 110000. https://doi.org/10.1016/j.enbuild.2020.110000

Kizilkan, O., Dincer, I., 2012. Exergy analysis of borehole thermal energy storage system for building cooling applications. Energy and Buildings 49, 568–574. https://doi.org/10.1016/j.enbuild.2012.03.013

Klepikova, M., 2013. Imaging of fractured rock properties from flow and heat transport : field experiments and inverse modelling (phdthesis). Université Rennes 1.

Konikow, L.F., 2011. The Secret to Successful Solute-Transport Modeling. Groundwater 49, 144–159. https://doi.org/10.1111/j.1745-6584.2010.00764.x

Lakshmanan, E., 2011. Hydraulic Conductivity - Issues, Determination and Applications.

Lamarche, L., Beauchamp, B., 2007. A new contribution to the finite line-source model for geothermal boreholes. Energy and Buildings 39, 188–198. https://doi.org/10.1016/j.enbuild.2006.06.003

Lanini, S., Delaleux, F., Py, X., R.Olivès, Nguyen, D., 2014. Improvement of borehole thermal energy storage design based on experimental and modelling results. Energy and Buildings 77, 393–400. https://doi.org/10.1016/j.enbuild.2014.03.056

Lazzarotto, A., Mazzotti Pallard, W., Abuasbeh, M., Acuña, J., 2020. Performance Evaluation of Borehole Thermal Energy Storage Systems Through Energy and Exergy Analysis. Presented at the World Geothermal Congress 2020, Reykjavik.

Le Borgne, T.L., Bour, O., Dreuzy, J.R. de, Davy, P., Touchard, F., 2004. Equivalent mean flow models for fractured aquifers: Insights from a pumping tests scaling interpretation. Water Resources Research 40. https://doi.org/10.1029/2003WR002436

Luo, J., Rohn, J., Bayer, M., Priess, A., Xiang, W., 2014. Analysis on performance of borehole heat exchanger in a layered subsurface. Applied Energy 123, 55–65. https://doi.org/10.1016/j.apenergy.2014.02.044

Luo, J., Rohn, J., Xiang, W., Bertermann, D., Blum, P., 2016. A review of ground investigations for ground source heat pump (GSHP) systems. Energy and Buildings 117, 160–175. https://doi.org/10.1016/j.enbuild.2016.02.038

Maréchal, J.C., Dewandel, B., Subrahmanyam, K., 2004. Use of hydraulic tests at different scales to characterize fracture network properties in the weathered-fractured layer of a hard rock aquifer. Water Resources Research 40. https://doi.org/10.1029/2004WR003137

Mielke, P., Bauer, D., Homuth, S., Götz, A.E., Sass, I., 2014. Thermal effect of a borehole thermal energy store on the subsurface. Geothermal Energy 2, 5. https://doi.org/10.1186/s40517-014-0005-1

Molina-Giraldo, N., Bayer, P., Blum, P., 2011a. Evaluating the influence of thermal dispersion on temperature plumes from geothermal systems using analytical solutions. International Journal of Thermal Sciences 50, 1223–1231. https://doi.org/10.1016/j.ijthermalsci.2011.02.004

Molina-Giraldo, N., Blum, P., Zhu, K., Bayer, P., Fang, Z., 2011b. A moving finite line source model to simulate borehole heat exchangers with groundwater advection. International Journal of Thermal Sciences 50, 2506–2513. https://doi.org/10.1016/j.ijthermalsci.2011.06.012

Moradi, A., Smits, K.M., Massey, J., Cihan, A., McCartney, J., 2015. Impact of coupled heat transfer and water flow on soil borehole thermal energy storage (SBTES) systems: Experimental and modeling investigation. Geothermics 57, 56–72. https://doi.org/10.1016/j.geothermics.2015.05.007

Nastev, M., Savard, M.M., Lapcevic, P., Lefebvre, R., Martel, R., 2004. Hydraulic properties and scale effects investigation in regional rock aquifers, south-western Quebec, Canada. Hydrogeology Journal 12, 257–269. https://doi.org/10.1007/s10040-004-0340-6

Neuman, S.P., 2005. Trends, prospects and challenges in quantifying flow and transport through fractured rocks. Hydrogeol J 13, 124–147. https://doi.org/10.1007/s10040-004-0397-2

Neuman, S.P., 1990. Universal scaling of hydraulic conductivities and dispersivities in geologic media. Water Resources Research 26, 1749–1758. https://doi.org/10.1029/WR026i008p01749

Nguyen, A., Pasquier, P., Marcotte, D., 2017. Borehole thermal energy storage systems under the influence of groundwater flow and time-varying surface temperature. Geothermics 66, 110–118. https://doi.org/10.1016/j.geothermics.2016.11.002

Nguyen, A., Pasquier, P., Marcotte, D., 2015. Influence of groundwater flow in fractured aquifers on standing column wells performance. Geothermics 58, 39–48. https://doi.org/10.1016/j.geothermics.2015.08.005

Nilsson, E., 2020. Borehole Thermal Energy Storage Systems for Storage of Industrial Excess Heat : Performance Evaluation and Modelling.

Nordell, B., 1994. Borehole Heat Store Design Optimization. Luleå University of Technology, Luleå.

Nordell, B., Scorpo, A.L., Andersson, O., Rydell, L., Carlsson, B., 2016. Long-term Long Term Evaluation of Operation and Design of the Emmaboda BTES. : Operation and Experiences 2010-2015. Luleå tekniska universitet.

Nußbicker, J., Mangold, D., Heidemann, W., Müller-Steinhagen, H., 2003. Solar Assisted District Heating System with Duct Heat Store in Neckarsulm-Amorbach (Germany).

Ozgener, L., Hepbasli, A., Dincer, I., 2005. Energy and exergy analysis of geothermal district heating systems: an application. Building and Environment 40, 1309–1322. https://doi.org/10.1016/j.buildenv.2004.11.001

Ozudogru, T.Y., Ghasemi-Fare, O., Olgun, C.G., Basu, P., 2015. Numerical Modeling of Vertical Geothermal Heat Exchangers Using Finite Difference and Finite Element Techniques. Geotech Geol Eng 33, 291–306. https://doi.org/10.1007/s10706-014-9822-z

Pacheco, F.A.L., 2013. Hydraulic diffusivity and macrodispersivity calculations embedded in a geographic information system. Hydrological Sciences Journal 58, 930–944. https://doi.org/10.1080/02626667.2013.784847

Pahud, D., Hellström, G., Mazzarella, L., 1996. Heat Storage in the Ground. Duct Ground Heat Storage Model for TRNSYS (TRNVDST). User Manual for the October 1996 Version (Report). Ecole Polytechnique Fédérale de Lausanne.

Pruess, K., 1985. A Practical Method for Modeling Fluid and Heat Flow in Fractured Porous Media. Society of Petroleum Engineers Journal 25, 14–26. https://doi.org/10.2118/10509-PA

Rapantova, N., Pospisil, P., Koziorek, J., Vojcinak, P., Grycz, D., Rozehnal, Z., 2016. Optimisation of experimental operation of borehole thermal energy storage. Applied Energy 181, 464–476. https://doi.org/10.1016/j.apenergy.2016.08.091

Rezaie, B., Reddy, B.V., Rosen, M.A., 2015. Exergy analysis of thermal energy storage in a district energy application. Renewable Energy 74, 848–854. https://doi.org/10.1016/j.renene.2014.09.014

Rivera, J.A., Blum, P., Bayer, P., 2015. Analytical simulation of groundwater flow and land surface effects on thermal plumes of borehole heat exchangers. Applied Energy 146, 421–433. https://doi.org/10.1016/j.apenergy.2015.02.035

Rovey, C.W., 1994. Assessing flow systems in carbonate aquifers using scale effects in hydraulic conductivity. Geo 24, 244–253. https://doi.org/10.1007/BF00767085

Rybach, L., Eugster, W.J., 2010. Sustainability aspects of geothermal heat pump operation, with experience from Switzerland. Geothermics, Special Issue on the Sustainable Utilization of Geothermal Energy 39, 365–369. https://doi.org/10.1016/j.geothermics.2010.08.002

Rybach, L., Mongillo, M., 2006. Geothermal sustainability-A review with identified research needs. Transactions - Geothermal Resources Council 30, 1083–1090.

Selroos, J.-O., Walker, D.D., Ström, A., Gylling, B., Follin, S., 2002. Comparison of alternative modelling approaches for groundwater flow in fractured rock. Journal of Hydrology 257, 174–188. https://doi.org/10.1016/S0022-1694(01)00551-0

Shapiro, A.M., 1987. Transport Equations for Fractured Porous Media, in: Bear, J., Corapcioglu, M.Y. (Eds.), Advances in Transport Phenomena in Porous Media, NATO ASI Series. Springer Netherlands, Dordrecht, pp. 405–471. https://doi.org/10.1007/978-94-009-3625-6_10

Sharqawy, M.H., Mokheimer, E.M., Habib, M.A., Badr, H.M., Said, S.A., Al-Shayea, N.A., 2009. Energy, exergy and uncertainty analyses of the thermal response test for a ground heat exchanger. International Journal of Energy Research 33, 582–592. https://doi.org/10.1002/er.1496

Shewchuk, J.R., 1996. Triangle: Engineering a 2D quality mesh generator and Delaunay triangulator, in: Lin, M.C., Manocha, D. (Eds.), Applied Computational Geometry Towards Geometric Engineering, Lecture Notes in Computer Science. Springer, Berlin, Heidelberg, pp. 203–222. https://doi.org/10.1007/BFb0014497

Signorelli, S., Kohl, Tomas, Rybach. Ladislaus, 2005. SUSTAINABILITY OF PRODUCTION FROM BOREHOLE HEAT EXCHANGER FIELDS, in: Proceedings of World Geothermal Congress 2005. Antalaya.

Sommer, W., Valstar, J., Gaans, P. van, Grotenhuis, T., Rijnaarts, H., 2013. The impact of aquifer heterogeneity on the performance of aquifer thermal energy storage. Water Resources Research 49, 8128–8138. https://doi.org/10.1002/2013WR013677

Sørensen, P.A., Larsen, J., Thøgersen, L., Andersen, J.D., Østergaard, C., Schmidt, T., 2013. Boreholes in Brædstrup. Final report.

Spitler, J.D., Bernier, M., 2016. 2 - Vertical borehole ground heat exchanger design methods, in: Rees, S.J. (Ed.), Advances in Ground-Source Heat Pump Systems. Woodhead Publishing, pp. 29–61. https://doi.org/10.1016/B978-0-08-100311-4.00002-9

Sutton, M.G., Nutter, D.W., Couvillion, R.J., 2003. A Ground Resistance for Vertical Bore Heat Exchangers With Groundwater Flow. J. Energy Resour. Technol 125, 183–189. https://doi.org/10.1115/1.1591203

Tordrup, K. W., Poulsen, S.E., Bjørn, H., 2017. An improved method for upscaling borehole thermal energy storage using inverse finite element modelling. Renewable Energy 105, 13–21. https://doi.org/10.1016/j.renene.2016.12.011

Tordrup, K.W., Poulsen, S.E., Bjørn, H., 2016. Calibration of a finite element model of a borehole thermal energy storage in FEFLOW: model and numerical considerations. Presented at the European Geothermal Congress, Strasbourg, p. 6.

Tordrup, Karl Woldum, Poulsen, U.V., Nielsen, C., 2017. A modular approach to inverse modelling of a district heating facility with seasonal thermal energy storage. Energy Procedia, 11th International Renewable Energy Storage Conference, IRES 2017, 14-16 March 2017, Düsseldorf, Germany 135, 263–271. https://doi.org/10.1016/j.egypro.2017.09.518

Tsang, C.-F., 1990. The Modeling Process and Model Validation. Ground Water 29.

U.S. National Committee for Rock Mechanics, 1996. Rock fractures and fluid flow contemporary understanding and applications. National Academy Press, Washington, D.C.

Wheatcraft, S.W., Tyler, S.W., 1988. An explanation of scale-dependent dispersivity in heterogeneous aquifers using concepts of fractal geometry. Water Resources Research 24, 566–578. https://doi.org/10.1029/WR024i004p00566

Wheatcroft, E., Wynn, H., Lygnerud, K., Bonvicini, G., Leonte, D., 2020. The Role of Low Temperature Waste Heat Recovery in Achieving 2050 Goals: A Policy Positioning Paper. Energies 13, 2107. https://doi.org/10.3390/en13082107

Yang, W., Chen, Y., Shi, M., Spitler, J.D., 2013. Numerical investigation on the underground thermal imbalance of ground-coupled heat pump operated in cooling-dominated district. Applied Thermal Engineering 58, 626–637. https://doi.org/10.1016/j.applthermaleng.2013.04.061

Zeng, H.Y., Diao, N.R., Fang, Z.H., 2002. A finite line-source model for boreholes in geothermal heat exchangers. Heat Trans. Asian Res. 31, 558–567. https://doi.org/10.1002/htj.10057

Zhang, C., Wang, Y., Liu, Y., Kong, X., Wang, Q., 2018. Computational methods for ground thermal response of multiple borehole heat exchangers: A review. Renewable Energy 127, 461–473. https://doi.org/10.1016/j.renene.2018.04.083

Zhang, L., Zhao, L., Yang, L., Hu Songtao, 2015. Analyses on soil temperature responses to intermittent heat rejection from BHEs in soils with groundwater advection. Energy and Buildings 107, 355–365. https://doi.org/10.1016/j.enbuild.2015.08.040

PUBLICATION 3 : Design methodology for laboratory scale borehole storage: An approach based on analytically-derived invariance requirements and numerical simulations
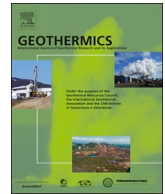
Design methodology for laboratory scale borehole storage: An approach based on analytically-derived invariance requirements and numerical simulations

Willem Mazzotti Pallard*, Alberto Lazzarotto, José Acuña Sequera, Björn Palm

KTH Royal Institute of Technology, Department of Energy Technology, Brinellvägen 68, 100 44 Stockholm, Sweden

ABSTRACT

This paper presents a methodology for designing Laboratory Borehole Storages (LABS) intended to generate reference Thermal Response Functions (TRFs) for model validation. The design method is based on analytically-derived invariance requirements demanding the conservation of the Fourier and Biot numbers. Accordingly, convective boundary conditions (BCs) need to be up-scaled when downscaling the borehole field, especially for short boreholes. Indeed, numerical simulations show that natural convection as top BC leads to TRF values more than 14 % higher than a Dirichlet BC. In addition, this BC effect is proposed as a possible explanation for previously reported differences between experimental and analytical results. Finally, the numerical simulations are used to find suitable size – height and radius of twice the borehole length–and test durations for the LABS.

1. Introduction and literature review

Ground-source heat pump (GSHP) systems with vertical, closed-loop borehole heat exchangers (BHEs) are among the most energy-efficient systems for heating and cooling buildings, when properly designed. A key part in the design process of these systems is the borehole field sizing, performed in such a way that the secondary fluid circulating in the BHEs remains within pre-determined temperature limits over the lifetime of the installation. The long-term changes in secondary fluid temperature are predominantly influenced by heat transfer phenomena in the ground; accurately modelling these phenomena is thus important to reach a proper design. For a given borehole field geometry, a common method to calculate temperature changes over time is to use a Thermal Response Function (TRF) linking the increase in temperature at the borehole wall to a constant heat injection rate, given ground properties.

1.1. Thermal Response Functions (TRFs) and ground heat transfer modelling

Broadly-cited TRFs are Eskilson's g-functions (1987) which are dependent on similarity parameters of the borehole field, namely the borehole-radius-to-length ratio, $r_b^* = r_b/H$, the borehole-spacing-to-

height ratio, $B^* = B/H$, and the dimensionless time, $t^* = t/t_s = 9Fo_H$. Eskilson's g-functions may be defined by the following equation relating the temperature increase at the borehole wall, $T_{bh} - T_0$, to the depth-averaged heat rate per meter, $\bar{q}$, and the thermal conductivity, λ

$$T_{bh} - T_0 = \frac{\bar{q}}{2\pi\lambda} g(r_b^*, B^*, t^*) \tag{1}$$

Eskilson generated g-functions numerically, assuming that all boreholes in the field have the same wall temperature, which is additionally uniform with depth. Claesson and Eskilson (1987) furthermore introduced an analytical solution based on uniform heat injection along a Finite-Line-Source (FLS) in a semi-infinite medium. Zeng et al. (2002) later discussed the importance of using the integral mean borehole wall temperature, instead of the mid-length temperature, when using the FLS to design borehole fields. Lamarche and Beauchamp (2007) provided a simplified expression of the mean integral temperature obtained with the FLS, thereby enabling faster computation of TRFs. Claesson and Javed (2011) developed another simplification that can be used for boreholes with an arbitrary buried depth, D. Lamarche (2011) generalized his and Beauchamp's simplification by partly applying it in the case of inclined boreholes, using the FLS solution for inclined boreholes reported by Cui et al. (2006) and Marcotte and Pasquier (2009). Spatial and temporal superposition may be applied to

---

Nomenclature

Symbols

B	borehole spacing (m)
Bi	Biot number
D	buried depth (m)
Fo	Fourier number
g	g-function
h	heat transfer coefficient (W/(m²·K))
H	borehole depth or LABS height (m)
$\dot{m}$	mass flow rate (kg/s)
q	heat rate per meter (W/m)
R	thermal resistance (m·K/W)
r	radius (m)
t	time (s)
T	temperature (K)
$U(x, p)$	extended uncertainty of variable x with confidence level p (K)
$\dot{V}$	volume flow rate (m³/s)
z	vertical direction (m)
α	ground thermal diffusivity (m²/s)
β	geometric scale factor-
γ	thermal diffusivity scale factor-
η	effective borehole resistance factor-
λ	ground thermal conductivity (W/(m·K))
τ	time scale factor-
φ	azimuth angle rad or (°)
Ω_b	dimensionless borehole resistance

$\mathbb{R}$	real numbers-

Superscripts

*	dimensionless ratio or effective parameter (borehole resistance)
′	LABS parameter (downscaled)
+	positive real numbers
-	depth-integral mean
+	positive real numbers
-	depth-integral mean
b/bh	borehole
c	convection
cond	conduction
D	buried depth
f	fluid (heat transfer fluid)
a	internal (thermal resistance)
geo	geothermal
lim	limit
g	grout
H	borehole length
i	initial value
m	LABS' dimensions (overall height and radius)
p	pipe
ref	reference model
s	borehole characteristic time
ss	steady-state / test duration
0	initial condition
12	direct coupling resistance

---

the FLS solution in order to determine the temperature response of a borehole field and a time-varying load, respectively.

Although convenient for fast computation, the different FLS methods failed to reproduce Eskilson's g-functions for large borehole fields because of the difference in boundary conditions (BCs) applied along the borehole wall in the two models (Fossa, 2011). Although none of these BCs duly represents a real case, g-functions will better represent temperature changes in the borehole field when all boreholes are fed in parallel, as highlighted by Cimmino et al. (2013). Cimmino and Bernier (2014) proposed an alternative analytical model addressing the observed discrepancy between FLS and g-function. The authors modelled boreholes as a stack of FLS segments, each segment having a constant heat injection rate. Using this method, the authors could use the FLS solution while imposing a uniform temperature BC. They thus obtained TRFs similar to Eskilson's g-functions. This stack-FLS method was generalized by Lazzarotto (2016) and Lazzarotto and Björk (2016) for inclined boreholes.

Although the uniform temperature BC better represents boreholes fed in parallel, it will differ from what happens in real systems. Indeed, as the fluid temperature varies along the length of the borehole, it is likely that the borehole wall temperature will also vary. This issue was tackled by coupling a stacked FLS model to a quasi-steady-state borehole heat transfer model while imposing the same inlet temperature for all boreholes in the field (Cimmino, 2015).

Besides Eskilson (1987), other authors have numerically generated TRFs. A novel approach to numerically model borehole fields was presented by Monzó et al. (2015). The authors used a highly conductive material (HCM) as a heat distribution network between boreholes. As the total heat load is applied at the network top boundary, heat naturally distributes in the borehole field and along the length of each borehole. Since the HCM is in direct thermal contact with the ground, the resulting condition at the borehole wall is a near-uniform temperature. The authors could therefore replicate Eskilson's g-functions. A similar approach was used by Priarone and Fossa (2016). In a newer

version (Monzó et al., 2018), the authors added a thin thermal resistive layer at the borehole interface in order to reproduce more realistic conditions at the borehole wall. Naldi and Zanchini (2019) proposed to generate numerical TRFs with uniform temperature BC through iterations. First, the authors apply a constant heat flux BC at the borehole wall. The resulting time-varying temperature is then applied as a new BC at the borehole wall for the next simulation. The depth-averaged heat flux from the previous simulation is used to correct to initial TRF. Finally, this correction is used as new BC for a new simulation. The authors find results in agreement with those of Monzó et al. (2015) and Cimmino and Bernier (2014). Other numerical models have been used for simulating heat transfer in borehole fields but are not discussed here (e.g. Lee and Lam, 2008; Ozudogru et al., 2014).

Similarly, short-term models simulating heat transfer phenomena within boreholes (e.g. Beier, 2014; Hellström, 1991; Lamarche, 2015; Pasquier and Marcotte, 2014), as well as models considering convection in the ground (e.g. Lee and Lam, 2012; Molina-Giraldo et al., 2011; Nguyen et al., 2017), have been developed but are not reviewed in this article.

1.2. Experimental and monitoring work

As highlighted in the previous section, many authors have focused on developing analytical and numerical models or methods to predict temperature changes in borehole fields, with the aim to improve the accuracy of GSHP design. However, due to the slow transient nature of heat transfer phenomena in long boreholes, long-term experimental and monitoring studies have been scarce. This has been emphasized in the literature (Cimmino and Bernier, 2015; Cullin et al., 2015; Gehlin et al., 2018; Montagud et al., 2011; Spitler and Bernier, 2016, 2011). Spitler and Bernier (2016) identified the relevance and usefulness of long-term monitoring of thermally unbalanced borehole fields.

Some research work have reported monitoring and performance analysis of GSHP installations over extended periods, typically more

than two years. A GSHP system in a Spanish research facility was monitored over 11 years, providing a reference datasets for validation of GSHP models (Montagud et al., 2011; Ruiz-Calvo et al., 2016; Ruiz-Calvo and Montagud, 2014). Michopoulos et al. (2013) reported the eight years monitoring of a GSHP system in Northern Greece. Spitler et al. (2017) investigated the performance of the GSHP system during two years at the ASHRAE headquarters in Atlanta, USA, and compared it with an air-source VRF system at the same facility. The GSHP system of an office building in Nuremberg, Germany, was monitored continuously during four years, with detailed temperature measurements in two monitoring boreholes outside of the boreholes, upstream and downstream of groundwater flow (Luo et al., 2015). Cullin et al. (2015) compared two design methods using monitored data from four different installations as input. Other studies reported monitoring data over shorter periods (Gehlin et al., 2018; Mikhaylova et al., 2015; Monzó et al., 2017; Naiker and Rees, 2011; Ozyurt and Ekinci, 2011; Sivasakthivel et al., 2016; Stafford, 2011; Yavuzturk and Spitler, 2001; Yu et al., 2011). None of the studies mentioned above tried to validate long-term ground heat transfer models, because it was not the primary objective of the studies, because of a lack of data and/or important parameters, among other reasons. The fact the heat loads are balanced in most of the cases is also a limitation since the influence of the long-term effects on the temperature response become negligible.

Monzó et al. (2018) used data from two real systems (Iglesias et al., 2012; Puttige et al., 2016; Ruiz-Calvo et al., 2016) to validate a numerical model. Root-mean square errors of 1.4 K and 1.8 K were reported for daily mean fluid temperatures over four and ten years, respectively. Again, the heat loads were balanced which limits the influence of long-term effects, as highlighted by the similarity between models with different BCs.

Although long-term monitoring of GSHP installations should be encouraged, as it is very valuable for researchers and practitioners, validation of ground heat transfer models in real systems is difficult because of the long time scales involved; the typical lifetime of a GSHP

being about 20–25 years and even longer for the borehole field (Huang and Mauerhofer, 2016; Koroneos and Nanaki, 2017). Moreover, uncontrolled or unknown parameters such as groundwater flow, thermal properties or geological conditions may complicate the validation process in real installations. Practical difficulties such as data gaps, unknown control strategies or lack of documentation may also arise. Additionally, uncertainties are hard to assess in real systems. Few of the mentioned field studies reported measurements and parameter uncertainties.

An alternative is to perform lab experiments in small-scale physical models. Such lab-scale models (LABSs) are attractive because the time scale is reduced and the tests can be performed in a controlled environment. A lab-scale apparatus was successfully built by Cimmino and Bernier (2015) based on a previous work (Salim Shirazi and Bernier, 2014). Some other physical LABSs were constructed although their use was limited to analysis of short-term models or other purposes (Akrouch et al., 2016; Beier et al., 2011; Eslami-nejad and Bernier, 2011; Hellström and Kjellsson, 2000; Kramer et al., 2015). The apparatus built by Cimmino and Bernier (2015) consists of a 1.35 m high cylinder of radius 0.7 m filled with Ottawa sand C-109. The cylindrical tank is insulated both at the bottom and on its circumference. Only one BHE is modelled, using a 40 cm long U-pipe of outer diameter 3.2 mm. The U-pipe itself is contained in a stainless steel tube of outer nominal diameter 0.5 in representing the borehole. This stainless steel tube is filled with sand. Temperature in the tank and at the borehole wall is recorded using thermocouples. The top surface of the tank is subjected to convection and radiation from the surroundings and the temperature appears to be uncontrolled.

The authors managed to obtain an experimental g-function using the test apparatus, which is compared to a semi-analytical method. In the reviewed literature, this is the only attempt to validate ground heat transfer models over the whole time span of a borehole field. A discrepancy between the experimental TRF and the analytical one was observed, although the difference is comprised within the measurement
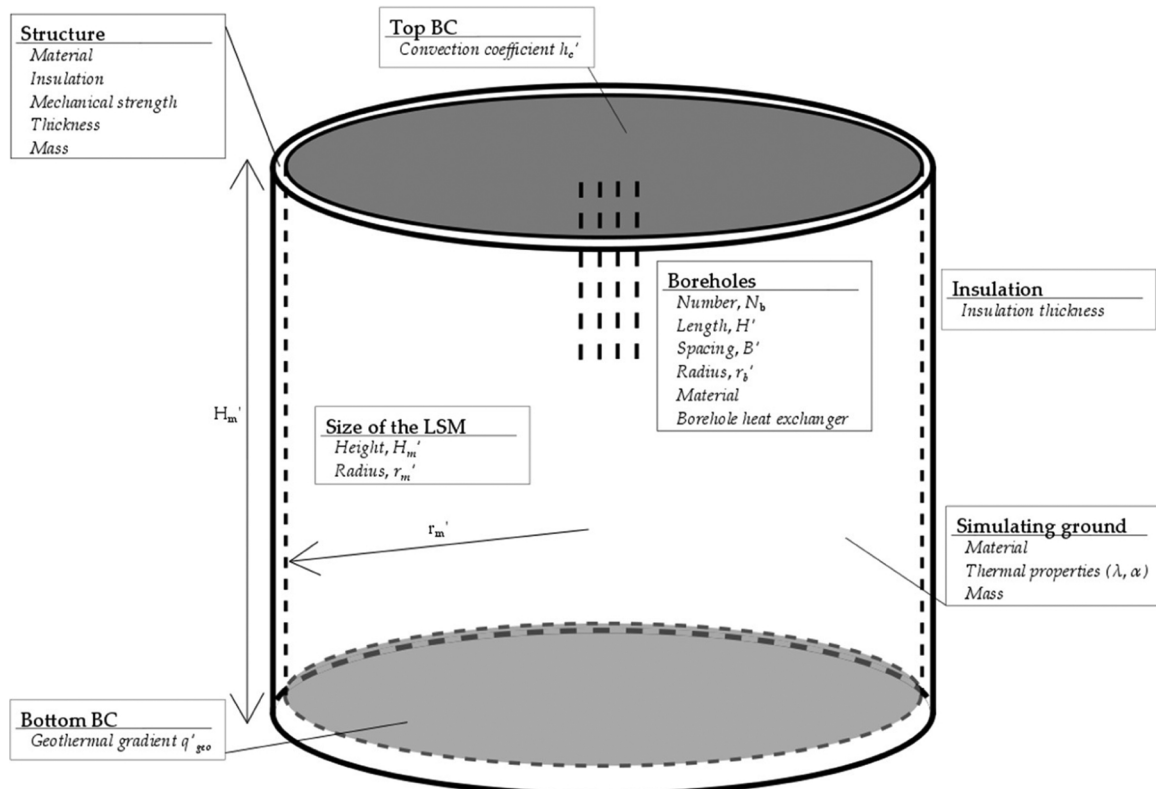

Fig. 1. Preliminary outline of the lab-scale model (LABS) including important parameters to be determined through the design process.

uncertainty at a 95 % confidence level (Cimmino and Bernier, 2015). The authors proposed an explanation for this observed difference based on the air temperature variation above the tank. The effect of this variation on the temperature field could be analytically quantified and a corrected temperature response was thus calculated by superposition. It appears that the top surface temperature was assumed equal to the ambient air temperature. Though reducing the difference between the experimental and analytical results, the proposed correction did not fully succeed in reproducing the observations.

While Cimmino and Bernier (2015) have used a successful approach and provided useful results, some questions remain as regards the discrepancy between experimental and analytical TRFs. For instance, it seems that the experimental TRF is systematically higher than the analytical TRF, although the difference is comprised within the uncertainty bounds. Is this the indication of a flaw in the modeling, a measurement bias or an experiment bias, i.e. a bias caused by some experiment design pitfall? In the latter case, would the bias "add up" for borehole fields, since the thermal response at a given borehole then consists of the thermal response of the borehole on itself and the contributions from all other boreholes?

In this article, a design methodology for LABS, based on analytical invariance requirements and experimental constraints, is proposed. The present work is an extension and generalization of a previous study (Mazzotti et al., 2018). Here, the design methodology is formalized in order to make it reproducible. In addition, the invariance requirements are generalized through nondimensionalization. The implications of the found invariance requirements are investigated numerically for different borehole fields. Here, again, the present study is made more general by investigating three different borehole spacings. A notable result is that invariance requirements applied to the top surface BC offers a possible explanation for the observed discrepancy in Cimmino and Bernier (2015). Through the application of the design methodology to a case study, insights about potential practical difficulties, experimental biases and sources of systematic errors are given. In particular,

the bias introduced by heat losses through the containing envelope is investigated dynamically, while a steady-state model was used in the previous study. Correctly characterizing the sources of systematic errors reinforce the trustworthiness of results from LABS. In turn, those results can be used as a reference dataset for validation of ground heat transfer models with greater confidence.

2. Methodology

The main goal of this work is to develop a design methodology for LABS so that adequate dimensions, materials and experimental conditions can be determined. Due to the physics of the problem, it is natural to think of the LABS as a vertical cylindrical container filled with a material simulating the ground. Boreholes would then be placed at the center of the container as shown in Fig. 1. This figure also includes important parameters to be determined during the design process. For the case study, it is later chosen to limit the LABS to a quarter of a cylinder by using symmetry. The first, and most important, step in the scaling process is to ensure that the results obtained with the LABS will be the same as in a real-scale installation. A general analytical analysis of the effect of downscaling on heat transfer is thus performed. Then, using the requirements derived from the analytical analysis, the design process shown in Fig. 2 is initiated. This design process is not unique – for instance, if the temperature constraint is not respected (step 4), one could also modify the borehole field instead of just changing the simulating ground – but it provides a structure for understanding what parameters are important when designing LABS and how these parameters influence each other. Some parameters shown in Fig. 1 do not appear in Fig. 2 because the latter specifically refer to the sizing of the simulating ground.

2.1. Invariance of the solution under downscaling: analytical requirements

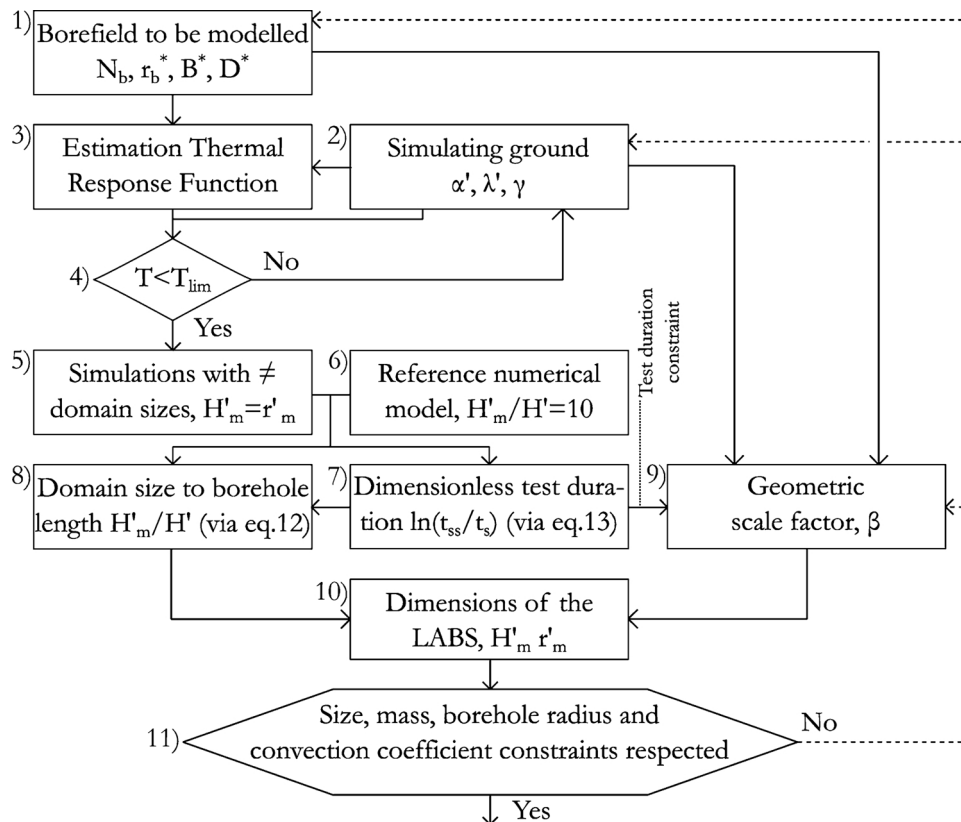Some invariance requirements may be obtained analytically by

Fig. 2. Flow chart of LABS design process for the simulating ground.

stating the governing equations for the real and lab-scale cases. Assuming constant and uniform thermal properties, the two heat equations may be written, respectively, as

$$\frac{1}{\alpha}\frac{\partial T}{\partial t} = \frac{1}{r}\frac{\partial}{\partial r}\left(r\frac{\partial T}{\partial r}\right) + \frac{1}{r^2}\frac{\partial^2 T}{\partial \varphi^2} + \frac{\partial^2 T}{\partial z^2} \tag{2}$$

And

$$\frac{1}{\alpha'}\frac{\partial T'}{\partial t'} = \frac{1}{r'}\frac{\partial}{\partial r'}\left(r'\frac{\partial T'}{\partial r'}\right) + \frac{1}{r'^2}\frac{\partial^2 T'}{\partial \varphi'^2} + \frac{\partial^2 T'}{\partial z'^2} \tag{3}$$

Note that the apostrophe symbol refers to the lab-scale parameters and variables. The behavior of the real and lab-scale cases will be the same if the governing equations are the same, as well as the initial (IC) and boundary conditions (BCs). By introducing a proportional and isotropic geometrical scale factor, β, a thermal diffusivity scale factor, γ, as well as a time scale factor, τ, defined as ratios between real-scale and LABS variables, such that

$$\begin{cases} \beta = \dfrac{r}{r'} = \dfrac{z}{z'} = \dfrac{H}{H'} \\ \tau = \dfrac{t}{t'} \\ \gamma = \dfrac{\alpha}{\alpha'} \end{cases} \tag{4}$$

and applying the corresponding change of variables, eq.2 may be rewritten as

$$\frac{\beta^2}{\gamma\tau}\cdot\frac{1}{\alpha'}\frac{\partial T}{\partial t'} = \frac{1}{r'}\frac{\partial}{\partial r'}\left(r'\frac{\partial T}{\partial r'}\right) + \frac{1}{r'^2}\frac{\partial^2 T}{\partial \varphi'^2} + \frac{\partial^2 T}{\partial z'^2} \tag{5}$$

Note that $\varphi = \varphi'$ and that an anisotropic scaling would require an anisotropic material in the LABS, which is not convenient. We note that

$$\frac{\beta^2}{\gamma\tau} = \frac{Fo_{r'}}{Fo_r} = \frac{Fo_{H'}}{Fo_H} \tag{6}$$

where H and H' are the active lengths of the boreholes in the real and lab-scale cases, respectively. Thus, perhaps non-surprisingly, eqs. 3 and 5 have the same solution if the Fourier number is conserved, for similar IC and a set of BCs. This constitutes a first invariance requirement. One of the advantages of downscaling becomes clear from eq.6, as the time scale factor τ is proportional to β^2, which takes large values ($\beta \gg 1$).

As previously mentioned, the IC and BCs must also be analogous in order to obtain the same solutions for the real and LABS cases. Dirichlet BCs will not be affected by the downscaling whereas Neumann and convective BCs will be modified by the downscaling. Such BCs may arise at the borehole wall, as well as the bottom and top domain boundaries. At the borehole wall, the heat flow balance may be expressed as

$$-\lambda\frac{1}{H}\int_D^{D+H}\frac{\partial T}{\partial r}(r_b, z, t)dz = \frac{\bar{q}}{2\pi r_b} \quad \forall \, (z, t) \in ([D; D+H] \times \mathbb{R}^{+*}) \tag{7}$$

Applying the same change of variable as for the heat equation, the following equation is obtained

$$-\lambda'\frac{1}{H'}\int_{D'}^{D'+H'}\frac{\partial T'}{\partial r'}(r_b', z', t')dz' = \frac{\lambda'}{\lambda}\frac{\bar{q}}{2\pi r_b'} = \frac{\bar{q}'}{2\pi r_b'} \quad \forall \, (z', t')$$
$$\in ([D'; D'+H'] \times \mathbb{R}^{+*}) \tag{8}$$

Hence, the heat rate per unit length that should be applied in the LABS is the same as in the real scale case, adjusted for the potential change in thermal conductivity. Relations for the geothermal heat flux BC and the top convective BC can be obtained in a similar manner, leading to

$$\frac{\lambda'}{\lambda}\beta q_{geo} = q_{geo}' \tag{9}$$

And

$$\frac{\lambda'}{\lambda}\beta h_c = h_c' \tag{10}$$

Note that eqs.8-10 may be expressed in dimensionless form by using the dimensionless numbers

$$\begin{cases} TRF = \dfrac{2\pi\lambda(\overline{T}_{bh} - \overline{T}_0)}{\bar{q}} \\ q_{geo}^* = H\dfrac{q_{geo}}{\lambda(T_{i,D} - T_{i,D+H})} = 1 \\ Bi = \dfrac{h_c \cdot H}{\lambda} \end{cases} \tag{11}$$

$T_{i,D}$ and $T_{i,D+H}$ are initial temperatures at depth D and $D + H$, respectively. Eqs. (8)–(10) are additional invariance requirements that can equivalently be expressed in terms of the invariance of the TRF, the dimensionless geothermal heat flux q_{geo}^* and the Biot number, Bi. It is gratifying that one of the outcomes of the analysis is the invariance of the TRF, since this is precisely what is supposed to be achieved.

An important observation is that the geometrical scale factor, β, appearing in Eqs. (9) and (10) implies large increases in the geothermal heat flux and convection coefficient when downscaling the model ($\beta \gg 1$). For instance, a 300 m deep borehole field modelled by a 0.5 m LABS will lead to $\beta = 600$. For a natural convection coefficient of 10 W.m^{-2}.K^{-1} on top of a real-scale system, the required convection on top of the corresponding LABS would be of 6000 W.m^{-2}.K^{-1} for equal thermal conductivities. Thus, forced convection will be required at the top of the LABS in order to reproduce the behavior of a real-scale installation having natural convection as top BC. Note that radiation is accounted for in the convection coefficient.

It is later shown that, in a real size borehole field, a convective BC with a natural convection coefficient of 10 W m^{-2} K^{-1} leads to similar results as a Dirichlet BC at the top of the borehole field. This validates the assumption that constant temperature is "quite sufficient" (Eskilson, 1987) as BC at the ground surface for long boreholes. For shorter boreholes however (e.g. energy piles or lab-scale borehole fields), the latter assumption may become invalid. In lab conditions, the convection coefficient at the top of the apparatus must be appropriately up-scaled in order to properly reproduce TRFs.

2.2. Step 1 – Choice of the borehole field to be modelled

Having derived some design requirements from the analytical invariance analysis, the design process shown in Fig. 2 can be initiated. Since TRFs only depend on relative geometrical characteristics for a given configuration and a given thermal diffusivity, choosing absolute values for the borehole length, spacing, buried depth and radius is not critical per se. One can instead restrict the choice to the geometrical aspect ratios, namely $r_b^* = \frac{r_b}{H}$, $B^* = \frac{B}{H}$ and $D^* = \frac{D}{H}$. For the sake of the case study, r_b^* and B^* were varied in the ranges $1.92 \cdot 10^{-4} - 2.50 \cdot 10^{-3}$ and $0.0167 - 0.0667$, respectively, whereas D^* was taken constant as 0.0167. Note that, in practice, for a given length, H, the values that r_b^* can take are dictated by the standard drill bit dimensions. Therefore, r_b^* values do not always represent standard realistic cases.

The number of boreholes and their configuration is also a key characteristic of the borehole field. Here it was chosen to investigate a 4×4 borehole field with vertical boreholes. This initial choice was not changed during the design process.

2.3. Steps 2–4 – Choice of the simulating ground and structural materials, estimation of the TRF and the maximum reached temperature

The simulating ground refers to the material in the LABS, as opposed to the simulated ground that refers to the real-scale material. The thermal properties of the simulating ground are of primary importance

since they directly influence the heat diffusion process in the LABS. Indeed, a larger thermal diffusivity will lead to shorter test durations but the heat plume will reach further away from the boreholes, thereby increasing the required LABS size. On the other hand, lower thermal diffusivity will lead to a larger temperature increase that may create some practical problems such as material compatibility or changes in thermal properties. Therefore, a high temperature limit for the simulating ground should be set (step 4). For the sake of the case study, this limit was set as 70 °C. For a given simulating ground, it is possible to check if this limit is exceeded through the TRF of the borehole field. The latter can be estimated through the FLS solution (Claesson and Javed, 2011). The dimensionless steady-state time of $\ln(t/t_s) = 2.3$ reported by Cimmino and Bernier (2015) is used as a first approximation for the test duration, i.e. the time at which the temperature is the largest in the simulating ground. Since the FLS solution tends to overestimate the thermal response of borehole fields, it can be considered as a safety factor in the determination of the maximum temperature.

Saturated sand was chosen as simulating ground for the case study because it allows keeping the temperature below the high limit and because it is an easily interchangeable and manageable material. The thermal properties assumed for the simulated and simulating ground are as follow: $\lambda = 3.5$ W m^{-1} K^{-1}, $\alpha = 1.58\cdot10^{-6}$ m$^2\cdot$s^{-1} and $\lambda' = 3.0$ W m^{-1} K^{-1}, $\alpha' = 7.00\cdot10^{-7}$ m$^2\cdot$s^{-1}, respectively (Arkhangelskaya and Lukyashchenko, 2017; Sundberg, 1991; Tarnawski et al., 2011). The thermal properties of the simulating ground should be well characterized before experiments are to be performed.

For structural and practical reasons, steel was chosen as a structural material for the case study. Since steel has a relatively high thermal conductivity, the container should be thermally isolated from the simulating ground to avoid thermal disturbances. An insulation layer is thus needed between the steel and the simulating ground. This insulation layer moreover reduces the potential thermal influence from the environing air as well as heat losses. The magnitude of the heat losses are evaluated through a 3D numerical model presented in the next section.

2.4. Steps 5 and 6 – Numerical models

In order to find suitable domain dimensions for a given borehole length, a numerical model is developed with COMSOL Multiphysics® (COMSOL Mutliphysics®, 2018) based on the work of Monzó et al. (2015). A screenshot of the model geometry and mesh, including a zoom on the boreholes, is presented in Fig. 3. Symmetry is used so that the numerical model is reduced to an eighth-cylinder geometry with boreholes by a Highly Conductive Material (HCM). This allows to indirectly apply a uniform temperature BC (see Monzó et al. (2015) for more details). All vertical boundaries are set as adiabatic, the bottom boundary is either adiabatic or subject to a constant geothermal heat flux of 0.05 W·m m^{-2}, the top boundary is either subject to constant temperature or convection. Which BC and convection heat transfer coefficient are applied is specified in the result section, if applicable. The total heat rate is applied at the uppermost surface of the HCM and is chosen to obtain a heat rate per unit length of 22 W m^{-1}. The IC is either uniform temperature, set as zero, or a linear increase of temperature with depth in the cases in which a geothermal heat flux is set as bottom BC. Since the domain size varies as well as the spacing and borehole radius, the size of the mesh also varies but is comprised between 270 000–390 000 elements. A mesh independence study is performed for the numerical model with the largest domain size – later called reference model – with a borehole-to-domain-size ratio of 10. It is found that the relative error between a finer mesh (about 485 000 elements) and the mesh used in this study (about 385 000) does not exceed 1% of the total temperature change, both in terms of the RMSE and the maximum absolute error. Other verifications on the numerical model are provided in previous studies (Mazzotti et al., 2018; Monzó et al., 2015).

A second numerical model is used in this study in order to assess heat losses from the side of the LABS. The insulation and structure are therefore also included in the numerical modeling as can be shown in Fig. 4. Note that, as opposed to the model shown in Fig. 3, the domain in the second model is a quarter cylinder. The reason is that this second model was also used to investigate non-symmetrical features (e.g. horizontal piping connections) which are not presented here. The insulation thickness is set as a fifth of the borehole length and it wraps all
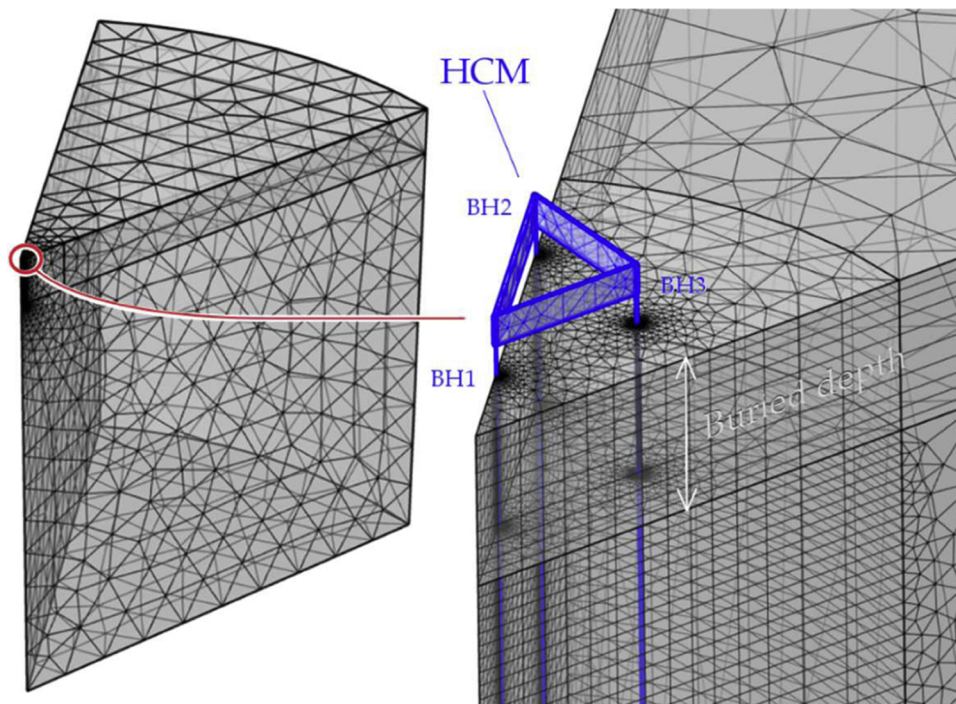

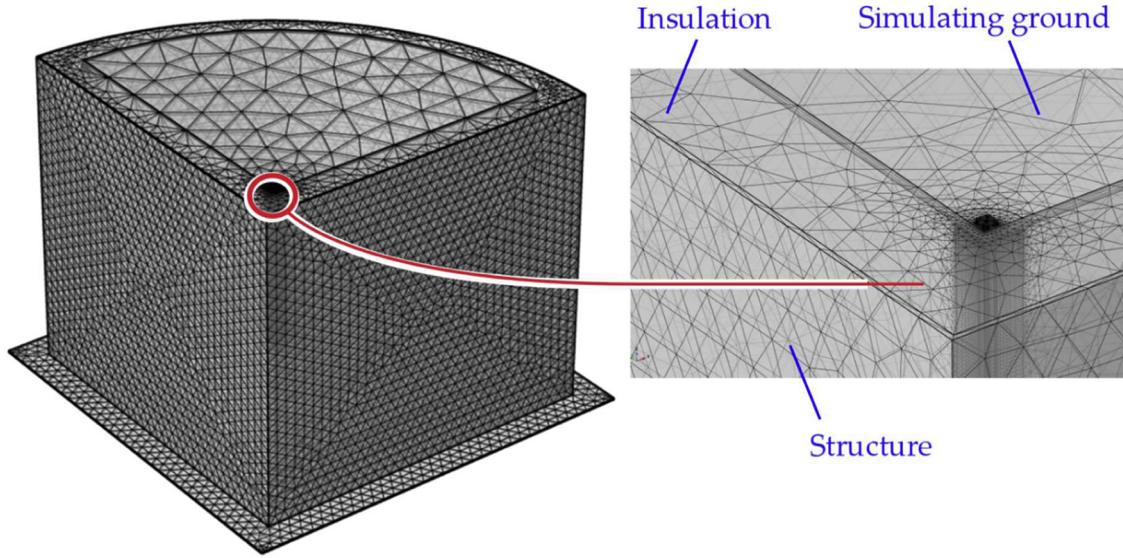**Fig. 3.** Screenshots of the numerical model used for sizing the LABS.

Fig. 4. Screenshots of the numerical model used to evaluate heat losses through the side of the LABS.

the simulating ground except for the top. The structure thickness is set as 1% of the borehole length. The dimensionless geometrical parameters are as such: $r_b^* = 2.50 \cdot 10^{-3}$, $D^* = 0.0167$ and B^* was varied in the range $0.0167 - 0.0667$. The vertical boundaries – now structural metal sheets – are not adiabatic anymore but subject to convection with a coefficient of $10\,\mathrm{W\,m^{-2}\,K^{-1}}$. A convection heat transfer coefficient of $3\,\mathrm{W\,m^{-2}\,K^{-1}}$ is applied at the bottom of the structure while a geothermal heat flux of $0.05\,\mathrm{W\,m^{-2}}$ is still applied through an internal boundary heat source at the interface between the bottom insulation and the simulating ground. For the top boundaries, a Dirichlet BC is applied for the simulating ground while a convective BC is applied for the insulation and the structure. A thermal conductivity of $50\,\mathrm{W\,m^{-1}\,K^{-1}}$ and diffusivity of $1.30 \cdot 10^{-5}\,\mathrm{m^2\,s^{-1}}$ are set for the structure while the same properties are of $0.03\,\mathrm{W\,m^{-1}\,K^{-1}}$ and $3.47 \cdot 10^{-7}\,\mathrm{m^2\,s^{-1}}$, respectively, for the insulation. The used mesh consists of about 515 000 elements.

2.5. Steps 7–11 – sizing and time criteria, practical constraints

In order to find what domain size is adequate for the LABS, some criteria must be defined. Since the main goal of the LABS is to validate TRFs, one first criterion may be expressed as

$$|\Delta \bar{T}(r_b, t_{ss}) - \Delta \bar{T}_{ref}(r_b, t_{ss})| < U(\Delta \bar{T}, 95\%) \tag{12}$$

where $\Delta \bar{T}(r_b, t_{ss})$ refers to the depth-integral mean of the temperature increase at the borehole wall at the end of the test, t_{ss}, and $\Delta \bar{T}_{ref}$ is also a depth-integral mean but emanates from the reference model. This first criterion ensures that the boundaries do not have a significant effect on the thermal response of the borehole field. The term $U(\Delta \bar{T}, 95\%)$ is the design-stage extended uncertainty of the temperature increase at the borehole wall at a 95 % confidence level, and is equal to $0.33\,\mathrm{K}$. The upper bound in eq.12 is chosen to limit the uncertainty in the determination of the TRF.

The test duration, t_{ss}, expressed in eq.12 corresponds to the time at which heat transfer is close to steady-state, which constitutes a second criterion defined by

$$\forall\, t > t_{ss}\,,\quad \frac{|\Delta \bar{T}_{ref}(r_b, t) - \Delta \bar{T}_{ref}(r_b, t_{ss})|}{\Delta \bar{T}_{ref}(r_b, t)} < 0.5\% \tag{13}$$

A time close to the steady-state regime is chosen because this is when the highest uncertainty in the TRF is expected to appear, due to heat losses and effects from the boundaries among other things. The maximum value for the test duration t_{ss} is fixed to one week.

For a given borehole length, eqs.12–13 give the smallest domain

size that fit the defined criteria. The results may be generalized by introducing the ratio $H_m'/H' = r_m'/H'$. Similarly, t_{ss} may be generalized to any borehole length by considering the ratio $\ln(t_{ss}/t_s)$ or the Fourier number.

Given the upper bound of one week for t_{ss}, the diffusivity ratio, γ, and the real-scale length, H, the geometrical scale factor, β, may be determined through eq.6. Note that all ratios in eq.6 should be equal to one due to the conservation of the Fourier number. From β, the downscaled borehole length can be determined, which in turn gives the size of the LABS by using the ratio H_m'/H' obtained previously.

Once the LABS size is determined, several arbitrarily-set design constraints related to the case study may be checked. Firstly, the LABS must fit in the lab facilities so its size is limited to $1.8\,\mathrm{m}$ in height and radius. Secondly, the total mass of the LABS, including structural materials, must not exceed $1.5\,\mathrm{tonnes}$ for mobility and structural issues. Thirdly, the borehole radius of the LABS should be larger than $1\,\mathrm{mm}$ due to practical construction issues and pressure drop considerations. Finally, the required heat transfer coefficient at the top of the LABS should not exceed $1500\,\mathrm{W.m^{-2}.K^{-1}}$ to be feasible. In practice, it is impossible to respect all constraints as will be discussed in the result section. Other constraints are also considered throughout the process, e.g. establishment of the initial temperature gradient (see Mazzotti et al. (2018) for an analysis regarding this matter), heat losses, pressure drop and mechanical stresses. Tests constraints such as flow distribution, release of dissolved air and power stabilization should be kept in mind but are not discussed here.

3. Results and discussions

3.1. Real-scale vs lab-scale numerical models

In order to verify the analytical invariance relations derived previously, numerical simulations are performed for borehole fields having similar dimensionless ratios but different absolute dimensions and different thermal properties of the ground. A geometrical scale factor, β, of 600 is used between the real and lab-scales. For both real-scale and Lab-Scale Numerical Model (LSNM), constant temperature is implemented as top BC and geothermal heat flux is applied as bottom BC. Geothermal heat flux implies a vertical temperature gradient making the determination of the g-function not formally possible. However, a TRF may be defined in a similar way as

$$T_{bh} - \bar{T}_0 = \frac{\bar{q}}{2\pi\lambda} TRF(r_b^*, B^*, D^*, t^*) \tag{14}$$

The TRFs obtained for each model are presented in Fig. 5. The maximum relative difference is lower than 0.7 % for all times, compared to the TRF value at the largest time. The LSNM thus give very similar result to the real-scale numerical model on the long-term, the observed discrepancies being attributed to slightly different meshes and solver time stepping.

3.2. Dimensionless test duration and LABS size-to-borehole-length ratio

The dimensionless test duration $\ln(t_{ss}/t_s)$ is determined using reference models. Dimensionless test durations of 2.48 and 2.82 for $B^* = 0.0167$ and $B^* = 0.0667$, respectively. In other words, borehole field with larger spacing will take longer time to reach steady-state. LNSMs with different domain sizes are then run to find a size matching the criterion expressed in eq.12. Each model has equal radius, r'_m, and height, H'_m for the domain. The resulting differences in borehole average temperature between the reference solution and the solutions for different domain-size-to-borehole-length ratios, H'_m/H', are shown in Fig. 6. These differences are shown for the two values B^* mentioned above. The limit in criterion 12 is also represented by the black dashed line. It can be seen that the differences are higher for $B^* = 0.0667$. There are two explanations for this: the dimensionless test duration is longer and the boreholes are closer to the outer boundary.

Of all tested ratios, the smallest one that satisfies eq.12 is $H'_m/H' = 2$ for both values of B^*. Such a ratio leads to average borehole temperatures respectively 0.19 K and 0.29 K higher than the reference model for $B^* = 0.0167$ and $B^* = 0.0667$ at the test duration defined by eq.13. The results shown in Fig. 6 could also be used to choose domain size for numerical simulations of similar borehole fields.

3.3. Influence of the geometric scale factor and final design for the case study

The most important parameter to be determined through the design process is the geometric scale factor, β. It is indeed related to the test duration, the size and mass of the LABS and its boreholes, as well as the requirements on the BCs. The influence of β on the test duration, the mass of the simulating ground, the size of the LABS, the borehole radius in the LABS and the required heat transfer coefficient on the top of the LABS is shown in Fig. 7 for three different real-scale lengths. Colored dashed lines represent values that go beyond the fixed limits while grey horizontal dashed lines represent the set design constraints. Note that the graphs are in logarithmic scale and that the heat transfer coefficient is length-independent. The influence of β on the LABS borehole spacing is not shown although there is one. A final value of $B^* = 0.0667$ is chosen and the reasons for this choice are detailed in further sections.

One may observe that no β value lead to all design constraints being respected. In fact, the test duration set the largest lower bound for acceptable β values. As can be seen on Fig. 7, this lower bound is about 520 for a real-scale length of 300 m, which is the chosen length to be simulated. Since the next largest lower bound, for the mass, is just about 500, it is tempting to accept a small excess of the test duration and use $\beta = 500$; however, the mass constraint is for the whole mass of the LABS while Fig. 7 only shows the mass of the simulating ground. Hence, $\beta = 500$ would leave no margin for the mass of the metal structure and $\beta = 600$ is therefore chosen as geometrical scale factor.

$\beta = 600$ implies a borehole length downscaled to 0.5 m and, in turn, a LABS of 1 m in height and radius. The resulting mass of the simulating ground is about 1.2 tonnes. On the other hand, a reduction in scale of 600 leads to a borehole radius of about 0.1 mm and a required heat transfer coefficient of more than $5000\,W\,m^{-2}\,K^{-1}$ (based on a heat transfer coefficient for the real-scale model of $10\,W\,m^{-2}\,K^{-1}$). Each of the two latter obtained values is challenging to implement in a LABS and the effect of these two parameters on the TRF is therefore studied more in details in the next sections.

3.4. Challenges with the borehole radius

As noted in the previous section, a problem arising from the chosen scale factor ($\beta = 600$) and radius-to-depth ratio ($r_b^* = 1.92 \cdot 10^{-4}$) is that the borehole radius becomes very small in the LABS (0.1 mm), which is challenging to reproduce in a physical model. One could instead choose to simulate a borehole field with larger r_b^* but this may not always represent realistic cases, as noted in part 2.1 and in a previous study (Cimmino and Bernier, 2015). One could also try to correct for the effect of the borehole radius on the TRF. Such a correction would also be useful for generation of TRFs: in practice the standard drilling bit dimensions constrain the application of a given set of the dimensionless parameter r_b^* to specific borehole lengths. Having a radius correction factor would allow to extend the range of applicability of TRFs calculated for a given r_b^*. Perhaps with this idea in mind, Eskilson (1987) suggested such a correction factor

$$g(r_1^*, B^*, t^*) = g(r_2^*, B^*, t^*) + \ln(r_2^*/r_1^*) \qquad (15)$$

which was derived by assuming steady-state radial conduction between the two radii. This approximation may be valid for small differences in radius but larger differences may lead to changes in axial effects as well as changes in the heat distribution between boreholes and along their depth. This could lead to underestimated values of the TRF for large times. In contrast, the correction will lead to overestimated values of the TRF for short times, when the quasi-steady-state regime has not yet been established between the two considered radii. These two features can be observed in Fig. 8 (a) and (b) which shows numerically-generated TRFs for three different r_b^* and three different B^* in graph (a), while graph (b) shows the same TRFs corrected with eq.15. It can be seen that Eskilson's correction is not satisfactory for the considered r_b^* and B^*. Thus, large r_b^* are employed for LABS simulations, which is still useful for TRF validation as shown in previous work (Cimmino and Bernier, 2015). For the case study, a r_b^* value of 0.0025 is chosen.

With regard to heat transfer inside the borehole, the effect of downscaling can be understood by looking at how the effective borehole thermal resistance is influenced. Hellström (1991) gives the following formula for a uniform temperature BC at the borehole wall

$$R_b^* = R_b \cdot \eta \coth\eta \qquad (16)$$

with

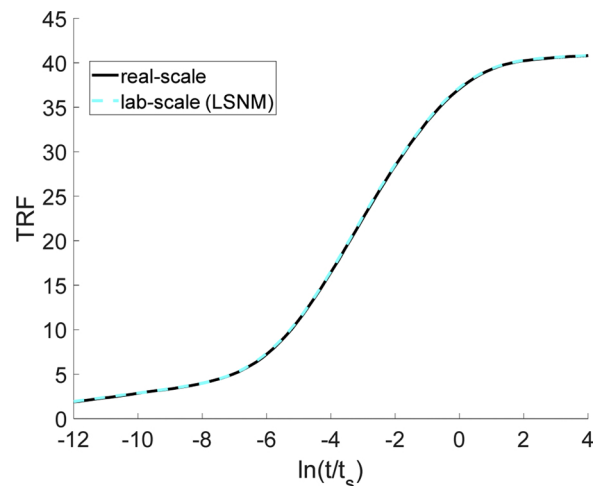$$\eta = \frac{H}{\rho_f c_f V_f} \frac{1}{2R_b} \sqrt{1 + 4\frac{R_b}{R_{12}}} \qquad (17)$$

Fig. 5. Comparison of real-scale and lab-scale models in terms of the TRF for a 4×4 borehole field with $r_b^* = 1.917 \cdot 10^{-4}$ and $B^* = D^* = 0.0167$
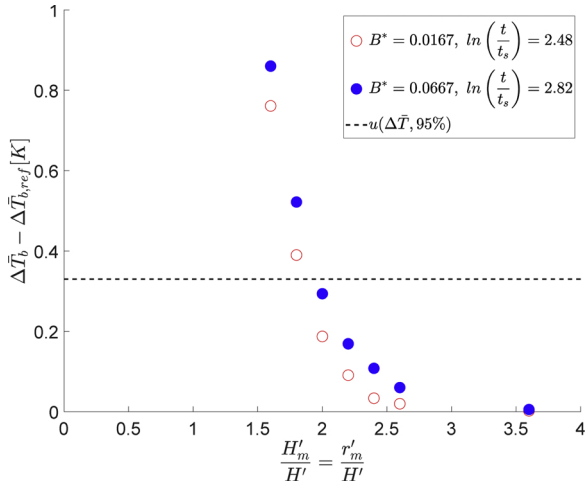
Fig. 6. Difference in borehole average temperature between the reference model and models with different domain-size-to-borehole-length ratios. Calculated for $\lambda' = 3.0$ W·m^{-1} K^{-1}, $\alpha' = 7.00 \cdot 10^{-7}$ m^2·s^{-1}, r* = 1.92·10^{-4} and D* = 0.0167.

The local borehole resistance, R_b, can be expressed as a sum of three components (Lamarche et al., 2010)

$$R_b = R_g + R_{p,cond} + R_{p,c} \tag{18}$$

The two first components depend on ratios of radii and distances so they do not change under downscaling if the same materials are used in the real-scale and lab-scale borehole field (if not a simple proportionality constant must accounted for). The third component may be expressed as

$$R_{p,c} = \frac{1}{4\pi r_p h_c} = \frac{1}{2\pi Nu\lambda_f} \tag{19}$$

Typically the Nusselt number depends on the Reynolds and Prandtl numbers. The Reynolds number is conserved if the flow rate is scaled down proportionally to the geometrical scale factor

$$\dot{V}_f' = \frac{\dot{V}_f}{\beta} \tag{20}$$

This last equality also lead to the conservation of η under downscaling (which can verified by replacing H by $\beta H'$ and $\dot{V}_f$ by $\beta \dot{V}_f'$ in eq.17). Now, why should η be conserved? This can be understood by looking at the study from Cimmino (2015) in which three invariants are given for obtaining similar TRFs accounting for the borehole thermal transfer process: the dimensionless borehole thermal resistance, $\Omega_b = 2\pi\lambda R_b$, the dimensionless borehole internal thermal conductance, $R_a^* = \frac{H}{\dot{m}_f c_f R_a}$ and the dimensionless flow rate $\dot{m}_f^* = \frac{2\pi\lambda H}{\dot{m}_f c_f}$. Since $R_a = \frac{4R_{12}R_b}{4R_b + R_{12}}$, we have that $\eta^2 = \frac{R_a^* \cdot \dot{m}_f^*}{\Omega_b}$ and the conservation of η becomes a necessity for obtaining similar TRFs.

3.5. Influence of the top convective BC

As noted through the analytical invariance analysis, the convection heat transfer coefficient, h_c, at the top boundary layer must be scaled up when downscaling the borehole field. This is a direct consequence of the conservation of the Biot number. Values of h_c around 10 W m^{-2} K^{-1} can be expected at the top of real size borehole fields, corresponding to a h_c' of 5142 W m^{-2} K^{-1} ($Bi = 857$) given the chosen scale factor and thermal conductivities for the case study. The latter value is challenging to achieve; hence, the LSNM is utilized in order to assess the possible
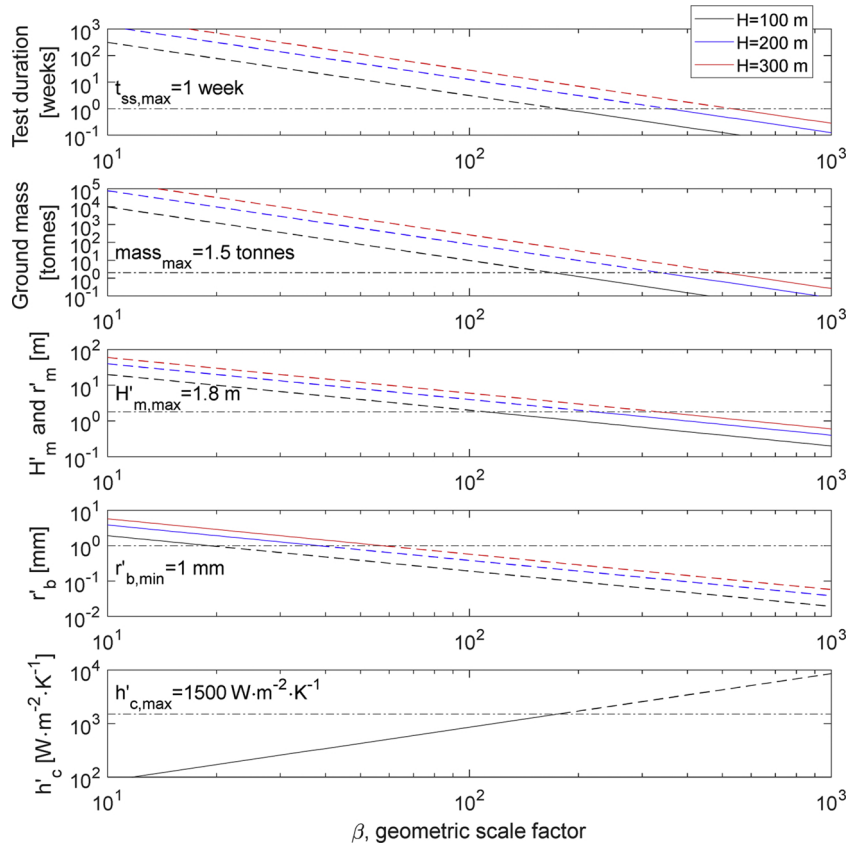
Fig. 7. Influence of the geometrical scale factor on several design parameters. Calculated for three different real-scale borehole lengths, r* = 1.92·10^{-4} and D* = 0.0167.
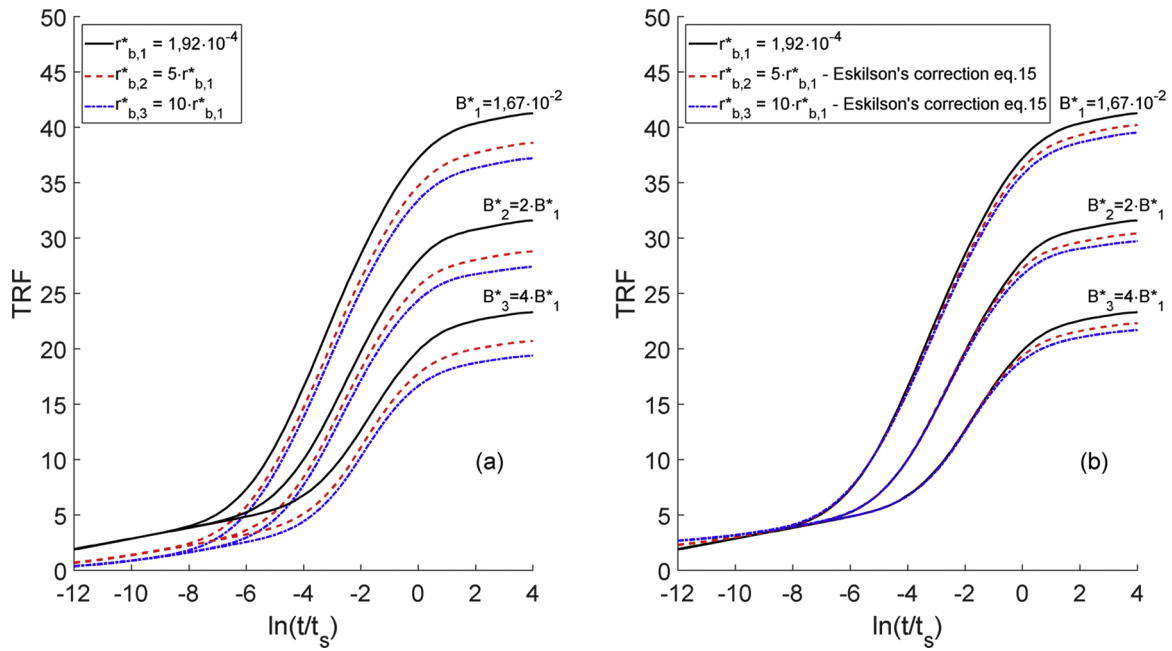
Fig. 8. Influence of the borehole radius aspect ratio on the numerically generated TRFs for a 4×4 borehole field: (a) without correction, (b) with Eskilson's correction eq.15.

deviations in TRF for lower h_c', namely 514.2, 51.42 and 5.142 W m^{-2} K^{-1} corresponding to h_c of 1, 0.1 and 0.01 W m^{-2} K^{-1}, or Biot numbers of 85.7, 8.57 and 0.857. Three different dimensionless spacing are applied for the simulations, namely $B^* = 0.0167$, $B^* = 0.0333$ and $B^* = 0.0667$, but only Biot numbers of 857 and 85.7 are tested for the two last B^*. Note that the ambient temperature is set as 0 °C.

The resulting TRFs are shown in Fig. 9 together with the TRF obtained for a Dirichlet BC at the top. As could be expected, decreasing h_c' leads to increasing TRF values: if heat cannot "easily" escape through the top boundary, it will accumulate in the ground, leading to a higher temperature at the borehole wall. At $\ln(t/t_s) = 2.4$ and for $B^* = 0.0167$, relative differences with the TRF generated with constant temperature BC are of 0.41 % 2.9 %, 14.0 % and 34.3 % for Bi of 857, 85.7, 8.57 and 0.857, respectively. For $B^* = 0.0333$ relative differences of 0.26 % and 3.3 % are observed for Bi of 857, 85.7 while those differences become 0.34 % and 3.4 % for the same Biot numbers but $B^* = 0.0667$. Although the relative differences are of similar magnitude, it may be preferable to use larger spacing leading to lower absolute systematic errors introduced by the top convective BC.

It may be observed that a h_c of 10 W m^{-2} K^{-1} in real size borehole fields ($Bi = 857$, $h_c' = 5142$ W m^{-2} K^{-1} in the LABS) leads to an almost identical TRF than the Dirichlet BC (). This outcome can be expected since the Biot number is typically large (several hundreds to one thousand) for real size borehole fields with somewhat long boreholes. For fields with short lengths (10–30 m) however, a h_c of 10 W m^{-2} K^{-1} can lead to Biot numbers as low as 30 which would imply that using a Dirichlet BC for the modeling could significantly underestimate the TRF. This can have implications for short boreholes or energy piles for example.

A h_c', of 514.2 W m^{-2} K^{-1} leads to a reasonable error while being easier to achieve than 5142 W m^{-2} K^{-1}. A value of 514.2 W m^{-2} K^{-1}, or higher, can be reached by circulating constant temperature water in micro-channels. Kim et al. (2017) report local values between 1400 and 3000 W m^{-2} K^{-1} for single-phase convection in mini-channel. Note that the diverging TRF for $Bi = 0.857$ is due to the finite size of the LSNM, the adiabatic BC on the sides and the close-to-adiabatic BC at the top.

As previously noted, the top BC appears to have been left uncontrolled in Cimmino and Bernier (2015), entailing natural convection on the surface. In those conditions, one may expect convection heat

transfer coefficients between 1 to 6 W m^{-2} K^{-1}. Considering radiation, heat transfer coefficients could go up to 15 W m^{-2} K^{-1} (Bergman et al., 2011). A LSNM reproducing as faithfully as possible the conditions reported by Cimmino and Bernier (2015) is made using values of h_c' of 1 and 10 W m^{-2} K^{-1}, as well as a Dirichlet BC on top. The results are shown in Fig. 10 which also displays results for $h_c' = 10$ W m^{-2} K^{-1} and borehole radius changing by ± 0.5 mm due to the uncertainty on the actual borehole radius used during the tests. A convection coefficient of 10 W m^{-2} K^{-1} seems to reproduce fairly well the behavior observed during their test with differences of 3.5 % and 1.1 % at the first and last reported time points, respectively. The top convective BC could thus contribute to the systematic error between experimental and analytical results that is observed in Cimmino and Bernier (2015).

3.6. Impact of heat losses on TRF

Heat losses through the sides of the LABS have been disregarded so
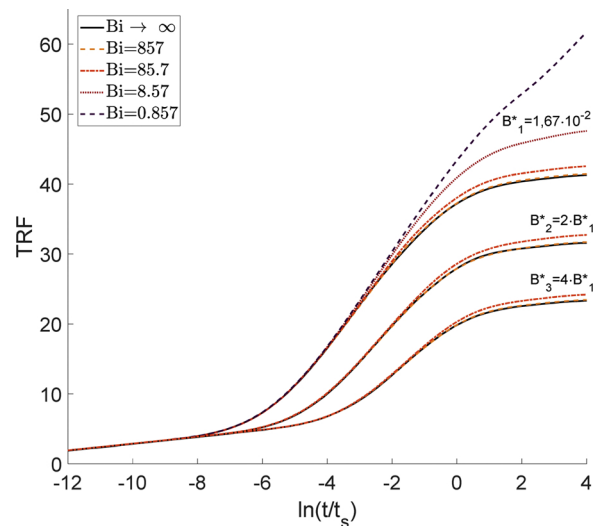

Fig. 9. Influence of the top BC convection heat transfer coefficient (Biot number) on the TRF for three different spacing B*.
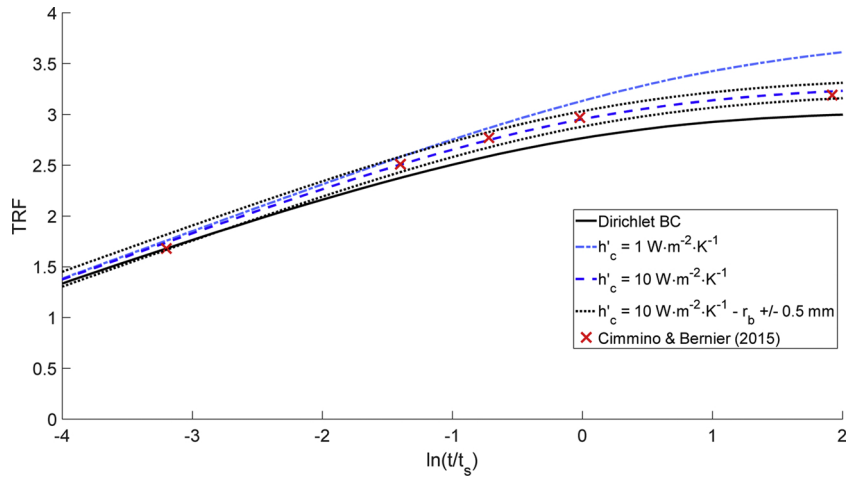
Fig. 10. Numerical reproduction of the test performed by Cimmino and Bernier (2015).

far but there will be losses and it is important to limit them as much as possible. Heat losses were investigated through a 2D steady-state model in Mazzotti et al. (2018) but the influence on the TRF could not be evaluated. Here the heat losses are assessed dynamically through a numerical model. The results in terms of TRFs for perfectly adiabatic boundaries and for boundaries with heat losses are represented in Fig. 11 for three different dimensionless spacings. There is a noticeable discrepancy at large time with a maximum relative difference of 5–6 % for all spacings. Again, the relative differences are of similar magnitude for different spacings, but it may be preferable to use larger spacing leading to lower absolute systematic errors. Additional insulation and low emissivity layers were stated as possible solution for this issue (Mazzotti et al., 2018); however, extra insulation or a low emissivity layer do not prevent heat from penetrating the insulation in contact with the simulating ground. Therefore, this potential source of systematic error should be accounted for when analysing hypothetical results from LABS.

4. Conclusion

A design methodology for LAboratory-scale Borehole Storage (LABS) and its application to a case study were investigated in this work. The design methodology is largely based on invariance requirements analytically derived from the heat equation. Numerical models are then used to verify the found invariance requirements, determine test duration, find a suitable size for the LABS, as well as investigate boundary condition (BC) and practical issues. This work is based on a previous study (Mazzotti et al., 2018). Here, the design process is clarified through a flowchart that allow other researchers to implement and build on the proposed methodology. In addition, the present study is made more general by nondimensionalizing the invariance requirements and simulating borehole fields with different borehole spacing.

The analytical analysis shows that the invariance of the Fourier and Biot numbers is a requirement for generating lab-scale results similar to those that would be obtained in a real-scale installation. As a consequence, Neumann or convective BCs are scaled up, proportionally to the geometrical scale factor, when downscaling. This BC scale-up is notably proposed as a possible explanation for the observed bias between experimental and analytical results in Cimmino and Bernier (2015). A numerical reproduction of their experiment indeed shows a good agreement with their test results when convection is accounted for.

Through the case study, a LABS with a 4 × 4 borehole field and vertical boreholes, it is found that natural convection as top BC of the LABS leads to TRF values more than 14 % higher than those obtained with a Dirichlet BC. Natural convection as top BC for a real-scale

borehole field with long boreholes will however lead to results similar to that of a Dirichlet BC, which validates the use of the latter as top BC. For short boreholes (about 10–30 m), or possibly energy piles, using a Dirichlet BC may however lead to underestimation of TRFs. This can be easily understood through considerations of the Biot number: small scale requires higher convection coefficient for the Biot number to be conserved. For LABS, forced convection must therefore be applied on the top BC to accurately reproduce TRFs.

For the case study, a geometrical scale factor of 600 is found suitable. This implies simulating a real-scale borehole of 300 m by a 50 cm long "in-lab" borehole. The corresponding test duration is then about 5.5 days. Domain-size-to-borehole-length ratios of two are found appropriate for this configuration of boreholes, hence leading to a LABS of radius and height 1.0 m. For these dimensions, the borehole temperature increase induced by boundary effects is indeed less than 0.29 K, which is below the determined design uncertainty of the change in average borehole wall temperature. The borehole radius is chosen as 1.25 mm while the spacing is of 3.3 cm. Symmetry is used to reduce the LABS to a ¼ cylinder, thereby reducing the weight of the sand used as simulating ground to 1.2 instead of 4.9 tonnes.

Because of the low geometrical aspect ratios of boreholes, it becomes challenging to reproduce realistic borehole radius in LABS. LABS are however still useful for model validation. The effect of the borehole
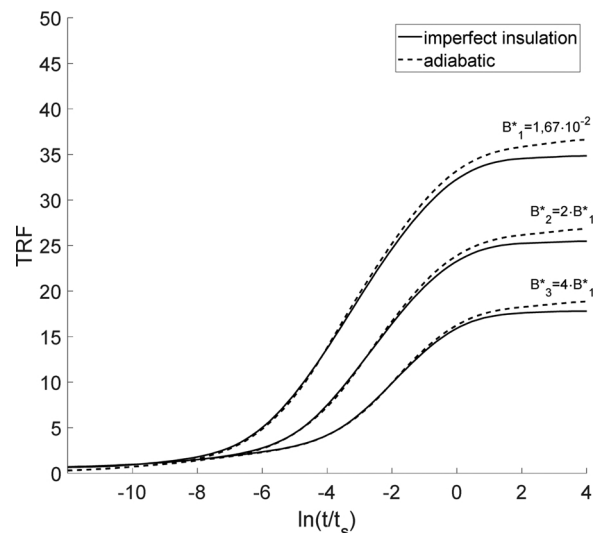

Fig. 11. Influence of the heat losses on the TRF of a 4 × 4 borehole field for three different dimensionless spacing and with $r_b^* = 0.0025$ and $D^* = 0.0167$

radius on TRFs is numerically investigated and it is found that Eskilson's radius correction (1987) is not fully satisfactory.

Finally, heat losses through the side of the LABS – investigated here dynamically as opposed to a steady-state model in Mazzotti et al. (2018) – are found to influence the TRF at large times with maximum relative differences of 5–6 %. This potential source of systematic error should be accounted for when analyzing results from LABS.

Through the analytical and numerical analyses presented in this work, the authors believe that they have provided a solid background for designing LABS. Moreover, some potential sources of systematic errors have been highlighted, which strengthen the need of such pre-experimental studies. Identifying potential sources of systematic error should reinforce the trustworthiness of results from LABS, which can be used to generate reference Thermal Response Function under controlled conditions. In turn, this would fill a data gap highlighted in the literature and contribute to strengthen the trustworthiness of long-term ground heat transfer models.

CRediT authorship contribution statement

Willem Mazzotti Pallard: Conceptualization, Methodology, Software, Validation, Formal analysis, Investigation, Data curation, Writing - original draft, Writing - review & editing, Visualization, Project administration. **Alberto Lazzarotto:** Conceptualization, Methodology, Validation, Writing - review & editing, Supervision. **José Acuña Sequera:** Conceptualization, Methodology, Writing - review & editing, Supervision, Project administration, Funding acquisition. **Björn Palm:** Conceptualization, Methodology, Writing - review & editing, Supervision, Project administration.

Declaration of Competing Interest

The authors declare that they have no known competing financial interests or personal relationships that could have appeared to influence the work reported in this paper.

Acknowledgments

References

Akrouch, G.A., Sánchez, M., Briaud, J.-L., 2016. An experimental, analytical and numerical study on the thermal efficiency of energy piles in unsaturated soils. Comput. Geotech. 71, 207–220. https://doi.org/10.1016/j.compgeo.2015.08.009.

Arkhangelskaya, T., Lukyashchenko, K., 2017. Estimating soil thermal diffusivity at different water contents from easily available data on soil texture, bulk density, and organic carbon content. Biosyst. Eng. https://doi.org/10.1016/j.biosystemseng.2017.06.011.

Beier, R.A., 2014. Transient heat transfer in a U-tube borehole heat exchanger. Appl. Therm. Eng. 62, 256–266. https://doi.org/10.1016/j.applthermaleng.2013.09.014.

Beier, R.A., Smith, M.D., Spitler, J.D., 2011. Reference data sets for vertical borehole ground heat exchanger models and thermal response test analysis. Geothermics 40, 79–85. https://doi.org/10.1016/j.geothermics.2010.12.007.

Bergman, T.L., Incropera, F.P., Dewitt, D.P., Lavine, A.S., 2011. Fundamentals of Heat and Mass Transfer, 7th ed. Wiley, Hoboken, NJ.

Cimmino, M., 2015. The effects of borehole thermal resistances and fluid flow rate on the g-functions of geothermal bore fields. Int. J. Heat Mass Transf. 91, 1119–1127. https://doi.org/10.1016/j.ijheatmasstransfer.2015.08.041.

Cimmino, M., Bernier, M., 2014. A semi-analytical method to generate g-functions for geothermal bore fields. Int. J. Heat Mass Transf. 70, 641–650. https://doi.org/10.1016/j.ijheatmasstransfer.2013.11.037.

Cimmino, M., Bernier, M., 2015. Experimental determination of the g-functions of a small-scale geothermal borehole. Geothermics 56, 60–71. https://doi.org/10.1016/j.geothermics.2015.03.006.

Cimmino, M., Bernier, M., Adams, F., 2013. A contribution towards the determination of g-functions using the finite line source. Appl. Therm. Eng. 51, 401–412. https://doi.org/10.1016/j.applthermaleng.2012.07.044.

Claesson, J., Eskilson, P., 1987. Conductive Heat Extraction by a Deep Borehole. Analytical Studies. (Technical Report). University of Lund, Lund.

Claesson, J., Javed, S., 2011. An analytical method to calculate borehole fluid temperatures for time-scales from minutes to decades. ASHRAE Trans. 117, 279–288.

COMSOL Mutliphysics®, 2018. COMSOL AB. Stockholm, Sweden. .

Cui, P., Yang, H., Fang, Z., 2006. Heat transfer analysis of ground heat exchangers with inclined boreholes. Appl. Therm. Eng. 26, 1169–1175. https://doi.org/10.1016/j.applthermaleng.2005.10.034.

Cullin, J.R., Spitler, J.D., Montagud, C., Ruiz-Calvo, F., Rees, S.J., Naicker, S.S., Konečný, P., Southard, L.E., 2015. Validation of vertical ground heat exchanger design methodologies. Sci. Technol. Built Environ. 21, 137–149. https://doi.org/10.1080/10789669.2014.974478.

Eskilson, P., 1987. Thermal Analysis of Heat Extraction Boreholes. Lund University, Sweden.

Eslami-nejad, P., Bernier, M., 2011. Coupling of geothermal heat pumps with thermal solar collectors using double U-tube boreholes with two independent circuits. Appl. Therm. Eng. 31, 3066–3077. https://doi.org/10.1016/j.applthermaleng.2011.05.040.

Fossa, M., 2011. The temperature penalty approach to the design of borehole heat exchangers for heat pump applications. Energy Build. 43, 1473–1479. https://doi.org/10.1016/j.enbuild.2011.02.020.

Gehlin, S., Spitler, J.D., Larsson, A., Annsberg, Å., 2018. Measured performance of the university of Stockholm studenthuset ground source heat pump system. Proceedings Book. Presented at the The 14th International Conference on Energy Storage. Çukurova University, Adana, Turkey, pp. 210–224.

Hellström, G., 1991. Ground Heat Storage: Thermal Analyses of Duct Storage Systems. PhD Thesis. Lund University, Lund, Sweden.

Hellström, G., Kjellsson, E., 2000. Laboratory measurements of heat transfer properties for different types of borehole heat exchangers. In: Proc. of Terrastock. Presented at the Terrastock. Stuttgart, Germany.

Huang, B., Mauerhofer, V., 2016. Life cycle sustainability assessment of ground source heat pump in Shanghai. China. J. Clean. Prod. 119, 207–214. https://doi.org/10.1016/j.jclepro.2015.08.048.

Iglesias, M., Rodriguez, J., Franco, D., 2012. Monitoring of building heating and cooling systems based on geothermal heat pump in Galicia (Spain), in: EPJ web of conferences. Presented at the 2nd European Energy Conference 05004. https://doi.org/10.1051/epjconf/20123305004.

Kim, Y., Kim, M., Ahn, C., Kim, H.U., Kang, S.-W., Kim, T., 2017. Numerical study on heat transfer and pressure drop in laminar-flow multistage mini-channel heat sink. Int. J. Heat Mass Transf. 108, 1197–1206. https://doi.org/10.1016/j.ijheatmasstransfer.2016.12.025.

Koroneos, C.J., Nanaki, E.A., 2017. Environmental impact assessment of a ground source heat pump system in Greece. Geothermics 65, 1–9. https://doi.org/10.1016/j.geothermics.2016.08.005.

Kramer, C.A., Ghasemi-Fare, O., Basu, P., 2015. Laboratory thermal performance tests on a model heat exchanger pile in sand. Geotech. Geol. Eng. 33, 253–271. https://doi.org/10.1007/s10706-014-9786-z.

Lamarche, L., 2011. Analytical g-function for inclined boreholes in ground-source heat pump systems. Geothermics 40, 241–249. https://doi.org/10.1016/j.geothermics.2011.07.006.

Lamarche, L., 2015. Short-time analysis of vertical boreholes, new analytic solutions and choice of equivalent radius. Int. J. Heat Mass Transf. 91, 800–807. https://doi.org/10.1016/j.ijheatmasstransfer.2015.07.135.

Lamarche, L., Beauchamp, B., 2007. A new contribution to the finite line-source model for geothermal boreholes. Energy Build. 39, 188–198. https://doi.org/10.1016/j.enbuild.2006.06.003.

Lamarche, L., Kajl, S., Beauchamp, B., 2010. A review of methods to evaluate borehole thermal resistances in geothermal heat-pump systems. Geothermics 39, 187–200. https://doi.org/10.1016/j.geothermics.2010.03.003.

Lazzarotto, A., 2016. A methodology for the calculation of response functions for geothermal fields with arbitrarily oriented boreholes – part 1. Renew. Energy 86, 1380–1393. https://doi.org/10.1016/j.renene.2015.09.056.

Lazzarotto, A., Björk, F., 2016. A methodology for the calculation of response functions for geothermal fields with arbitrarily oriented boreholes – part 2. Renew. Energy 86, 1353–1361. https://doi.org/10.1016/j.renene.2015.09.057.

Lee, C.K., Lam, H.N., 2008. Computer simulation of borehole ground heat exchangers for geothermal heat pump systems. Renew. Energy 33, 1286–1296. https://doi.org/10.1016/j.renene.2007.07.006.

Lee, C.K., Lam, H.N., 2012. A modified multi-ground-layer model for borehole ground heat exchangers with an inhomogeneous groundwater flow. Energy, Asia-Pacific Forum on Renewable Energy 2011 (47), 378–387. https://doi.org/10.1016/j.energy.2012.09.056.

Luo, J., Rohn, J., Bayer, M., Priess, A., Wilkmann, L., Xiang, W., 2015. Heating and cooling performance analysis of a ground source heat pump system in Southern Germany. Geothermics 53, 57–66. https://doi.org/10.1016/j.geothermics.2014.04.004.

Marcotte, D., Pasquier, P., 2009. The effect of borehole inclination on fluid and ground temperature for GLHE systems. Geothermics 38, 392–398. https://doi.org/10.1016/j.geothermics.2009.06.001.

Mazzotti, W., Jiang, Y., Monzó, P., Lazzarotto, A., Acuña, J., Palm, B., 2018. Design of a laboratory borehole storage model, in: research Conference proceedings. In: Presented at the International Ground Source Heat Pump Association Research Conference. Stockholm, Sweden. https://doi.org/10.22488/okstate.18.000038.

Michopoulos, A., Zachariadis, T., Kyriakis, N., 2013. Operation characteristics and experience of a ground source heat pump system with a vertical ground heat exchanger. Energy 51, 349–357. https://doi.org/10.1016/j.energy.2012.11.042.

Mikhaylova, O., Johnston, I.W., Narsilio, G.A., Kivi, A.V., Aditya, R., Noonan, G., 2015. Performance of borehole ground heat exchangers under thermal loads from a school

building: full-scale experiment in Melbourne, Australia. in: Proceedings World Geothermal Congress 19–25.

Molina-Giraldo, N., Blum, P., Zhu, K., Bayer, P., Fang, Z., 2011. A moving finite line source model to simulate borehole heat exchangers with groundwater advection. Int. J. Therm. Sci. 50, 2506–2513. https://doi.org/10.1016/j.ijthermalsci.2011.06.012.

Montagud, C., Corberán, J.M., Montero, Á., Urchueguía, J.F., 2011. Analysis of the energy performance of a ground source heat pump system after five years of operation. Energy Build. 43, 3618–3626. https://doi.org/10.1016/j.enbuild.2011.09.036.

Monzó, P., Mogensen, P., Acuña, J., Ruiz-Calvo, F., Montagud, C., 2015. A novel numerical approach for imposing a temperature boundary condition at the borehole wall in borehole fields. Geothermics 56, 35–44. https://doi.org/10.1016/j.geothermics.2015.03.003.

Monzó, P., Lazzarotto, A., Acuña, J., 2017. First measurements of a monitoring project on a btes system. In: Presented at the International Ground Source Heat Pump Association Conference. Denver. https://doi.org/10.22488/okstate.17.000523.

Monzó, P., Puttige, A.R., Acuña, J., Mogensen, P., Cazorla, A., Rodriguez, J., Montagud, C., Cerdeira, F., 2018. Numerical modeling of ground thermal response with borehole heat exchangers connected in parallel. Energy Build. 172, 371–384. https://doi.org/10.1016/j.enbuild.2018.04.057.

Naiker, S.S., Rees, S.J., 2011. Monitoring and performance analysis of a large non-domestic ground source heat pump installation. CIBSE.

Naldi, C., Zanchini, E., 2019. A new numerical method to determine isothermal g-functions of borehole heat exchanger fields. Geothermics 77, 278–287. https://doi.org/10.1016/j.geothermics.2018.10.007.

Nguyen, A., Pasquier, P., Marcotte, D., 2017. Borehole thermal energy storage systems under the influence of groundwater flow and time-varying surface temperature. Geothermics 66, 110–118. https://doi.org/10.1016/j.geothermics.2016.11.002.

Ozudogru, T.Y., Olgun, C.G., Senol, A., 2014. 3D numerical modeling of vertical geothermal heat exchangers. Geothermics 51, 312–324. https://doi.org/10.1016/j.geothermics.2014.02.005.

Ozyurt, O., Ekinci, D.A., 2011. Experimental study of vertical ground-source heat pump performance evaluation for cold climate in Turkey. Appl. Energy 88, 1257–1265. https://doi.org/10.1016/j.apenergy.2010.10.046.

Pasquier, P., Marcotte, D., 2014. Joint use of quasi-3D response model and spectral method to simulate borehole heat exchanger. Geothermics 51, 281–299. https://doi.org/10.1016/j.geothermics.2014.02.001.

Priarone, A., Fossa, M., 2016. Temperature response factors at different boundary conditions for modelling the single borehole heat exchanger. Appl. Therm. Eng. 103, 934–944. https://doi.org/10.1016/j.applthermaleng.2016.04.038.

Puttige, A.R., Rodriguez, J., Monzó, P., Cerdeira, F., Fernández, A., Novelle, L., Acuña, J.,

Mogensen, P., 2016. Improvements on a numerical model of borehole heat exchangers. In: Presented at the European Geothermal Congress. Strasbourg.

Ruiz-Calvo, F., Montagud, C., 2014. Reference data sets for validating GSHP system models and analyzing performance parameters based on a five-year operation period. Geothermics 51, 417–428. https://doi.org/10.1016/j.geothermics.2014.03.010.

Ruiz-Calvo, F., De Rosa, M., Monzó, P., Montagud, C., Corberán, J.M., 2016. Coupling short-term (B2G model) and long-term (g-function) models for ground source heat exchanger simulation in TRNSYS. Application in a real installation. Appl. Therm. Eng. 102, 720–732. https://doi.org/10.1016/j.applthermaleng.2016.03.127.

Salim Shirazi, A., Bernier, M., 2014. A small-scale experimental apparatus to study heat transfer in the vicinity of geothermal boreholes. HVACR Res. 20, 819–827. https://doi.org/10.1080/10789669.2014.939553.

Sivasakthivel, T., Murugesan, K., Kumar, S., Hu, P., Kobiga, P., 2016. Experimental study of thermal performance of a ground source heat pump system installed in a Himalayan city of India for composite climatic conditions. Energy Build. 131, 193–206. https://doi.org/10.1016/j.enbuild.2016.09.034.

Spitler, J., Bernier, M., 2011. Ground-source heat pump systems: the first century and beyond. HVACR Res. 17, 891–894. https://doi.org/10.1080/10789669.2011.628221.

Spitler, J., Bernier, M., 2016. 2 - vertical borehole ground heat exchanger design methods. In: Rees, S.J. (Ed.), Advances in Ground-Source Heat Pump Systems. Woodhead Publishing, pp. 29–61. https://doi.org/10.1016/B978-0-08-100311-4.00002-9.

Spitler, J.D., Southard, L.E., Liu, X., 2017. Ground-source and air-source heat pump system performance at the ASHRAE headquarters building, in: proceedings. In: Presented at the 12th IEA Heat Pump Conference. Rotterdam. pp. 12.

Stafford, A., 2011. Long-term monitoring and performance of ground source heat pumps. Build. Res. Inf. 39, 566–573. https://doi.org/10.1080/09613218.2011.603599.

Sundberg, J., 1991. Termiska Egenskaper I Jord Och Berg (No. 12). Swedish Geotechnical Institute.

Tarnawski, V.R., Momose, T., Leong, W.H., 2011. Thermal conductivity of standard sands II. Saturated conditions. Int. J. Thermophys. 32, 984–1005. https://doi.org/10.1007/s10765-011-0975-1.

Yavuzturk, C., Spitler, J.D., 2001. Field validation of a short time step model for vertical ground-loop heat exchangers / Discussion. ASHRAE Trans. Atlanta 107, 617.

Yu, X., Wang, R.Z., Zhai, X.Q., 2011. Year round experimental study on a constant temperature and humidity air-conditioning system driven by ground source heat pump. Energy 36, 1309–1318. https://doi.org/10.1016/j.energy.2010.11.013.

Zeng, H.Y., Diao, N.R., Fang, Z.H., 2002. A finite line-source model for boreholes in geothermal heat exchangers. Heat TransferAsian Res. 31, 558–567. https://doi.org/10.1002/htj.10057.

PUBLICATION 4 : Integrated Combined Heat and Power Plant with Borehole Thermal Energy Storage

Energiforsk

Integrated Combined Heat and Power Plant with Borehole Thermal Energy Storage

Amol Yevalkar

		Master of Science Thesis
		TRITA-ITM-EX 2019:704
		Integrated Combined Heat and Power Plant with Borehole Thermal Energy Storage
		Amol Yevalkar
Approved	Examiner Björn Laumert	Supervisor Monika Topel
	Commissioner Bengt Dahlgren AB	Contact person José Acuña

Abstract

Countries like Sweden, that experience temperatures below 0^oC, have a high heating demand during winters. The heating demand in Sweden is satisfied through district heating, electric heating, heat pumps and biofuel boilers. The fossil fuels account for around 5 % of the heating market. Sweden is currently looking for alternative solutions in order to replace the fossil fuels. One of the solutions being studied is to have a Borehole Thermal Energy Storage (BTES) system that can store the excess heat produced from a Combined Heat and Power (CHP) plant during the summer.

In previous studies, a dynamic model of BTES system was developed which was limited for a specific case. In order to design the BTES systems for different cases as well, a generic steady-state sizing model was developed. This generic steady-state sizing model is flexible can be used to determine the size of BTES in terms of number of boreholes, borehole depth, etc. as per the requirements of the user.

Few key results for different input parameters from the newly developed steady-state sizing model and the existing dynamic model were compared for several simulations in order to validate the new steady-state model. The results for a reference case of 240 m borehole depth and 0.8 kg/s mass flow rate in the borehole loop were presented. Further a sensitivity analysis was done by varying the borehole depth and the mass flow rate in the borehole loop. It showed that the Net Present Value (NPV) of the entire system after 20 years and BTES efficiency were higher for lower borehole depth and higher mass flow rate in the borehole loop.

Sammanfattning

Länder som Sverige, som upplever temperaturer under 0^oC, har ett högt värmebehov under vintrarna. Värmebehovet i Sverige tillgodoses genom fjärrvärme, elvärme, värmepumpar och pannor eldade med biobränsle. Fossila bränslen står för cirka 5 % av värmemarknaden. Sverige letar för närvarande efter alternativa lösningar för att ersätta de fossila bränslena. En av lösningarna som studeras är att ha värmelagring i borrhål (Borehole Thermal Energy Storage, BTES) som kan lagra överskottsvärmen som produceras från en kraftvärmeanläggning under sommaren.

I tidigare studier utvecklades en dynamisk modell av ett BTES-system som var begränsat till ett specifikt fall. För att utforma BTES-system även för andra fall, utvecklades en generisk modell. Denna generiska dimensioneringsmodell för stabiliseringsstatus är flexibel och kan användas för att bestämma storleken på BTES när det gäller antalet borrhål, borrhålsdjup etc. enligt användarens krav.

Några nyckelresultat för olika ingångsparametrar från den nyutvecklade statiska dimensioneringsmodellen och den befintliga dynamiska modellen jämfördes för flera simuleringar för att validera den nya statiska modellen. Resultaten för ett referensfall på 240 m borrhålsdjup och 0,8 kg/s massflödeshastighet i borrhålslingan presenterades. Dessutom utfördes en känslighetsanalys genom att variera borrhålens djup och massflödeshastigheten i borrhålslingan. Det visade sig att både nettonuvärdet (net present value, NPV) för hela systemet efter 20 år och BTES-effektiviteten var högre för lägre borrhåldjup och högre massflödeshastighet i borrhålsslingan.

Acknowledgement

Abbreviations

ATES	Aquifer Thermal Energy Storage
BHE	Borehole heat exchanger
BTES	Borehole Thermal Energy Storage
CAPEX	Capital Expenditure
CHP	Combined Heat and Power
CTES	Cavern Thermal Energy Storage
DH	District Heating
DST	Duct Ground Heat Storage
GSHP	Ground Source Heat Pump
HEX	Heat Exchanger
HP	Heat Pump
HT-BTES	High Temperature - Borehole Thermal Energy Storage
KPI	Key Performance Indicator
MATLAB	Matrix Laboratory
NPV	Net Present Value
OPEX	Operational Expenditure
SEK	Swedish Krona
SPF	Seasonal Performance Factor
TES	Thermal Energy Storage
TRNSYS	TRaNsient SYstems Simulation Program
UTES	Underground Thermal Energy Storage

Table of Contents

List of Figures

List of Tables

1 Introduction

In the countries that experience cold winters with temperatures below $0^{o}C$, additional heating needs to be supplied to all the buildings in order to increase the indoor temperatures. For humans, there are various factors that affect the thermal comfort and air temperature around the human body is one of them. During low outdoor temperatures there is a certain heating demand as additional heat needs to be supplied to maintain the indoor air temperature. This additional heat can be supplied in various ways.

In Sweden, the heating market is one of the most predominant energy markets. As of 2014, the demand for space heating and hot tap water is accounted to be approximately 100 TWh/year. The four ways of heating that exists are district heating, electric heating, heat pumps and biofuel boilers. District heating accounts for a bit more than 50% whereas the electric heating and heat pumps accounts for approximately 30%. The biofuel boilers have a share of approximately 10% in the heating market. The fossil fuels account for around 5% in the heating market (Dzebo A., 2017). The environmentally heating market plays an important role in Sweden's ambition for sustainable development (Rydén B., 2014).

Sweden is looking for alternative solutions to replace the heating due to fossil fuels, in order to achieve the goal of net-zero greenhouse gas emissions. Tekniska Verken AB is a municipality owned company located in Linköping, Sweden that offers services in district heating and cooling, waste treatment, electricity, lighting, water, biogas and energy efficiency (Anon., n.d.). Tekniska Verken owns two CHP-plants called Gärstadverket and KV1 in Linköping. Among these two plants, Gärstadverket is the main plant and covers most of the heating demand in Linköping. But due to uneven heating demand over the annual period, Gärstadverket cannot satisfy the peak heating demand during the winter period and Tekniska Verken needs to operate the KV1 plant to satisfy the peak heating demand. The boilers in the Gärstadverket plant are mainly fed by the household and industrial waste whereas the boilers in the older KV1 plant are operated by biofuels, coal and oil (M., 2017). In order to decrease the use of fossil fuels, Tekniska Verken is looking for alternative solutions that are sustainable and could substitute the heat and power produced by the KV1 plant. One of the proposed solutions is to store the surplus heat produced during summer by the Gärstadverket plant into a Borehole Thermal Energy Storage (BTES) system.

A BTES is a seasonal storage system that is used to store the excess heat energy under the ground during summer, which can be extracted later during the winter. Some possible sources of heat energy could be a CHP plant, solar thermal and industrial waste heat. Figure 1 and Figure 2 shows the summer and winter operation of a borehole thermal energy storage system.
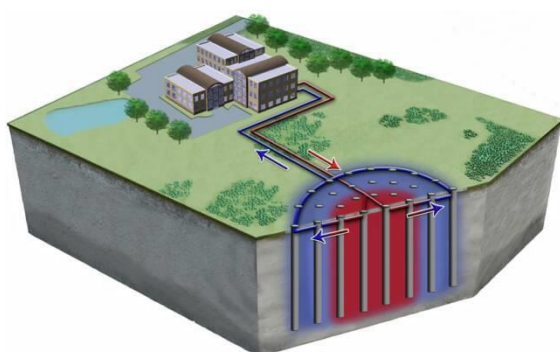
Figure 1. BTES summer-time operation (M., 2017)
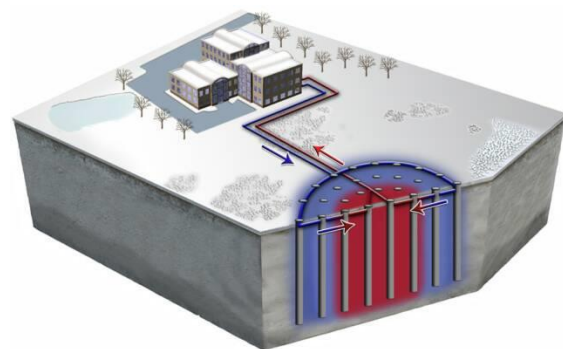
Figure 2. BTES winter-time operation (M., 2017)

Previously, some studies have been performed at KTH and Bengt Dahlgren AB and a dynamic model was developed to analyze the performance of a BTES system connected to a CHP plant in Linköping, Sweden. Initially, the dynamic model was simulated without a heat pump. In the later studies, a dynamic model was developed that considered the interaction between the BTES and the Gärstadverket. A heat pump was connected in between the BTES and the district heating network to control the power output as per the required heating demand.

The previous dynamic model was developed for a specific case and is not flexible for analyzing the performance of BTES system in different locations which can have different thermodynamic and geometric constraints. In this master thesis a generic steady-state sizing model was developed which can be flexible and used for the evaluation of BTES system under different operating conditions as per the requirement of the user.

Figure 3 shows the process flowchart involved in the Dynamic Energy Systems Optimizer tool also called as DYESOPT. It is a tool that is used for dynamic modeling of the power plants and assess the thermo-economic performance. The purpose of the optimization tool is to find out the optimal configuration for any power plant. The entire process can be divided in 4 main stages: input design parameters, steady-state sizing, dynamic simulation and thermo-economic calculations. The dynamic model already existed before and the steady-state model was developed in this master thesis.
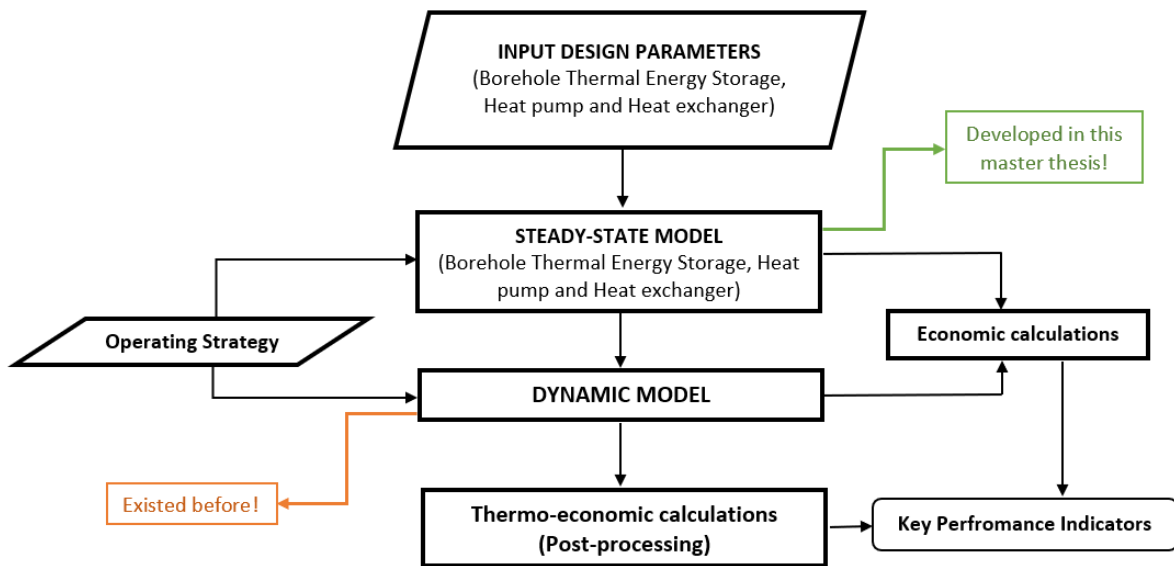
Figure 3. DYESOPT structure

1.1 Aims & Objectives

The aim of this master thesis is to generalize an existing BTES-GSHP sizing model in order to evaluate the technical and economic feasibility of the system. The objectives of the master thesis are:

1. To analyze the existing dynamic model on BTES-GSHP and develop the generalized steady state model.
2. To validate the generalized steady state model against an already existing dynamic model.
3. To perform a sensitivity analysis and assess some technical & economic key performance indicators (KPI's).

1.2 Methodology

Firstly, a literature review was done to understand all the technologies involved in this master thesis study. The different types of underground thermal energy storage systems and existing BTES systems were studied. The previous work done so far on this topic was studied to get a better understanding of the research done till now. The existing dynamic model developed at KTH and Bengt Dahlgren AB along with the BTES system layout provided by Tekniska Verken AB was studied to understand the working of the entire system of BTES connected to the Gärstadverket CHP plant in Linköping. Then the Dynamic Energy Systems Optimizer tool also called as DYESOPT was studied to understand the link between the steady-state model and dynamic model.

Further the working of the BTES was understood and the heat transfer equations required for the generic sizing of BTES were noted. The heat pump model developed in the previous work was studied as well. Then the generic steady-state sizing model was developed for the three main components of the system; heat exchanger, heat pump and the borehole thermal energy storage. The newly developed steady-state model was validated by comparing the key results from the steady-state sizing and the dynamic model by running several simulations.

In the end, a techno-economic analysis was done to find out the best configuration of the system by comparing some of the key performance indicators (KPI's). As a part of the techno-economic analysis, a sensitivity analysis was performed by varying some of the input parameters and the results of interest were obtained and discussed.

2 Thermal Energy Storage systems

Thermal Energy Storage (TES) systems are gaining popularity nowadays and they are used for efficient thermal energy management given that there is an imbalance between the energy generation and demand due to seasonal variations (Rapantova N., 2016). With the help of TES systems, the energy demand can be balanced between the winter and summer seasons. There are several thermal energy sources, such as combined heat and power plant (CHP) that generates surplus heat during the summer, industrial waste heat and the heat generated from the renewable energy sources that exceed the grid demand (Rapantova N., 2016). Even in few cases the solar thermal systems are used to store heat in the TES systems during the summer and the heat is then distributed to the houses during winter through a low temperature space heating system (Malmberg M, 2018).

The earth is increasingly being used for storing thermal energy and it is termed as underground thermal energy storage (UTES) (Sannera B., 2003). There are significant advantages of the UTES systems such as enormous amount of energy can be stored and extracted later for heating or cooling purposes, profitable in the long term compared to the other conventional storage systems (K.S., 2013). The UTES systems can be classified into two categories such as 'closed' systems and 'open' systems. The systems where a fluid, mostly water, is circulated through heat exchangers in the ground are called 'closed' systems (K.S., 2013). The systems where the groundwater is pumped out and then injected into the ground through underground caverns or wells are called 'open' system. Since the 1970's, the different types of UTES systems developed are aquifer thermal energy storage (ATES), borehole thermal energy storage (BTES), cavern thermal energy storage (CTES), pit storage and water tank (Novo A. V., 2010).

Aquifer thermal energy storage (ATES) is an example of 'open' system and uses natural water in a saturated and permeable underground layer called an aquifer as the storage medium. The groundwater is extracted from the aquifer and its temperature is raised by transferring thermal energy to it and is reinjected in a well located nearby (Novo A. V., 2010). ATES is the least expensive UTES system and its application has recently become popular for heating and cooling of buildings (Rapantova N., 2016).

Borehole thermal energy storage is a 'closed' system that consists of vertical heat exchangers placed in boreholes which are responsible for the heat transfer between the ground and the heat carrier fluid. This type of system can be drilled into rocks, clays or soils and is flexible with any type of ground conditions (Malmberg M, 2018). The depth of the boreholes can vary between 20-300 m. The heat source for the BTES could be either from solar thermal, combined heat and power (CHP) or heat from industrial waste.

Cavern thermal energy storage is another example of the 'open' system and uses water in large underground caverns to store heat. Caverns can be either man-made or natural. Even though this technology is feasible, its application is limited as it requires extremely specific site conditions (K.S., 2013). Pit storage and water tank is also called as man-made aquifer are artificial tanks built under the ground. They are insulated both on the top and along the walls up to certain depth (Novo A. V., 2010). In this master thesis, only the borehole thermal energy storage (BTES) system will be discussed further.

2.1 BTES system description

The BTES, also called as the duct ground heat storage (DST) system is defined as a system where heat is directly stored in the ground. A duct or channel is used to transfer heat between the ground and the heat carrier fluid. The heat transfer in the ground is mainly done by heat conduction. The borehole thermal energy storage system consists of two basic components: the geological medium that provides the storage capacity and the ground heat exchanger (Hellström, 1991).

2.1.1 Storage Volume

The storage volume can be defined as the ground region perforated by the ducts. The geometry of the storage volume is usually cylindrical or cubical with vertical symmetry axis (Reuss, 2015). The cylindrical geometry is better as there are reduced heat losses at the edges and the surfaces of the storage volume

(Mangold, 2015). The heat transfer mechanism between the heat carrier fluid and the water is mainly through heat conduction. The heat transfer depends on the ground thermal properties such as the thermal conductivity and the heat capacity of the ground.

The fraction of heat losses to the surrounding ground decreases as the size of the storage volume increases. A compact heat store is usually preferred as it would have less heat losses due to the minimum exposure to the surrounding ground. The spacing between the boreholes is usually 4-6 m (Barth J., 2012). The ground surface above the storage region can also be insulated to avoid heat losses (Hellström, 1991).

2.1.2 Ground heat exchangers

The purpose of the ground heat exchanger is to transfer the heat energy between the heat carrier fluid and the surrounding ground. The ground heat exchanger, also called as borehole heat exchanger (BHE) are of two types: U-pipe and coaxial. The U-pipe BHE is mostly used in the single BHE installations (Acuña, 2013). The U-pipe BHE consists of two tubes inserted in the borehole and the two tubes are connected at the bottom end making it a closed system. There can be either single, double or triple U-pipes placed inside the borehole. For triple U-pipes, the heat exchange is better due to reduced thermal resistance and head loss in the pipes. Figure 4 shows an example of a U-pipe borehole heat exchanger.
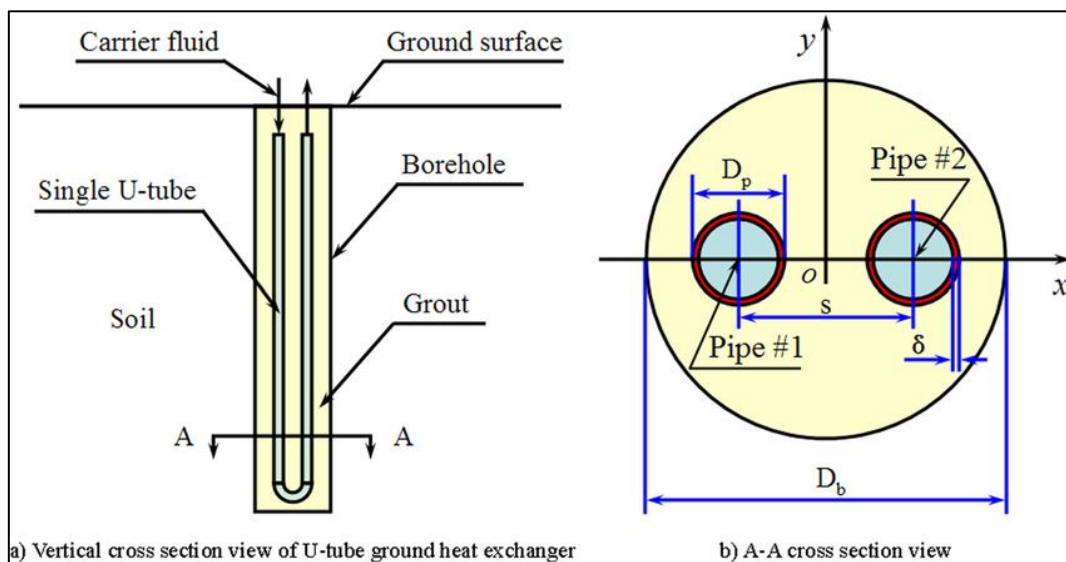
Figure 4. Schematic diagram of a U-pipe borehole heat exchanger (Liao Q., 2012)

On the other hand, the co-axial BHE has one or more flow channels in the upward and the downward directions. It can also be termed as borehole with concentric inner tube where a single plastic tube is placed in the center of the borehole. The hot fluid flows in downward direction in the inner tube and in upward direction between the tube and borehole wall. In this system, the fluid comes in direct contact with the borehole wall and is called an open system. Being an open system, the co-axial BHE has better heat exchange than the U-pipe BHE (Hellström, 1991). Figure 5 shows the schematic diagram of a co-axial borehole heat exchanger. The diagram on the left side shows the flow direction while charging the ground and the diagram on the right shows the flow direction while discharging the ground.
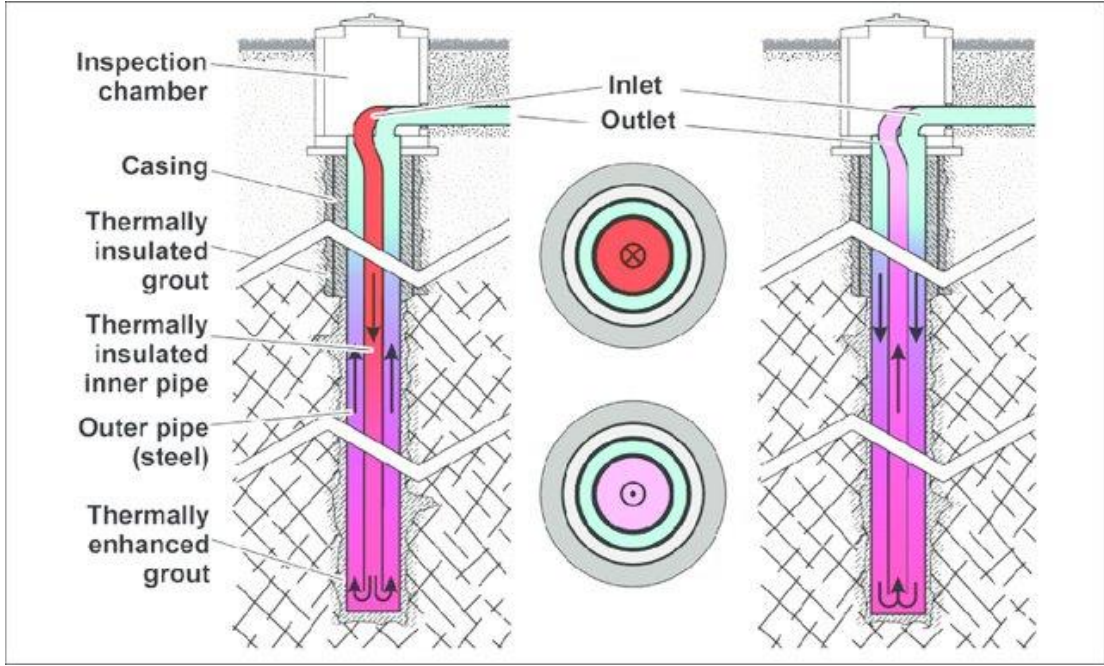
Figure 5. Schematic diagram of a co-axial borehole heat exchanger (Homuth S., 2016)

3   Theoretical Background of the DST model

In this chapter, the theoretical background in modelling a duct ground heat storage (DST) system is explained along with an example. The duct ground heat storage system is defined as a system where heat is directly stored in the ground (Hellström, 1989). The heat transfer to the ground occurs by the circulation of heat carrier fluid in the ducts or channels. The heat transfer between the ducts and the surrounding ground takes place in the form of heat conduction.

The duct or channel can also be called as a ground heat exchanger. These ground heat exchangers have a specific arrangement which depends on the geological medium. There are some fundamental differences in the design of the ground heat exchanger for rock when compared to softer medium like clay, sandy soil and peat (Hellström, 1989).

For solid rock, the duct system typically consists of many boreholes uniformly placed in the storage region. In Sweden, most of the BTES systems use the vertical boreholes with a diameter of 4-6" and a spacing of about 4 meters between the two adjacent boreholes. A customized arrangement is required for the sites where the ground surface area available is limited. The boreholes form a diverging bundle towards the bottom end thus increasing the duct spacing with the depth (Hellström, 1989).

For clay, sandy soil, or peat deposits, the duct system can be obtained by inserting vertical U-shaped loops of thin plastic tubes. For the existing systems, the spacing between each borehole is shorter and is typically about 2 meters due to the lower thermal conductivity of clay when compared to rock. Another alternative could be using two U-shaped loops inserted down together. For shallow deposits, horizontal pipes could be used as a ground heat exchanger (Hellström, 1989).

3.1 Description of Thermal Processes

The thermal process in the storage region with the duct system is complicated. The thermal process in a ground storage region can be divided into a local process around each borehole and a macroscale global process in the storage volume and the surrounding ground (Hellström, 1991). There is a large-scale heat flow between the different parts of the store and the surrounding ground. The heat exchange process in the ground heat exchangers occurs in the form of convective heat transfer and further the heat is distributed in the surrounding ground in the form of conductive heat transfer. The global heat flow process in the ground is thus coupled to the local thermal process around each ground heat exchanger. The character of the local thermal process is essentially the same throughout the storage region (Hellström, 1989).

3.1.1 Fundamental Thermal Processes

The thermal processes require an accurate description that govern the thermal behavior of the storage region. The thermal interaction between the duct system, the heat capacity of the surrounding ground and the heat transfer properties within the duct system must be considered. The large-scale heat flow will also have some heat losses from the storage region in all the three dimensions which needs to be accounted for. The ground consists of different geological material in the horizontal strata and the thermal properties may vary accordingly. To reduce the heat losses an insulating material is placed on the ground surface above the store. All these heterogeneous factors of the thermal properties will influence the global thermal process.

3.1.2 Secondary Thermal Processes

There are some other processes that can affect the thermal behavior of the ground heat store and are of secondary importance as their influence is usually small. The regional ground water flow may increase the heat losses from the heat store if it is in a permeable ground layer. The ground water flow takes place in the bedrock through fissures and fractured zones in the rock. The magnitude of the flow depends on various factors such as the number of fissures, the width of the fissures, extension of the fractured zones and the local hydraulic gradients. These factors are usually very site-specific. A study by van Meurs (Meurs, 1985)

suggests that a protecting hydraulic screen is required for the heat store if the ground water flow exceeds 50 mm/day.

As the heating of water-saturated ground material will take place, natural convection will be induced due to the varying density of water as the temperature changes. This will lead to buoyancy flow which will cause the warmer water to flow upwards. The magnitude of the buoyancy flow depends on many factors such as the temperature of the storage region and the surrounding ground, the depth of the store and the permeability of the ground in the horizontal and vertical direction. Normally, the thermal performance of the ground heat store will be affected if the permeability of the ground exceeds 10^{-12} m² (Meurs, 1985).

A homogeneous infiltration by the cold rainwater at the ground surface is not important but any change of the water content in the unsaturated soil layers will affect the thermal properties of the ground. The small-scale inhomogeneities will influence the local heat transfer process around the duct if they occur close to the duct otherwise, they are insignificant.

3.1.3 Local Thermal Processes

The local thermal process around each borehole is important. The basic problem involved in the analysis of the borehole thermal energy storage system is the interaction between the local thermal process around a borehole and the global temperature process throughout the storage volume and the surrounding ground. The local thermal process needs to be described precisely in order to obtain the right amount of heat injected and extracted from the bore field (Hellström, 1989). The heat transfer from the boreholes to the ground is dependent on the inlet fluid temperature, the heat transfer properties of the ground and the temperature of the surrounding ground near the borehole. The heat flow and the temperatures will vary along the ducts. The value of global temperature in the local region is necessary for the local problem (Hellström, 1989).

3.2 Different types of problems

The entire process of simulating a DST model involves superposition of three parts: global problem, local problem and steady-flux problem.

3.2.1 Global problem

The Global problem is a heat conduction problem which accounts for the heat transfer on a large scale. It accounts for the interaction between the different parts of storage volume, between the entire storage volume and the surrounding ground, the influence of external conditions at the ground surface, etc. The simulated volume by the DST model includes the storage volume and a sufficient part of the surrounding ground to account for the heat losses from the storage to the surrounding ground. The storage volume, arrangement of ducts, thermal properties and temperature field are assumed to exhibit cylindrical symmetry with respect to the central axis of the storage volume (Hellström, 1989).

3.2.2 Local problem

The Local problem accounts for the thermal process using a one-dimensional radial mesh around the individual ducts due to variations in every time-step of the simulation. The local problem is assumed to be the identical around each pipe in each subregion. The entire storage region V is divided into N subregions (Hellström, 1989).

3.2.3 Steady-Flux problem

The steady-flux solution gives the temperature field around a pipe for a constant heat injection/extraction rate. It is used for pulses that vary slowly in time. The net energy contribution to each subregion due to the steady-flux part is zero as it only deals with the adjustment of Global mesh temperature by redistribution of heat within the storage for every time-step. The adjustment of temperature is usually of the order 10^{-1} ºC. The heat source term for the steady-flux part depends only on the temperature of an individual cell (Hellström, 1991).

3.3 Superposition of temperatures

In the DST model, the temperature at any given point in the storage volume is a superposition of three parts: a local radial solution around the borehole, a steady-flux solution and a global solution (Hellström, 1991). The entire storage volume is divided into a certain number of subregions. Each subregion has its own local solution. The flow path of the heat carrier fluid is also defined by the subregions. The short-time variations of the heat injection or extraction through the borehole ducts are simulated as local solutions. The local solution is assumed to be the same for all the borehole ducts in that subregion. The heat is slowly redistributed in the storage region during the heat injection or extraction process and it is accounted by the steady-flux solution. The interaction between the storage region and the surrounding ground is accounted by the global solution (Hellström, 1989).

3.4 Working of DST model – an example of 19 boreholes

In this section, the working of DST model will be explained with the help of an example. The DST model calculates the amount of heat transferred between the circulating fluid in the borehole and the ground. The model assumes the boreholes to be placed uniformly. The heat transfer problem is solved by dividing the entire borehole storage volume into several meshes, thus splitting the problem into simpler problems and making it easier to solve the problem. The various solutions are superimposed for successive time-steps using the linearity of heat conduction equation to get the final solution. The DST model superimposes the two numerical solutions of the Local problem and the Global problem. The steady flux solution redistributes the energy into the nearby storage volume (Chapuis S., 2009).

Mesh networks:

As shown in the Figure 6, the DST model uses three meshes defined as: Subregion, Local and Global. The example shows bore field of 19 boreholes. The boreholes are divided into 3 radial regions and 5 vertical regions. The BTES volume, V_{BTES} is considered to have a cylindrical shape and its radius, R_{BTES} is given by the following equation:

$$V_{BTES} = \pi . R_{BTES}^2 . H \tag{1}$$

where H is the borehole depth. The BTES volume is divided into subregions, using a 2D (r, z) axisymmetric mesh network with respect to the central axis of BTES. The total number of subregions equals the number of vertical regions times the number of radial regions. In this case, the total number of subregions are 15. The height of the vertical regions is assigned by an algorithm imposing shorter heights at the top and bottom ends of the BTES where there are steep gradients. The radial regions can have more than one subregion. As shown in the Figure 6, the subregions #1 to #5 are closest to the center axis of BTES. The length of the radial region is calculated depending on the number of boreholes assigned by the code to that region. The boreholes connected in series are placed in consecutive radial regions from the BTES center towards the BTES periphery. If the number of radial regions defined are less than the number of boreholes connected in series, then the code will distribute the boreholes will be distributed proportionally in every radial region. For example, if the user specified a bore field with 25 boreholes with 5 boreholes connected in series and only 3 radial regions (Chapuis S., 2009). The code will distribute the boreholes in the following way:

- $\frac{2}{5} \times 25$ boreholes in the radial region 1;
- $\frac{2}{5} \times 25$ boreholes in the radial region 2;
- $\frac{1}{5} \times 25$ boreholes in the radial region 3.

The last radial region will have half the surface area of the boreholes as compared to the other two radial regions.
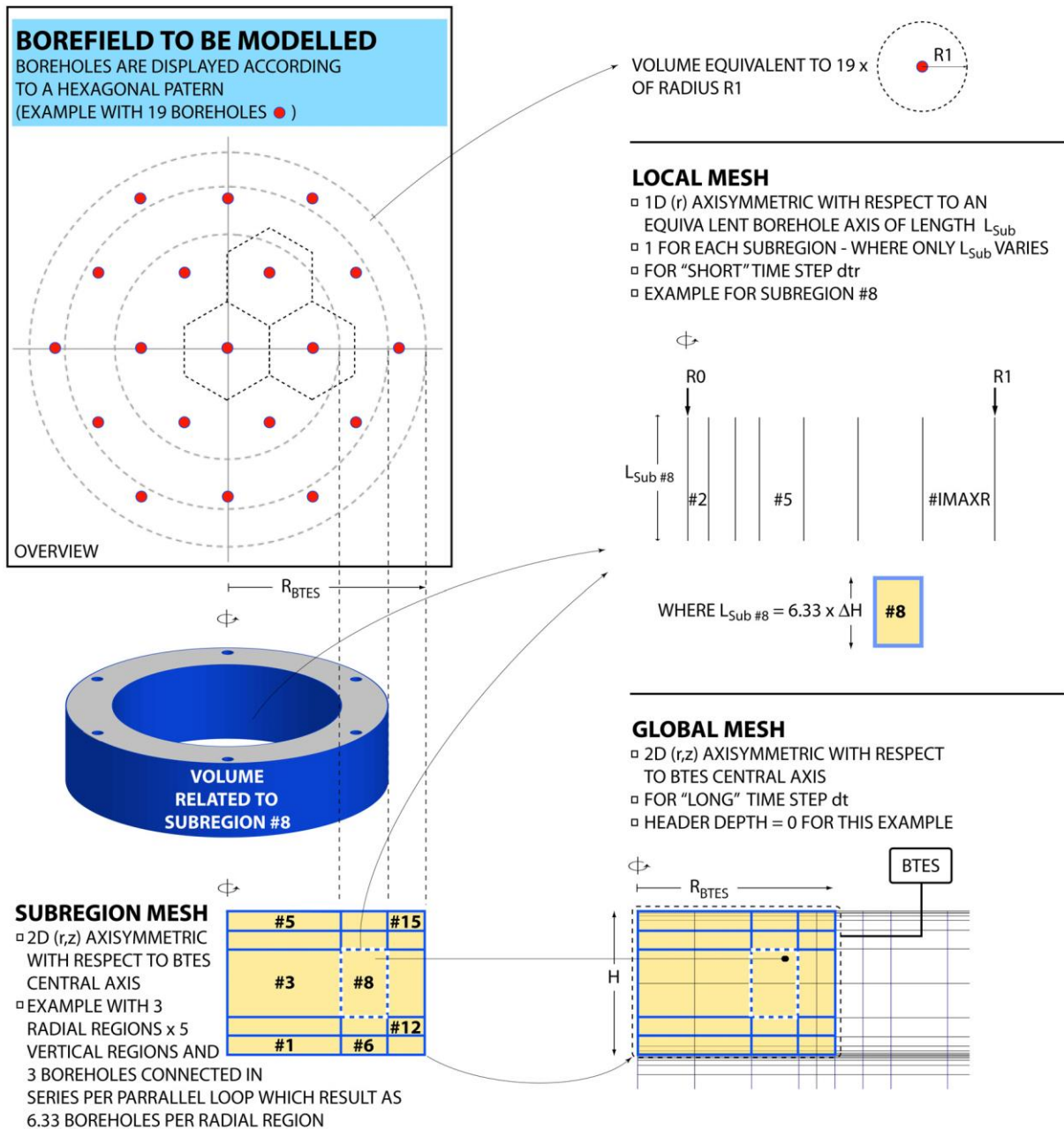
Figure 6. Mesh networks used in the DST model (not to scale) (Chapuis S., 2009)

The borehole length, L_{sub}, is assigned to each subregion. It is defined as the total number of boreholes in the subregion times the height of the subregion. As shown in the Figure 6, the 15 subregions are placed successively from 1 to 15 starting from the bottom left corner. The fluid circulates in the BTES either from the center starting from subregion #1 to the periphery of the BTES or from subregion #15 to the subregion #1 to the center as specified by the user.

Further a Global mesh network is developed using the subregion mesh network as shown in the bottom right of Figure 6. The Global mesh accounts for the heat transfer inside the BTES as well as the BTES and its surroundings. This mesh consists of radial and vertical meshes which are not the same as defined earlier for the subregion mesh network and are generated by an algorithm using the number of simulation years and the ground thermal properties specified by the user. The Global mesh corresponds to the subregion limits, but it can have finer mesh than the subregion mesh.

Every subregion has its own Local mesh network as shown in the middle right of Figure 6. This Local mesh network accounts for heat transfer from fluid circulating in the borehole ducts to the surrounding ground and is called as Local problem. Every borehole duct in the radial region has its own Local mesh and its covers the ground region from the borehole radius $R0$ up to the radius $R1$. The radius $R1$ is calculated using the equation below:

$$V_{BTES} = \pi.R1^2.H.NBH_{tot} \tag{2}$$

where NBH_{tot} is the total number of boreholes. All the Local meshes have the same dimensions except the length of the borehole as the height of each subregion varies.

3.5 Heat transfer for the heat carrier fluid

Due to the temperature difference between the heat carrier fluid and the storage region, there will be heat transfer either from the fluid to the ground or vice-versa. The temperature of the fluid will vary along the flow path through the storage volume. The outlet temperature from the storage volume is expressed as:

$$T_{fout} = \beta.T_{fin} + (1 - \beta).T_a \tag{3}$$

T_{fin} is the fluid inlet temperature, T_a is the surrounding ground temperature and β is the damping factor which is defined as:

$$\beta = e^{-\frac{\alpha_v.V}{C_f.Q_f}} = e^{-\frac{\alpha_p.L_p}{C_f.Q_f}} \tag{4}$$

V is the storage volume, L_p is the total pipe length in the storage volume, Q_f is the total fluid flow rate, C_f is the volumetric heat capacity of the fluid, α_p is the heat transfer coefficient is between the fluid and the point in the surrounding ground with temperature T_a. When the fluid flow rate tends to reach zero the outlet temperature gets closer to the surrounding ground temperature T_a. On the other hand, the outlet temperature tends to get closer to the inlet temperature when the fluid flow rate goes to infinity. The total heat injected $'Q'$ to the storage volume is given by the equation:

$$Q = C_f.Q_f.(T_{fin} - T_{fout}) \tag{5}$$

Using the equation (3) of the outlet temperature T_{fout} and normalizing to unit volume, the total heat injected given by equation (5) changes to:

$$q = \frac{C_f.Q_f}{V}.(1 - \beta).(T_{fin} - T_{fout}) \tag{6}$$

The above equations are used to find out the temperature variations along the fluid flow path both in the local problem and steady-flux problem.

4 Model - Sizing of the components

In this chapter, the entire system and the generic sizing model of the heat exchanger, heat pump and BTES developed is discussed in detail.

4.1 System Description

Figure 7 shows the system layout for the specific case of Tekniska Verken AB. The valves for charging the BTES are placed after the steam condensers; KV50, KV61 and KV62. The charging temperature that goes to the BTES is constant at 95^oC during the summer. The discharge valves are placed between the flue gas condensers and the steam condensers. The flue gas condensers in the district heating network preheats the return water to an approximate temperature of 55.5^oC. During the discharge period in the winter, this temperature is the input temperature for the condenser section of the heat pump. The previous model was designed for a maximum of 50 MW heating output from the heat pump as the district heating network at Tekniska Verken can sustain a maximum of 50 MW power supply (M., 2017).
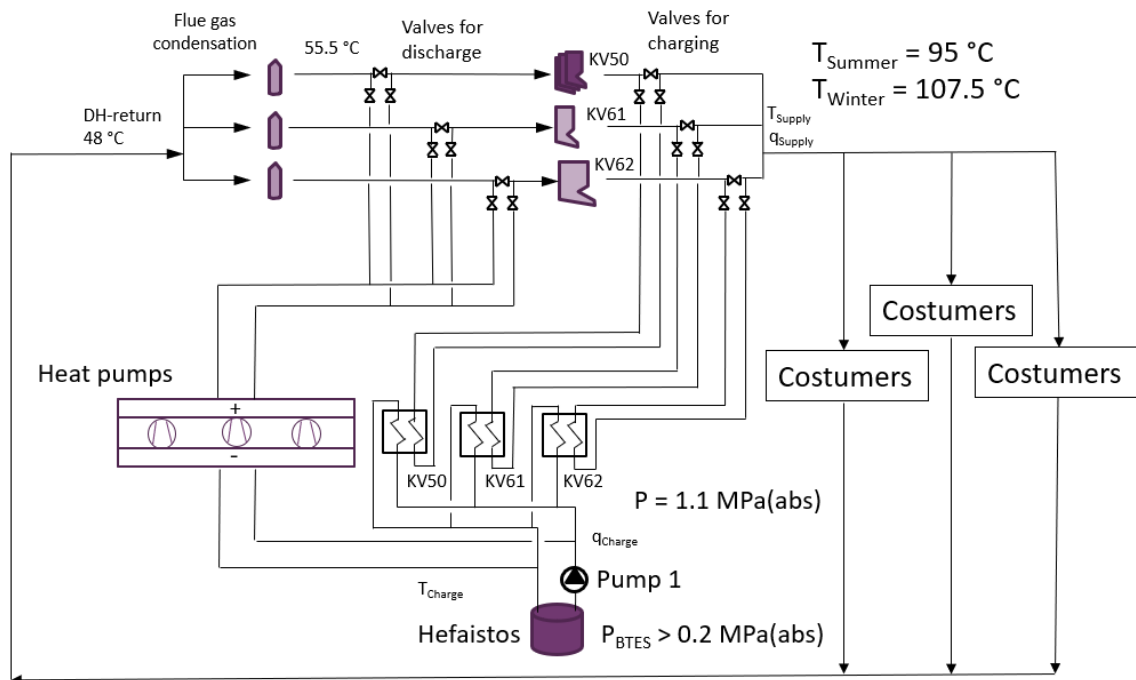
Figure 7. Flowchart for Gärstadverket including the BTES and heat pumps (Provided by Tekniska Verken AB) (M., 2017)

Based on flowchart provided by Tekniska Verken AB, a schematic diagram of the entire system was developed and is shown in Figure 8. There are total 15 temperature points defined on the diagram and each point has been described in the Table 1 below. There are two loops L1 and L2 that defines that fluid flow process in the BTES during the charging and discharging phase respectively.

Figure 8. Flow chart of the entire system with temperatures defined at different points in the system

Table 1. Description of the different temperature points in the system shown in Figure 8

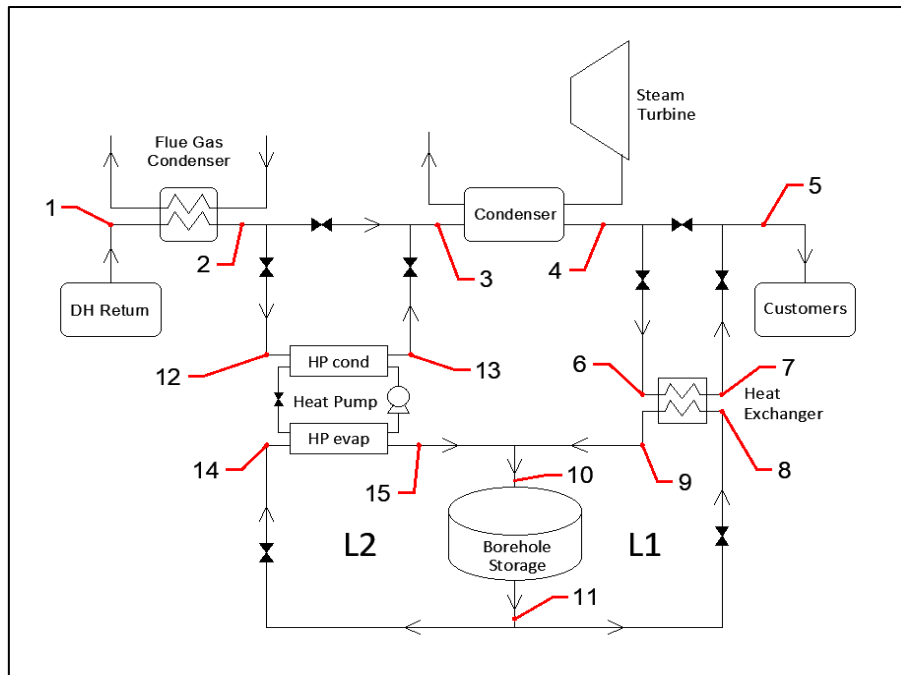| Points	Description
1	The temperature of fluid from the District heating (DH) network.
2	The temperature of fluid after passing through the flue gas condenser.
3	The temperature of fluid before entering the condenser of the Rankine cycle of the Power plant.
4	The temperature of fluid leaving the condenser of the Rankine cycle of the Power plant.
5	The temperature of the fluid that is being supplied to the customers.
6	The hot side inlet fluid temperature of the heat exchanger
7	The hot side outlet fluid temperature of the heat exchanger
8	The cold side inlet fluid temperature of the heat exchanger
9	The cold side outlet fluid temperature of the heat exchanger
10	The inlet temperature to the Borehole thermal energy storage
11	The outlet temperature from the Borehole thermal energy storage
12	The temperature of fluid at the inlet of heat pump condenser
13	The temperature of fluid at the inlet of heat pump condenser
14	The temperature of fluid at the inlet of heat pump evaporator
15	The temperature of fluid at the inlet of heat pump evaporator

4.2 Process Flowchart

This section includes the description of modelling process of the HEX-HP-BTES steady-state model. The steady-state model was developed in the MATLAB tool. The entire modelling process is shown below in the flowchart (Figure 9). Initially, the model is given some input parameters as per the requirements. For few parameters such as power available in the DH network and inlet temperatures the input can be given in two ways: a data file provided from the power plant or a fixed input value. The input parameters include the length of simulation (years), mass flow rates, temperatures, initial guess of boreholes etc. Based on the input parameters the three components; heat exchanger heat pump and the borehole thermal energy storage (BTES) are designed.
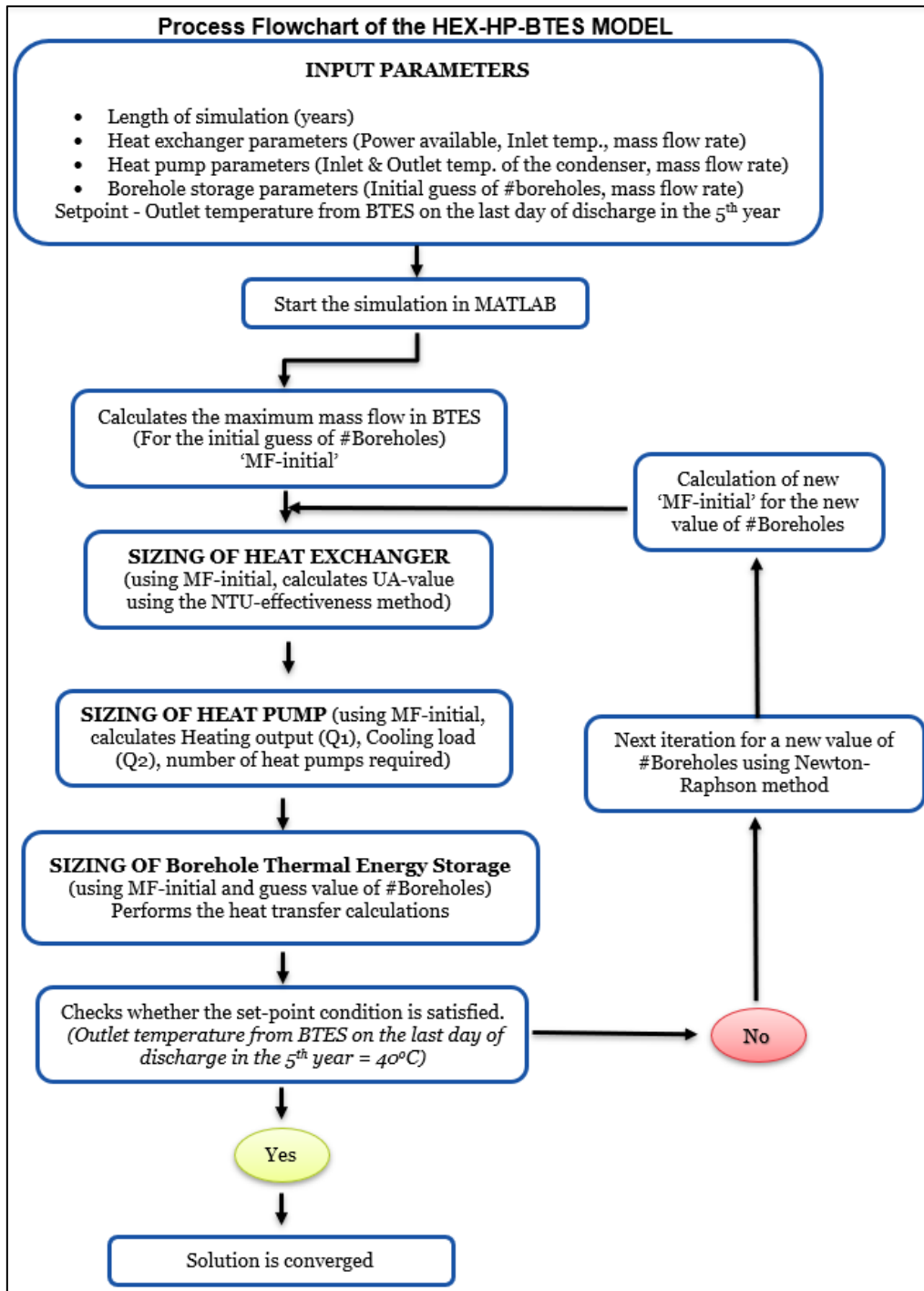

Figure 9. Process Flowchart of the HEX-HP-BTES Model

After setting the input parameters, the simulation in MATLAB can be started. As the simulation begins, the model will first calculate the total mass flow rate that can be allowed in the BTES loop for the initial guess of the number of boreholes. In the next step, it will size the heat exchanger and calculate the required UA value for the heat exchanger.

It will further size the heat pump. Based on the input parameters, the model will calculate the required heating output from the heat pump, the cooling load of the heat pump and the number of heat pumps required. In the next step, the model will perform heat transfer calculations using a simplified DST approach for the BTES with the initial guess of the boreholes for a period of 5 years. The BTES is designed in such a way that it must satisfy the cooling load of the heat pump for the entire period of the simulation and another condition is that the outlet temperature of the BTES on the last day of the discharge should be 40^oC which is the set point condition.

If the required set point condition is not satisfied, then the model will do another iteration for a new guess of boreholes. For the new guess value, the new mass flow rate in the BTES loop will be calculated. Using this updated mass flow rate and new guess of boreholes, the model will again size the heat exchanger, heat pump and the borehole thermal energy storage and check if the required condition is satisfied or not. The model will keep doing iterations for different values of boreholes which are determined using the Newton-Raphson's method until it finds the convergence point where the condition is satisfied.

After finding the size of BTES, the model will create an input file and write all the calculated values for the different components in the steady-state model. This input file then sends the input values to the TRNSYS model and runs a dynamic simulation. After the end of the dynamic simulation, the model will extract the output data and do the post-processing calculations in MATLAB in the last step.

4.3 Heat exchanger (HEX)

The heat exchanger is used during the charging period of the BTES. It is used to transfer the heat energy available in the district heating network to the BTES. In the case of Gärstadverket, as there are three steam condensers, KV50, KV61 and KV62, it was assumed that each steam condenser is of equal size and so each of them share 1/3 of the total district heating mass flow rate respectively. In the previous dynamic model, there were two counter flow heat exchanger components of Type 5b. The first heat exchanger component represented the steam condenser KV50 while the second one represented the steam condensers KV61 and KV62. The district heating flow to the two components was controlled using two flow diverters that allowed 1/3 flow to pass through KV50 and 2/3 flow to pass through KV61-62.

In the new dynamic model, for simplification purpose only one counter flow heat exchanger component is used, and it handles the entire district heating mass flow rate. The model in steady-state sizes the heat exchanger using the effectiveness-NTU method (Havtun H., 2016). The equations used for the sizing of the heat exchanger are mentioned below. First, the heat capacity rates are calculated for the hot side and cold side of the heat exchanger.

$$C_h = \dot{m}_{DH,charge} \cdot c_{p,h} \tag{7}$$

$$C_c = \dot{m}_{BTES\_loop} \cdot c_{p,c} \tag{8}$$

Based on the specific heat capacities and the input mass flow rates, the minimum and maximum heat capacity rates on the either side of the heat exchanger are calculated.

$$C_{MIN} = \min(C_h, C_c) \tag{9}$$

$$C_{MAX} = \max(C_h, C_c) \tag{10}$$

The ratio of the heat capacities is given by:

$$RAT = C_{MIN}/C_{MAX} \tag{11}$$

The effectiveness of the heat exchanger is given by the equation 12 (D., 2013), as a function of the minimum approach temperature ΔT_{min} and the total temperature difference across the heat exchanger ΔT_{tot} from the inlet of the hot stream to the inlet of the cold stream.

$$\varepsilon = 1 - \frac{\Delta T_{min}}{\Delta T_{tot}} \tag{12}$$

The number of transfer units (NTU) is calculated using the following mathematical equation:

$$NTU = \left(\log\left(\frac{\varepsilon - 1.0}{\varepsilon * RAT - 1.0}\right) \right) * \left(\frac{1}{RAT - 1.0}\right) \tag{13}$$

The overall heat transfer coefficient, UA-value is finally calculated using the following equation:

$$UA = NTU * C_{MIN} \tag{14}$$

The calculated parameters, UA-value of the heat exchanger, the specific heat capacities on the hot side inlet and cold side inlet are further sent to the dynamic model as inputs.

4.4 Heat pump (HP)

The heat pump is used during the discharging period of the BTES. A heat pump consists of four components: condenser, compressor, evaporator and expansion valve. As shown in the Figure 10, the heat energy extracted from the boreholes through a circulating loop is passed through the evaporator section to satisfy the cooling load of the heat pump. The compressor then increases the pressure level of the refrigerant which also increases the temperature. Further in the condenser section, the heat is ejected and transferred to the water flowing in the district heating network. After the condenser section, the cold fluid is passed through the expansion valve where the temperature of the fluid is decreased further before entering back into the evaporator and the process continues in a cycle.
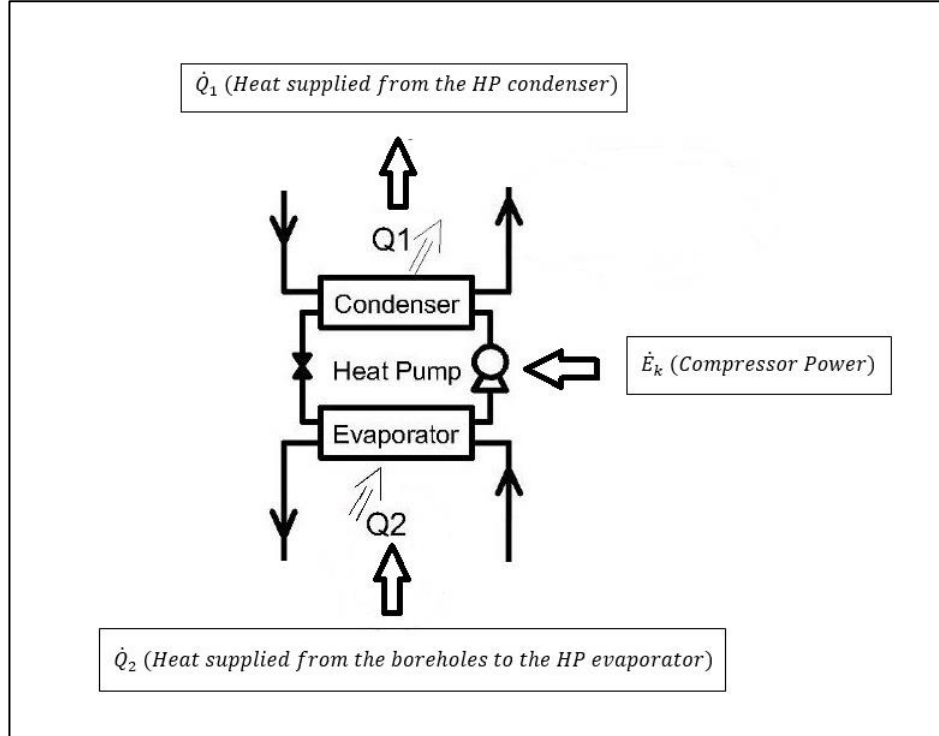

Figure 10. Function of a ground source heat pump (M., 2017)

In the previous studies, the heat pump model was created in the form of polynomial based on the calculated heat pump performance data provided by the manufacturer called Star Renewable Energy. The general polynomial used for the heat pump model is given by equation 15 (M., 2017), where $\dot{m}_{BH}$ is the volumetric

mass flow rate in the borehole loop through the HP's evaporator, $\dot{m}_{DH}$ is the volumetric mass flow rate in the district heating loop through the HP's condenser and T_{BH} is the temperature in Kelvin, of the water flowing out the boreholes and entering the evaporator section of the heat pump.

$$\dot{Q}_1, \dot{Q}_2, \dot{E}_k = C + a_1 * \dot{m}_{BH} + a_2 * \dot{m}_{BH}{}^2 + b_1 * \dot{m}_{DH} + b_2 * \dot{m}_{DH}{}^2 + c_1 * T_{BH} + c_2 * T_{BH}{}^2 \quad (15)$$

In this master thesis, the same heat pump model is used as a reference for sizing the heat pump in the steady state. The constants C, a_1, a_2, b_1, b_2, c_1 and c_2 are calculated in using least root mean square difference method. According to this model, one heat pump has a maximum heating capacity of 10 MW and if more heating output is required then more heat pumps are connected in series thus adding up the heating output.

While sizing the heat pump, the heating output can be varied either by changing the mass flow rate or the temperature at the outlet of the condenser which is connected to the district heating network. The temperature entering the inlet of the condenser is kept constant at 55^oC as it is a standard value for DH return temperature in Sweden. Based on the input mass flow rates and temperatures, the total heating output $\dot{Q}_{1,total}$ is calculated using the equation 16.

$$\dot{Q}_{1,total} = \dot{m}_{DH} * c_p * (T_{cond,in} - T_{cond,out}) \quad (16)$$

There are three possible cases for sizing the heat pump:

1. Changing the mass flow rate in the district heating loop
2. Changing the condenser outlet temperature
3. Changing both, mass flow rate and condenser outlet temperature

4.4.1 Changing the mass flow rate

As the heat pump model is developed based on the manufacturer data which had an average mass flow rate of 900 kg/s in the condenser section. In this case, 900 kg/s is assumed to be the reference mass flow rate, the return temperature of water in the district heating network that enters the inlet of HP condenser is assumed to be constant at 55^oC and the HP condenser outlet temperature is kept fixed at 68^oC for the reference case which gives heating output of around 50 MW. For these inputs, a maximum of 5 heat pumps can be connected in series which gives a heating output of up to 50 MW. For a mass flow rate higher than 900 kg/s, if the heating output requirement exceeds 50 MW then the additional heat pumps would be connected in parallel. A scaling factor of 'X' is introduced and defined as ratio of the input mass flow rate to the ideal mass flow rate in the district heating loop.

$$X = \frac{\dot{m}_{DH}}{\dot{m}_{DH,ideal}} \quad (17)$$

This factor 'X' is used to either scale up or down the mass flow rate to always size 5 heat pumps connected in series. If the mass flow rate is lower than 900 kg/s, the scaling factor X<1, then the total heating output would be less than the maximum capacity of 50 MW for 5 heat pumps and so the heat pumps are assumed to be running at partial load satisfying the required heating demand.

If X>1, then the heat pumps are assumed to be connected in parallel combination with 5 heat pumps connected in series each and the mass flow rate is equally divided between the two segments. All of them are assumed to be operating at partial load as per the required heating demand. The number of heat pumps connected in series are always 5 as it is the maximum that can be connected for the ideal case mentioned earlier.

4.4.2 Changing the condenser outlet temperature

In the second case, the condenser outlet temperature is varied between the range of 60^oC to 80^oC, keeping the mass flow constant at the ideal value of 900 kg/s. For the ideal mass flow rate and a fixed condenser inlet temperature of 55^oC, the total heating output $\dot{Q}_1$ is calculated. The number of heat pumps connected

in series would vary in this case and assuming one heat pump having a capacity of 10 MW, the total number of heat pumps connected in series are calculated as below:

$$num_{HP} = (\dot{Q}_1/10) \tag{18}$$

Based on the manufacturer data provided, a maximum of 9 heat pumps could be connected in series.

4.4.3 Changing both, mass flow rate and condenser outlet temperature

In the third possible case, both the mass flow rate and the condenser outlet temperature are varied. For any given condenser outlet temperature, if X<1, then the heat pumps are connected in series operating at a partial load. If X>1, then the heat pumps are assumed to be connected in a series and parallel combination, distributing the mass flow rates as mentioned in the section 4.4.1.

Further, assuming the Coefficient of Performance (COP) of the heat pump equal to 5 and using the total heating demand $\dot{Q}_1$, the cooling load at the evaporator section $\dot{Q}_2$ is calculated using the formula:

$$\dot{Q}_2 = \dot{Q}_1 * (1 - \left(\frac{1}{COP}\right)) \tag{19}$$

The calculated cooling load $\dot{Q}_2$ is further used for sizing of the BTES. The scaling factor calculated for the mass flow rate and the number of heat pumps are sent to the dynamic model as inputs.

4.5 Borehole Thermal Energy Storage (BTES)

After the sizing of heat exchanger and heat pump, the Borehole Thermal Energy Storage is sized. The heat exchanger is connected to the BTES during the charging period. The power available on the hot side of the heat exchanger (DH loop) is transferred to the BTES through the fluid circulating in the BTES loop. On the other hand, the heat pump is connected to the BTES during the discharging period and the power is extracted from BTES to satisfy the cooling load of the heat pump at the evaporator section. While sizing the BTES only the number of boreholes is changed based on the cooling load of the heat pump, keeping the rest of the parameters of BTES constant that are mentioned in Table 2.

Table 2. Input parameters for sizing of BTES

Parameters	Value	Unit
Length of simulation	5	years
Borehole depth	300	m
Borehole radius ($r0$)	0.055	m
Borehole spacing	5	m
Outer radius of the local problem ($r1$)	0.525* (Borehole spacing)	m
Number of boreholes in series	3	--
Fluid to ground resistance (Rm_{pipe})	0.05	(m*K)/W
Ground storage thermal conductivity (k_g)	2.9	W/(m*K)
Ground storage heat capacity (C_{st})	2241	kJ/(m³*K)
Initial temperature of the storage volume	8	ºC
Number of vertical regions ($Nzloc$)	10	--
Number of radial regions ($Nrloc$)	3	--

Assumptions made for the steady-state sizing of BTES:

1. No heat losses to the surrounding ground were considered.
2. The mesh distribution was assumed to be uniform in the storage volume.
3. The interaction between adjacent local problems were not considered.
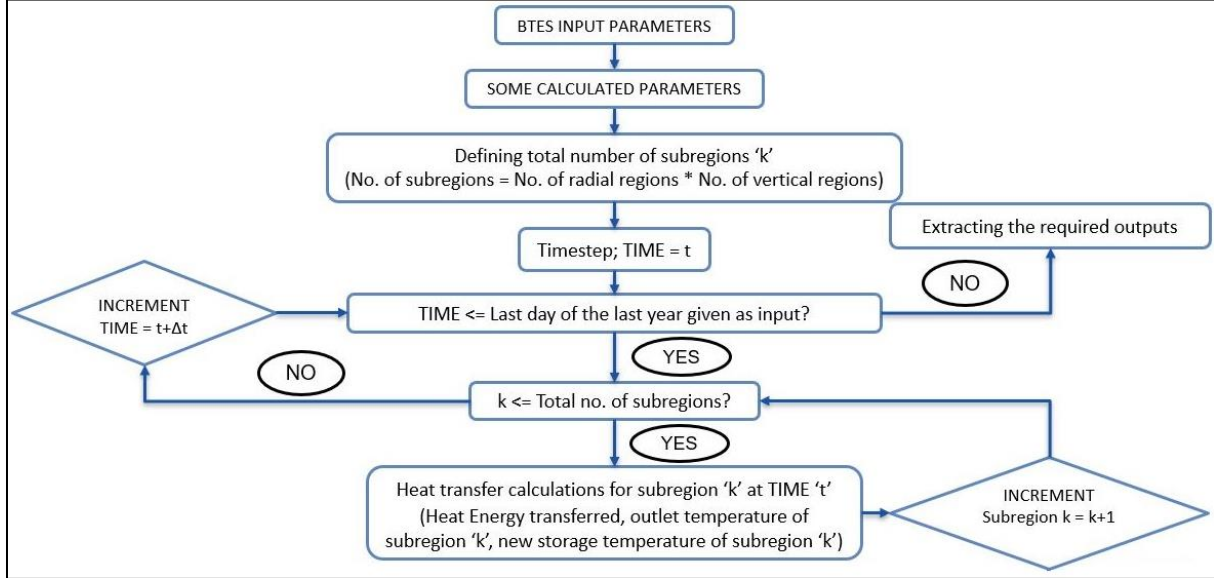4. The number of radial regions is equal to number of boreholes connected in series.

Figure 11. Working Process of simplified BTES model

Figure 11 shows the working process of the simplified BTES model. The steps involved in the sizing of the BTES system are described in detail below. The BTES input parameters that are defined at the very beginning of the sizing process are used to do some preliminary calculations before calculating the actual heat transfer process. The preliminary calculations include, overall heat conductance, depth of each subregion which was defined in chapter 3, the total duct length in the subregion, total heat capacity of each subregion and total mass flow rate.

The overall heat conductance 'α_k' for a local problem is calculated by:

$$\alpha_k = (2 * \pi)/\left(\left(\log\frac{\bar{r}/r0}{k_g}\right) + \left(2 * \pi * Rm_{pipe}\right)\right) \tag{20}$$

where $\bar{r} = (r1 - r0)/2$. The depth of each subregion '$Depth_{sub}$' is given by dividing the borehole depth to the total number of vertical regions. In the simplified BTES, it is assumed that the length of each subregion is identical.

$$Depth_{sub} = Borehole\ depth/Nzloc \tag{21}$$

The total duct length 'L_s' in each subregion is calculated by:

$$L_s = Depth_{sub} * \frac{num_{BH}}{num_{BH,(in\ series)}} \tag{22}$$

The total heat capacity '$Cinr$' accounted by the total number of ducts in a subregion is given by:

$$Cinr = C_{st} * \pi * (r1^2 - r0^2) * L_s \tag{23}$$

The total mass flow rate in the BTES loop is limited by a flow rate per borehole loop. The boreholes connected in series of 3 is considered as one borehole loop which gives the total mass flow rate by:

$$\dot{m}_{BH,total} = \dot{m}_{BH,loop} * \frac{num_{BH}}{num_{BH,(in\ series)}} \qquad (24)$$

The damping factor defined in chapter 3 is calculated using the equation:

$$\beta = e^{-\frac{\alpha_k . L_s}{C_f . Q_f}} \qquad (25)$$

Where, $Q_f = \dot{m}_{BH,total}$ is the total mass flow rate in the BTES, C_f is the heat capacity of the water, L_s is the total duct length in each subregion and α_k is the overall heat conductance for a local problem. All the above calculated values are further used as inputs for simulating the heat transfer process in the BTES for a period of 5 years with a timestep 't' of 1 day. The total number of subregions are given by multiplying the number of radial regions with the number of vertical regions. As shown in the figure 11, if the timestep 't' is less than the last day of the simulation period given as input, then it proceeds to the next step else it will end the timestep calculations and extract the required outputs. Within each timestep there are calculations done for every subregion. The model checks if the subregion 'k' is less than the total number of subregions calculated by equation 26 and if it less than the simulation proceeds to next step and calculates the heat transfer process for that subregion. After heat transfer calculations for all the subregions for a timestep 't' it will proceed to the next timestep of 't+Δt' and repeat all the heat transfer calculations for all the subregions. This process repeats until the last day of simulation period. Figure 12 shows an example of 3 boreholes connected in the series and the respective subregion mesh structure. As in this case we have 3 boreholes connected in series, the number of radial regions were also considered to be 3. Each radial region consists of one borehole that is connected in the series.

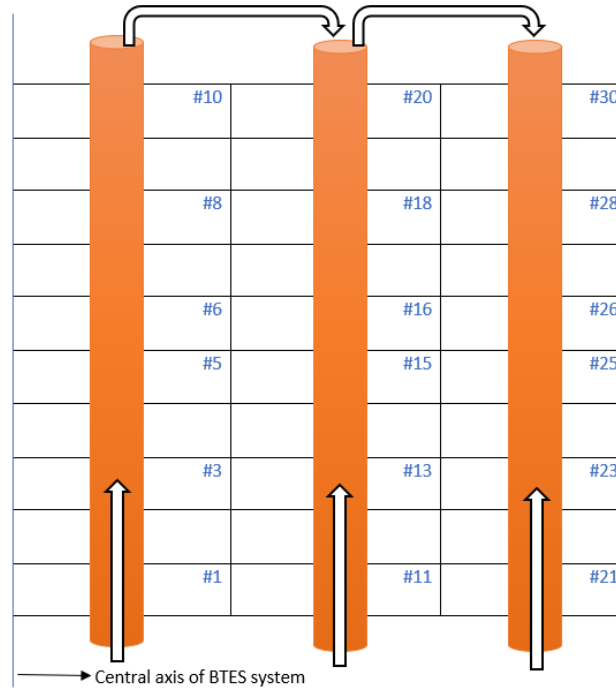$$Number\ of\ subregions = Nrloc * Nzloc \qquad (26)$$

Figure 12. Subregion mesh structure

The inlet temperature to the BTES system varies for every timestep 't'. While charging the heat carrier fluid flows through the heat exchanger and gains heat energy, thus increasing the temperature of the fluid before entering the BTES system. The temperature of fluid cannot exceed a certain maximum set temperature which is defined during the sizing of heat exchanger and is calculated using the inlet temperature of hot water entering the heat exchanger. While discharging, the BTES system is connected to the heat pump and

the heat carrier fluid flows through the heat pump evaporator satisfying the cooling load. For every subregion 'k' and timestep of 't', the heat transfer calculations are done using the following set of equations:

The heat energy transferred is calculated using the equation 27 given below where Q_f is the total mass flow rate, C_f is the specific heat capacity of the fluid and $T_{a_t}^{\ k}$ is the average storage temperature of subregion 'k' at a given timestep 't'.

$$Q_t^k = C_f . Q_f . (1 - \beta) . (T_{fin_t}^{\ \ k} - T_{a_t}^{\ k}) \tag{27}$$

The outlet temperature is calculated using the equation 28,

$$T_{fout_t}^{\ \ k} = \beta . T_{fin_t}^{\ \ k} + (1 - \beta) . T_{a_t}^{\ k} \tag{28}$$

The total energy in 'kWh' injected or extracted is given by the equation 29:

$$Energy_{t+1}^k = Energy_t^k + (Q_t^k * 3600 * 24) \tag{29}$$

The new value of storage temperature is calculated based on the superposition principle by the equation 30 given below:

$$T_{a_{t+1}}^{\ k} = T_{a_t}^{\ k} + ((Energy_{t+1}^k - Energy_t^k)/Cinr) \tag{30}$$

The outlet temperature of subregion 'k' becomes the inlet temperature for the next subregion 'k+1'.

$$T_{fin_t}^{\ \ k+1} = T_{fout_t}^{\ \ k} \tag{31}$$

The heat carrier fluid flows from the first subregion to the last subregion and exits the BTES system from the last subregion. In the above Figure 12, the fluid enters in subregion #1 and exits from subregion #30. The outlet temperature from the BTES system for every timestep 't' is given by:

$$T_{fout,BTES} = T_{fout_t}^{\ \ number\ of\ subregions} \tag{32}$$

The average storage temperature is given by adding the storage temperature for all the subregions and dividing it by the total number of subregions 'N_{sub}':

$$Avg\ storage\ temp = \frac{\sum_{k=1}^{N_{sub}} T_{a_t}^{\ k}}{N_{sub}} \tag{33}$$

The average power input/output in 'MW' is given by the total energy injected or extracted for every timestep. The total energy is injected or extracted is calculated by adding the energy transferred for all the subregions.

$$Avg. power = Total\ energy_{injected,extracted}/(3600 * 24 * 10^6) \tag{34}$$

For an initial guess value of the number of boreholes and above input parameters, using the simplified DST approach the model simulates the performance of the system over the period of 5 years under the defined conditions. The solver in MATLAB runs several iterations using the Newton-Raphson's method until the number of boreholes for which the set-point condition is satisfied. In this case, the set-point is to have the outlet temperature from the BTES on the last day of the 5th year equal to 40^oC. Once the BTES is sized, the storage volume V is calculated by the formula:

$$V = \pi * h * N * (0.525 * d)^2 \tag{35}$$

After sizing the BTES, all the input parameters along with the calculated parameters, the number of boreholes, maximum mass flow rate in BTES and the storage volume are sent to the dynamic model as inputs. The existing dynamic model in TRNSYS was modified so that the model can read the calculated input parameters that are sent after the sizing of the components.

5   Validation of the steady-state model of BTES (DST)

In this chapter, the procedure followed for validation of simplified DST (steady-state model of BTES) against the actual DST is discussed. For the validation study, a basic model of BTES which was developed in the TRNSYS software that represents an actual DST model. TRNSYS is a transient system simulation software tool used worldwide by researchers and consultant engineers which is used for modeling of a wide range of thermal energy systems, with the possibility of combining a large variety of system components (Simulation Studio components) (Pahud, 1996). Figure 13 shows the basic model of BTES developed in TRNSYS that performs simulation as per the actual DST and it was used to validate the performance of simplified DST. Table 3 shows the list of components used in the model.
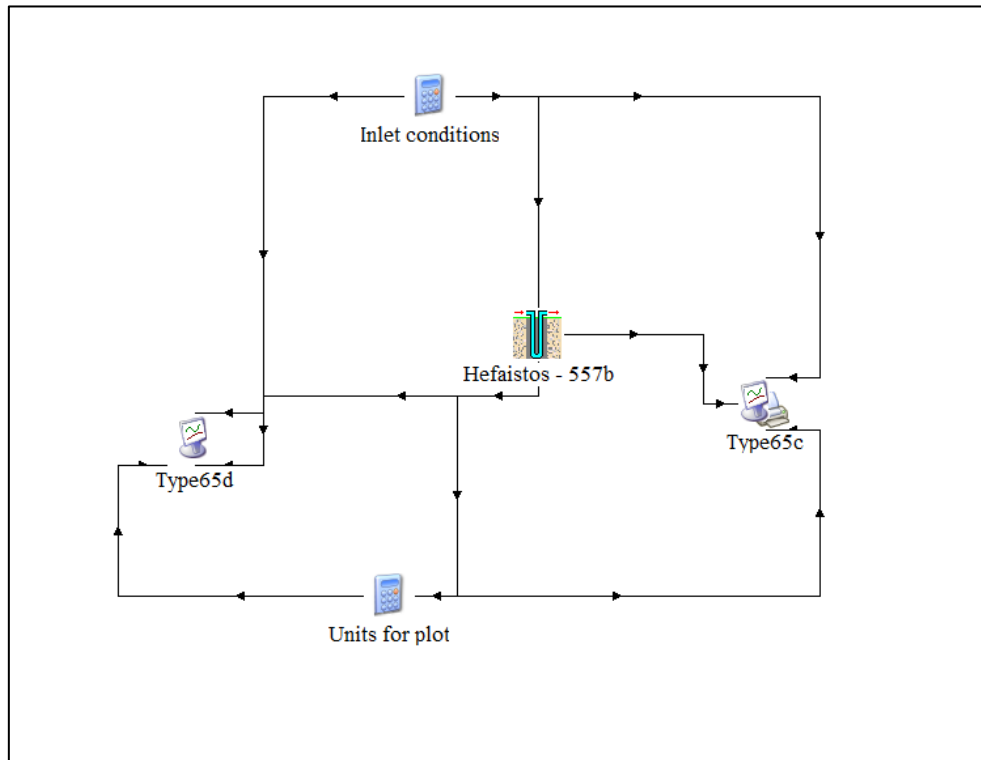

Figure 13. Basic model of BTES in TRNSYS

Table 3. List of components used in the TRNSYS model

Name in the TRNSYS model	Description
Hefaistos – 557b	Borehole thermal energy storage
Type 65c	Online plotter with file
Type 65d	Online plotter without file
Inlet conditions	Equation
Units for plot	Equation

The component named Hefaistos – 557b is the borehole storage component which follows the actual DST approach to analyze the heat transfer process. The inlet conditions component has inputs in the form of equations. The main inputs from the 'Inlets conditions' component to the 'Hefaistos – 557b' are the total mass flow rates, inlet temperature to the BTES while charging and discharging. The inlet temperature while charging was set to be 95°C and while discharging the inlet temperature was set to be 40°C. After running

several simulations for different periods of 5, 10 and 20 years with different input parameters, it was found that the size of the BTES system does not vary much and for this study, the length of simulation was defined to be 5 years as it was time-efficient.

For the validation study, several simulations were done by giving the same inputs to the simplified DST model and actual DST model. The inputs consisted the geometric and thermodynamic properties associated with the borehole storage such as the total mass flow rate, borehole depth and the number of boreholes. For this study, the total mass flow rate was varied in the interval between 500 to 1000 kg/s, the borehole depth was varied between 100 to 300 m and the number of boreholes was varied between 500 to 1500. The interesting outputs such as the average storage temperature, the outlet temperature from the BTES, the average power output, energy charged, and energy discharged were plotted. These outputs of the actual DST model were further compared to outputs of the simplified DST model and the difference was calculated in terms of error percentage as given by equation 36:

$$Error \% = \frac{(Output_{simplified\ DST} - Output_{actual\ DST})}{Output_{actual\ DST}} \times 100 \qquad (36)$$

6 Techno-economic analysis

Techno-economic analysis is a method that is used to analyze the technical and economic performance of the system for different system configurations and find out the best possible configuration as per the requirements. For the techno-economic analysis of the system, the reference case was defined with the input parameters mentioned in the Table 4.

Table 4. Input parameters for the reference case

Parameter	Value	Unit
Borehole depth	240	m
Mass flow rate/borehole loop	0.8	kg/s
Borehole radius	0.055	m
Power available for charging the BTES	50	MW
District Heating (DH) mass flow rate	900	kg/s
Heat Pump (HP) condenser inlet temperature	55	°C
Heat Pump (HP) condenser outlet temperature	68	°C

A sensitivity analysis was done for selective parameters of interest and then the output results of some key performance indicators (KPI's) for the different possible configurations were compared. For this study two parameters, the maximum allowed mass flow rate per borehole loop, '$\dot{m}_{BH,loop}$' and the borehole depth were chosen for performing the sensitivity analysis. The maximum allowed mass flow rate per borehole loop was varied between 0.6 - 1.0 kg/s and the borehole depth was varied between 180 – 300 m.

6.1 Key Performance Indicators (KPI's)

The Key Performance Indicators are used to compare the different configurations and find out the best possible configuration. The three KPI's defined are: BTES efficiency, seasonal performance factor (SPF) and the Net Present Value (NPV).

6.1.1 BTES efficiency

The BTES efficiency 'η_{BTES}' is defined as ratio of the amount of heat energy extracted from the borehole storage volume while discharging '$Q_{extracted}$' to that of the total amount of heat energy injected into the borehole storage volume while charging '$Q_{injected}$' (McDaniel B., 2016).

$$\eta_{BTES} = \frac{Q_{extracted}}{Q_{injected}} * 100 \tag{37}$$

6.1.2 Seasonal Performance Factor (SPF)

The seasonal performance factor (SPF) is defined as the ratio of heating energy $\dot{Q}_1$ delivered by the heat pump annually to that of the total compressor power $\dot{E}_k$ required by the heat pump annually. It can also be defined as the average coefficient of performance (COP) of the heat pump for a year.

$$SPF = \frac{\dot{Q}_{1(annual)}}{\dot{E}_{k(annual)}} \tag{38}$$

6.1.3 Net Present Value (NPV)

To perform an economic analysis of the entire BTES system, NPV was chosen as the economic performance indicator. The NPV is calculated for a period 't' of 20 years using equation 39, which includes the total investment costs (CAPEX), operational costs ($Cash_{out}$), profit ($Cash_{in}$), maintenance costs and the discounted rate of return 'r' is assumed to be 10%.

$$NPV = \sum_{t=0}^{20}[\frac{Cash_{in} - (Cash_{out} + Maintenance\ costs)}{(1+r)^t} - CAPEX] \tag{39}$$

6.1.3.1   Total Investment costs

The capital expenditure (CAPEX) includes the initial investment costs for the three components of the BTES system. The CAPEX of the borehole thermal energy storage was estimated using the equation 40 developed from a survey mentioned in (Mazzotti W., 2018).

$$CAPEX_{BH} = (C_1 + C_2.H^2 + C_3).N_b.H + C_o \tag{40}$$

where H is the borehole depth, N_b is the number of boreholes, $C_1 = 158.53$ SEK/m and $C_2 = 3.38\times10^{-4}$ SEK/m³ are constants. $C_3=100$ SEK/m is the lumped price for the BHE, casing and other extra prices related to drilling, $C_o=9300$ SEK is the fixed price related to the establishment of the drilling rig on site.

The CAPEX for a heat pump was 250 pounds/kW as it was estimated from the heat pump manufacturer Star Renewable Energy. The conversion rate of pound to SEK (SEK/£) was assumed to be 12. The total cost of the heat pump is then calculated using the equation 41.

$$CAPEX_{HP} = Max.Heating\ output\ (kW) * 250 * 12 \tag{41}$$

The CAPEX of the heat exchanger was calculated using the equation 42 mentioned in (Hackl R., 2013). The equation uses the area of the heat exchanger to calculate the investment costs, so based on the UA-value calculated during the steady-state the respective area of the heat exchanger is calculated assuming a U-value of 1.5 kW/m²K (Anon., n.d.).

$$CAPEX_{HX} = C_B.\left(\frac{K}{K_B}\right)^M.CEPCI_{HX}.(\frac{SEK}{US\$}) \tag{42}$$

Where $C_B=32800$ \$ is the known base cost, $K_B=80$ m² is the base capacity, $M = 0.68$, $CEPCI_{HX}$ is the index used to update the costs of heat exchangers from 2000 (370.6) to 2018 (603.1) i.e. $CEPCI_{HX} = (603.1/370.6) = 1.627$ (Anon., n.d.) and the conversion rate from SEK/US\$ is assumed to 9.8.

The total CAPEX costs of the entire system were calculated by adding the three individual CAPEX costs of the boreholes, heat pumps and the heat exchanger.

6.1.3.2   Operational and Maintenance costs

The operational costs (OPEX) of the system consist of the amount spent on the electricity for the operation of the compressors and water circulation pumps and is termed as '$Cash\_out$'. The price of electricity used for the calculations was 0.7 SEK/kWh (Anon., n.d.). The profit was calculated from the amount of heat energy sold during the discharging period and is termed as '$Cash\_in$'. The district heating selling price used for the calculations was 0.9 SEK/kWh (Anon., 2018). During the charging period, it was assumed that the heat energy available to store in the BTES is for free of cost. As the performance of the borehole storage system becomes stable in the 5th year, all the '$Cash\_out$' and '$Cash\_in$' values were assumed to be the same as 5th year from the year 6 to year 20. The maintenance costs were assumed to be 4% of the total CAPEX costs and was accounted for every year in the NPV calculations.

7 Results & Discussion

The results extracted from the newly developed sizing model during the post-processing will be summarized and discussed in this chapter. The steady-state model of DST was validated against the dynamic model of DST by presenting the error percentage between some of the key outputs of both the models. From the techno-economic analysis, few important results are presented for a reference case with the borehole depth of 240 m and the maximum allowed mass flow rate in the borehole loop of 0.8 kg/s. Further the results for the sensitivity analysis are presented. The sensitivity analysis was done by varying two parameters, borehole depth and maximum allowed mass flow rate per borehole loop with respect to the reference case.

7.1 Validation of simplified DST against the actual DST

The steady-state sizing model of BTES also called as simplified DST model was validated against the actual DST model that calculates the heat transfer process in dynamic state. A basic model was developed in TRNSYS software to analyze the performance of actual DST as mentioned in the chapter 5. In the Table 5, the different cases with different input parameters that were used for validation of simplified DST are shown. The outputs of average storage temperature, average power output, outlet temperature from the BTES, energy charged, and energy discharged were compared.

Table 5. Different cases used for validation of the simplified DST against the actual DST

Case No.	Mass flow rate in the BTES		Borehole Depth (m)	Number of Boreholes (-)
	Total (kg/s)	Per Borehole loop (kg/s)		
1	500	1	300	1500
2	600	1.2	300	1500
3	700	1.4	300	1500
4	800	1.6	300	1500
5	900	1.8	300	1500
6	1000	2	300	1500
7	1000	2	100	1500
8	1000	2	150	1500
9	1000	2	200	1500
10	1000	2	250	1500
11	1000	2	300	1500
12	1000	6	300	500
13	1000	5	300	600
14	1000	4.28	300	700
15	1000	3.75	300	800
16	1000	3.33	300	900
17	1000	3	300	1000

18	1000	2.72	300	1100
19	1000	2.5	300	1200
20	1000	2.30	300	1300
21	1000	2.14	300	1400
22	1000	2	300	1500

In Figure 14, the error percentage for the average storage temperature at the end of 5th year is shown. The error percentage between the simplified DST and the actual DST varied within the range of -0.9% to 1% for different input parameters. The average error for the average storage temperature is around 0.05%.
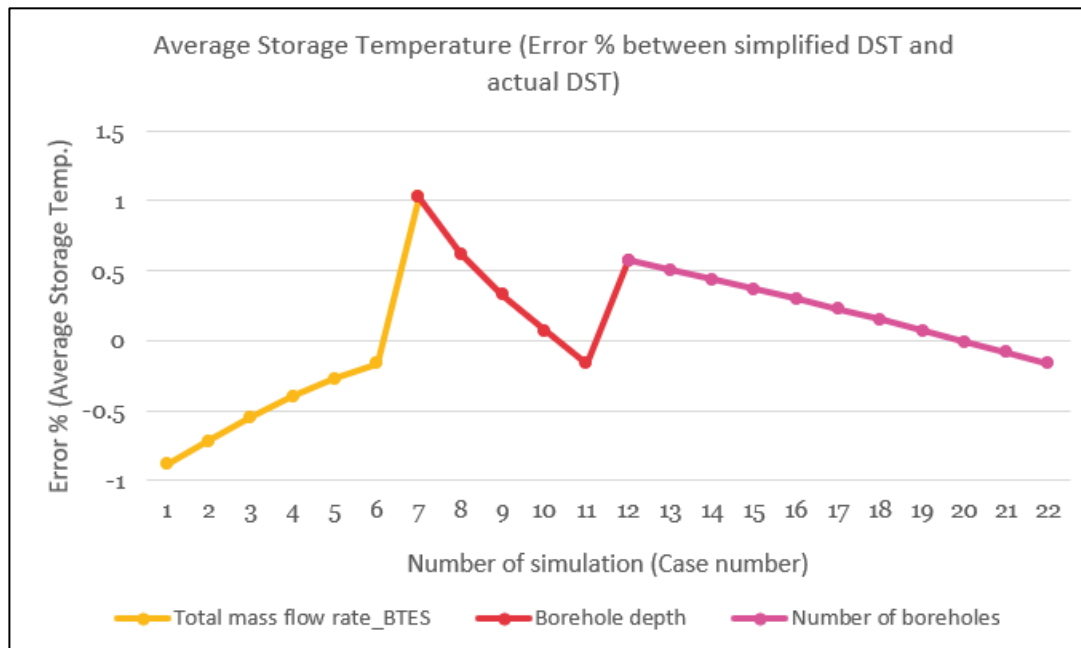

Figure 14. Average Storage Temperature (Error between simplified DST and actual DST)

In Figure 15, the error percentage for the average power output at the end of 5th year is shown. The error percentage varies within a range of 3.5% to 12%. The average error is around 5.09%. For most of the cases, the error is below 6% and only for lower mass flow rates in the BTES the error is high. The power output in the actual DST is less when compared to the simplified DST and the main reason for this is due to no heat losses to the surrounding ground being considered in the simplified DST which are mentioned in the assumptions in section 4.5. As the actual DST considers heat losses it is expected to give a less heating output when compared to simplified DST.
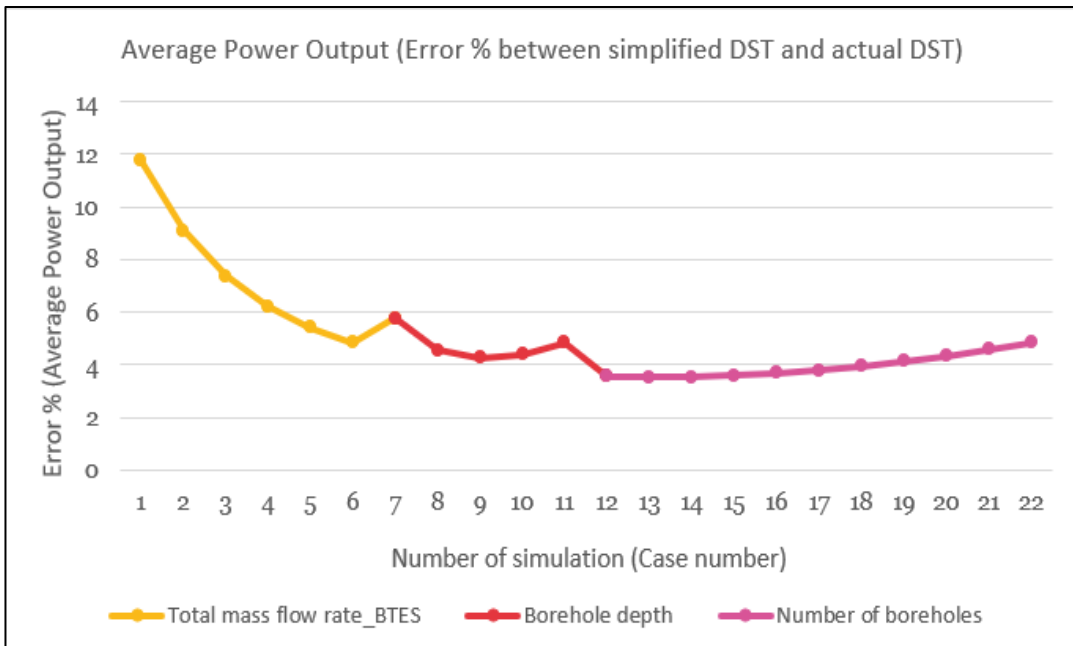
Figure 15. Average Power Output (Error between simplified DST and actual DST)

In Figure 16, the error percentage for the outlet temperature from the BTES at the end of 5th year is shown. The error percentage varies within the range of 0.1% to 2.1% and the average error is around 0.53%.
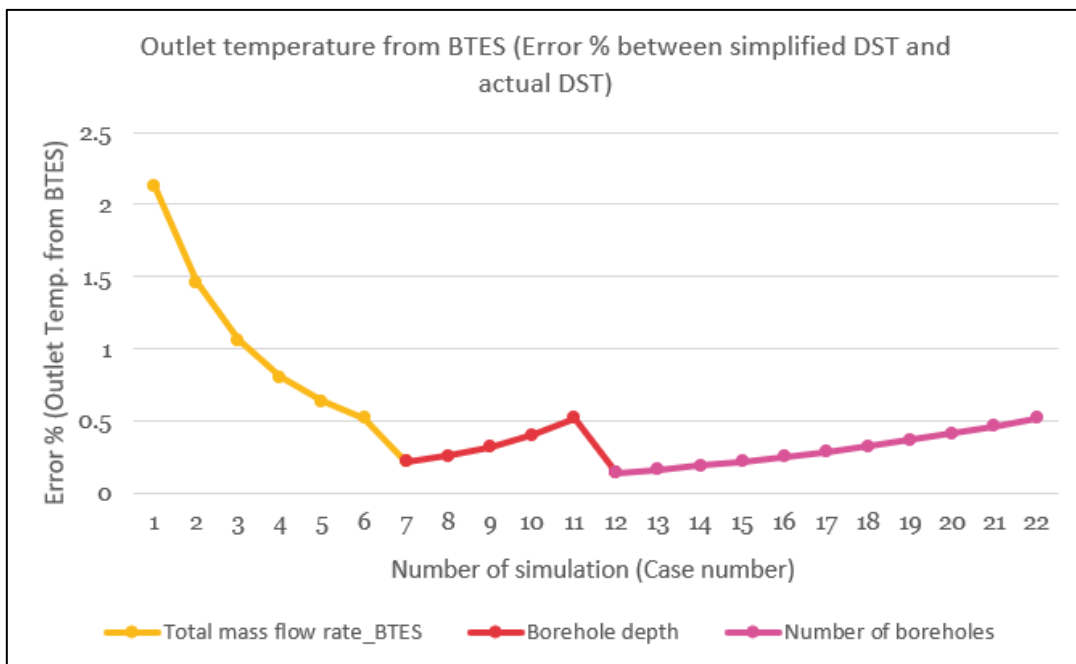

Figure 16. Outlet Temperature from BTES (Error between simplified DST and actual DST)

In Figure 17, the error percentage for the energy charged in the 5th year is shown. The error percentage between the simplified DST and the actual DST varies within the range of -3% to 7% and the average error is around 0.29%.
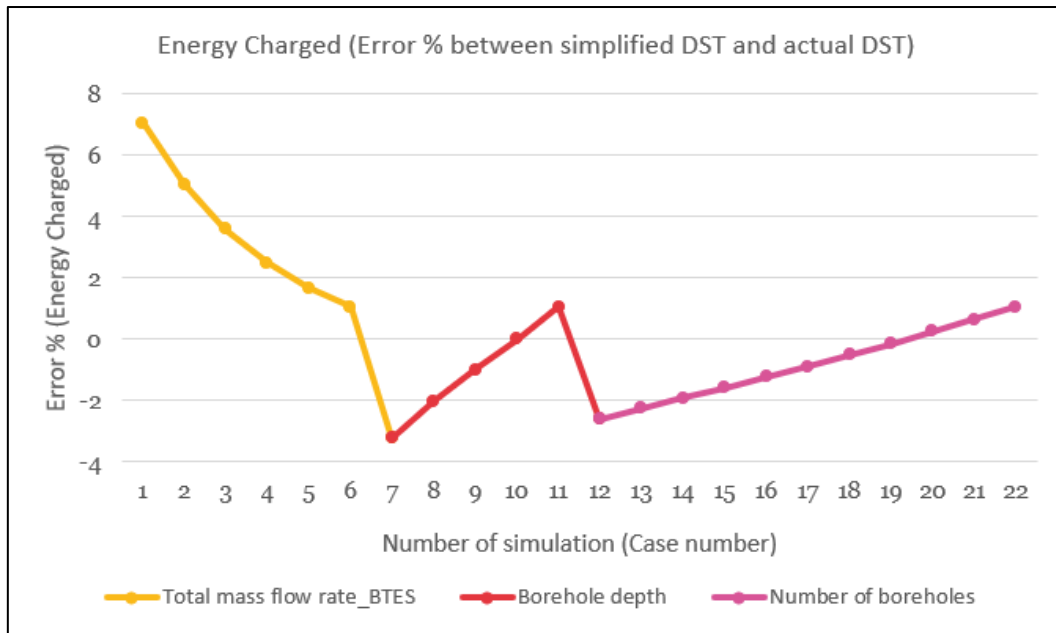
Figure 17. Energy charged in the 5th year (Error between simplified DST and actual DST)

In Figure 18, the error percentage for the energy discharged from the BTES in the 5th year is shown. The error percentage varies within a range of 4% to 14%. The average error is around 6.28 %. The energy discharged in the simplified DST is higher than the actual DST which gives a high error. The argument for this high error is the same as the one for average power output and the main reason is due to no heat losses being considered in the simplified DST.
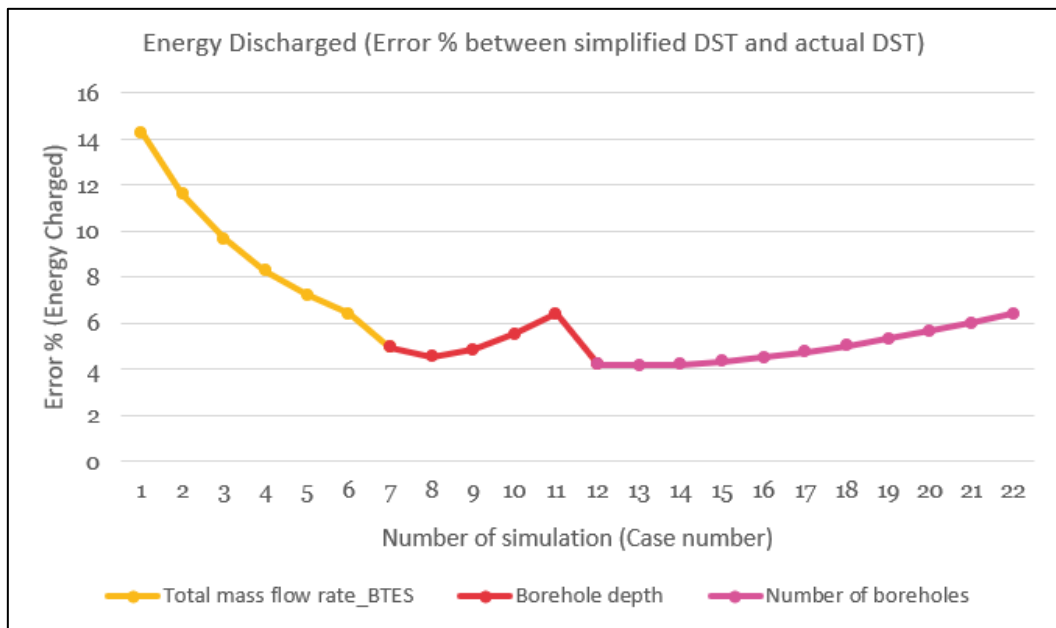

Figure 18. Energy discharged in the 5th year (Error between simplified DST and actual DST)

The average error for the average storage temperature, outlet temperature from the BTES and the energy charged was close to 0% for different cases whereas for average power output and energy discharged the error was higher due to no heat losses considered in the simplified DST.

7.2 Outputs for the reference case

For a reference case mentioned in the chapter 6, the outputs for the key performance indicators (KPI's) of Net Present Value (NPV), BTES efficiency in the 5th year, Seasonal Performance Factor (SPF) in the 5th year and number of boreholes that were sized are presented in the Table 6.

Table 6. Key outputs for the reference case

Key Performance Indicator (KPI)	Value	Unit
Net Present Value (NPV)	715	million SEK
BTES efficiency	88.1	%
Seasonal Performance Factor (SPF)	9.79	--
Number of boreholes	2073	--

In Figure 19, the variation of average storage temperature of the BTES is shown over the period of 5 years for the reference case. During the first year, for the initial six months the BTES is only being charged and there is no discharge, so the average storage temperature is almost constant during the last 6 months of the first year and only decreases by a small margin due to heat losses to the surroundings. Second year onwards the storage temperature increases gradually. For the reference case, the average storage temperature reaches a maximum of 75°C in the 5th year at the end of charging period.
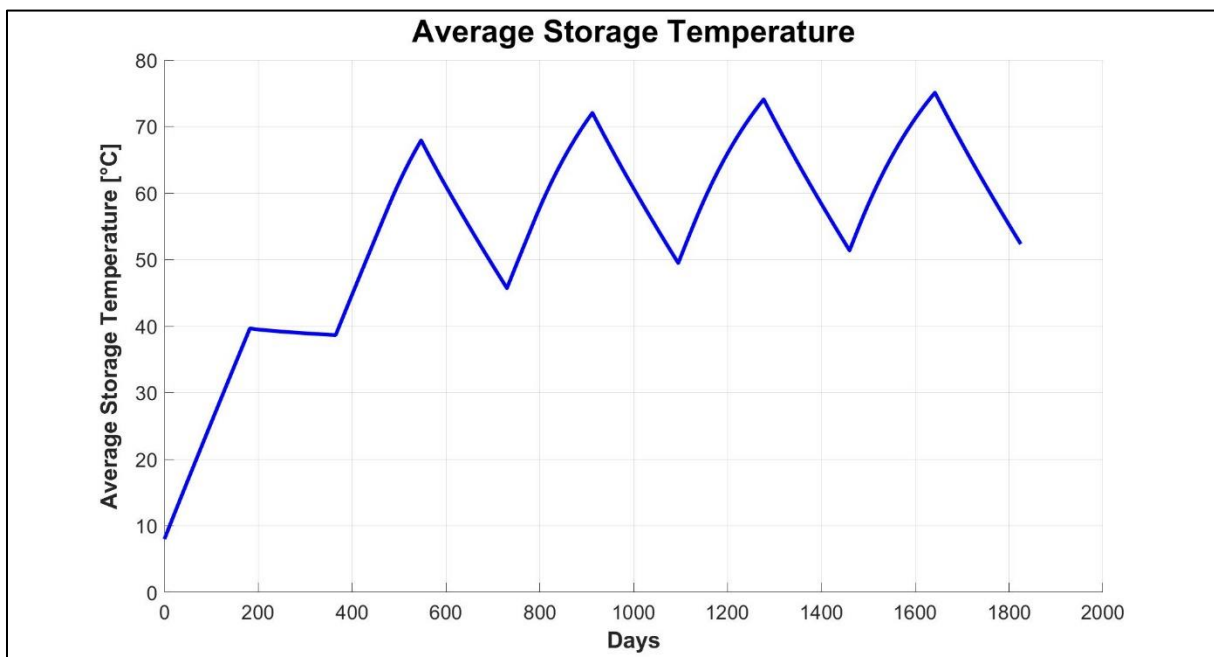
Figure 19. Average Storage Temperature (for reference case)

Figure 20 shows the amount of energy charged and discharged during the BTES simulation period of 5 years for the reference case. The energy charged decreases for the later years and this due to the increase in the storage temperature in the later years which reduces the capacity to store heat energy. On the other hand, almost the same amount of energy is being discharged from the storage volume. The mean discharge temperature is around 55°C at the end of 5th year and the BTES storage efficiency is around 88.1% at the end of 5th year.

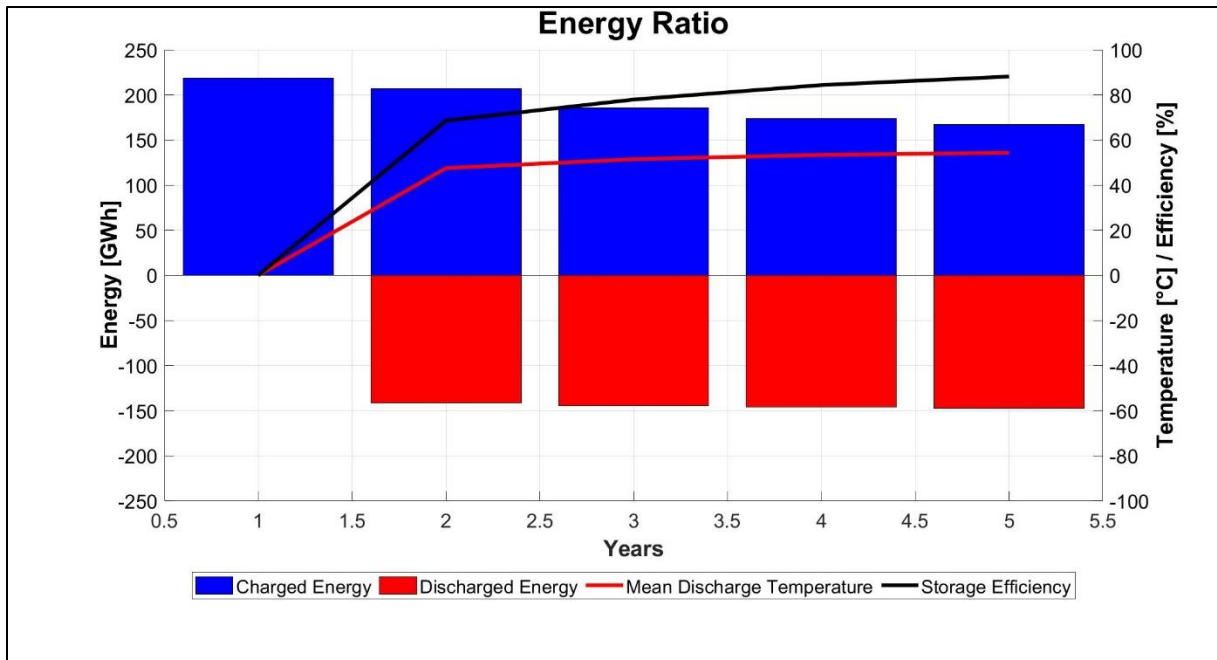*Figure 20. Energy Ratio (for reference case)*

Further a sensitivity analysis was done by varying only the borehole depth and mass flow rate per borehole loop and the results are discussed in the next section.

7.3 Sensitivity analysis

In this section, the results from the sensitivity analysis are presented comparing the different configurations of BTES systems formed by varying the depth and mass flow rate. Figure 21 shows the Net Present Value (NPV) after 20 years for different mass flow rates and borehole depth varied by 25% below and above the reference case. The NPV of the system increases when the borehole depth is decreased and is around 800 million SEK for a system with lower borehole depth. For the varying mass flow rate, the NPV of the system increases as the mass flow rate increases.
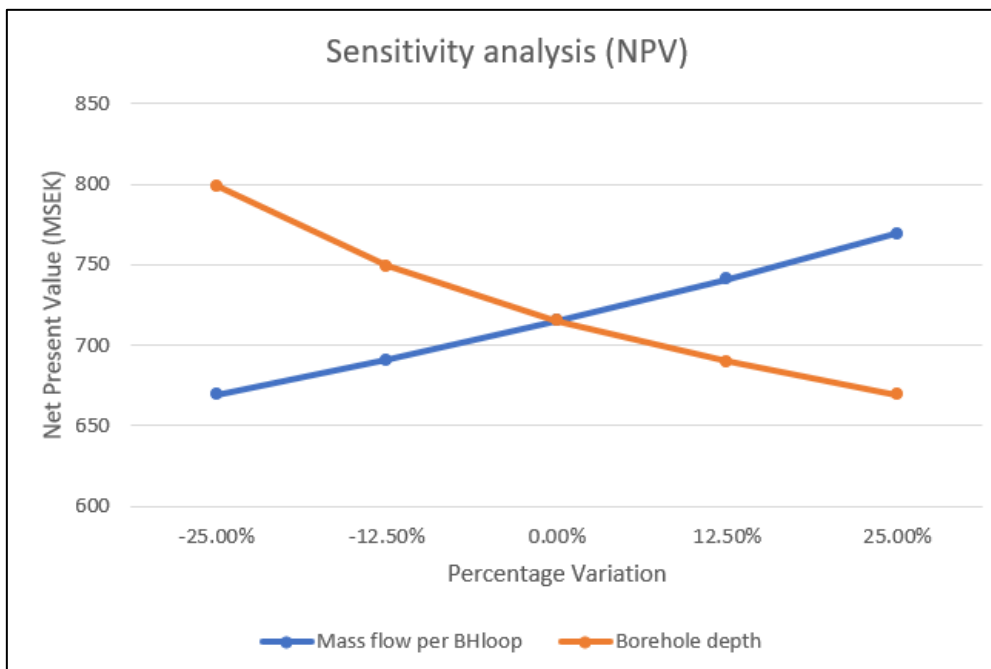

Figure 21. Sensitivity analysis (Net Present Value)

In Figure 22, another KPI of BTES efficiency in the 5th year is compared for different system configurations. It can be observed from the graph that the BTES efficiency increases as the mass flow rate in the borehole loop increases. At the maximum mass flow rate, the BTES efficiency is around 88.42%. For variation in the borehole depth, the BTES efficiency is around 88.22% for the lowest borehole depth which decreases as the borehole depth increases and then is almost constant for higher values of borehole depth.
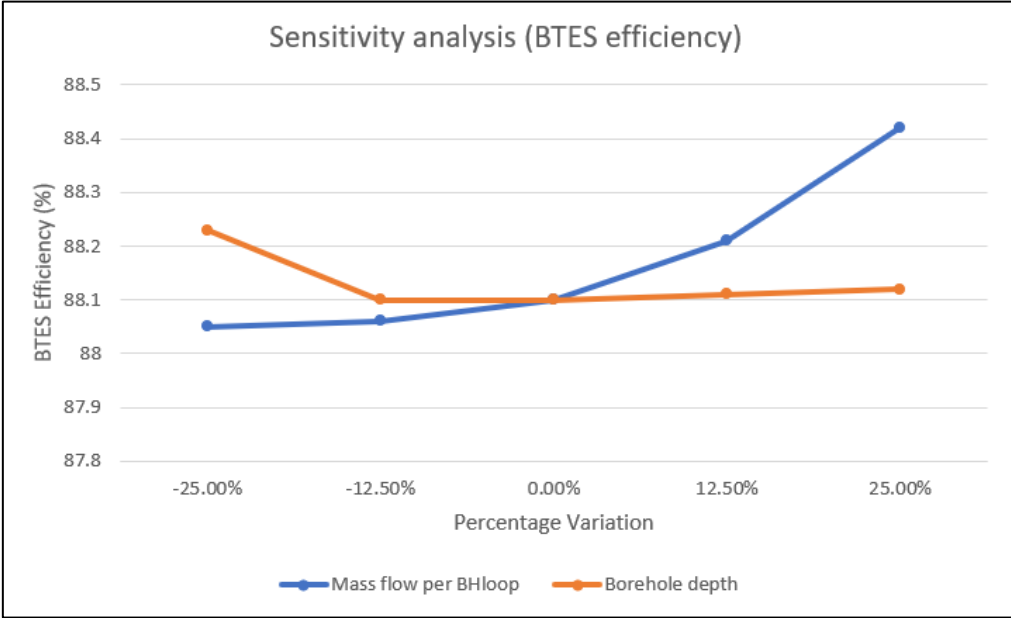
Figure 22. Sensitivity analysis (BTES efficiency)

The Figure 23 shows the variation in the seasonal performance factor (SPF) for the different system configurations. For the sensitivity study, the SPF at the 5th year of the simulation period was used. The SPF is higher when the mass flow rate in the borehole loop is the lowest and is around 12.5. It decreases when the mass flow rate is increased. The SPF increases as the borehole depth is increased.

Figure 23. Sensitivity analysis (Seasonal Performance Factor)

Figure 24 shows the variation in the sizing of the borehole storage system in terms of the number of boreholes. The variation in the mass flow rate does not affect the sizing of the borehole storage too much but as the borehole depth increases the size of the storage decreases. This is obvious as we increase the size of storage vertically it will require less horizontal space to store the same amount of energy thus decreasing the number of boreholes. For the reference case, the size of BTES was around 2073 number of boreholes.
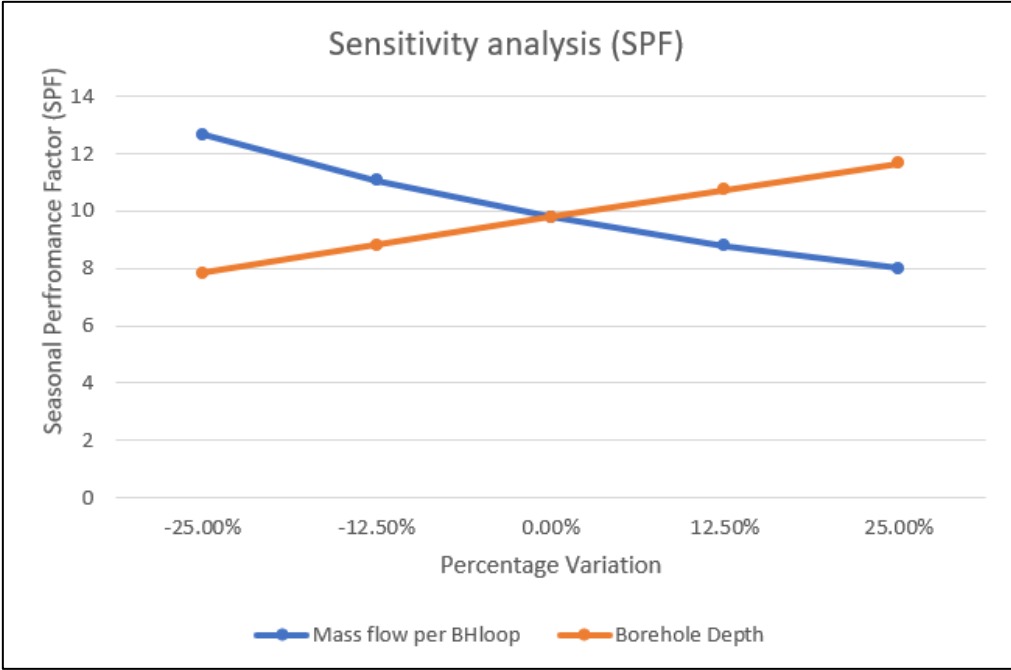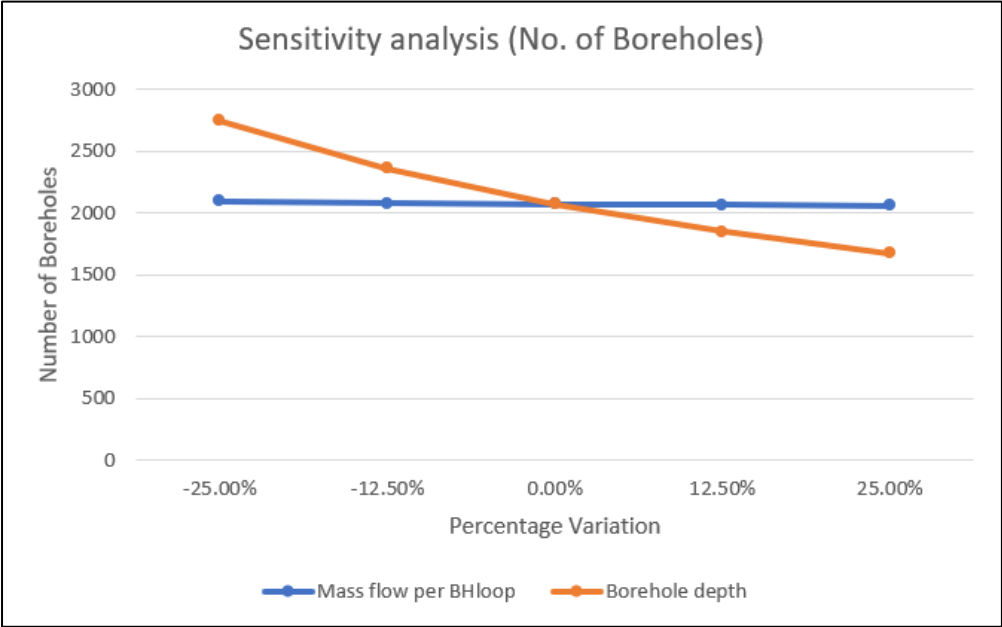

Figure 24. Sensitivity analysis (Number of boreholes)

From the sensitivity analysis, it can be found that the NPV and the BTES efficiency are higher for lesser value of borehole depth even though the BTES system has larger number of boreholes. This type of system configuration would lead to higher initial investment costs but will be profitable and give a better performance in terms of efficiency in the longer run. The SPF is higher for higher value of borehole depth, but as the other KPI's suggest that the BTES system with lower borehole depth has higher NPV and BTES efficiency, the sensitivity analysis shows that it is better to have lower borehole depth.

For a higher mass flow rate in the borehole loop, the NPV after 20 years and BTES efficiency are higher, whereas the SPF decreases and the size of BTES is not affected much, so this study shows that it is better to have a higher mass flow rate.

8 Conclusion

In this master thesis, the previously developed dynamic model of the HT-BTES system was studied and the function of all the components was understood. The heat transfer calculations involved in the borehole thermal energy storage system was further studied. Based on the DST model developed by Hellström G., another simplified version of DST model called as steady-state model was developed which can be used for sizing of the borehole storage i.e. the number of boreholes as per the requirements of any specific location. A steady-state heat pump sizing model was developed using the model that is being used in the previously developed dynamic model and also a steady-state model to size the heat exchanger used for injected heat in the ground was developed.

The validation study was done for the steady state model of BTES (simplified DST) alone against the dynamic model (actual DST). The error between the key outputs of simplified DST model and the actual DST model was within the interval of -5% to +5% for most of the tested input values. This shows that the newly developed simplified DST model is robust.

In the techno-economic analysis, for a reference case of borehole depth 240 m and mass flow rate of 0.8 kg/s in the borehole loop, the Net Present Value (NPV) of the system after 20 years was estimated to be around 715 million SEK, the BTES efficiency in the 5th year was 88.10%, the seasonal performance factor (SPF) was around 9.79 and the BTES system was sized with 2073 number of boreholes, connected in a series of 3. The average stoarge temperature in the 5th year reached around a maximum of 75^oC at the end of the charging period and the mean discharge temperature at the end of 5th year was around 55^oC.

Futher a sensitivity analysis was done by varying the borehole depth and the mass flow rate in the borehole loop upto 25% below and above the reference case. It showed that the NPV and BTES efficiency were higher for lower borehole depth and higher mass flow rate per borehole loop. On the other hand, the SPF was higher for a higher borehole depth and a lower mass flow rate per borehole loop.

8.1 Future work

An optimization study could be done comparing different system configurations to find out the best possible configuration as per the requirement of any specific case. The steady-state sizing model developed in this master thesis could be linked to an optimization tool called DYESOPT to perform the optimization study.

Also, as part of the techno-economic analaysis, it would be interesting to do an exergy analysis and use it as a key performance indicator to compare the perfromance of different configurations and find out the optimal configuration of the system.

9 Bibliography

Acuña, J., 2013. *Distributed thermal response tests – New insights on U-pipe and Coaxial heat exchangers in groundwater-filled boreholes,* Stockholm: KTH Royal Institute of Technology.

Anon., 2018. *Energy in Sweden - Facts and Figures 2018,* Stockholm: Swedish Energy Agency.

Anon., u.d. *Chemical Engineering essentials for the CPI professional.* [Online] [Använd 24 10 2019].

Anon., u.d. *Engineering Page.* [Online] Available at: https://www.engineeringpage.com/technology/thermal/transfer.html [Använd 24 10 2019].

Anon., u.d. *Statista.* [Online] Available at: https://www.statista.com/statistics/596262/electricity-industry-price-sweden/ [Använd 24 10 2019].

Anon., u.d. *Tekniska Verken i Linköping AB.* [Online] Available at: https://www.tekniskaverken.se/om-oss/ [Använd 24 10 2019].

Barth J., A. O., 2012. *Geoenergin i samhället: En viktig del i en hållbar energiförsörjning,* u.o.: Geotec och Svensk Geoenergi.

Chapuis S., a. B. M., 2009. *SEASONAL STORAGE OF SOLAR ENERGY IN BOREHOLE HEAT EXCHANGERS.* Glasgow, Scotland, Building Simulation 2009.

D., S. J., 2013. *Hybrid Solar Gas-Turbine Power Plants - A Thermoeconomic Analysis,* Stockholm: KTH Royal Institute of Technology.

Dzebo A., N. B., 2017. *Swedish heat energy system – new tensions and lock-ins after a successful transition,* Stockholm: Stockholm Environment Institute.

Hackl R., H. S., 2013. *Identification, cost estimation and economic performance of common heat recovery systems for the chemical cluster in Stenungsund,* Göteborg, Sweden: CHALMERS UNIVERSITY OF TECHNOLOGY.

Havtun H., B. P., 2016. *Sustainable Energy Utilization.* Stockholm, Sweden: KTH Royal Institute of Technology.

Hellström, G., 1989. *Duct Ground Heat Storage Model - Manual for Computer Code,* Lund: University of Lund, Department of Mathematical Physics.

Hellström, G., 1991. *Ground heat storage : thermal analyses of duct storage systems.* Lund: University of Lund, Department of Mathematical Physics.

Homuth S., H. W. K. H. S. I. a. S. T., 2016. Down-the-Hole Water-Powered HammerDrilling Method for medium-deep GeothermalEnergy Drilling. 132(3).

K.S., L., 2013. *Underground Thermal Energy Storage.* Springer, London: Green Energy and Technology.

Liao Q., Z. C. C. W. J. T., 2012. *New Correlations for Thermal Resistances of Vertical Single U-Tube Ground Heat Exchanger.* u.o., Journal of Thermal Science and Engineering Applications.

M., M., 2017. *Transient modeling of a high temperature borehole thermal energy storage coupled with a combined heat and power plant,* Stockholm: KTH Royal Institute of Technology.

Malmberg M, M. W. A. J. L. H. L. A., 2018. High temperature borehole thermal energy storage – A case study.

Mangold, D. &. D. L., 2015. *Seasonal Thermal Energy Storage - Report on State of the Art and Necessary Further R+D,* Stuttgart: International Energy Agency - Solar Heating & Cooling Programme (SHC), Task 45 Large Systems.

Mazzotti W., A. J. L. A. P. B., 2018. *Deep Boreholes for Ground-Source Heat Pump,* Stockholm: Energimyndigheten.

McDaniel B., K. D., 2016. Modeling of combined heat and power plant performance with seasonal thermal energy storage. Volym 7.

Meurs, v., 1985. *Seasonal Heat Storage in the Soil,* Delft: Ph.D. Thesis, Department of Applied Physics,.

Novo A. V., B. J. R. C.-F. D. R.-H. J., 2010. *Review of seasonal heat storage in large basins: Water tanks and gravel-water pits.* Spain: Applied Energy.

Pahud, D. &. H. G., 1996. *The New Duct Ground Heat Model for TRNSYS.* Eindhoven, Netherlands, u.n.

Rapantova N., P. P. K. J. V. P. G. D. R. R., 2016. *Optimisation of experimental operation of borehole thermal energy.* Czech Republic, Applied Energy.

Reuss, M., 2015. The Use of Borehole Thermal Energy Storage (BTES) Systems. i: *Advances in Thermal Energy Storage Systems: Methods and Applications.* u.o.:Woodhead Publishing.

Rydén B., S. H., 2014. *The heating market in Sweden - an overall picture,* u.o.: Profu.

Sannera B., K. C. M. D. R. L., 2003. Current status of ground source heat pumps and underground thermal energy storage in Europe. *Geothermics,* pp. 579-588.

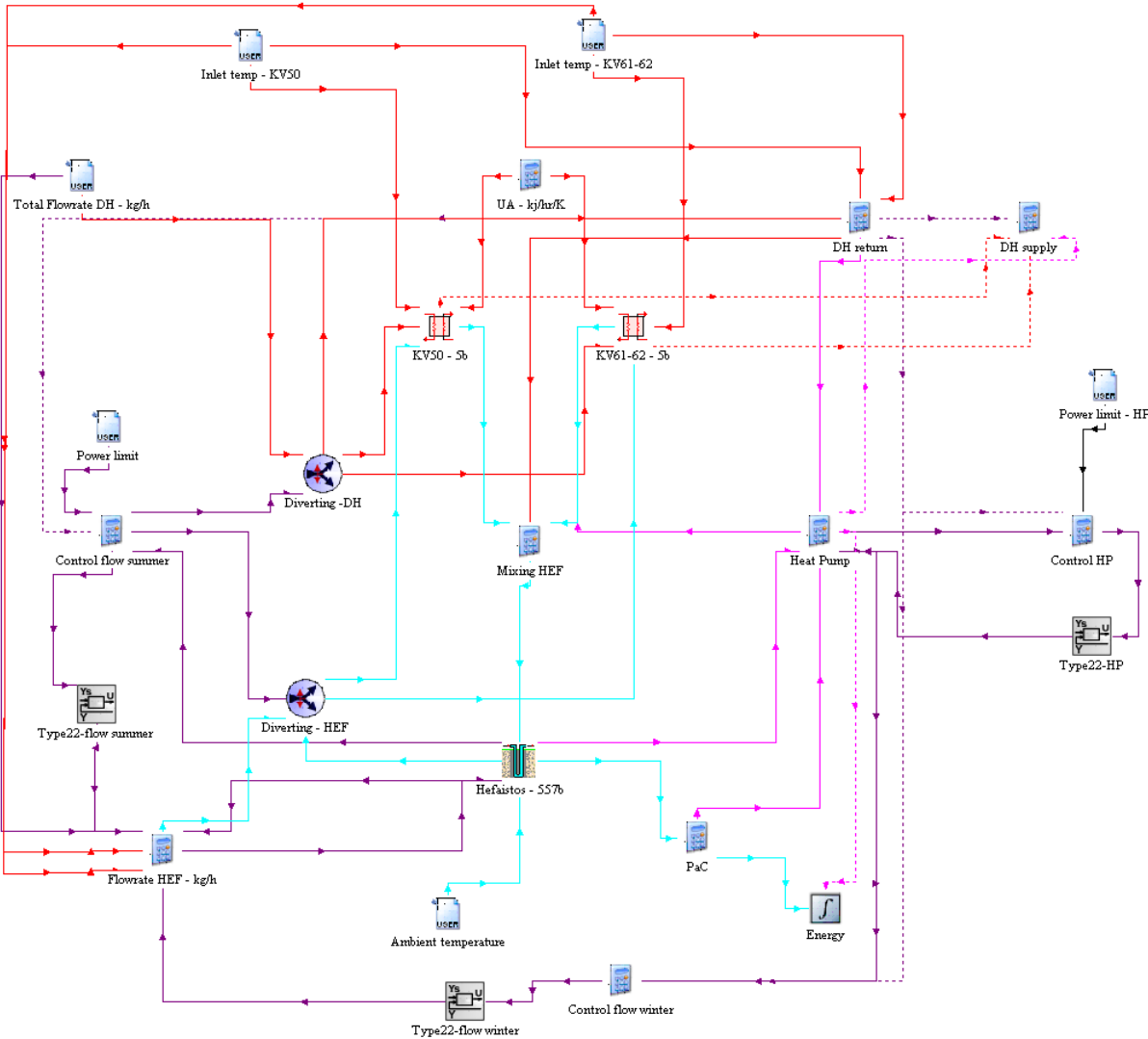# Appendix 1 – Dynamic model developed in the previous work

Figure 25. Dynamic model developed in the previous work (M., 2017)

PUBLICATION 5 : High temperature borehole thermal energy storage – A case study

Energiforsk

High temperature borehole thermal energy storage – A case study

Malin Malmberg   **Willem Mazzotti**   **José Acuña**

Henrik Lindståhl   **Alberto Lazzarotto**

ABSTRACT

Combining High-Temperature Borehole Thermal Energy Storages (HT-BTES) with existing Combined Heat and Power (CHP) systems running on waste fuels seems to be a promising approach to increase the energy efficiency of district heating systems through recovery of excess heat summertime from the waste-to-energy operation. This paper presents a case study from Sweden where the potential for charging and discharging waste heat at 95°C from a CHP-plant in summer into and from a HT-BTES is investigated. The interaction between the HT-BTES and the CHP-plant has been simulated with the software tool TRNSYS using the DST (Duct Ground Heat Storage Model) and a number of other TRNSYS tools. The aim of the study has been to design the size and operation of the HT-BTES with regard to energy and power coverage. Several different potential system configurations are presented in this paper, with 1 300 to 1 500 boreholes of 300 m depth. The result shows that it is possible to retrieve around 93 GWh/year of stored heat winter time, with the use of heat pumps using ammoniac as refrigerant. The discharge temperatures from the BTES range between 40-60°C, and up to 70°C in the initial discharge period.

INTRODUCTION

In the 1980s, Sweden was first in constructing a High Temperature Borehole Thermal Energy Storage (HT-BTES) in bedrock: the Luleå Heat Store (Nordell, 1994; Hellström, 1991). New interest for HT-BTES has arose during recent years in Sweden, especially within the district heating sector. A large part of the Swedish district heating production takes place in Combined Heat and Power (CHP) plants. These plants are often waste-to-energy plants that run at high loads and work almost continuously when they constitute a part of a waste management system, resulting in large quantities of waste heat in summer when the district heating demand is low. Furthermore, due to uneven heating demand over the year, the capacity of the CHP plants is often insufficient during peak heat demand in winter and is hence complemented by auxiliary boilers using fossil fuels or expensive biofuels as primary energy source. Operation during peak demand is costly and contributes to a larger carbon footprint. Due to the few annual operational hours the capital invested in such peak load plants is also poorly utilized.

Based on this background, the possibility of shifting some of the surplus heat from summer to winter has been investigated through a case study, in order to increase the flexibility between energy supply and demand in the district heating network and to phase out fossil fuels. The investigated case involves the connection of a HT-BTES to a CHP-plant with large quantities of surplus heats in the summer (approximately 260 MWh).

A BTES system consists of closely placed vertical boreholes working as ground heat exchangers. It can be drilled in rocks, clays or soils and is applicable in most locations. It is therefore one of the most popular forms of Underground Thermal Energy Storage (UTES) systems. In Sweden, the procedure for authority approvals is usually somewhat simple, the ground loop is easy to construct, and the system requires limited maintenance when using closed borehole heat exchanger loops.

When the Luleå Heat Store was constructed in the 80s, it was built for experimental and demonstrational purpose for Luleå University of Technology. The storage was charged with excess heat from gas combustion in the steelwork of the Swedish Steel Company (SSAB) and supplied space heating for one of the university buildings. This HT-BTES was taken out of operation in 1990 due to lower performance than expected regarding energy storage and extraction (Nordell, 1994). Nonetheless, this project managed to show the potential of HT-BTES and provided experiences about the design, construction and operation of such systems. Twenty years after, a large storage was constructed in Emmaboda, Sweden, and started to operate in 2010 (Nordell, 2016). The HT-BTES in Emmaboda works both as an energy research project and as a part of the Xylem Water Solutions AB plant with the aim to increase the energy efficiency of the plant. Another HT-BTES installation in Sweden is the Anneberg residential area where solar thermal heat is seasonally stored in boreholes and distributed to houses through a low temperature space heating system (Lund and Dalenbäck, 2007). The system has been operated since 2003 with overall good performance.

Several other HT-BTES have also been built outside of Sweden, such as the HT-BTES in Brædstrup, Denmark (Tordrup, et al. 2017; PlanEnergi, 2013), and in Necklarsum and Crailsheim in Germany (Nußbicker, et al., 2003; Schneider, 2013), Okotoks, Canada (Sibbitt, et al., 2015) and in Paskov, Czech Republic (Grycz, et al., 2014; Rapantova, et al., 2016). In Table 1 a summary including years of operation, storage volume and maximal storage temperature reached for the above-mentioned HT-BTES, including the ones in Sweden, is given. The installations in Sweden are constructed in hard crystalline bedrock which is especially suitable for BTES due to the relatively easy drilling procedure. The borehole depth for the HT-BTES presented in Table 1 reaches between 30 m (Necklarsum) to 150 m (Emmaboda) and is, except the Swedish ones, mostly built in soils and clay.

The HT-BTES in Anneberg, Necklarsum, Crailsheim and in Okotoks are all seasonal storages of solar thermal energy and are connected to local low-temperature district heating networks supplying heat to residential areas, whereof the system in Okotoks (Drake Landing Solar Community) has reached a solar fraction as high as 97% after the fifth year of operation. Furthermore, the BTES in Brædstrup is solar-assisted while being connected to the local CHP-plant supplying district heating to the community.

The BTES in Paskov is an experimental HT-BTES charged by excess heat from a CHP-unit taken into operation in 2011 (Grycz, et al., 2014; Rapantova, et al., 2016). The storage was built for experimental purpose with the aim to study the storage system and the rock environmental behavior during different operating states of charging and discharging. The use of a CHP unit gives a continuous supply of heat compared to storing of solar collector heat. The project was initiated to gain more knowledge of BTES with high heat carrier temperatures of 70-90°C.

Table 1. Design Parameters of Existing HT-BTES

Location	Years of operation	Storage volume [m³]	Maximum storage temperature [°C]	Source of charge
Luleå, Sweden	1983-1990	115 000	65	Industrial waste heat
Emmaboda, Sweden	2010-	323 000	45	Industrial waste heat
Anneberg, Sweden	2003-	50 600	45	Solar thermal
Brædstrup, Denmark	2012-	19 000	60	Solar thermal
Necklarsum, Germany	1999-	63 360	65	Solar thermal
Crailsheim, Germany	2008-	37 500	65	Solar thermal
Okotoks, Canada	2007-	34 000	74	Solar thermal
Paskov, Czech Republic	2011-	Unknown	78	CHP

In the majority of these HT-BTES the boreholes have been grouted. The regulations for grouting the boreholes with a sealing material differ between countries. In Sweden groundwater filled boreholes are most common, except in water protected areas or in risk of salt water contamination as it can decrease the risk for contamination of groundwater significantly (Gehlin, 2016). In the case of BTES the magnitude of induced natural convection from groundwater flow in fractures and cracks can furthermore be reduced (Gehlin, 2002).

METHODOLOGY

The aim of this work has been to evaluate potential system configurations for effective extraction and storage of excess heat from a CHP-plant in connection to a HT-BTES. The software TRNSYS (Klein, et al. 2004) has been used to simulate the system performance. TRNSYS is a transient system simulation software tool used worldwide by researchers and consultant engineers which enables modeling of a wide range of thermal energy systems, with the possibility to combine a large variety of system component models (Simulation Studio components). The system has been simulated with two different configurations, with and without heat pumps during discharge of the HT-BTES. Figure 1 and 2 below shows a flow chart of the CHP-plant connected to the HT-BTES respectively the layout of the TRNSYS model used for the simulations, both with the configurations including heat pumps. The TRNSYS model has been iteratively developed at the *Royal Institute of Technology (KTH)* and *Bengt Dahlgren AB*.

The vertical BHEs and their interaction with the surrounding rock has been model with Type 557b available in TESS library in TRNSYS. Type 557b assumes uniformly placed ground heat exchangers in a hexagonal pattern, based on the well-known DST approach, developed by Claesson et al. (1981), Hellström (1989;1991) and Pahud & Hellström (1996). The Type 557b has been widely used for dimensioning of BTES. The temperature in the ground, at a specific point, is derived by superposition of three parts: the global temperature, a local solution and a steady-flux part. The local and the global part are solved using the explicit finite difference method (FDM) while the steady-flux part is solved by an analytical solution. The temperature response is derived through thermal interaction between the BHE regarding the injected/extracted load of the modelled BTES (Hellström 1989).
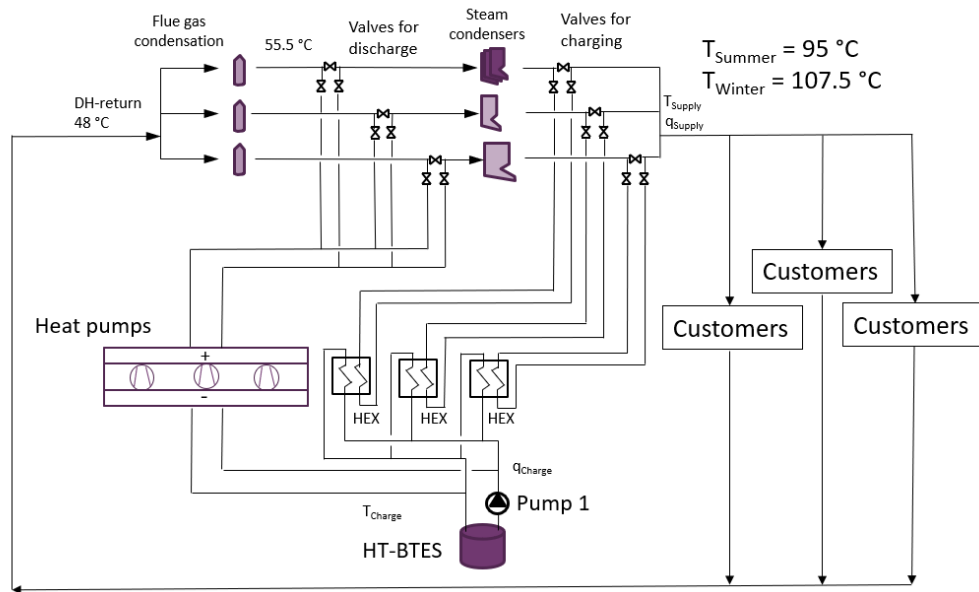

Figure 1   Flow chart for the CHP-plant including a HT-BTES and heat pumps.

In addition to simulation studio components, custom equations were utilized in the TRNSYS model. Furthermore, different data reader components are included. These contains pre-determined input data for operation of the CHP-plant such as district heating temperature, flow rates and power levels. The input data is given as daily mean values. However, the simulations are carried out with a timestep of one-hour. The simulation start corresponds to the first of May and a simulation period of 10 years has been used. The discharge period of the HT-BTES is considered to be between the end of October to the beginning of April. In the simulations the HT-BTES is not discharged during the first year of operation in order to heat up the surrounding ground. This means that it is charged for two periods before discharged.
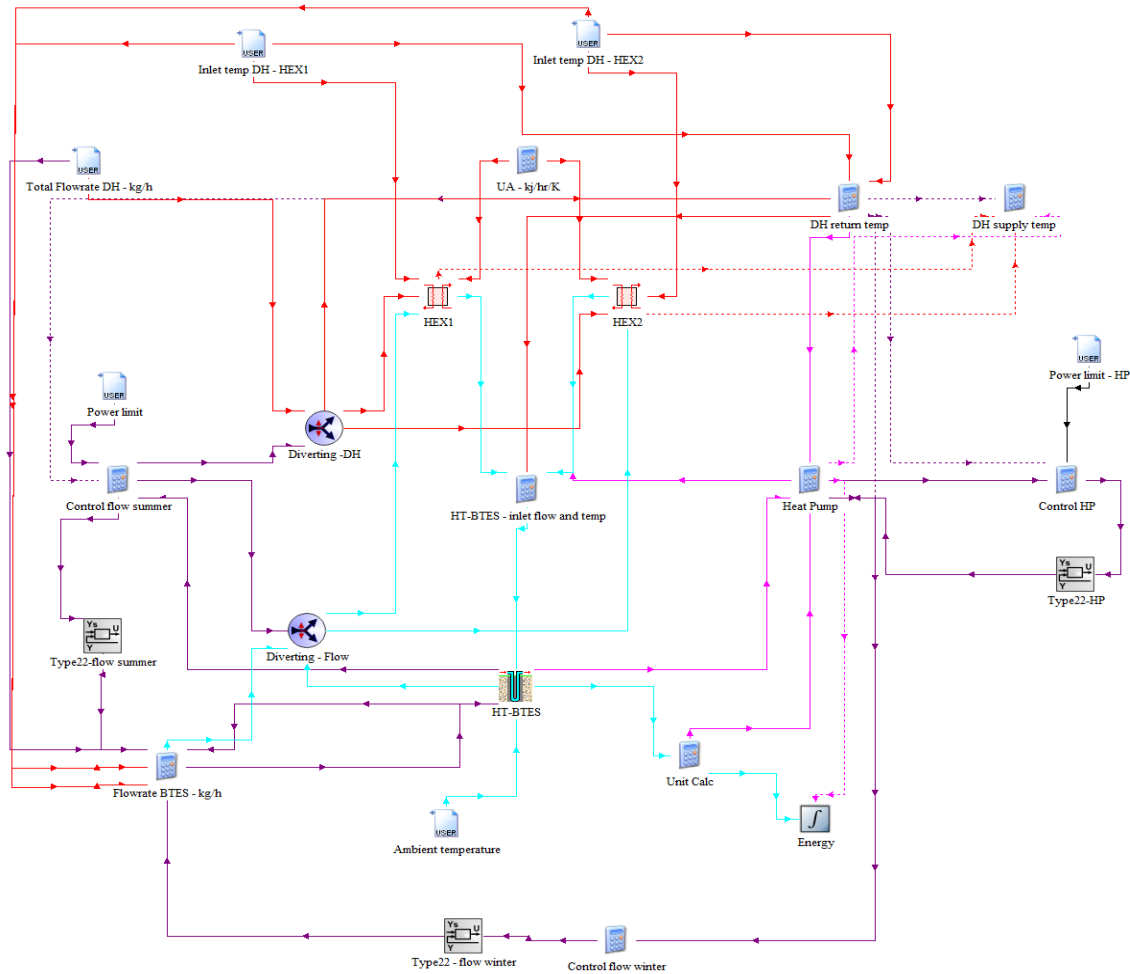
Figure 2   TRNSYS model of the interaction between the CHP-plant, the BTES and the heat pumps.

In the considered system layout (Figure 1) the HT-BTES is charged using the steam condensers of the electricity production unit in the CHP plant. The temperature at the condenser outlet is assumed to be maintained constant at 95°C during summer operation, corresponding to the required district heating supply temperature. During discharge, the HT-BTES is considered to be connected to the CHP-plant with discharge valves placed placed before the steam condensers, but after the flue gas condensers. Depending on the configuration the HT-BTES is discharged through heat pumps (Figure 1) alternatively directly through heat exchangers. In this way, the BTES preheats the district heating return flow without affecting the efficiency of the flue gas condensers. A more thoroughly investigation of how this

configuration would affect the operation of the CHP-plant is needed but has not been included in this study.

The district heating return temperature after passing the exhaust gas condensation is considered to be around 55°C winter time. During discharge phases of the HT-BTES, this temperature is used as inlet temperature to the water side of the heat pumps' condensers (or heat exchangers). The district heating flow varies over the year to obtain the desired supply temperature to the district heating network, with higher flowrates during the colder months when the demand is high. In Figure 3 a) the temperature levels and flowrates used for the simulations in the district heating system can be seen, as well as the ambient temperature.

In Figure 3 b) the power limits for charge and discharge of the BTES is shown in the form of a load duration curve. This limits the maximum possible power levels available or deliverable in the CHP-plant as excess heat (charge) and peak heat demand (discharge including heat pumps). The maximum delivered discharge power, with the use of heat pumps, has been limited to a maximum of 50 MW in the simulations, estimated as the maximum additional power supply that can be handled through the CHP-plant.
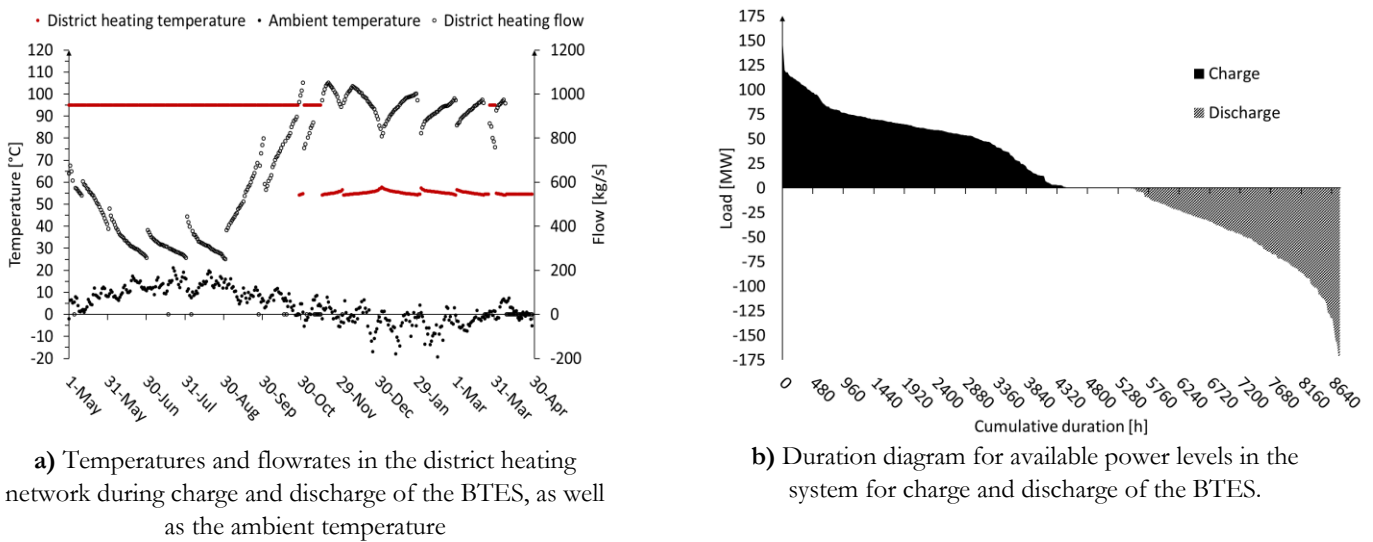

a) Temperatures and flowrates in the district heating network during charge and discharge of the BTES, as well as the ambient temperature

b) Duration diagram for available power levels in the system for charge and discharge of the BTES.

Figure 3   Input data used in the simulations regarding temperatures, flowrates and power levels in the district heating system.

When simulated without heat pumps the charge and discharge of the BTES was made through heat exchangers with the volumetric flow rate in the BTES loop controlled to match respectively not exceed the power limit in Figure 3 b). When simulated with heat pumps different control strategies have been applied in TRNSYS for summer and winter operation of the BTES, during charging and discharging, respectively. In summer mode, the system is controlled in a way similar to the case without heat pumps, with heat exchangers and control of the flow in the BTES. In the winter mode heat pumps are running for discharge of the BTES, connected in parallel to the heat exchangers. The number of heat pumps running during discharge, as well as the compressor speed (indirectly handled in the model) are controlled so that the delivered heating power from the heat pumps match the power limit shown in Figure 3 b), but at maximum 50 MW.

The heat pump model used for the simulations has been developed through a regression analysis from manufacturer's data for a two-stage high-temperature industrial heat pump unit, consisting of five individual 10 MW heat pumps which evaporators and condensers are respectively connected in series. The heat pump model has been applied to the TRNSYS model using custom equations. In winter mode the flow in the HT-BTES loop is furthermore controlled to give a

temperature difference of around 2 K over each evaporator. The number of heat pumps running in the model is not necessarily an integer, but it is representing an equivalent number of heat pumps running on full capacity (3600 RPM). The actual number of heat pumps is always rounded up and works with variable compressor speed at the high stage compressor. See Equation 1. The first compressor in each heat pump is always running on nominal speed (2950 RPM). The heat pump model is a simplification of the reality but is capturing the general behavior of the system.

$$RPM_{2^{nd}\ compressor} = 3600 \cdot \left(\frac{Number\ of\ HP}{Equivivalent\ number\ of\ HP_{Full\ speed}} \right) \qquad (1)$$

The HT-BTES has been simulated with the number of boreholes varied between 1000-2000, borehole depth varied between 250-300 m and borehole spacing varied between 4-6 m, with a serial connection of up to three boreholes to induce thermal stratification of the storage. The system was furthermore simulated with two different borehole heat exchangers (BHEs): double U-pipes and coaxial. Some general input values used in the simulations are shown in Table 2 below. With regard to the higher density gradient of water at the operating temperatures, the borehole resistance is assumed to be 0.05 K·m·W^{-1} for double U-pipes and 0.025 K·m·W^{-1} for coaxial collectors, based on experience from field tests. The thermal conductivity of the ground is assumed as 2.9 W·m^{-1}·K^{-1}. All simulations have been made without regard of heat losses occurred due to ground water flow.

Table 2. Assumed Input Data for the Simulations

Parameter	Value
Borehole radius [m]	0.055
Heat transfer conductivity ground [W/(m·K)]	2.9
Heat capacity of the rock [kJ/(m³·K)]	2241
Heat capacity of the heat carrier fluid [kJ/(m³·K)]	4.2
Density of the heat carrier fluid [kg/m³]	976
Insulation thickness (on top of storage) [m]	0.4
Heat transfer conductivity insulation [W/(m·K)]	0.13
Undisturbed ground temperature [°C]	8.0
Borehole resistance (double U-pipes) [(K·m)/W]	0.05
Borehole resistance (coaxial) [(K·m)/W]	0.025

RESULTS

Results from the initial simulations, all made with 1 500 boreholes, 300 m depth and 5 m borehole spacing, showed that the use of a heat pumps are required if the system is to deliver the desired power and temperature level to the CHP-plant during discharge. With the use of heat pumps the discharged energy showed to increase with up to 84%. The heat pumps require operational energy as opposed to direct heat exchange. The TRNSYS simulations furthermore showed that when boreholes were coupled in series of three, compared to all being coupled in parallel, the available energy discharge increased with up to 17%. When increasing the flow in the BTES, from 0.5 m³/s to 1.0 m³/s the discharge energy also showed to increase with up to 17%, though the discharge temperature decreased with 5-7%. The result furthermore shows about 30% lower operational energy for the circulation pumps in the BTES when simulated with coaxial BHE compared to double U-pipes.

Based on several simulations three designs were found with similar performance: 1 400 boreholes with double U-pipes and a borehole depth of 300 m (Case 1), 1 300 boreholes with coaxial BHEs and a borehole depth of 300 m (Case 2), and a design with 1 500 boreholes and 275 m borehole depth with double U-pipes (Case 3) – all three designs with a borehole spacing of 5 m and with loops of 3 boreholes connected in series. The three BTES designs showed similar

results with a potential to store around 107 GWh/year and to extract around 93 GWh/year with the use of a GSHP after the fourth simulation year.

In Figure 4 a)-c) some results from the simulations with 1 300 boreholes, coaxial collectors and a borehole depth of 300 m is shown. Figure 4 a) shows how the control of the heat pumps is handled in the simulations, as was previously explained. In Figure 4 b) the system temperatures can be seen for the fifth simulation year for the heat pumps, BTES and district heating system. The resulting discharge temperature from the BTES ranges between 40-60°C and up to 70°C in the initial discharge period with the mean temperature during discharge reaching almost 60 °C in the tenth simulation year. In Figure 4 c) the corresponding system power levels are presented for the fifth simulation year. As can be seen the charged and discharged power of the BTES is respecting the power limit of the district heating network, and the maximum power delivered from the heat pumps is limited to 50 MW.

In general, the capacity of the system increases with time. Experience from existing HT-BTES, and the simulations, the system requires 3-4 years of operation before reaching its expected performance. The energy output-to-input ratio, calculated as the ratio between charged and discharged energy of the HT-BTES increases with time to reach about 90% in the tenth simulation year (Figure 4 d). As can be seen in Figure 4 d the performance of the HT-BTES is similar for the three configurations presented in this paper.
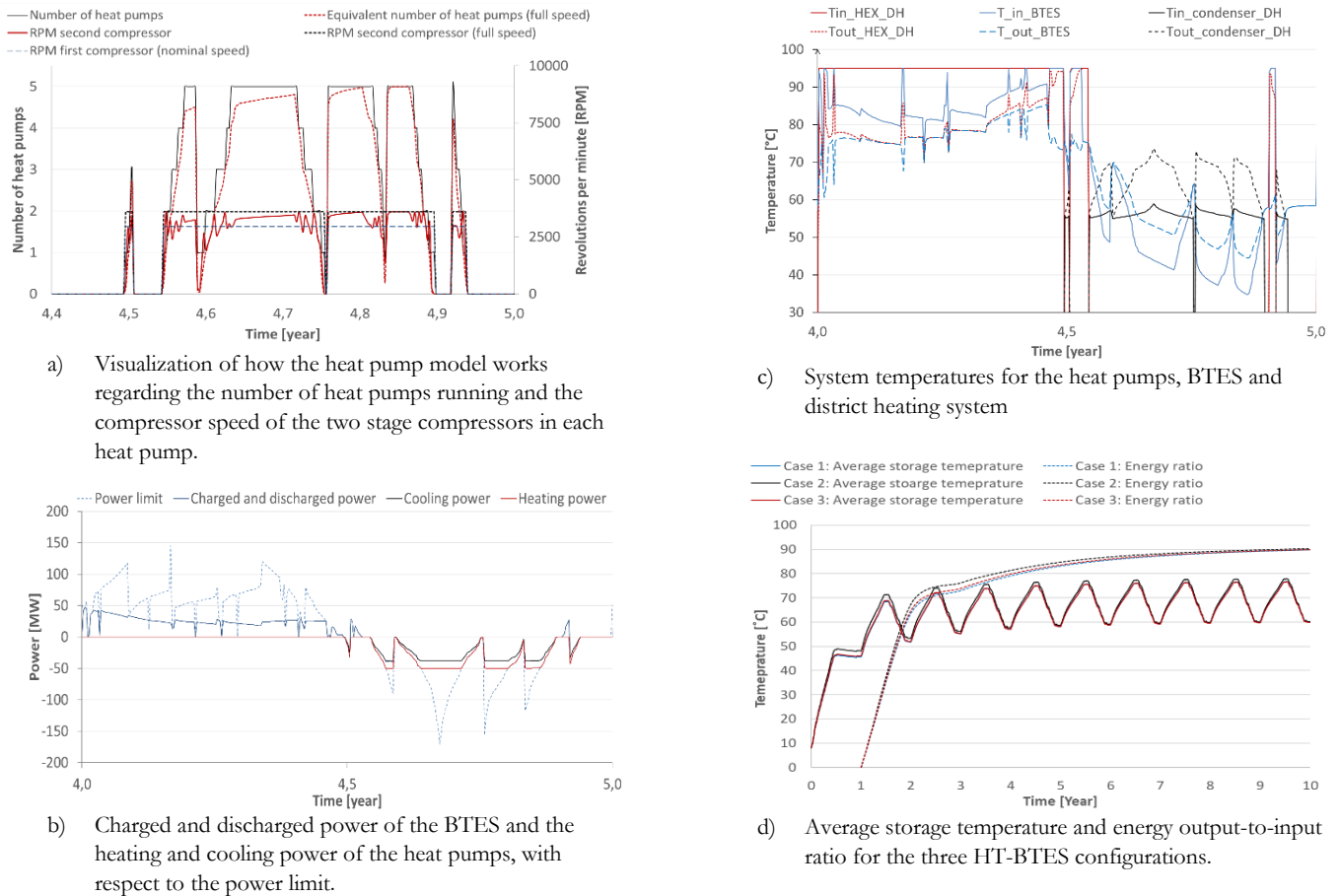

a) Visualization of how the heat pump model works regarding the number of heat pumps running and the compressor speed of the two stage compressors in each heat pump.

c) System temperatures for the heat pumps, BTES and district heating system

b) Charged and discharged power of the BTES and the heating and cooling power of the heat pumps, with respect to the power limit.

d) Average storage temperature and energy output-to-input ratio for the three HT-BTES configurations.

Figure 4   a)-c) Results from the TRNSYS simulations for the case with 1 300 boreholes and coaxial collectors; d) performance of the three HT-BTES configurations.

DISCUSSIONS AND CONCLUSION

In this project, a HT-BTES for seasonally storing excess heat from summer operation of a CHP-plant has been simulated in the software tool TRNSYS using the DST (Duct Ground Heat Storage Model). With the use of a HT-BTES as a part of the district heating system the flexibility between energy supply and demand in the district heating network can be increased. The BTES was simulated with two different BHEs: double U-pipes and coaxial. The tested geometries that showed the most favorable results consists of 1 400 boreholes and 1 300 boreholes with double U-pipes and coaxial collectors respectively, both with a borehole depth 300 m and a spacing of 5 m. When simulating with a lower borehole resistance, corresponding to coaxial collectors, the storage capacity of the system increased due to the improved heat exchange in the BHE and the size of the BTES could be decreased. Furthermore, a geometry with 1 500 boreholes and 275 m borehole depth with double U-pipes showed similar results regarding energy, power and system temperatures. The three systems showed a potential to store around 107 GWh/year and to extract around 93 GWh/year with the use of a GSHP. The resulting discharge temperature from the BTES ranges between 40-70°C.

The pressure drop in the BHE is overall rather high for the simulated systems, with up to 6 bars with double U-pipes, a borehole depth of 300 m and 3 boreholes in series. If the number of boreholes in series would be reduced the pressure drop would decrease significantly, both as the total collector length is decreased in each loop and that the number of borehole loops would increase resulting in a lower volumetric flowrate in each loop. How this would affect the thermal performance should be investigated further. Coaxial collectors would decrease the pressure drop, and thus the required operational energy for the circulation pumps in the BTES by about 30%. Using coaxial collectors should then be considered as they both improve the heat exchange and leads to lower pressure drop in the BHEs and thereby decreasing the required pumping energy. Further investigation is needed to ensure the market availability of a coaxial BHE that can withstand the high temperatures of this application.

Another subject where further investigation is needed is the influence on microbiology and geochemistry in HT-BTES applications. BTES systems operating at temperatures above 40°C can increase the risk of causing geochemical disturbance and affecting the microbiological balance in the ground (Gehlin, 2016). Several studies have shown no evidence for increasing number of bacteria or growth of pathogens related to increased temperature in the ground, but have showed a change in the composition of bacterial species (Bonte, et al., 2011). However, this is one subject regarding HT-UTES where the information is very limited.

Abbreviations

BHE   =   Borehole heat exchangers
BTES   =   Borehole thermal energy storage
CHP   =   Combined heat and power
GSHP   =   Ground source heat pump
HT   =   High temperature
RPM   =   Revolutions per minute
TRNSYS =   TRansient system simulation program
UTES   =   Underground thermal energy storage

REFERENCES

Bonte, M., Stuyfzand, P. J., Hulsmann, A. & Beelen, P. V., 2011. *Underground Thermal Energy Storage: Environmental Risks and Policy Developments in the Netherlands and European Union.* Ecology and Society, 1 March.16(1)(22).

Claesson, Eftring, Hellström, Johansson. 1981. *Duct storage model*, Dept. of mathematical physics, Lund institute of technology, Sweden.

Erlström, M. et al., 2016. *Geologisk information för geoenergianläggningar: en översikt*, s.l.: Sveriges Geologiska Undersökning (SGU).

Gehlin, S., 2002. *Thermal Response Test - Method Development and Evaluation,* Luleå: Luleå University of Technology.

Gehlin, S., 2016. *Borehole Thermal Energy Storage.* in: S. J. Rees, red. Advances in Ground-Source Heat Pump Systems. u.o.:Woodhead Publishing, pp. 295-327. ISBN: 978-0-08-100322-0.

Grycz, D., Hemza, P. & Rozehnal, Z., 2014. *Charging of the Experimental High Temperature BTES Via CHP Unit - Early Results.* Energy Procedia, Volume 48, pp. 355-360.

Hellström, G., 1989. *Duct Ground Heat Storage Model - Manual for Computer Code,* Lund: University of Lund, Department of Mathematical Physics.

Hellström, G., 1991. *Ground heat storage : thermal analyses of duct storage systems*, Lund: University of Lund, Department of Mathematical Physics.

Klein, S. A., et al. 2004. *TRNSYS 16 – A TRaNsient SYstem Simulation program*, Solar Energy Laboratory. Univ. of Wisconsin. USA.

Lundh, M., Dahlenbäck, J.-O. 2007. *Swedish solar heated residential area with seasonal storage in rock: Initial evaluation. Renewable Energy*, Volume 33, pp. 703–711.

Mangold, D. & Deschaintre, L., 2015. *Seasonal Thermal Energy Storage - Report on State of the Art and Necessary Further R&D,* Stuttgart: International Energy Agency - Solar Heating & Cooling Programme (SHC), Task 45 Large Systems.

Nordell, B., 1994. *Borehole heat store design optimization,* Luleå: Luleå University of Technology.

Nordell, B. o.a., 2016. *Long Term Evaluation of Operation and Design of the Emmaboda BTES: Operation and Experiences 2010-2015,* Luleå: Luleå University of Technology.

Pahud, D. & Hellström, G., 1996. *The New Duct Ground Heat Model for TRNSYS.* Eindhoven, Netherlands. 25-27 March, s.n.

PlanEnergi, 2013. *Boreholes in Brædstrup,* u.o.: Brædstrup Totalenergianlæg, Via University College, GEO, P. Aersleff, SOLITES.

Rapantova, N. et al., 2016. *Optimisation of experimental operation of borehole thermal energy storage.* Applied Energy, Volume 181, pp. 464-476.

Rees, S. J. 2016. *Advances in Ground-Source Heat Pump Systems.* Duxford, UK: Woodhead Publishing.

Reuss, M., 2015. The Use of Borehole Thermal Energy Storage (BTES) Systems. In: L. F. Cabeza, ed. *Advances in Thermal Energy Storage Systems: Methods and Applications.* s.l.:Woodhead Publishing , pp. 117-147. ISBN 978-1-78242-096-5.

Schneider, B., 2013. *Storing Solar Energy in the Ground,* Eggenstein-Leopoldshafen: FIZ Karlsruhe - Leibniz Institute for Information Infrastructure.

Sibbitt, B., McClenahan, D., Djebbar, R. & Paget, K., 2015. *Groundbreaking solar - Case study Drake Landing Solar Community.* High Performing Buildings (HPB), July, pp. 36-46.Sibbitt, B. et al., 2012. *The Performance of a High Solar Fraction Seasonal Storage District Heating System – Five Years of Operation.* Energy Procedia, Volume 30, pp. 856-865.

Tordrup, K.W., Poulsen, S.E., & Bjørn, H. 2017. *An improved method for upscaling borehole thermal energy storage using inverse finite element modelling.* Renewable Energy, Volume 105, pp. 13-21.

TOOLS FOR DESIGN OF HIGH TEMPERATURE BOREHOLE STORAGE IN DISTRICT HEATING PRODUCTION

Här beskrivs en ny modell för design av ett borrhålslager i ett fjärrvärmesystem där man tar hänsyn till grundvattenflöden. Forskarna har utvecklat ett beräkningsverktyg som kan användas av energibolag som undersöker potentialen för högtemperaturlagring i borrhål.

Geoenergilager för att ta hand om spillenergi vid temperaturer under 100 grader har diskuterats i Sverige under de senaste åren. Tidigare forskning visar att ungefär hälften av den globala produktionen av primär energi går till spillo.

Här har ett fristående beräkningsverktyg för design, simulering och optimering utvecklats. Värmen lagras i borrhål som interageras med kraftvärmeverk. Verktyget underlättar beräkningen av preliminär storlek på borrhålslager och värmepumpsystem och hur olika faktorer påverkar prestandan. Det kan användas i förstudier där man undersöker potentialen för temperaturlagring inom effektområdet 10–50 MW.

Till rapporten hör en öppen källkod som används för att undersöka inverkan av grundvattenrörelse på ett lagers prestanda.

Energiforsk